PhD degree in Molecular Medicine (curriculum in Molecular Oncology)

European School of Molecular Medicine (SEMM),

University of Milan and University of Naples "Federico II"

Settore disciplinare: Med/04

β-catenin signaling in *CCM3* null endothelial cells contributes to Cerebral Cavernous Malformation pathology

Luca Bravi

IFOM, Milan

Matricola n. R09408

Supervisor: Prof.ssa Elisabetta Dejana

IFOM, Milan

Added Supervisor: Dr.ssa Maria Grazia Lampugnani

IFOM, Milan

Anno accademico 2013-2014

"Stay hungry, stay foolish" S.J.

TABLE OF CONTENTS

LIST OF ABBREVIATIONS

AF6: Afadin

AJ: Adherens Junction

Alk: anaplastic lymphoma receptor tyrosine kinase

ANG1: Angiopoietin1

APC: Adenomatous Polyposis Coli

BBB: Blood Brain Barrier

BMP: Bone Morphogenic Proteins

BSA: bovine serum albumin

CBP: CREB-Binding Protein

CCM: Cerebral Cavernous Malformation

CD: Cluster of Differentiation

CK1: Casein Kinase 1

CNS: Central Nervous System

COUP-TFII: chicken ovalbumin upstream promote transcription factor 2

DAPI: 4', 6-diamidino-2-phenylindole

DEP1: Density-enhanced protein tyrosine phosphatase-

DKK: Dickkopf

DLL4: Delta Like 4

DN: dominant negative

DPN: day post natal

DVL: Dishevelled

E: embryonic day

EC: Endothelial Cell

ECKO: Endothelial cell-specific knockout

ECM: Extracellular Matrix

EndMT: Endothelial to mesenchymal transition

ERK/MAPK: Extracellular-signal-Regulated Kinases/Mitogen-Activated Protein Kinase

ESAM: Endothelial cell-selective adhesion molecule

FAK: Focal Adhesion Kinase

FGF: Fibroblast Growth Factor

FoxO1: Forkhead-box O1

FZD: Frizzled

GAPDH: glyceraldehyde-3-phosphate dehydrogenase

GCKIII: germinal center kinase III

GEF: guanine nucleotide exchange factor

GFP: green fluorescent protein

GLUT1: Glucose transporter 1

GOF: gain-of-function

GSK3β: Glycogen Synthase Kinase 3 β

HEG: heaert of glass

HEY: Hes-related proteins

ID1: DNA-binding protein inhibitor

IMG: intussusceptive microvascular growth

JAM: Junctional Adhesion Molecule

KD: Knockdown

Klf4: Krüppel-like factor

KO: Knockout

LEF: Lymphoid enhancer-binding factor

LOF: loss-of-function

LRP5/6: Low-density lipoprotein receptor-related protein 5/6

LY6A: Lymphocyte antigen 6 complex

MLC: Myosin light chain

MSH: MutS Homolog

MST: mammalian STE20-like protein kinase 4

MYC: myelocytomatosis oncogene

NICD: Notch intracellular domain

NSAIDS: nonsteroidal anti-inflammatory drugs

NVU: Neurovascular Unit

PAR: partitioning defective protein

PDCD10: Programmed Cell Death 10

PECAM: Platelet Endothelial Cell Adhesion Molecule

PI3K: PhosphatidylInositol 3-Kinase

PKC: Protein Kinase C

PL-VAP: Plasmalemma vesicle-associated protein

PLC: phospholipase C

PNVP: Perineural vascular plexus

PP2A: Protein phosphatases 2a

RAC: Ras-related C3 botulinum toxin substrate 1

RAF: Rapidly Accelerated Fibrosarcom

RAP: Ras-related protein

ROCK: Rho-associated protein kinase

RPM: Revolutions per minute

SAN: Santa

sFRPs: secreted Frizzled-Related Proteins

SHH: Sonic Hedgehog

SMAD: Small mother against decapentaplegic

SOX: sex-determining region (SRY)-box

STK: Serine/threonine-protein kinase

STRIPAK: Striatin-interacting phosphatase and kinase

TCF: T-Cell Factor

TGF: Transorming Growth Factor

TGFβR: Transforming Growth Factor beta Receptor

Tiam: T-Cell Lymphoma Invasion And Metastasis

TJ: Tight Junctions

VE-cadherin: Vascular Endothelial cadherin

VE-PTP: Vascular endothelial protein tyrosine phosphatase

VEGF: Vascular Endothelial Growth Factor

VEGFR2: Vascular Endothelial Growth Factor Receptor 2

VTN: Valentine

vWF: von Willebrand factor

WIF: Wnt inhibitory factor

WNT: Int/Wingless

WT: wild type

ZO: Zonula Occludens

ZONAB: ZO-1-associated nucleic acid binding protein

ZPLD1: zona pellucida-like domain containing 1

βTrCP: beta-transducin repeat containing protein

FIGURE INDEX

INTRODUCTION

MATERIALS AND METHODS

RESULTS

DISCUSSION

ABSTRACT

Cerebral cavernous malformation (CCM) is a vascular disease that affects blood vessels in the central nervous system, which become malformed, leaky and prone to hemorrhage. The organ location is critical, both for neurological consequences and therapeutic intervention, which is exclusively surgical to date. The cause of CCM can be either sporadic or genetic. Mutations in three genes named *CCM1/Krit1*, *CCM2/Malcavernin* and *CCM3/Pdcd10* are associated with hereditary CCM.

Here we describe a novel murine model of the disease that develops after endothelial cell-selective ablation of the *CCM3* gene in newborn mice and that we use to investigate the molecular mechanisms behind the development of CCM.

We report enhanced transcription activity of β-catenin in *CCM3*-knockout endothelial cells in *in vitro* and *in vivo* models and we demonstrate that such activation is critical at early stage of the pathology development. In particular, we found that β-catenin is fundamental to trigger the process of endothelial-to-mesenchymal transition (EndMT), which has been previously demonstrated to be crucial for CCM development. Noteworthy, the activation of β-catenin pathway results Wnt-independent, while it correlates with the impaired state of endothelial cell-to-cell junctions typical of vessels developing CCM lesions.

We also show that a pharmacological screening of a panel of drugs targeting β-catenin signaling revealed the NSAIDs sulindac sulfide and sulindac sulfone as potent inhibitors of this signaling pathway in endothelial cells. Moreover, we found that sulindac sulfide and sulindac sulfone are able to attenuate β-catenin transcription activity and to significantly reduce the number and dimension of vascular lesions in the central nervous system of mice with endothelial cell-specific *CCM3*-knockout. These NSAIDs thus represent pharmacological tools for inhibition of the formation of CCM3 vascular lesions, particularly with a view to

patients affected by the genetic variant of CCM, who continue to develop new malformations over time.

INTRODUCTION

1. VASCULAR ENDOTHELIUM

William Harvey in 1628 was the first to describe circulating blood in vertebrates. Anyway, only some years later thanks to Malphigi's experiments the existence of an intricate and complex grove of tubes able to transport blood and nutrients throughout the entire body, known as vascular network, became clear[1]. We had to wait until the XIX century to find a first detailed description, thanks to the work of Von Reckingausen first and Starlings later, of the cellular components of blood vessels and in 1865 Wilhem His coined the term "endothelium" to differentiate the inner lining of body cavities from "epithelium".

However, all these studies looked to the endothelium as a selective but merely static physical barrier. A decisive change of direction occurred immediately after the advent of the electron microscopy during the second half of the XX century when Palade and other scientists described more in details the physiological characteristic of endothelial cells and their interaction with other cell types such as the lymphocytes[1]. These studies led scientific world to consider the endothelium as a dynamic and active organ able to supervise to different biological functions. In 1973 Jaffe and Gimbrone have been able to culture endothelial cells derived from umbilical veins definitively laying the foundation for the modern era of vascular biology[2, 3].

Nowadays the concept that vascular endothelium, as a monolayer of cells forming a barrier between the vessel lumen, where blood stream flow, and surrounding tissue, plays a pivotal role in the regulation of vascular function and structure, is fully accepted. This regulation involve the release of various biochemical mediators and the interactions with other cell types including vascular smooth muscle cells, circulating cells and organ specific cellular constituents.

Altogether these elements constitute the vascular micro-environment which is crucial for endothelial homeostasis, signaling and differentiation as it will be discuss more in details in the next chapters.

1.1 Endothelial differentiation

The endothelium lines the blood-exposed surface of the entire vascular network and the interior heart (where it is called endocardium). However, the endothelial cells (ECs) are very heterogeneous at different levels. The maturation of the endothelium from an undifferentiated progenitor toward a mature and fully functional biological entity is a complex process, which involves different steps and a wide range of physiological signaling, which lead the differentiating ECs to acquire a repertoire of unique functional and molecular characteristics[4, 5].

In mammals a first level of specification occurs very early during embryonic development when two mains processes contribute to the establishment of the vascular system: vasculogenesis and angiogenesis[6, 7]. Vasculogenesis refers to the *de novo* formation of a primitive vascular network starting from a pool of poorly-differentiated endothelial precursors, known as haemangioblasts, which takes place in mouse embryo between embryonic day (E) 6.5 and E9.5. At this stage haemangioblast progenitors start to express the first endothelial-specific marker, the Vascular endothelial growth factor receptor 2 (Vegfr2)[8, 9]. Starting from this primitive plexus another important process, known as angiogenesis, takes place starting from E8.5-E9 in mouse embryo, leading to the formation of new blood vessels through the extension and remodeling of pre-existing ones. Angiogenesis is supported by two different mechanisms: endothelial sprouting and intussusceptive microvascular growth (IMG). The sprouting process is based on endothelial cell migration, proliferation and tube formation, while the IMG or non-sprouting angiogenesis consists in the remodeling of existing vessels

that branch due to the formation of interstitial tissue into the vessel lumen[10]. This maturation process includes the acquisition by ECs of specific endothelial markers such as Platelet Endothelial Cell Adhesion Molecule (Pecam) and the Vascular Endothelial (VE-) cadherin[7].

During embryonic development, both vasculogenesis and angiogenesis contribute to the formation of blood vessels. In the adult, the formation of new blood vessels is restricted to certain physiological conditions (during female reproductive cycle, in the placenta during pregnancy and during wound healing) and occurs mainly through angiogenesis[9].

When deregulated, the formation of new blood vessels has a major impact on our health and contributes to the pathogenesis of many disorders such as ischemic, inflammatory, infectious and immune disorders and malignancies[11] as it will be discuss later.

1.2 Arterial-venous specification

During embryonic angiogenesis in mammals the primitive plexus is remodeled into a highly organized and hierarchical structure where different vessels acquired peculiar characteristic differentiating into artery or veins. The specification of vascular network into two distinct, even if strictly inter-connected, types of blood vessel possessing unique structural characteristic is regulated by a variety of genetic and extrinsic factors working in concert to determine endothelial cell fate[12, 13]. A third type of vessel, the lymphatic vasculature, also starts to develop in mouse embryos at E10.5, when the cardiovascular system is already functioning. The lymphatic circulation subsequently becomes separated from the blood circulation thanks to poorly understood mechanisms[14].

Arteries and veins are usually described as big vessels that drive the blood flow respectively away or toward the heart. From both arteries and veins depart an intricate network of smaller vessels called arterioles and venules, which, in turn, finally branches into capillaries, the smallest and thinnest vessels in the body that connect arterial and venous

districts. Lymphatic vessels derive from embryonic cardinal vein and their development requires the further specification of a subpopulation of venous ECs to a lymphatic fate via signals distinct from those that specify venous endothelium.

Cardiac contractions start very early during mouse development (around E8.5)[15] generating a high-pressure blood flow through arterial vessels, which needs to be supported by a system of smooth muscle cells and extracellular matrix components. On the contrary, venous district collects blood returning to the heart under low pressure. This difference between hemodynamic forces in arteries and veins is crucial for ECs fate determination and different studies have shown a link between local environment and blood vessels specification[16] in terms of physiology and markers expression[17].

However, several studies suggest that arteries and veins possess distinct molecular identity even before blood flow ensues arguing that genetic determinants may play a pivotal role in regulating the very initial steps of arterial-venous differentiation during development[18]. Indeed, through extensive characterization of *in vitro* (ECs in culture) and *in vivo* models (such as mouse, frog, and zebrafish) recent studies identified an array of molecules differentially expressed between arterial and venous ECs and many of them have been found to regulate signaling pathways crucial in the determination of arterial-venous fate[14].

One of the firsts molecular determinants of arterial-venous specification described were the Eph receptors and their ligand Ephrins. The expression of these two classes of molecules is very precocious during development and the binding of Ephrins to EphB receptors stimulates the transduction of intracellular signals essential to guide vessels remodeling. In particular, Ephrin B2 is specifically expressed on the surface of arterial ECs, whereas EphB4 receptor is peculiar of venous endothelium. The complementary expression between these two molecules results in the separation of the two compartments probably via mediating a repulsive signal that separates arterial and venous ECs. However, deletion of either EphrinB2 or EphB4 does

not impair initial specification of arteries and veins but EphrinB2-EphB4 signaling is required for maintenance of the arterial-venous interaction[19, 20]. This limited role leads to the subsequent identification of upstream factors such as Notch in the process of arterial-venous differentiation.

Evolutionarily conserved across diverse species, Notch signaling occurs when a member of the single-pass transmembrane Notch receptors are activated by engagement of ligands, from Delta and JAG/Serrate family, presented by neighboring cells. The binding allows the cleavage by metalloprotease enzymes of the receptor extracellular domain. An enzymatic complex known as γ-secretase then cleaves the Notch transmembrane domain, releasing a Notch Intracellular Domain (NICD) able to translocate to the nucleus and to form complexes with other DNA-binding proteins[21].

In vivo experiment in zebrafish and mammals identified the Notch pathway as the main determinant of initial arterial-venous specification. Indeed, Notch signaling and the activation of downstream transcription factors (Hes-related proteins 1 and 2, Hey1 and Hey2) are required to promote arterial differentiation and to suppress venous fate choice[22]. Conversely, the transcription factor COUP-TFII is required for venous identity since it is able to inhibit the Notch signaling[23].

Recently, it has been demonstrated that both Sonic Hedgehog (Shh) and VEGF signaling pathways act upstream of Notch pathway to determine arterial cell fate[24]. In particular Shh is able to activate VEGF, which in turn induces the expression of Notch pathway genes, including Notch1 and its ligand, Delta-like 4 (Dll4).

Lymphatic ECs differentiate from venous endothelium. The transcriptional factor Sox18, in cooperation with COUP-TFII, progressively promotes expression of Prox1, a master gene in lymphatic determination and maintenance. Venous ECs start to express Prox1 at E9.75 in mouse embryo and by E11.5, clusters of Prox1-positive lymphatic progenitor cells emerge

along the anterioposterior axis of the cardinal vein. These clusters generate intermediate structures known as lymph sacs, from which lymphatic vessels emerge by a combination of sprouting and migration of lymphatic ECs from the cardinal vein[25].

In addition to the mechanisms cited above for arterial-venous differentiation, at least two other signaling pathways have been shown to be crucial for endothelial fate determination: Wnt pathway[26] and Transforming Growth Factor (Tgf)β/Bone Morphogenic Proteins (Bmp) pathway[27]. Indeed, Corada et al.[28] found that during vascular development in the embryo, the downstream effector of Wnt pathway, β-catenin, induces activation of the Notch pathway. In particular, β-catenin triggers the transcription of the Notch ligand Dll4, which, in turn, activates Notch1 and Notch4 receptors. Overexpression of β-catenin both in *in vitro* and *in vivo* models leads to a series of alterations of vascular morphology comparable to those described by overexpression of Dll4, resulting in a strong endothelial cell arterialization and lack of venous specification. Only recently a novel transcription factor called Sox17, a known regulator of endoderm differentiation and selectively expressed in arteries, has been shown to be a key mediator of arterial determination and the molecular link between Wnt and Notch pathway. Indeed, β-catenin is able to induce Sox17 expression, which, in turn, promotes Notch signaling upregulating Hey1, Dll4, Dll1 and Notch4[29]. It appears, therefore, that Wnt and Notch pathways act synergistically in modulating arterial differentiation.

Another pathway important for EC fate determination is Bmp pathway. Bmps are a family of growth factors implicated in a multitude of biological processes including physiological and pathological angiogenesis[27]. In particular, during embryonic development in zebrafish Bmp2 promote endothelial specification and subsequent venous differentiation. Evidences showed that within the caudal vein plexus, Bmp2 expression is restricted to the developing caudal vein, and axial veins sprout in response to Bmp2. Downstream effectors of BMP signaling, Small mothers against decapentaplegic (Smads) and Extracellular signal-

regulated kinase (Erks), mediate this effect by transcriptionally activating a program regulating venous sprout initiation and length[30]. However, the factors responsible for this differential responsiveness between arteries and veins are still obscure.

Although it is now clear that specific molecular pathways guide the arterial-venous-lymphatic determination of ECs, the contribution of other environmental cues, such as flow dynamics, to this process is still under investigation. Some experiments showed that transplanted vessels after grafting, switch their gene expression profile to match that of the host vessels[31, 32]. Moreover, overexpression or loss-of-function experiments of critical molecular determinants of specification can also reprogram a differentiated EC, thus indicating that ECs have a remarkable phenotypic plasticity[33]. Taken together this data suggest a model in which genetic predetermination coordinate initial arterial-venous specification and the environmental inputs regulate subsequent vascular remodeling.

1.3 Endothelial heterogeneity among and within tissues

For long time ECs have been considered as a homogeneous population of cells lining the blood vessels. Nowadays, it is fully accepted the idea that ECs can express specific phenotypes, although displaying many common features, depending on multiple factors such as tissues localization, vessel size and age. This heterogeneity is the primary mechanism by which the endothelium adapts to and sustains the specific functions of distinct tissues and organs.

From a structural point of view the endothelium can be classified into three main types: continuous non-fenestrated, continuous fenestrated and discontinuous or sinusoidal[34-36]. Continuous non-fenestrated endothelium is distinctive of vessels in organs that need to strictly control the passage of substances across the vessel wall such as the brain, the skin and the heart. The presence of highly specialized structures such as tight junctions guarantee the

sealing of cell-to-cell contacts thus the extracellular molecules can cross the barrier mainly by the active process of transcytosis mediated by peculiar structures including caveolae, vesiculo-vacuolar organelles and specific transporters[37]. Continuous fenestrated endothelium is characterized by the presence of transcellular pores (about 70 nm in diameter) on the surface of ECs called fenestrae, allowing a rapid exchange of molecules between the circulation and the surrounding tissue. This kind of endothelium is permeable to water and small solutes and typically occurs in organs characterized by increased filtration or trans-endothelial transport such as glands, digestive tract and kidney. Finally, the discontinuous endothelium is marked out by large heterogeneous fenestrae (100-200 nm in diameter) with few caveolae. This endothelium is found in certain sinusoidal vascular beds most notably bone marrow and liver which need to allow cellular trafficking[37] (**see Fig.1**).

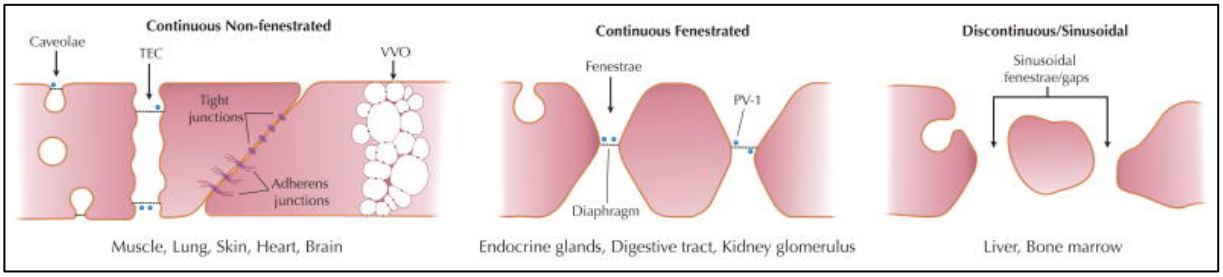

Figure 1. **Endothelial cell heterogeneity.** Capillaries mediate transfer of fluids and solutes between blood and underlying tissue. In continuous non-fenestrated endothelium, water and small solutes (molecular radius, <3 nm) pass between ECs, whereas larger molecules pass through ECs either via transendothelial channels or transcytosis. The latter process is mediated mainly by caveolae, which are particularly prevalent in capillaries of heart and skeletal muscle but rare in brain. Continuous fenestrated endothelium demonstrates high permeability to water and small solutes but not for albumin and larger macromolecules (the diaphragms of the fenestrae act as molecular filters). Discontinuous endothelium is characterized by fenestrae (without diaphragms), gaps, and poorly organized basement membrane. These ECs contain many clathrin-coated pits, which play an important role in receptor-mediated endocytosis (that includes endosomal and lysosomal compartments) and transcytosis. TEC indicates transendothelial channel; VVO, vesiculo-vacuolar organelles[37].

Beside structural differences, ECs from different tissues are heterogeneous also for the expression of markers. For example, von Willebrand factor (vWF), used commonly as a marker for ECs, is not expressed uniformly by the endothelium of all types of vessels[38] and the expression of Glucose transporter 1 (Glut1) is limited *in vivo* to brain vascular ECs[39].

Indeed, microvascular ECs in the brain, liver, and other organs each expresses distinct patterns of cell surface markers, protein transporters, and intracellular enzymes. Some of these tissue-specific phenotypic differences can be only transiently maintained under tissue culture conditions, but they are then lost, indicating the need of specific regulators coming from different tissues[40]. Many evidences have been accumulated in last years suggesting that ECs heterogeneity arise as a result of exposure of ECs to tissue-specific environmental stimuli. Indeed, numerous exogenous factors impact on ECs phenotype including mechanical forces, cytokines exposure, contact with tissue specific cell types, circulating cells, extracellular matrix and soluble growth factors. The regulation of the endothelial phenotype through the microenvironment has been referred as trans-differentiation[41]. The expression and activity of general angiogenic factors such as Vegf or Angiopoietin1 (Ang1) greatly impact on ECs differentiation and varies in different tissues. For example Ang1 stimulates angiogenesis in the skin but suppresses vascular growth in the heart[42, 43].

Additional signaling molecules, such as members of the Tgfβ/Bmp superfamily, contribute to the resolution and maturation phases of angiogenesis, but in a pleiotropic manner. Tgfβ/Bmp family ligands are able to dimerize and bind to a heteromeric receptor complex composed by two type I and two type II receptor proteins. Endoglin is a type III receptor, which facilitates binding of Tgfβ/Bmp to the type II receptors. Once the ligand-receptor complex is formed the kinetic domain of type I receptors phosphorylates and activates Smad proteins. Phosphorylated Smads can dimerize and translocate to the nucleus where they can regulate the transcription of several target genes[11]. Different members of the

Tgfβ/Bmp family can associate with different receptor complexes and trigger different physiological responses. Both pro- and anti-angiogenic properties have been ascribed to Tgfβ/Bmp factors, through effects on ECs and other cell types. For example at low doses, Tgfβ1 contributes to the angiogenic switch by upregulating angiogenic factors and proteinases, whereas at high doses, Tgfβ1 inhibits EC growth, promoting basement membrane deposition and stimulating smooth muscle cells differentiation and recruitment[44].

Vascular heterogeneity acquires even more prominence considering that several human vascular diseases such as vasculitis, atherosclerosis[45] and rare diseases as Cerebral Cavernous Malformation (CCM)[46], which will be described in details in the next chapters, show predilection to specific types of vessels (for schematic summary of endothelial heterogeneity see **Fig.2**).

The basis for such vascular district-specific diseases is poorly understood, but may lie, in part, in the heterogeneity of ECs themselves and for this reason a detailed and deep knowledge of EC biology is crucial to find pharmacological solutions.

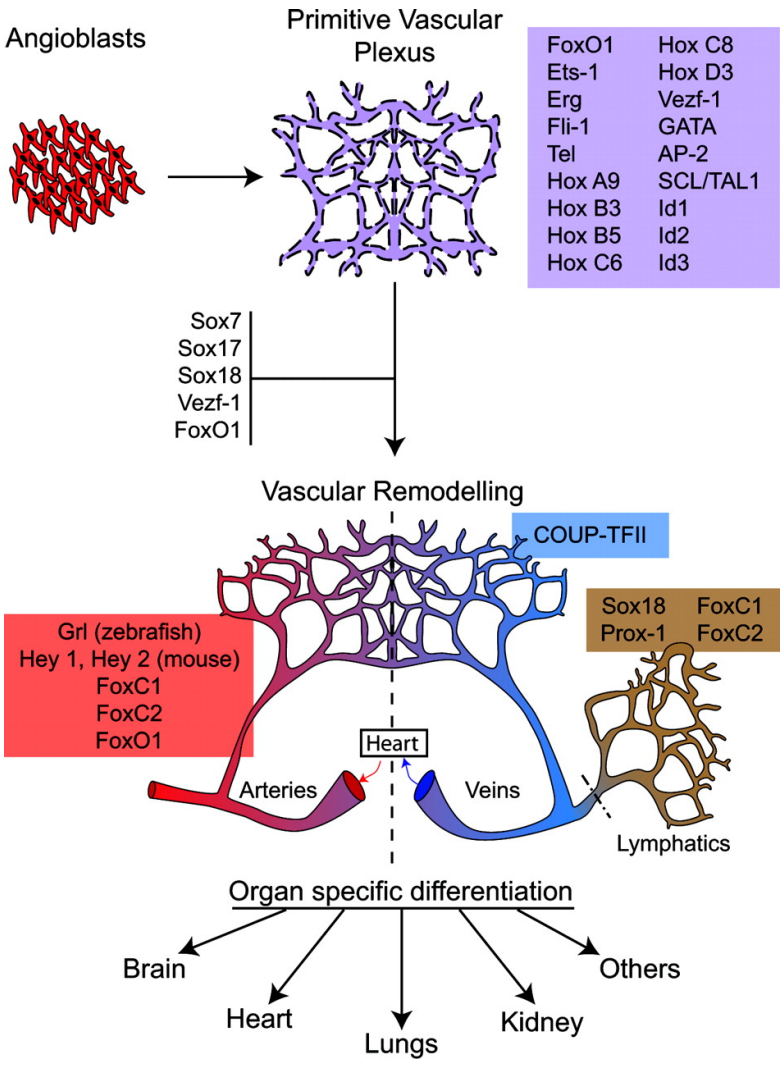

Figure 2. **Schematic representation of different stages of vascular development.** Endothelial cells differentiate from mesodermal progenitors called angioblasts, acquire specific markers, and form the primitive vascular plexus. The plexus undergo further remodeling in large and small vessels, arteries, veins, and lymphatics. Endothelial cells then acquire organ-specific characteristics induced by the crosstalk with cells of the surrounding tissues. All of these steps of endothelial differentiation are regulated by sets of transcription factors[26].

2. A SPECIALIZED ENDOTHELIUM: THE BLOOD BRAIN BARRIER

Among different type of specialized endothelia, one of the most surprising and complex is for sure the brain endothelium, a continuous non-fenestrated monolayer that, thanks to its unique barrier characteristic is able to form, together with other cellular components, a sophisticated structure referred as Blood Brain Barrier (BBB)[47, 48]. Lewandowsky was the first in 1900 to coin the term "Blood Brain Barrier", when he observed that all the organs except the brain rapidly took up neurotoxic compounds injected into the vasculature and that only direct applications into the brain could lead to neuronal cell death. However, the BBB cellular and molecular basis remained unclear for decades. Today, we know that BBB is a peculiar multicellular interface that separates the central nervous system (CNS) from the peripheral blood circulation and carries out a fine control of both the trafficking of molecules and the delivering of nutrients and oxygen across the endothelium according to neuronal needs. This tight control allows BBB to protect the brain from toxins and pathogens, and to maintain the environment that allows neurons to function properly[49].

The BBB is present at all levels of the vascular tree within the CNS even if some regional differences are reported[50], supporting a sub-specialization of the BBB functions. For example, there is a higher expression of nutrients transporters in the capillaries closer to neurons, whereas a finer regulation of leukocytes trafficking and immune modulation occurs in post capillary venules, which are surrounded by the perivascular space[51].

In the BBB the brain endothelium is constituted by ECs with peculiar molecular structure and characteristic allowing them to be the gatekeepers of the brain. These characteristics include continuous intercellular tight junctions, lack of fenestration, extremely low rate of transcytosis and consequently limited paracellular and transcellular movements of molecules through the EC layer. The trafficking of molecules across the endothelial layer is regulated by a series of specific transporters in both directions. Moreover, immune cell

infiltration in the CNS is very rare due to the low expression of leukocyte adhesion molecules on EC surface[48, 49]. Beside ECs, other cellular and non-cellular elements are extremely important for BBB development and maintenance in particular pericytes, astrocytes, neurons and the extracellular matrix (ECM), which enwrapped ECs to provide both structural and functional support. All this elements, together with the contribution of microglial cells and peripheral immune cells, constitute a peculiar microenvironment, which regulates BBB homeostasis known as neuro-vascular unit (NVU)[52] (see **Fig.3**).

In the last years, extensive efforts have been done in order to better characterize BBB unique structural and functional components. Comprehensive *in vitro* and *in vivo* analysis provided the elements for better understanding some of the molecular mechanism and signaling pathways at the basis of BBB complexity that will be discussed in the next chapter.

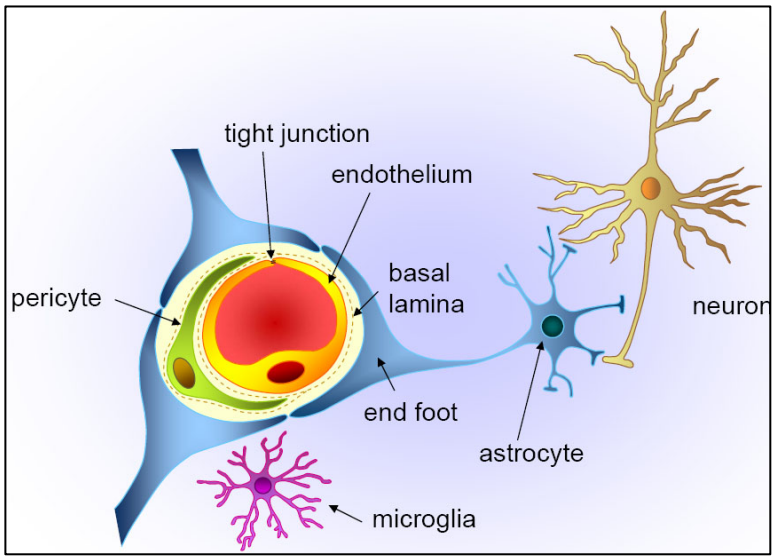

***Figure 3*. The neurovascular unit at capillary level.** Several cell types work in close association to maintain optimal brain function. Together they form the neurovascular unit. Cerebral endothelial cells are the main substrate of the BBB. Pericytes partially envelop the endothelial cells and share a common basal lamina with them. Astroglial endfeet envelope the microvessel wall. Pericytes and astrocytes are important in barrier induction and maintenance, and astrocytes provide links to neurons. Microglia are CNS-resident immune cells[53].

2.1 Wnt/β-catenin signaling

Recently different studies put a great effort trying to elucidate the molecular basis of BBB specialization. Extensive high-throughput genomic and proteomic approaches identified the Int/Wingless (Wnt)/β-catenin signaling as one of the master regulator pathways in CNS angiogenesis[50].

Wnt proteins belong to an incredibly evolutionary conserved family of secreted glycoproteins acting as ligands for receptor-mediated signaling pathways regulating different processes during the development and in the adults. 19 members of the Wnt family have been described so far, able to trigger different pathways. Wnt proteins are ~40 kDa in size, contain many conserved cysteines[54] and undergo several post-translational modifications[55] before being secreted from cells. One of such post-translational modification consists in the attachment of a mono-unsaturated fatty acid (palmitoleic acid) to a conserved serine. This event takes place in the endoplasmic reticulum by the action of Porcupine enzyme. Wnt palmitoilation is required for efficient ligand activity and secretion[56]. Once secreted, Wnt proteins act as morphogens, molecules that exert their action across a distance in tissues forming a gradient that determines cell fate in a concentration-dependent manner.

Wnt ligands interact with target cells recognizing a heteromeric receptor complex composed by both a receptor of the Frizzled (Fzd) family and a Lrp5/6 co-receptor[57]. Depending on the type of the ligand and on the molecular composition of the receptor complex, Wnt proteins can trigger different pathways. The best studied is the canonical Wnt/β-catenin pathway[57], while the non-canonical pathways, including planar cell polarity pathway and calcium pathway, are still poorly understood[58]. In the canonical Wnt/β-catenin pathway, the association of the ligand with the receptor complex induces a conformational change of the receptor followed by phosphorylation of key target proteins such as Lrp5/6[59], which, in turn, activate an intracellular signaling cascade that has in β-catenin the main

downstream effector. In resting condition, free cytoplasmic β-catenin is maintained at very low levels due to the activity of the 'destruction complex', a multiprotein complex able to trigger β-catenin degradation through the proteasomal machinery. In particular the 'destruction complex' harbors scaffold proteins, such as Axin and Adenomatous polyposis coli (APC), and kinases, such as Glycogen synthase kinase (GSK3) and casein kinase 1 (CK1), able to trigger sequential β-catenin phosphorylation at the level of serine 45 (by CK1) and then at threonine 41, serine 37 and serine 33 (by GSK3). β-catenin phosphorylation creates a binding site for the E3 ubiquitin ligase β-Trcp, leading to β-catenin ubiquitination and degradation[60]. The ligand-dependent activation of Wnt receptor complex initiates a series of events that culminate in the recruitment at cell membrane of members of the 'destruction complex' with the help of an adaptor protein called Dishevelled (Dvl)[61]. As a consequence, the 'destruction complex' is no more active on β-catenin, which can accumulate into the cytoplasm and then translocate to the nucleus. Noteworthy, the Wnt pathway transduces signals differently from most of the other pathways. In many signaling cascades, the phosphorylation of downstream effectors amplifies the signal since individual kinases can target multiple substrate molecules. In contrast, Wnt stimulus titrates away negative regulators, the 'destruction complex' members, providing a stoichiometric rather than a catalytic mechanism of signal transduction[57].

The ultimate step of Wnt signaling cascade occurs in the nucleus where β-catenin is able to act as co-factor for the transcription of several target genes. The canonical partners of nuclear β-catenin are the transcription factors of the lymphoid-enhancer/T-cell factor (Lef/Tcf) family. When Wnt signaling is switched off the Lef/Tcf interact with Groucho transcriptional repressors, preventing gene transcription[57, 62]. When Wnt pathway becomes activated, the association with β-catenin transiently converts Lef/Tcf factors into transcriptional activators of target genes, with additional modulation of Lef/Tcf coming from phosphorylation[63]. Most of

the Wnt target genes are tissue or developmental stage specific and a multiplicity of molecular partners can modulate β-catenin transcriptionally response. However, Axin2 and Nkd1 genes are regarded as general transcriptional targets of β-catenin and therefore general indicators of Wnt pathway activity[64]. Among the most common transcriptional partners of β-catenin are CREB binding protein (Cbp) and P300, histone-modifier proteins able to induce DNA epigenetic activation[57] (for a schematic representation of Wn/β-catenin signaling cascade see **Fig.4**).

Other important β-catenin interactors are Smad proteins. These transcription factors are associated to Tgfβ/Bmp receptors and, upon receptor activation, are phosphorylated and translocate to the nucleus[65]. Smad–induced transcription is further dependent on co-activators that stabilize their association to DNA. Among others, Smads combined to β-catenin and this complex is crucial for the expression of genes involved in cell motility and endothelial to mesenchymal transition[66-68].

Wnt/β-catenin signaling can be modulated at many levels by physiological regulators including various secreted antagonists. Among these are molecules that bind Wnt proteins thus inhibiting ligand-receptor association such as secreted Frizzled-related proteins (sFrps) and Wnt inhibitory factors (Wifs). Other Wnt inhibitors include proteins of the Dickkopf (Dkk) family, which antagonize signaling by binding Lrp5/6 co-receptor disrupting Wnt-induced Fzd-Lrp complex formation[57].

The broad implications of Wnt/β-catenin signaling in different fundamental processes of health and disease make the pathway a prime target for pharmacological research and development. The complex regulation of β-catenin at its various locations provides alternative points for therapeutic interventions and many studies directed their attention to chemicals compounds screening trying to find pharmacological inhibitors of the Wnt/β-catenin pathway.

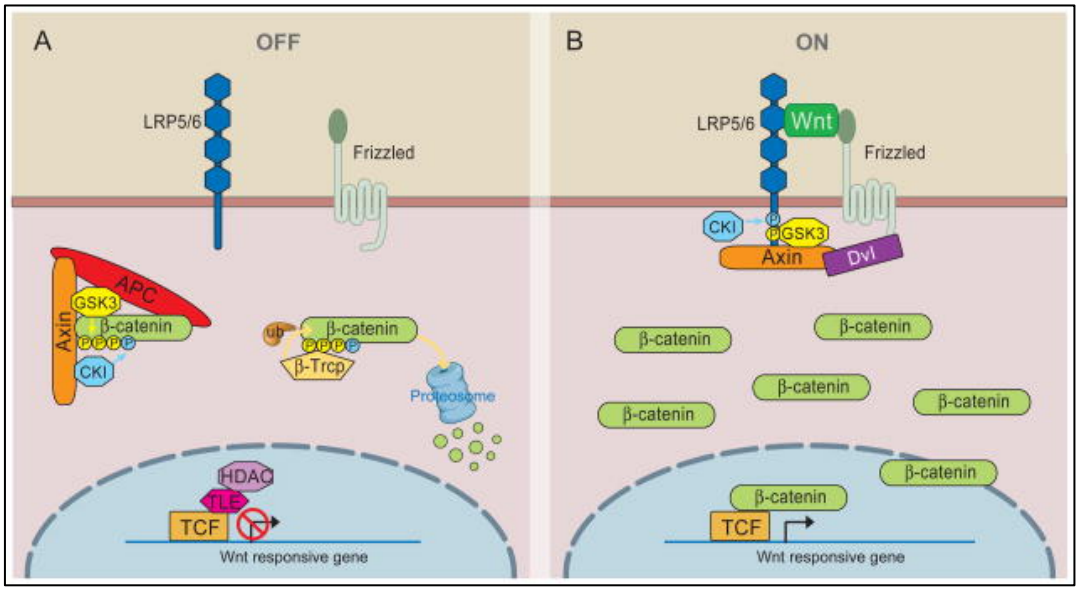

Figure 4. **Wnt signaling cascade.** (**A**) In the absence of Wnt, cytoplasmic β-catenin is engaged in a complex with Axin, APC, GSK3 and CK1 and is phosphorylated by CK1 and subsequently by GSK3. Phosphorylated β-catenin is then uiquitinated by the E3 ubiquitin ligase β-Trcp, which targets β-catenin for proteosomal degradation. Wnt target genes are repressed by Tcf-TLE/Groucho and histone deacetylases (HDAC). (**B**) In the presence of Wnt ligand, Fzd and Lrp5/6 form a receptor complex and recruit Dvl, which, in turn, induces Lrp5/6 phosphorylation and Axin recruitment. In this way degradation of β-catenin is impaired and allow β-catenin to accumulate in the nucleus where it serves as a co-activator for Lef/Tcf to activate Wnt target genes[69].

2.2 Development and maturation of Blood Brain Barrier

The vascularization of CNS in mouse embryo starts at E9 exclusively via angiogenesis from a previously developed perineural vascular plexus (PNVP)[70, 71]. At E9.5 vascular sprouts start from PNVP and radially invade the neural tube toward the ventricular zone where they begin to remodel into capillaries[70, 71]. This process is not intrinsic to brain ECs but requires crosstalk with other cellular elements of the developing BBB. Indeed, transplantation experiments demonstrated that embryonic brain tissue from one species transplanted into ectopic sites of the embryo of a different species induced invasion of vessels from the non-brain host tissue, which developed BBB characteristic[72]. These experiments provide evidences that ECs differentiate into BBB-forming vessels under the influence of the microenviroment.

More recently it became clear that the ability to induce BBB properties of neuroblasts implicate the activation of Wnt pathway[73].

During embryogenesis in mouse the Wnt/β-catenin pathway has been found activated in CNS endothelium but not in ECs of other districts, therefore pointing to a specific role of Wnt signaling in the CNS[74]. Several Wnt ligands and Fzd receptors can act at different time and in different regions of the CNS vasculature. In particular, the expression pattern of the most studied ligands such as Wnt1, 3a and 7b have been described and they were found to be expressed in very defined domain of CNS at early time point (E8.5 of mouse embryo development)[74, 75]. In particular Wnt1 and Wnt3a show a dorsal expression pattern while Wnt7b is ventrally distributed[74-76]. This defined distribution suggests a differential role for distinct Wnt factors to regulate CNS vascularization and barrier properties.

While Wnt signaling is important at early steps of angiogenesis, it is likely down regulated in healthy, resting vasculature[77]. Evidences come from genetic experiments where different members of Wnt pathway have been selectively inactivated. For instance, mice knockout for Wnt7b but not Wnt7a die between E11.5 and E12.5 due to severe brain hemorrhages and abnormal vessel morphology in ventral regions. Combined inactivation of both ligands causes even more severe defects in CNS angiogenesis[74, 78]. These vascular defects are phenocopied by endothelial-specific inactivation of β-catenin[74] in the CNS suggesting that Wnt7a/Wnt7b exert their function activating the canonical Wnt signaling pathway in the endothelium. Conversely, ablation of Fzd5 and Wnt2 leads to defects in placenta vascularization and, at least in the absence of Fzd5, to a defective remodeling of yolk sac vasculature[26]. Moreover, both loss-of-function (LOF) and gain-of-function (GOF) mutations of Fzd4 and Lrp5 recapitulate severe vascular defects resulting in early embryonic lethality[26]. Lack of the Wnt pathway effector β-catenin in ECs affects the development of the whole embryonic vasculature and results in early lethality due to diffuse hemorrages[79]. Similarly, the

induction of an endothelial-specific GOF for β-catenin results in even more dramatically vascular phenotype including lack of vascular remodeling, defects in branching and loss of venous identity[28, 80]. Consistent with these findings the endothelial-specific GOF of Fzd4 induces a similar vascular phenotype[26]. Taken together these data indicate that Wnt/β-catenin signaling needs to be finely regulated in CNS endothelium and that either too much or too little can lead to major vascular aberrations.

In addition to promote angiogenesis, Wnt/β-catenin signaling could contribute to vascular differentiation in the CNS by regulating the expression of the BBB genes including the transporter Glut1, Plasmalemmal vesicle-associated protein (Pl-Vap) and the tight junction protein Claudin3[77]. Wnt/β-catenin signaling is high in ECs of CNS during embryonic life, while it dramatically drops soon after birth[77]. Nevertheless, a detectable signal subsists during the first post-natal days and decline slowly with the time, suggesting that BBB maturation is still ongoing. Therefore, the induction of EC migration into the CNS and the acquisition of BBB characteristics are driven by the same signaling pathway, suggesting a CNS-specific angiogenic program that imparts barrier-specific properties to the vasculature controlled by Wnt/β-catenin.

The unique anatomical properties of CNS vessels suggest a continuous crosstalk with elements of the neurovascular unit. This is supported by the observation that ECs from CNS microvasculature lose rapidly their barrier characteristics when put in culture. This effect can be partially restored by co-culturing them with pericytes or astrocytes or by adding exogenous Wnt ligands[81]. As far as the maintenance of the BBB phenotype beyond the embryonic and neonatal phase, it has been recently shown that Norrin via Fzd4 is important to maintain endothelial barrier properties in the retina (another type of vasculature with BBB properties) and cerebellum of adult mice[82]. Indeed, the inactivation of either the gene or its cognate receptor Fzd4 leads to the loss of barrier characteristics and up regulation of the permeability-

associated gene Pl-Vap[82]. This finding suggests that Wnt/β-catenin signaling can have a role in BBB maintenance throughout lifetime in addition to its role in BBB development and differentiation. Also in this case Wnt/β-catenin signaling needs to be tightly regulated during BBB development as suggested also by a recent work demonstrating that radial glia is involved in nascent vessel stabilization in cerebral cortex by inhibiting Wnt/β-catenin in ECs[83].

Finally, a further degree of complexity is proposed by the less-investigated possibility that different Wnt can determine region-specific effects potentially resulting in different 'subtypes' of BBB with different functional meaning.

2.3 Wnt/β-catenin signaling in pathology and pharmacological treatment

Taking into consideration the critical role that Wnt signaling exerts during vascular angiogenesis and BBB maturation and maintenance, it is not surprising that many vascular pathologies and neurological disorders can derive from Wnt pathway deregulation and the resulting loss of BBB integrity. Characteristic tracts of BBB dysfunction are edema, recruitment of inflammatory cells and neuronal cell death, as observed for example in multiple sclerosis and ischemic brains in animal models for stroke. Mutations in either Fzd4 or Lrp5 have been found in patients affected by familial exudative vitreoretinopathy characterized by defective retinal vascularization. The same phenotype has been observed in patients with Norrie disease carrying Norrin mutations. These findings leaded to the identification of Norrin as a ligand for Fzd4/Lrp5 receptor complex previously discussed[26]. Also brain tumors often show impaired BBB due to a continuous tumor-induced angiogenesis[84].

In addition to the CNS, mutations in different genes involved in Wnt/β-catenin signaling cascades have been reported in pathologies affecting different organs. For example mutations in Lrp5 have been found in patients with osteoporosis pseudoglioma syndrome, a recessive

disorder characterized by low bone mass and abnormal eye vasculature. Tcf4 is also implicated in type II diabetes even if the mechanisms are still unknown[69]. Deregulation of Wnt/β-catenin signaling is often associated with cancer in particular with colorectal cancer[85]. In this case different genetic alterations lead to a sustained β-catenin nuclear signaling and therefore to excessive stem cell renewal and proliferation. For this reason β-catenin has been frequently investigated as possible target for pharmacological treatment. Many lines of evidence attribute the beneficial effects of nonsteroidal anti-inflammatory drugs (NSAIDs) in colorectal cancer therapy to their ability in inhibiting Wnt/β-catenin signaling[86, 87].

Several studies also reported β-catenin nuclear accumulation in blood vessels of glioblastoma multiforme characterized by abnormal vascular construction with glomeruloid appearance. Here the intracellular localization of β-catenin was found to be different from that of normal brain vessels. These data suggests an implication of endothelial Wnt/β-catenin signaling in tumor angiogenesis[84].

Identification of small molecules able to block Wnt/β-catenin signaling is a hot topic of modern research. Several compounds targeting different steps of Wnt/β-catenin pathway have been proposed for use in therapy, but few of them had a positive clinical outcome[88]. In preclinical models some of the most active compounds seem to be the Porcupine inhibitors, targeting the enzyme responsible for Wnt ligands post-translational processing and secretion. Other drugs, used up to now only in experimental models, include Tankyrases inhibitors[88], which block a class of molecules responsible for Axin degradation. Increased amount of cytoplasmic Axin leads to enhanced β-catenin turnover. Inhibitors of the Tcf/β-catenin complex have also been proposed. Some examples are PKF-118 and ICG-001[88]. Finally, some natural compounds with a less defined molecular mechanism have been described to inhibit Wnt/β-catenin signaling such as Silibinin, Curcumin and Resveratrol[89, 90].

Concluding, targeting Wnt/β-catenin could represent a potent tool allowing, from one side, to block altered pathological signaling and from the other to manipulate a complex system such as the BBB, critical for drug delivery into the CNS.

2.4 Endothelial cell-to-cell junctions and vascular permeability

Brain endothelium represents a very specialized vasculature with unique properties that ensure a tight control of permeability between blood and the nervous system. One of the cellular components involved in this process is the cell-to-cell junction complex. The presence of organized cell-to-cell junctions is a peculiar tract of all ECs. However, the molecular composition and physiological properties of these structures varies depending on the organ specific localization and vessels identity, suggesting context-specific functions[34, 35]. Here I will first focus on common features of endothelial cell-to-cell junctions, then discussing their role and organization in BBB.

2.4.1 Common features of cell-to-cell junctions

ECs are linked one to the other by adhesive proteins that are organized in highly specialized domains of the plasma membrane that control fundamental activities of the endothelium such as the barrier properties, growth and the response to soluble factors during physiological angiogenesis. At least two distinct macromolecular complexes can be distinguished in ECs: the tight junctions (TJs) and the adherens junctions (AJs) respectively[91, 92]. These molecular structures, which occupy different positions on the cell surface, are associated to different functions: in particular AJs, localized more basally, initiate cell-to-cell contacts promoting their maturation and maintenance, while TJs, which occupy the most apical position of the junctional cleft, act by strictly regulating the paracellular passage of ions and solutes[36].

Cell-to-cell junctions are not only mere sites of attachment between ECs but highly dynamic structures undergoing continuous remodelling. For this reason junctional clusters are subjected to multiple regulations that allow them to control crucial cell functions in vascular homeostasis. Likely, any change in junctional organization might either seriously impact on endothelial physiology or modify the normal architecture of the vessel wall.

Although the specific molecular properties of cell-to-cell junctions in the different endothelia of the organism wait to be defined in details, it is clear that these structures can convey signals to the cell. The signals transmitted by the junctional proteins are multiple and regulate several fundamental aspects of endothelial physiology, generally maintaining a resting quiescent condition. Therefore, it is not surprising that angiogenic stimuli rapidly induce substantial alteration of junctional architecture and are accompanied by increased vessel permeability and, more in general, changes in the endothelial barrier function[93]. In most cases, changes in the endothelial permeability are reversible and intercellular junctions are rapidly restored with the exception of pathological conditions, such as chronic inflammation.

Both AJs and TJs host a series of adhesive transmembrane molecules responsible for homophilic cell-to-cell adhesion, thus interacting with identical partners on adjoining cells (*trans* interactions) and on the same cell (c*is* interactions)[91]. In turn, the transmembrane proteins associate to a specific set of cytosolic partners forming multiprotein complexes, which have scaffold and signaling properties. The list of molecules that can localize at cellular contacts is constantly increasing suggesting the existence of distinct junctional complexes localized in discrete microdomain precisely regulating cellular response to specific conditions and stimuli[94]. What is clear is that, even if presenting several common general structural features, distinct molecules compose either TJs or AJs. In addition, many evidences support the concept that TJs and AJs are interconnected and that the state of AJs influences TJs organization.

2.4.2 Cell-to-cell junctions architecture

Several transmembrane adhesive molecules have been identified at endothelial cell-to-cell contacts including cell-type-specific proteins such as VE-cadherin at AJs[95] and Claudin5 at TJs[96]. ECs of all types of vessels express these two proteins. In particular VE-cadherin cannot be found in any other differentiated cell type and represents a hallmark of the endothelium, expressed early during development, as soon as cells become committed to the endothelial lineage. Although most components of endothelial junctions are not endothelial specific, some of them appear to play a selective role in endothelial physiology, as indicated by the specific vascular phenotype of KO mice and in some cases of zebrafish morphants and mutants[97]. Through their cytoplasmic tails, adhesion proteins of both types of junctions bind to actin microfilaments and transfer exogenous signals to the cell interior. The interaction of junctional adhesion proteins with the actin cytoskeleton is relevant in the maintenance of cell shape and polarity[98]. Many other actin-binding proteins and several kinases, adaptors and phosphatases cluster at endothelial junctions[94].

Tight junctions

The main components of TJs are the members of Claudin family, a large family with more than twenty members. ECs express only few of them and in particular Claudin5 is predominantly expressed all along the vascular tree[96]. Other Claudins are found in different types of vessels responding to different needs in term of control of permeability such as Claudin16/paracellin1, which is responsible for paracellular flux of Mg^{2+} and Ca^{2+} in the kidney[99], and Claudin3 that participates to the control of permeability in the brain endothelium[77]. In addiction Claudin5, but not Claudin12, critically control permeability of brain capillaries as indicated by the lethal leakage at brain capillaries observed early after birth in Claudin5 KO mice[96].

In addition to Claudins other transmembrane proteins have been found at TJs such as Junctional adhesion molecules (JAMs), Occludin and Endothelial cell-selective adhesion molecule (ESAM)[100, 101] contributing to intercellular adhesion in different ways. The intracellular aspect of TJs is characterized by the presence of multiple partners such as members of the Zona occludens (ZO) family (ZO1 and ZO2 in the endothelium), Cingulin, Zonula occludens associated nucleic-acid-binding protein (ZONAB), Partitioning defective protein (Par) 3 and Par6[102-104]. ZO proteins link Claudins and Occludin via Cingulin to intracellular actin cytoskeleton. Importantly, it has been shown that ZO1 and ZONAB are substrates of kinases such as Protein Kinase C (PKC), which is crucial for the formation and regulation of TJs[105]. Moreover different types of signaling components can bind the cytosolic domain of TJs such as GTP-binding proteins, kinases and phosphatases. For instance the signaling pathways transduced by Rho family members such as Rho have been implicated in the regulation of TJs[106].

Adherens junctions

At the level of AJs the main players delegated to mediate cell-to-cell adhesion are the members of the cadherin family. In particular VE-cadherin is ubiquitously expressed in all types of vessel. N-cadherin is also expressed in the endothelium but is infrequently at inter-endothelial contacts, except in some pathological situation such as tumors[107]. Several studies demonstrated that VE-cadherin is able to exclude N-cadherin from inter-endothelial junctions suggesting a differential role for these two molecules. Indeed, N-cadherin seems to promote endothelial communication with other cellular components of the vessels, such as pericytes and smooth muscle cells and to predispose ECs to a migratory phenotype[107].

Both VE- and N-cadherin bind catenins through their cytoplasmic domain: directly β-catenin, Plakoglobin (also known as γ-catenin) and p120[36] and indirectly α-catenin have a strong impact on the activity and stability of VE-cadherin[108]. Catenins, in turn, connect

cadherins to the cortical actin cytosckeleton and with several others molecules for the constitution of junctional signaling clusters. β-catenin, p120 and plakoglobin all contain homologous Armadillo repeats (the name of this domain come from the *Drosophila* orthologue of β-catenin, the segment polarity protein Armadillo, so-called because the mutants resemble armadillos) critical for their functions, which represents the binding site for most catenin-binding partners[109].

VE-cadherin can recruit several cytoplasmic molecules that regulate the local organization of the actin cytoskeleton. One of this is T-Cell lymphoma invasion and metastasis (Tiam)[110], a guanine nucleotide exchange factor that activates Ras-related C3 botulinum toxin substrate (Rac) 1 for organization of peripheral actin bundles. The small GTPase, Ras-related protein (Rap)1, that plays a crucial role in the stabilization of endothelial junctions[111], promotes the translocation to membrane of Tiam[112]. Rap1 links to VE-cadherin and can also mediate the association of the Rapidly accelerated fibrosarcom (Raf)1/Rho-associated protein kinase (Rock) complex to VE-cadherin to regulate the phosphorylation of Myosin light chain (MLC) 2 and actomyosin contractility at junction[113].

However, the classical cytoplasmic partner of VE-cadherin is β-catenin, which associates simultaneously to the carboxy-terminal cytoplasmic domain of cadherins and to α-catenin, thereby forming a ternary complex. β-catenin is a very versatile adaptor molecule, which binds and recruits several regulatory and scaffold molecules to cell junctions. Therefore β-catenin provides a fundamental contribution to the molecular architecture and function of endothelial junctions. Indeed, truncated VE-cadherin, lacking the carboxy-terminal of the cytoplasmic domain and unable to bind β-catenin, induces *in vivo* and *in vitro* vascular defects superimposable to those observed after null mutation of *VE-cadherin*[113, 114].

It has been reported that the phosphorylation of tyrosine residues of β-catenin can decrease its binding affinity to VE-cadherin in response to Vegf[115]. Also Focal adhesion

kinase (FAK) could contribute to the weakening of endothelial junctions in response to Vegf, phosphorylating the tyrosine residue 142 of β-catenin and decreasing its association to VE-cadherin *in vivo*[116]. However, other reports are in contrast with the model in which VE-cadherin/β-catenin complex is modulated by tyrosine phosphorylation of β-catenin and further investigation would be needed to better address this issue.

In some conditions of severely and constantly disorganized junctions, β-catenin can partially dissociates from VE-cadherin. For example, this has been reported in *CCM1*-silenced ECs[117]. A reasonable hypothesis is that in ECs even a limited decrease in the association between VE-cadherin and β-catenin is sufficient to create (subtle) local discontinuities in the molecular composition of cell-to-cell junctions that weaken the continuity of the monolayer and impair its barrier function.

In addition to its adaptor role at junctions, β-catenin is a crucial regulator of transcription[57]. The relative ratio between junctional-associated β-catenin and free β-catenin is critical since free β-catenin is released in the cytoplasm where is either rapidly degraded by the ubiquitin–proteasome pathway or translocates to the nucleus to regulate several target gene expression in association with members of the Tcf/Lef family of transcription factors as previously discussed.

Besides catenins, growth factor receptors like Vegfr2 also associate to cadherin cluster, as well as kinases (as Src) or phosphatases (such as vascular Endothelial protein tyrosine phosphatase (VE-PTP) and Density-enhanced protein tyrosine phosphatase1 (Dep1)). AJs can also recruit several other mediators such as Caveolin 1, CCM proteins, the polarity complex Par3–Par6, PKC and many others[36, 118-120]. For detailed lists of molecules associated to VE-cadherin see[121], while for a schematic representation of endothelial cell-to-cell junction organization see **Fig.5**.

Due to the central role of junction clusters in regulating the localization and the activity of several signaling molecules, cell junctions should not be considered only as adhesive complexes, but rather real signaling center conveying and processing myriads of exogenous and endogenous stimuli.

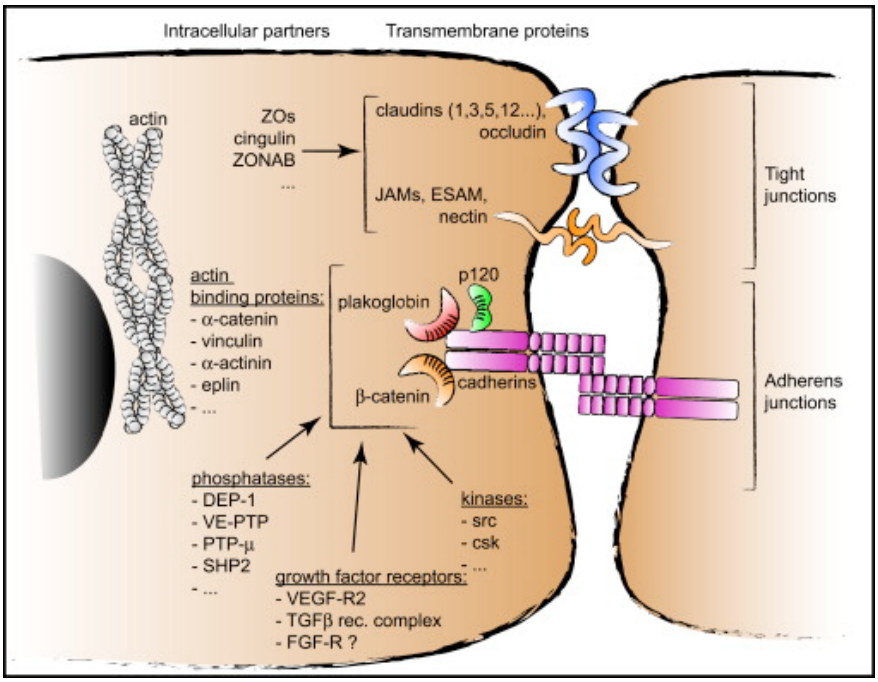

Figure 5. **Schematic representation of tight junctions and adherens junctions in endothelial cells.** In endothelial cells Claudins, Occludin, JAM proteins, and ESAM mediate adhesion at tight junctions. The cytoplasmic components of tight junctions are ZO proteins, cingulin, ZONAB, and others. At adherens junctions, adhesion is promoted by cadherins (VE-cadherin and N-cadherin), which directly bind to p120, β-catenin, and plakoglobin. Different actin binding proteins have been found to be associated to adherens junctions such as α-catenin, vinculin and others. In addition, phosphatases (Dep1, VE-PTP, etc.) and kinases (src and others) are directly or indirectly associated to adherens junction components. Growth factor receptors: Vegfr2 and TgfβR complex could bind to VE-cadherin complex. This interaction modulates their signaling properties[122].

2.4.3 Endothelial cells junctions and signaling

Besides regulation of endothelial functions, achieved through the local organization of specific signaling complexes to AJs as described in the previous paragraphs, the 'degree of tightness' of VE-cadherin association to junctions appears to regulate the transcriptional profile of ECs[123]. 'Degree of tightness' means distinct and specific molecular complexes

recruited by VE-cadherin to AJs as a function of the duration and stability of its engagement in an adhesive interaction. In general, the molecular details of the dynamic remodeling of such complexes are still poorly known. Some examples include the association of cell junction molecules with other angiogenic receptors. For example clustered VE-cadherin can modulate the activity of receptors that act as crucial regulators of vessel organization such as Vegfr2[124] and Tgfβr2[125]. Vegfr2, once activated by Vegf, becomes phosphorylated on different tyrosine residues (mainly Y951, Y1175 and Y1212)[126]. These phosphorylated tyrosines become docking sites for different mediators that can activate locally different signaling pathways[126] depending on the stability of the junctions. In particular, we have observed that when VE-cadherin is engaged in stable contacts, as in confluent endothelial monolayers, activated Vegfr2 associates to VE-cadherin through β-catenin and activates Phosphatidylinositol3-kinase (PI3K) (also associated to VE-cadherin through β-catenin) to phosphorylate Akt and to signal cell survival and resistance to apoptosis[123, 124]. When VE-cadherin is engaged in dynamic junctions, like in cells undergoing angiogenic responses, Vegf-activated Vegfr2 preferentially stimulates PLCγ and Mitogen-activated protein kinase (Mapk) pathway, inducing cell proliferation[127]. Such signaling can take place from endocytic compartments in which Vegfr2 is internalized in association to VE-cadherin through a clathrin-dependent process[127].

VE-cadherin clustered in stable contacts can modulate the endothelial behavior forming a complex with another regulator of vascular physiology, the Tgfβ receptors[125]. The functional consequence of such local regulation is the activation by Tgfβ of anti-proliferative and anti-migratory responses. Such signaling would contribute to the stability of the mature endothelial layer. On the contrary, in ECs with weakened junctions, as after treatment with a VE-cadherin blocking antibody[125], or with reduced level of VE-cadherin[128], Tgfβ receptors are not or less associated to VE-cadherin[125]. This dis-activates the anti-proliferative and anti-migratory

response elicited by Tgfβ and it can even re-direct Tgfβ signaling towards de-differentiation (mesenchymal transformation) of ECs.

VE-cadherin has been recently shown also to associate to the Fibroblast growth factor (Fgf) receptor 1 and reduce its phosphorylation in response to Fgf2 engaging the phosphatase Dep1 in a multiprotein complex[129].

AJs and TJs are not completely independent units but are strictly interconnected. For instance AJs can transfer signals that induce TJ assembly. Indeed, VE-cadherin clustered to cell-to-cell junctions activates a signaling pathway that up regulates the transcription and the deposition at junctions of Claudin5, the major transmembrane component of the TJs[123]. Clustered VE-cadherin recruits PI3K, through β-catenin as described above. This kinase locally activates Akt that, in turn, phosphorylates the transcription factor Forkhead-box O1 (FoxO1), a major repressor of Claudin5 transcription in association to β-catenin. The phosphorylated FoxO1 is excluded from the nucleus (phosphorylation on Thr24 promotes its exclusion from the nucleus and phosphorylation on Ser256 inhibits its binding to DNA), thus relieving the inhibition of Claudin5 transcription[123].

Among the interactors of VE-cadherin, β-catenin plays an important role in coordinating the state of junction compartment to the quality and type of transcription in the nuclear compartment. Although, such regulation is evident from a functional point of view, the details of the underlying molecular mechanism are still virtually unknown.

2.4.4 Cell junctions and nuclear β-catenin regulation

β-catenin can be engaged in AJs, where exerts a scaffold role, or recognized by the degradation complex which triggers its phosphorylation. For this reason β-catenin can subsists in ECs in a phosphorylated state (Thr41 to Ser37 and Ser33) destined to proteasomal degradation and in a de-phosphorylated state. De-phosphorylated β-catenin, referred as active

β-catenin, can localize at cell-to-cell contacts or in the nucleus where acts as a crucial regulator of transcription in association to Lef/Tcf transcription factors[57]. The relationship between junctional and nuclear pool of β-catenin remains at the present an unsolved general issue in cell biology, besides ECs. It is not known whether nuclear β-catenin originates from junctions or whether it comes from a distinct pool. In Drosophila the existence of two distinct pools, junctional and nuclear, of the β-catenin homologue armadillo, is ascertained[130], and confirmed in C. elegans[131]. In contrast, in mammalian epithelial cells, photo-activatable Green fluorescent protein (GFP)-tagged β-catenin has been observed to re-localize from E-cadherin to the nucleus upon dissociation of AJs[132].

While it is reasonable to hypothesize that some communication exists between these two pools, the molecular details of such connection are not defined. A possible mechanism through which cell-to-cell junctions could regulate the level of the cytoplasmic pool of β-catenin and indirectly the level of nuclear β-catenin has been reported in epithelial cells[133]. In these cells crucial components of the β-catenin phospho-destruction complex, such as axin, APC and GSK3β, are localized to cell-to-cell contacts where cadherins can promote N-terminal phosphorylation of β-catenin leading to its proteasomal degradation. As a consequence, when junctions are tightly organized N-terminal phosphorylation of β-catenin and its turnover are enhanced. The reduced pool of cytoplasmic β-catenin would limit the nuclear distribution of β-catenin and its transcriptional activity. Whether the phospho-destruction complex acts on β-catenin released from cadherin or on an independent pool is not yet clarified. However, such coordination between tightness of junctions and targeted degradation of β-catenin could regulate the cytoplasmic and nuclear amount of β-catenin and allow the cell to mount a transcriptional response, mediated by β-catenin, appropriate to the state of junctions.

2.4.5 Nuclear β-catenin in endothelial cells

In addition to the above general questions, ECs present a peculiarity respect to the classical model of a direct balance (proportion/ratio) between the cytoplasmic and nuclear level of β-catenin. In our experience, ECs can concentrate β-catenin in the nucleus without apparently requiring accumulation of (stabilized) β-catenin in the cytoplasm as generally observed after stimulation with Wnt in other cell types[124]. Constant finding in ECs is that when AJs are poorly organized β-catenin concentrates in the nucleus and regulates transcription. Examples of weak cell-to-cell contacts are ECs in non-confluent layers as during angiogenic responses, models of pathological conditions as after ablation of the *CCM1* gene[117] and the extreme experimental situation of VE-cadherin null ECs[124]. Remarkably, in each of these circumstances, although the total level of β-catenin can decrease, even to extremely low level, as in VE-cadherin null ECs, residual β-catenin concentrates into the nucleus where it is transcriptionally active. The mechanism of such nuclear localization of low total level of β-catenin is not yet defined at the present. Notably, β-catenin lacks nuclear localization sequences[117, 201]. Recently, FoxM1 has been reported to be required for nuclear localization of β-catenin in glioblastoma[134].

When junctions are poorly organized β-catenin induces a transcriptional profile characterized by loss of differentiation markers and acquisition of endothelial-to-mesenchymal transition (EndMT) markers[128] as discussed below.

2.4.6 Endothelial junctions and endothelial differentiation: the case of EndMT

Endothelial-to-mesenchymal transition (EndMT) represents a process of de-differentiation driven by transcriptional reprogramming that targets also the composition and function of cell-to-cell junctions[135, 136]. In the course of this process, the pro-migratory N-

cadherin partially substitutes for VE-cadherin[129]. The so-called cadherin switch, with N-cadherin substituting E-cadherin, is indeed a well-established trait of EMT (epithelial-to-mesenchymal transition) in epithelial cells[135, 137]. Transcriptional repression of E-cadherin is well defined in these cells and similar mechanisms involving Twist, Snai1 and Snai2 operate also in ECs[138]. Classical characteristics of mesenchymal phenotype are: increased proliferation, increased motility, loss of polarity, loss of contact inhibition, expression of mesenchymal markers such as α-SMA and S100a4. However, reorganization of cell-to-cell junctions might also represent a priming event of EndMT. Although the precise relationship between junctional and nuclear β-catenin is poorly defined, as discussed above, β-catenin might represent one of the molecular link(s) in the re-shaping of both junction organization and transcription profile that characterizes the EndMT. Indeed, β-catenin can drive the transcriptional up regulation of EndMT markers and properties also cooperating with the Tgfβ pathway[135].

A physiological example of EndMT takes place during the formation of the heart cushion in the embryo[139]. In this case, not only β-catenin is transcriptionally active in ECs undergoing the transformation, but also it is required for the initiation of the process, that is subsequently reinforced by the activation of ECs by Tgfβ2 produced in the heart tissue. At initial stages of transformation ECs co-express α-smooth muscle actin and the endothelial marker VE-cadherin[139]. Although the cells undergoing such transformation become highly motile, the organization of endothelial cell-to-cell junctions has not been examined in details, in particular it remains to be defined whether the expression of the pro-migratory N-cadherin is increased[129] (**Fig.6** summerize different stages of EndMT).

EndMT has been increasingly studied for its crucial contribution to various pathologies characterized by fibrosis (renal and cardiac fibrosis) as well as to cancer[135, 137]. As far as vascular pathology, EndMT takes place and has a causative role[128] in the Cerebral Cavernous

Malformation (CCM), as it will be discussed later. In this genetic vascular disease, endothelial AJs constitute an early target of the loss-of-function mutations of any of the three *CCM* genes. In the absence of CCM VE-cadherin and β-catenin become highly disorganized and the endothelium loses its barrier properties. Subsequently, N-cadherin substitutes VE-cadherin at junctions, which remain highly disorganized, as a consequence of delocalization of Rap1 and activation of Rho[117, 139, 140]. Reshaping of AJs is accompanied by induction of an array of EndMT markers, among which: CD44, S100a4, Ly6a, Klf4 and Id1 that contribute to the pathological vascular phenotype[128]. If and how disorganization of junctions has a causative role in the transcriptional reshaping and in the initiation of EndMT besides being a target of this process remains to be defined. In addition, EndMT is reinforced by activation of the Tgfβ/Bmp signaling that in *CCM1*-knockout ECs is cell autonomous, through the production of Bmp6[128]. These observations suggest that both β-catenin and Tgfβ/Bmp pathway can be involved in the control of EndMT.

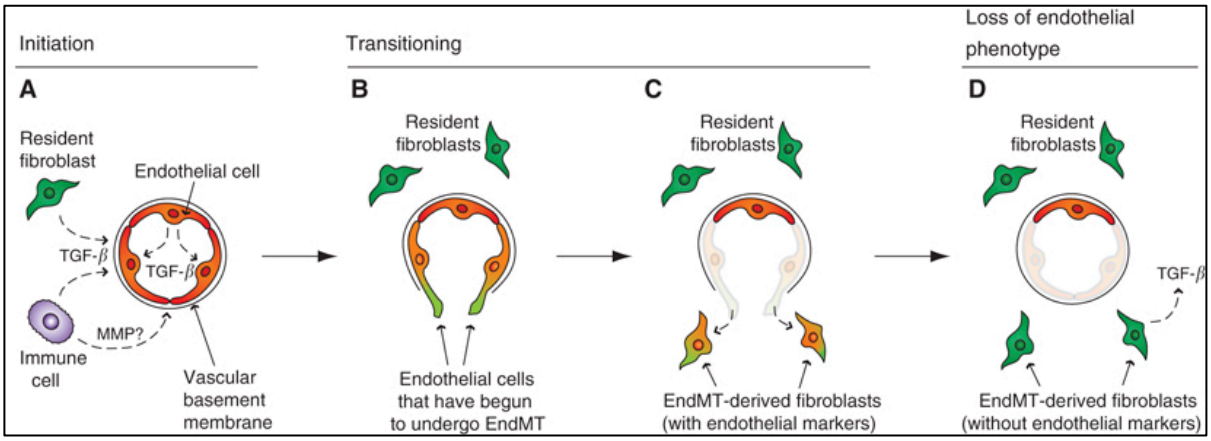

Figure 6. **Stages of endothelial-to-mesenchymal transition (EndMT).** (**A**) Different autocrine and/or paracrine stimuli can initiate EndMT such as the most studied Tgfβ. Possible sources include endothelial cells themselves, resident fibroblasts or immune cells. The vascular basement membrane is likely to be degraded by matrix metalloproteinases (MMPs) derived from local immune cells. (**B**–**C**) Transitioning endothelial cells acquire a migratory phenotype, invade underlying basement membrane and begin to express mesenchymal markers, such as S100a4, while still expressing endothelial markers. (**D**) Cells that have undergone EndMT completely loose their endothelial phenotype and contribute to the local fibroblast population[137].

2.4.7 Endothelial cell-to-cell junctions in the Blood Brain Barrier

Since brain barrier needs to be finely controlled in terms of vessel permeability, the composition and the regulation of endothelial cell-to-cell junctions is crucial for BBB homeostasis. For this reason TJs are particularly abundant and complex in the brain where they explain their important role not only for barrier function but also for the maintenance of cell polarity and for a correct differential distribution of molecules between luminal and abluminal compartments.

One of the main players involved in BBB integrity is Claudin5 as demonstrated by the fact that Claudin5-deficient mice exhibit a size-selective loosening of the BBB[97].

Claudin3 also participates in BBB control of permeability. Wnt3a-[77] or Wnt7a- or Wnt7b-dependent[78] activation of primary brain ECs *in vitro* and *in vivo* increases Claudin3 expression together with other molecules important for BBB maintenance. Consistently, selective loss of Claudin3 was observed in altered cerebral microvessels of human glioblastoma multiforme where permeability control was lost[141]. These findings suggest that the BBB can be manipulated to allow selective diffusion of small molecules

In parallel, Wnt induces stabilization of AJs, with increased localization to junctions of VE-cadherin and β-catenin[77, 78]. As far as AJs, both VE-cadherin and β-catenin appear to be more regularly disposed to cell-to-cell contact in Wnt3a-treated ECs from brain microvessels, however this is not the consequence of the transcriptional activation of these genes. The molecular mechanisms of strengthening of AJs in response to Wnt is not yet defined in ECs, although it might involve regulation of small GTPases[142].

All in all the transcriptional responses elicited by nuclear β-catenin appears to be coordinated to the state of endothelial cell-to-cell junctions. The molecular mechanisms that direct such alternative responses of ECs are still mostly unknown.

3. CEREBRAL CAVERNOUS MALFORMATIONS

Vascular malformations are defined as localized defects associated with abnormal angiogenesis, altered vascular integrity and bleeding. In particular, BBB integrity is crucial for CNS homeostasis and its break down is associated to different pathological conditions[47]. Among numerous pathologies affecting the BBB one of the most relevant is the Cerebral Cavernous Malformation (CCM), also referred as cavernoma or cavernous angioma. CCMs are vascular malformations that occur predominantly in the vasculature of the CNS even if also retina and skin can be interested by this pathology[143]. CCM lesions consist in mulberry-like enlarged clusters of sinusoids (caverns) lined by a thin layer of ECs surrounded by a thick, discontinuous basal membrane. Very few sub-ECs and no intervening parenchyma are features of the altered endothelium[144]. CCM lesions occur in the venous-capillary vascular bed and present low flow sometimes associated with thrombosis and calcifications[143]. The ultra structural analysis of ECs in the lesions revealed poorly developed TJs and AJs and the absence of enwrapping astrocyte end feet. The fragility of the endothelium within the lesions reflects a compromised BBB responsible for vessels leakiness and breaks. Indeed, clinical symptoms include strokes, intracranial hemorrhages, seizures and focal neurogical outcomes depending on the site of lesion[145]. No correlations between lesions development and defined anatomical region localization within CNS have been described. However, a CCM can also remain neurologically silent and it has been estimated that only approximately 60% of patients are symptomatic[146].

3.1 CCM genetics

CCM is a relatively common disease with prevalence in the general population of 1 out of 200 individuals and can occurs both in a sporadic (80% of cases) and familial form (20% of cases), inherited in an autosomal dominant manner with variable penetrance. Sporadic CCM

patients usually develops a single lesion that can be detected through cerebral magnetic resonance imaging, while the familial form presents multiple lesions with a strong association between the number and size of lesions and the age of the patients[146, 147].

In contrast with the sporadic form that it is not hereditated, the familial CCM is usually characterized (90% of familial CCM) by germ line mutations in three different *CCM* genes known as *CCM1/Krit1*, *CCM2/MGC4607/OSM/Malcavernin* and *CCM3/Pdcd10/TFAR15*[146, 147]. Recently a *CCM2* paralog called *CCM2L* was found expressed selectively in ECs during periods of active cardiovascular growth. Anyway, although important for cardiovascular development, there are no evidences of *CCM2L* relevance in the development of the cavernoma[148].

The progress of CCM lesions seems to occur following a 'second hit' mechanism. In this case loss of one allele in all cells (germ line mutation) would be followed in some ECs by a somatic mutation in the other allele (second hit). Anyway the detection of homozygous mutations inside the lesion is not easy and the results, still controversial, open the possibility that other additionally factors potentially specific for the neurovascular environment, could be necessary for the development of the lesions[149]. Animal models, in particular genetically modified mice constitutively knockout for *CCM1, CCM2* or *CCM3,* enforced the 'second hit' hypothesis since they die during embryogenesis due to cardiovascular defects, whereas heterozygous mice are viable and rarely develop CCM lesions[143, 150, 151] as discussed better in the next chapter. Moreover, *CCM1* heterozygous mice only when crossed with error prone background mice such as $p53^{-/-}$[152] or $Msh2^{-/-}$[153] develops vascular malformations.

Mutations in *CCM1* gene account for about 56% of familial CCM, whereas the *CCM2* gene occurs in 33% of the cases. Surprisingly, *CCM3* locus, show mutations only in a low percentage of familial cases (6%), suggesting the existence of, at least, a fourth *CCM* gene[154]. Recently a potentially new *CCM* gene, named '*zona pellucida-like domain containing 1*'

(*ZPLD1*), has been identified even if its functional role in CCM pathology remains to be determined[155]. CCM incidence can vary in certain populations, for example Hispanic populations of Mexican descent appear to be more susceptible to dominantly inherited CCMs (50% of the patients), due to a founder mutation[145].

Several causative mutations within the three *CCM* genes have been described mostly resulting in premature stop codons leading to nonsense-mediated mRNA decay or truncated proteins. *CCM* genes seem to be ubiquitously expressed in human tissues and not restricted to vasculature, suggesting a widespread functional significance even if endothelium is the election site for the disease (see above)[156].

The average age of onset is between the 2nd and 5th decades of life, but symptoms can start in early infancy or in old age. In particular, *CCM3* mutations are associated with a more severe phenotype and earlier age of onset. Indeed, *CCM3* mutations may confer a higher risk for cerebral hemorrhage, particularly during childhood. Additionally, *CCM3* is the most evolutionary conserved among the *CCM* genes (from humans to insects while *CCM1* and *CCM2* are conserved from human to fish).

3.2 Animal models for CCM

Several animal models have been developed to study CCM pathology. Due to its transparency and genetic tractability, significant amount of work has been carried out in zebrafish to determine the functions of the *CCM* genes. Initially two orthologue of *CCM* genes have been studied: *santa* (*san*, the zebrafish orthologue of *CCM1*) and *valentine* (*vtn*, the zebrafish orthologue of *CCM2*). Fishes with loss-of-function mutations in *san* or *vtn* developed dilated, thin-walled vessels that failed to form lumens very reminiscent of human CCM. This phenotype seems to be due to abnormal endothelial cell spreading, a potential mechanistic insight into CCM pathogenesis[157, 158]. Most recently, it has been shown that a

deletion of *pdcd10* (*CCM3* orthologue), which is duplicated in the zebrafish genome, results in the same abnormal phenotype of *san* and *vtn* mutants making the zebrafish the first non-human model organism to link all three *CCM* genes phenotypically[159]. Interesting *san, vtn* and *pdcd10* mutants share a common phenotype with fish lacking *heart of glass* (*heg*). Heg is a single-pass transmembrane protein expressed in the endocardial cells; its mutations in zebrafish lead to a dilated heart phenotype. Despite multiple studies demonstrated that Heg is an important binding partner of CCM1 suggesting a role for it within the CCM complex, mutations in the human orthologue of *HEG1* have not been identified in patients with CCM[160, 161].

Different mice models have been also developed to study the etiology of the pathology, showing a similar widespread expression patterns for *CCM1*, *CCM2* and *CCM3* genes[156]. Although CCM proteins are not endothelial–specific, they seem to have a specific activity in the endothelium. The constitutive and ubiquitous ablation in the mouse of any of the three *CCM* genes determines generalized vascular disorganization and early embryonic lethality (around E10)[140, 143, 150]. Mice with a gobal deletion of *CCM3* die earlier (E8.0 to E8.5) respect to CCM1 and CCM2 KO mice (E9.5). CNS-specificity for vascular lesions appears if gene ablation is induced after birth, using endothelial-restricted KO[128, 143], particularly in the venous bed. *CCM* gene selective deletion in other CNS cell types failed to give a pathological phenotype with the exception of neural-specific deletion of *CCM3*, which recapitulate CCM lesions as described by Louvi et al.[162]. Anyway, what is clear is that the vasculature of the CNS is particularly affected by CCM ablation with development of focal vascular malformations resembling human cavernomas in the brain, cerebellum and retina[163]. Unlike zebrafish, *Heg1*-knockout mice do not phenocopy *CCM* genes deletion[161].

The molecular mechanism of this typical organ specificity remains still to be explained. It might depend either on specific characteristics of the differentiated endothelium in the CNS

or on the persistence of endothelial precursors that could be particularly affected by *CCM* gene mutations[128]. This hypothesis may fit with the observation in the transgenic mice that the number of cavernomas and the rate of their appearance is maximal when gene recombination is induced soon after birth and decreases sharply when recombination is postponed even by few days[143]. In addition, it is described that ECs in the CNS acquire a fully differentiated phenotype early after birth[77].

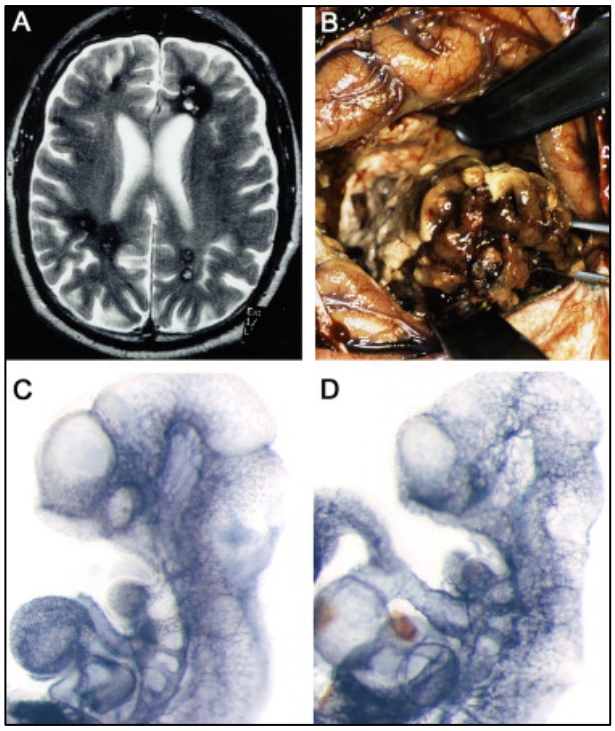

Figure 7. **CCM lesions from a human patient and abnormal vessel remodelling in murine CCM null model.** (**A**) Cerebral MRI showing multiple CCM lesions. (**B**) Surgical view of a CCM lesion. (**C** and **D**) Whole mount PECAM staining of control (**C**) and *CCM2* null mouse embryos (**D**) at E10.5 showing abnormal vascular remodeling in the aorta, outflow tract and head vessels[122].

3.3 CCM proteins function and pathological implications

Although independent loss-of-function mutations of any of the *CCM* genes lead to very similar clinical manifestations, CCM proteins are structurally distinct and share no sequence homology. Anyway, it is known that CCM proteins can associate in a multiprotein complex, at least in *in vitro* overexpression experiments[164, 165]. For instance interaction between CCM1 and

CCM2 protein is necessary for correct protein localization at cell-to-cell contact in ECs[166]. Moreover, overexpression of the newly identified CCM2L protein, able to compete with CCM2 for CCM1 binding but unable to bind to CCM3, mimics CCM2 deletion in EC cultures[167]. By contrast, single CCM proteins can have different intracellular localization and can interact with different unique partners[168]. Actually the role of CCM protein complex in the cavernoma physiopathology is still controversial even if some functions of the CCM proteins seem to require partial complex formation. By the way, either as a part of a complex or as single molecular entities, CCM proteins exert a critical role in ECs processes including cell-to-cell junctions integrity, cell polarity, cytoskeletal remodeling, lumen formation and angiogenesis[168].

Enhanced permeability is a peculiar characteristic of CCM lesions and now it is clear that CCM proteins prevent endothelial barrier dysfunction acting on endothelial junction formation and maintenance and actin remodeling. One of the mechanisms by witch CCM proteins contribute to the control of endothelial permeability is the regulation of small GTPase RhoA and Rho kinase[140, 166]. The consequence of Rho kinase activation by RhoA is the phosphorylation of a series of target proteins involved in stress fiber formation, motility, cell polarization and permeability. Alterations of these processes have been associated to CCM depletion in ECs. In particular endothelial ablation of *CCM1* leads to an increase in number of stress fibers and the inhibition of Rap1-mediated stabilization of cell junctions in a RhoA-dependent mechanism[117]. *CCM2* mutations in ECs share the same phenotype probably due to the role of CCM2 in RhoA degradation[169]. The relationship between CCM3 and RhoA is less clear and many controversial reports have been presented. Anyway, CCM3 is able to associate with the Striatin-interacting phosphatase and kinase (STRIPAK) complex proteins including Protein phosphatases 2a (PP2A) and Ser/Thr kinases of the Germinal center kinase (Gck)III family (Mammalian STE20-like protein kinase (MST)4, Serine/threonine-protein kinase

(STK)25 and STK24)[170], which, in turn, have been seen to activate RhoA inhibitor moesin[171]. In any case the role of STRIPAK in RhoA regulation needs to be further investigated.

CCM proteins are also crucial for the formation and maintenance of EC junctions. As aforementioned, Rap1 is a partner of CCM1, which act as a scaffold protein for a membrane-tethered complex containing VE-cadherin and β-catenin[117, 201]. Indeed, CCM1 deletion induces junction weakening and increase in permeability probably due to Rap1 mis-localization. Lack of CCM2 or CCM3 also increase EC permeability, but while for CCM2 AJs and TJs disruption is a well-established hallmark, in CCM3 mutants the effect on junction stability has been poorly investigated[140, 143].

Due to the critical role of cell-to-cell junctions not only as structural complexes but also in orchestrating intracellular signaling, impaired junctional stability, in the absence of CCMs, leads also to a de-regulation of several signaling pathways. For instance, β-catenin associates with VE-cadherin in resting conditions and it has been reported that knocking down the CCM1 protein in cultured aortic ECs promotes Wnt/β-catenin signaling[117, 201]. However, to date, there are no indications of the relevance of the β-catenin pathway in the formation of these vascular lesions *in vivo*.

In addition to their role in supervisioning to endothelial barrier properties, CCM proteins are also important in angiogenesis. *In vivo* deletion of *CCM* genes has already revealed that CCM proteins are essential for cardiovascular development and differentiation[140, 143, 150]. Indeed, loss of CCM1 results in an excessive angiogenesis due, at least in part, to a deregulation of Delta-Notch pathway[172]. Other angiogenic signaling pathways are affected by the absence of CCM proteins (e.g. Mapk and Akt pathway)[140, 150] but molecular functions have not yet been resolved and some of the data are still controversial.

Recently our group published very important data demonstrating that CCM pathogenesis is driven by EndMT[128]. This process consists, as previously described, in the acquisition of

mesenchymal and stem-cell-like characteristics by the endothelium and normally plays a key role in the heart cushion development[173]. Anyway, the acquisition of EndMT markers by the CNS endothelium results in a loss of endothelial stability and is crucial for the development of CCM. The molecular mechanisms linking CCM proteins to EndMT are still unknown even if one of the mediators of this process is for sure the Tgfβ/Bmp pathway, acting through its downstream effectors Smads to a transcriptional level[128]. However, other important signaling pathway can contribute to this process and some of them are already under investigation.

CCM3 has additional functions compared with CCM1 and CCM2 proteins[174]. For example it has been reported to associate to the Vegfr2 and to stabilize it therefore promoting Vegf signaling[150]. Anyway, most of the recent works pointed their attention on the association of CCM3 with the GckIII, which, in turn, can regulate proliferation, migration and apoptosis in ECs[174]. These studies suggested that the biological role of CCM3 might differ from those of CCM1 and CCM2, which may explain why mutations in *CCM3* gene lead to high risk for hemorrhages, in particular at younger age in human patients.

Despite the huge effort lavished in last years to understand CCM pathophysiology, the reasons behind how and why CCM lesions arise are still a mystery. Since CCM proteins seem to be crucial for EC homeostasis and are implicated in the regulation of several signaling pathways, one of the hypothesis is that loss of *CCM* genes could lead to a hyper-activation of the angiogenic program in CNS endothelium eventually resulting in irregular and unstable vascular structures. However, additional stimuli may be necessary to promote lesion development. Indeed, the endothelial-specific ablation of *CCM* genes in newborn mice (postnatal day 1) leads to the formation of severe multiple vascular malformations while, at least for CCM2, gene deletion in adult mice rarely results in cavernoma formation[143]. This indicates that an active angiogenesis program and environmental factors may promote cavernoma development. In the same direction can be interpreted the finding that *CCM3*

mutation in neuronal cells activates astrocytes and produces vascular lesions that resemble this pathology[162]. This thus reinforces the importance of cellular crosstalk within the neurovascular unit.

Another critical question is why CCM lesions arise predominantly in the CNS endothelium despite the fact that *CCM* genes are widely expressed in different cell types. One possible explanation is that CCM proteins are required to maintain BBB integrity, which is a unique structure that needs fine control of many different signaling pathways essential for its homeostasis.

3.4 Clinical intervention in CCM patients

Nowadays the only clinical option to remove the vascular malformations for CCM patients is neurosurgery. Anyway, often this treatment is not possible due to lesion localization that does not allow operating safely. For this reason most of the hopes for the future reside in the possibility to find new pharmacological treatment. Recently, Whitehead and colleagues proposed statins as pharmacological tool to inhibit RhoA activation and consequently vascular permeability[140]. Similarly Stockton et al. used Fasudil, a direct inhibitor of Rho kinase activity, to reduce lesions in mice models[166]. Another interesting insight is our recent work into the link between CCM and Tgfβ/Bmps pathway and its implication for potential therapeutics[128]. In this work we found that both inhibitors of TβRI (LY-364947), TβRII (LY-2109761) and Bmp (DMH1) are able to reduce CCM lesion extensions in murine models. Anyway, interventional drug treatments are still at the dawn of clinical strategies and much more work is still required in this direction.

For these reasons one of the main aims of this project is to investigate deeply the molecular mechanisms implicated in CCM development in order to find new targets for pharmaceutical intervention that can be developed in clinical trials for patient treatment.

AIM OF THE PROJECT

CCM is a vascular disease, which affects between 0.1 and 0.5% of the population. At the present the molecular mechanisms leading to CCM pathogenesis are still unknown. For this reason nowadays the only therapy available for CCM patients is neurosurgery that often it is not possible due to the CNS-specific location of CCM lesions. Recently, we have demonstrated that there is a physiological process known as EndMT, which is crucial for the development of CCM malformations even if the signaling pathways involved in this process are still largely unexplored.

The main aim of this project is to investigate and to identify new signaling pathways involved in CCM pathogenesis and in particular in EndMT process in order to select targets for novel therapeutic approaches. Taking in consideration this aspect, the second main aim of my thesis is to test in *in vivo* and *in vitro* models molecules potentially active on new identified targets that could be used and developed in future for patients treatment.

MATERIAL AND METHODS

Transgenic mice

Different transgenic mice have been used in this study:

- *CCM3*-flox/flox mice: these mice were generated at TaconicArtemis (Koeln, Germany) on a Black6/C57N background according to the knock-in procedures. In this case two P-lox sequences were inserted that flank exons 4 and 5 of the murine *CCM3* gene. P-lox sites can be targeted by the Cre-recombinase enzyme, which induces recombination and subsequent excision of the nucleotides inserted between P-lox sequences. These mice have been used to control in a time-dependent manner the deletion of *CCM3* gene.
- *Cdh5(PAC)-CreERT2* mice[175]: these mice have been kindly donated by Dr. R.H. Adams, (University of Munster, Munster, Germany) and present the CreERT2 gene under the VE-cadherin (*Cdh5*) promoter. Since VE-cadherin is an endothelial specific gene, the expression of CreERT2 is confined to the endothelial district. CreERT2 gene expresses a fusion protein in which Cre-recombinase has been fused together with the regulatory domain of the estrogen receptor. This domain is able to retain Cre-recombinase into the cytoplasm of ECs in resting conditions. Only after stimulation with estrogen or an analogue such as Tamoxifen CreERT2 fusion protein can dimerize and translocate to the nucleus where it can act on P-lox sites to drive homologous recombination. This model allows the operator to induce Cre-recombinase expression in an endothelial specific fashion just by Tamoxifen administration.
- *BAT-gal* mice[176]: these transgenic mice (kindly donated by Dr. S. Piccolo, Padova, Italy) harbor LacZ reporter gene under β-catenin/TCF consensus sequences. In particular 7 TCF/LEF consensus sequences and a Siamoisis minimal promoter are able

to control bacterial β-galactosidase expression in all cell types. This model allows the operator to monitor the activation of β-catenin transcription signaling *in vivo*.

- *Rosa 26-Enhanced Green Fluorescent Protein (EYFP) (Rosa26EYFP)* mice[177]: these mice (kindly donated by Dr. S. Casola, IFOM, Milan, Italy) express the EYFP gene in the Rosa26 locus. A stop codon flanked by P-lox sequences is present in the EYFP gene. This means that in normal condition EYFP protein is not expressed and only after Cre-recombinase activation the fluorescence protein can be detected in cells. This model is an important tool to monitor the expression of Cre-recombinase and its efficency *in vivo* through the expression of EYFP.

CCM3-flox/flox mice were bred with *Cdh5(PAC)-CreERT2* mice for Tamoxifen-inducible endothelial cell-specific expression of Cre-recombinase and *CCM3* gene recombination. The *CCM3*-flox/flox–Cdh5(PAC)-CreERT2 mice were further bred with BAT-gal mice to monitor the activation of β-catenin transcription signaling, and with *Rosa 26-EYFP* mice to monitor the expression of Cre-recombinase.

Endothelial cell-specific recombination in *CCM3*-flox/flox mice

In order to induce Cre-recombinase activation and *CCM3* recombination *in vivo* Tamoxifen (Sigma) was dissolved in corn oil and 10% ethanol (at 10 mg/ml), and then diluted 1:5 in corn oil before single intragastric administration to dpn 1-2 pups (35 mg/kg body weight) (see[175]). The control wild-type mice included *CCM3*-flox/flox–Cdh5(PAC)-CreERT2–BAT-gal mice treated with the vehicle used to dissolve the Tamoxifen (corn oil plus 2% ethanol), and $CCM3^{+/+}$–Cdh5(PAC)-CreERT2–BAT-gal mice treated with Tamoxifen or treated with the vehicle used to dissolve the Tamoxifen (corn oil plus 2% ethanol).

Mouse genotyping

The following probes were used for the mouse genotyping through genomic PCR: wild-type *CCM3* allele: 5’ GAT AGG AAT TAT TAC TGC CCT TCC 3’, 5’ GAC AAG AAA GCA CTG TTG ACC 3’; deleted *CCM3* gene after recombination induced by Cre recombinase: 5’ GAT AGG AAT TAT TAC TGC CCT TCC 3’, 5’ GCT ACC AAT CAG CTT CTT AGC CC 3’, *Cdh5(PAC)-CreERT2* gene: 5' CCA AAA TTT GCC TGC ATT ACC GGT CGA TGC 3', 5' ATC CAG GTT ACG GAT ATA GT 3'; *BAT-gal* gene: 5' CGG TGA TGG TGC TGC GTT GGA 3', 5' ACC ACC GCA CGA TAG AGA TTC 3'; *Rosa 26 EYFP* gene: 5' GCG AAG AGT TTG TCC TCA ACC 3', 5' GGA GCG GGA GAA ATG GAT ATG 3, 5' AAA GTC GCT CTG AGT TGT TAT 3'.

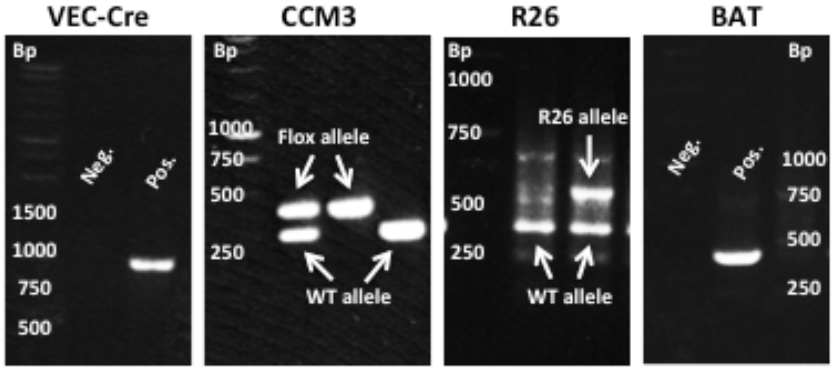

Figure 8. **Mice genotyping.** Representative genomic PCR using specific primer on mouse tail DNA run on a 1% agarose gel.

Immuno-staining for fluorescence microscopy of brain sections and retinas

Brains and eyes from mice pups were fixed in 3% paraformaldehyde immediately after dissection, and this fixing was continued overnight at 4 °C. The retinas were dissected from the eyes just before staining as the whole mount. Fixed brains were embedded in 4% low-melting-point agarose and sectioned along the sagittal axis (150 mm) using a vibratome (1000 Plus, The Vibratome Company, St. Louis, MO, US).

Brain sections and retinas (as whole-mount) were stained as floating samples in 12-well and 96-well plates, respectively. They were blocked overnight at 4 °C in 1% fish-skin gelatin with 0.5% Triton X100 and 5% donkey serum in phosphate-buffered saline (PBS) containing 0.01% thimerosal. The samples were incubated overnight at 4 °C with the primary antibodies diluted in 1% fish-skin gelatin with 0.25% Triton X100 in PBS containing 0.01% thimerosal. Following washing with 0.1% Triton X100 in PBS, the secondary antibodies were added for 4 h at room temperature in 1% fish-skin gelatin with 0.25% Triton X100 in PBS containing 0.01% thimerosal. The incubation with DAPI was in PBS for 4 h, which was followed by several washes in PBS, post-fixating with 3% paraformaldehyde for 5 min at room temperature, and further washes in PBS. The brain sections were mounted in Vectashield with DAPI, and the coverslips fixed with nail varnish; the retinas were mounted in Prolong gold with DAPI.

In vivo treatment with sulindac sulfide and sulindac sulfone

Sulindac sulfide (Sigma-Aldrich) and sulindac sulfone (Sigma-Aldrich) were both dissolved in DMSO and further diluted 1:50 in corn oil. They were administered intragastrically, daily (30 mg/kg body weight), starting one day after the induction of recombination. The control mice were treated in parallel with vehicle only (corn oil plus 2% DMSO). We did not observe either increased bleeding from vascular lesions or mortality in drug-treated *CCM3*-ECKO mice in comparison to vehicle-treated ones.

Assessment of lesion burden

For the classification and counting of lesions, entire brains from 9 dpn littermate pups were sectioned and immunostained for Pecam as described above. Sections were then examined under wide-field fluorescence microscopy (10× and 20×). Lesions were classified as

described in[178] as mulberry (multiple cavernae, group of more than two contiguous cavernae), single caverna (single dilated vessel with maximal diameter accommodating more than 25 red blood cells), or telangiectases, tortuous small vessels with abnormally dilated lumen).

As the sections were 150-mm thick, a correction was applied to the number of mulberry lesions, which can span two sections. Therefore, the number of mulberry lesions was divided by 2.5. The lesions were counted and classified independently by two observers who were blinded to the treatments.

The maximal diameter of the mulberry lesions and single cavernae was used for statistical comparison.

Quantification of endothelial-positive nuclei after immuno-staining for specific antigens

In order to assess the enrichment in malformed vessels of certain nuclear antigens a count of endothelial-positive nuclei has been performed after immune-staining with specific antibodies. Endothelial cell nuclei were counted in 50 random fields at 63× magnification of confocal acquisitions in brain sections from at least 5 *CCM3*-ECKO mice and 5 WT mice at both time points respectively. Nuclei were marked with DAPI. To better define the positive *versus* negative condition, pictures were modified using brightness and contrast Photoshop tool.

Cell cultures

The cell cultures used in this study were:

- ECs derived from brain of *CCM3*-flox/flox adult mice (8-10 weeks old). Briefly, brains were removed from mice and stored in buffer A [150mM NaCl, 5.6 mM KCl, 2.3 $CaCl_2$, 15 mM Hepes, 5% BSA] on ice. The remainder of the isolation took place under aseptic conditions. Each brain was rolled on Whatman 3MM chromatography

blotting paper to remove the meninges. The cortices were dissected away from the surrounding tissue and much of the brain white matter was subsequently removed. The cortices were mashed with forceps and thoroughly triturated, followed by a 1h digestion at 37°C with 0.7 mg/mL type 2 collagenase in buffer A. Afterwards, the enzyme solution was diluted with buffer A and centrifuged at 1000 g for 10 min at 4°C. The pellet was re-suspended in a 25% BSA solution and centrifuged for 20 min at 1000 g and 4°C to obtain a microvessel enriched cell pellet. Then, the pellet was further digested in 1 mg/mL collagenase/dispase 15 min and 39 U/mL Dnase I for 5 min at 37°C. The digested microvessel solution was diluted with buffer A and centrifuged at 700 g and 4°C for 10 min. The pellet was re-suspended and layered over 1% rat tail collagen I (BD 354236) coated plastic plates. A concentration of 4 μg/mL of Puromycin have been used to remove contaminating cell types without any noticeable BMEC growth inhibition. Cells were than infected with an adenovirus encoding GFP (control) or Cre-recombinase at culture day 1 to obtain *CCM3* deletion. These cells have been kept as primary culture for no longer than 2 weeks (see[77]).

- ECs derived from lung of *CCM3*-flox/flox mice. Briefly, lungs were removed from mice finely lungs with scalpels and disaggregate in 15-20 ml D-MEM+5% FBS N.A.+ Collagenase A (1.5 mg/ml, Roche)+ DNase (25 μg/ml, Roche). Suspension was incubate in agitation at 37°C for 2-3 hours and then filtered in 70 μm filters and then centrifuged at 1200 rpm for 5 min. Pellets were re-suspended in complete medium and cells seeded in gelatin 0.1% coated wells (24 wells plate) 30000 cells/wells. After two days endothelial cells were immortalized through retroviral expression of polyoma middle T gene[179] and than infected with an adenovirus encoding GFP (control) or Cre-recombinase to obtain *CCM3* deletion. In this case a continuous cell line has been established and kept in culture for more than 20 passages.

Brain ECs has been cultured in DMEM medium supplemented with 10% North American (NA) fetal bovine serum (FBS) (Hyclone), glutamine (2 mM), penicillin/streptomycin (100 units/l; Sigma) and sodium pyruvate (1 mM). Lung ECs have been cultured in MCDB 131 (GIBCO) medium with 20% FBS (HyClone), glutamine (2 mM; Sigma), penicillin/streptomycin (100 units/l; Sigma), sodium pyruvate (1 mM; Sigma), heparin (100 μg/ml, from porcine intestinal mucosa; Sigma), and EC growth supplement (ECGS) (5 μg/ml, made in our lab from calf brain) (complete culture medium). Starving medium was MCDB 131 (GIBCO) with 1% bovine serum albumin (BSA) (EuroClone), glutamine (2 mM), penicillin/streptomycin (100 units/l) and sodium pyruvate (1mM). All ECs were seeded on flask coated with 0.1% Difco™ gelatin (BD).

293T-Phoenix-Ecotropic packaging cells were provided by IFOM Cell Culture facility and cultured in DMEM medium supplemented with 10 % South American (SA) FBS (Hyclone), glutamine (2 mM) and sodium pyruvate (1 mM). Low passage AD-HEK293 cell line (human embryonic kidney, American Type Culture Collection, Manassas, VA), used for adenoviral production, were provided by IFOM Cell Culture facility and grown in DMEM medium supplemented with 10% FBS NA, glutamine (4 mM), penicillin/streptomycin (100 units/l), and sodium pyruvate (1 mM).

All cells were cultured at 37°C in a humidified atmosphere with 5% CO2.

Drug treatment of cells in culture

Drugs were added to confluent cells for 48 h before the indicated assays. The final concentrations used were: 135 mM sulindac sulfide (Sigma-Aldrich, Calbiochem), 125 mM sulindac sulfone (Sigma-Aldrich), 200 mM silibinin (Sigma-Aldrich), 40 mM curcumin (Sigma-Aldrich), 40 mM resveratrol (Sigma-Aldrich), 0.5 μg/ml Dkk1 (R&D system), 0.5, 2.5 and 5 μM IWP2 and IWP12 (Sigma-Aldrich). As all of these were dissolved in DMSO,

control treatment (vehicle) was 0.1% DMSO final concentration, as for drug treatment. Preliminary experiments to assess the right dose have been carried out before choosing the experimental conditions.

Lentiviral and adenoviral preparations

The following lentiviral constructs were used:

- Lef-ΔβCTA (in HIV3 vector): encoding a stabilized mutant of β-catenin was obtained from C. Brancolini, University of Udine, Udine, Italy[180].
- GFP control (in HIV3 vector)

Packaging plasmids were kindly donated by L. Naldini (HSR-TIGET, San Raffaele Telethon Institute for Gene Therapy, Milan, Italy). Lentiviral vectors were produced according to the following protocol: $4x10^6$ 293T-Phoenix-Ecotropic packaging cells were seeded in $158cm^2$ flasks and on day 1 were transfected with the viral vectors using calcium chloride (6mM) and HBS and incubated overnight with the transfection mix. On day 2 the medium containing the transfection mix was removed and 293T-Phoenix-Ecotropic cells were grown in as little medium as possible to concentrate the virus. On day 3 the medium containing the virus was removed, passed through a 0.45 μm diameter filter, supplemented with Polybrene (8 μg/ml, from IFOM Cell Culture facility) and placed on cells to be infected. The same procedure was repeated on day 4. Infected cells were selected with Puromycin 3 μg/ml. Cells were kept under selection until control non-infected cells died.

The dnTCF4 adenoviral construct was kindly donated by S. J. George (Bristol Heart Institute, Bristol, UK). Infectious viruses were purified and titered using standard techniques. Briefly, for adenovirus production AD-293T cells were infected with 2 pfu/cell in DMEM without serum for 1 h at 37°C. Then, the infection medium was removed and cells were grown

in an appropriate volume of DMEM + 5% horse serum until complete cell lysis is obtained (usually 72h later). The medium containing the viruses was then subjected to 3 freeze-and-thaw cycles in order to destroy all the cells and to set as many virions as possible free. The resulting supernatant was then centrifuged at 3000 rpm for 30 min at +4°C to eliminate the cellular debris, aliquoted and stored at -80°C. For the infection of ECs two consecutive cycles of infection [5h and overnight (O/N)] were performed with MOI of 300 in 1 ml of complete culture medium.

Western blot

Cells in culture have been solubilized to obtain total proteins lysates using Sample Buffer (SB) containing 2% SDS, 5% glycerol 0.05 M Tris-HCl (pH 6.8), 0.004% Bromophenol blue and 5% β-mercaptoethanol. Lysates were incubated for 5 minutes at 100°C to allow protein denaturation and then spinned for 5 min at 13000 rpm to discard cell debris. The supernatants were collected and the concentration of protein was determined using a BCA™ Protein Assay Kit (Pierce) according to manufacturer's instructions. Equal amounts of proteins were loaded on gel and separated by SDS-PAGE, transferred to a Protran Nitrocellulose Hybridization Transfer Membrane 0.2 μm pore size (Whatman) and blocked for 1 h at RT in 1X Tris Buffered Saline Tween (TBST) [150 mM NaCl, 10 mM Tris-HCl (pH 7.4), and 0.05% Tween] containing 5% (w/v) powdered milk. For phospho-protein analysis 5% BSA have been used instead of milk. The membranes were incubated overnight at 4°C with primary antibodies diluted in 1X TBST-5% BSA. Next, membranes were washed 3 times with 1X TBST for 5-10 minutes each and incubated for 45 minutes at RT with HRP-linked secondary antibodies (diluted in 1X TBST-5% BSA). Membranes were rinsed 3 times with TBST for 5-10 minutes each and specific binding was detected by the enhanced chemiluminescence (ECL) system (Amersham Biosciences) using HyperfilmTM (Amersham

Biosciences) or the ChemiDoc gel imaging system (BIORAD). The molecular masses of proteins were estimated relatively to the electrophoretic mobility of co-transferred prestained protein markers, Broad Range (Cell Signalling Technology).

Quantification of western blot bands optic densitometry was performed using ImageJ.

Cell fractionation

Experiments were carried out starting from 2 flasks with 75 cm^2 area of confluent cells for each cell types and all procedures were done in cold room at 4°C and on ice. Cells were washed 2 times with ice-cold PBS and finally collected in 5 ml volume. Lysates were transferred in 15 ml tubes and centrifuged at 5000 RPM for 5 minutes at 4°C. Supernatant were discard and pellet re-suspended in hypotonic buffer [10 mM Hepes, 100 mM KCl, 1.5 mM $MgCl_2$, 0.5 mM DTT] in a volume 3 times the pellet size. Suspensions were homogenized using Dounge homogenizer to induce cell breaks. Cells were transferred in a 15 ml tube and centrifuged at 1000 x g 4°C for 5 minutes. Supernatants representing the cytoplasmic fraction were collected. The pellet containing cells nuclei were washed 3 times with hypotonic buffer and then incubated with nuclear extract buffer [20 mM Hepes, 20 mM NaCl, 420 mM $MgCl_2$, 0.2 mM EDTA, 25% glycerol] 30 minutes 4°C under gently shacking. Nuclei were centrifugated 30 minutes at 15000 x g and supernatants, containing the nuclear fraction, collected. Nuclear extracts were diluted in order to reduce the high concentration of NaCl 1:2.8 (NaCl final concentration=150 mM). Hot SB 4x were added to cell fractions and boiled for 5 minutes. Also the pellet containing cell membranes were lysated with SB to obtain a third fraction. All the buffers contained freshly added protease inhibitor cocktail (IFOM Kitchen Facility). Protein concentration was determined with BCA™ Protein Assay Kit and an equal amount of protein was incubated with either immune antibodies overnight at +4°C as previously described for western blot.

Co-Immunoprecipitation

Cells were grown until confluent and starved overnight. Cells were then washed once with DMEM without serum and incubated with 0.4 mg/ml of dithiobis(succinimidyl)propionate (DSP) (Pierce) for 30 min at 37°C to induce molecules crosslinks. After several washes with ice-cold PBS, cells were lysed in ice-cold modified RadioImmunoPrecipitation Assay (RIPA) buffer (Tris HCl pH 7.5 100 mM, NaCl 150 mM, Deoxycholic acid 1%, SDS 0,1%, CaCl2 2 mM). The protein lysate was precleared with an appropriate volume of Protein G Sepharose 4B (Zymed) for 3 h at +4°C. Then, protein concentration was determined with BCA^{TM} Protein Assay Kit and an equal amount of protein was incubated with either immune antibodies or species- matched control antibodies overnight at +4°C. On the following day immunocomplexes were collected using Protein G Sepharose 4B for 3 h at +4°C. Beads were then washed several times with modified RIPA buffer and boiled in an appropriate volume of SB. Samples were analyzed by standard Western blot analysis as described above.

All the buffers contained freshly added protease inhibitor cocktail (IFOM Kitchen Facility).

Co-Immunoprecipitation for VE-cadherin shown in this work has been performed with two different antibodies against VE-cadherin.

RNA interference

Stealth RNAi Duplexes (Life Technologies) and the correspondent Medium GC Stealth RNAi Control Duplexes (Life Technologies) were used to knockdown VE-cadherin and CCM3. The sequences of the oligonucleotides used were the following: 5'-AGACAGACCCCAAACGUAA-3', 5'-GAAAAUGGCUUGUCGAAUU-3', 5'-AGGGAAACAUCUAUAACGA-3', 5'-CCGCCAACAUCACGGUCAA-3' for VE-cadherin

and 5'-ACUUCACCGAGUCCCUCCUUCGUAU-3', 5'-GGGCACUUAAGAUUCUCAGUAA-3', 5'-GACAAUCAAGGAUAUAGCUAGUGCA-3' for CCM3. Transfection was performed using LipofectAMINE 2000 (Invitrogen) according to the manufacturer's instructions.

Immuno-staining microscopy on cell culture

Immunofluorescence microscopy staining was performed using standard technique. Briefly, cells were fixed and permeabilized for 25 minutes with 1% paraformaldehyde, 0.875% tri-ethanol-ammine with 0.1% triton-100 and 0.1% NP40. Fixed cells were incubated for 1h in a blocking solution (5% BSA in PBS). Cells were then incubated overnight at 4 °C with primary antibodies diluted in blocking buffer. Appropriate secondary antibodies were applied on cells for 45 min at RT and mounted with VECTASHIELD with DAPI (Vector Biolabs).

Samples were observed under an epifluorescence microscope (DMR; Leica) or confocal microscope (Leica) using a 20X, 40X and 63X objectives. Images were processed with Adobe Photoshop using adjustments of brightness and contrast in the preparation of the figures. For comparison purposes, different sample images of the same antigen were acquired under constant acquisition settings.

rt-PCR

RNA extraction was performed with RNeasy kits (74106; Promega) according to the manufacturer's protocol. The RNA (1 μg) was reverse transcribed with random hexamers (High Capacity cDNA Archive kits; Applied Biosystems). The cDNA was amplified with TaqMan gene expression assays (Applied Biosystems) by the IFOM rq-PCR facility. For each sample, the expression levels were determined with the comparative threshold cycle (Ct)

method, and normalized to the housekeeping genes encoding 18S and glyceraldehyde-3-phosphate dehydrogenase (GAPDH). The probes to identify the *CCM3* mRNA transcript were custom designed, as: forward, CGAGTCCCTCCTTCGTATGG; reverse, GCTCTGGCCGCTCAATCA; reporter sequence, CTGATGACGTAGAAGAGTACA.

Probes (Applied Biosystems) that have been validated to recognize the following mouse transcripts in rt-PCR were used: Axin2, Lef1, Myc, Ccnd1, Klf4, Ly6a, S100a4, Cd44, Id1, Nkd1, Cdh5, Bmp2, Bmp6, Tuba1a, Tubb1.

Top/Fop-Flash assay

For the detection of β-catenin-dependent transcription of a reporter target, the Top-Flash plasmid was used (0.3 mg/cm^2 cell culture area), which contains seven Tcf/Lef binding sites that control the transcription of firefly luciferase[181] (kindly donated by Dr. M.P. Cosma, previously at Telethon Institute for Genetics and Medicine, Naples, Italy, now at Centre for Genomic Research, Barcelona, Spain). This was transfected into the ECs from lung using Lipofectamine 2000, according to the manufacturer's instructions (Invitrogen). The pCMV plasmid for constitutive expression of β-galactosidase was co-transfected (0.1 mg/cm^2), for normalization of luciferase expression over transfection efficiency. As the negative control, a Fop-Flash plasmid was used that contained six mutated (i.e., inactive) Tcf/Lef sites upstream of a minimal promoter and the firefly luciferase gene (0.3 mg/cm^2). This was co-transfected with the β-galactosidase plasmid, for normalization, as above. The Dual-Light Reporter Gene assay system (Applied Biosystems) for the combined detection of firefly luciferase and β-galactosidase was used. The cell extraction and detection of chemiluminescence (Glomax 96 microplate luminometer; Promega) was carried out according to the manufacture's instructions.

Affymetrix

Primary ECs have been derived from the brain of *CCM3*-flox/flox mice ten weeks old, put in culture (see cell cultures paragraph) and treated with recombinant Wnt3a (100 ng/ml, Peprotech, 315-20) or Ctr vehicle every 24h and infected with adeno Cre or adeno GFP virus. RNA was extracted and analyzed using Affymetrix GeneChip arrays Gene ST 1.0 covering 29.000 murine genes. For each condition, total RNA from three distinct extractions was used to measure biological variability. In order to identify the modulated genes, an initial filter was applied to select transcripts regulated at least 2 fold and with a statistical p-value below 0.05[182].

Active Rap1 pull-down assay

Active Rap1 pull-down assay was performed using the GST-fused Rap1-binding domain of Ral GDS obtained by transforming *E. coli* strain BL21 with a pGEX-2T-RalGDS-RBD expression vector (kindly donated by Ruggero Pardi, San Raffaele Scientific Institute, Milan, Italy)[183]. The fusion protein was affinity purified on Glutathione-Sepharose 4B beads (GE Healthcare) by standard methods.

Briefly, ECs were lysed by addition of 1 volume of cold 2x RIPA lysis buffer to cell suspension. Lysis was performed at 4°C for 10–30 min. Lysates were clarified by centrifugation at maximal speed in an Eppendorf centrifuge for 10 min at 4°C. Five μg of RalGDS-RBD coupled Glutathione-Sepharose 4B beads (GE Healthcare) were added to the supernatant and incubated at 4°C for 30–90 min with slight agitation. Beads were washed four times in 1x RIPA. After the final wash, Laemmli sample buffer was added to the samples. Next, proteins were fractionated by SDS–PAGE and transferred to Protran Nitrocellulose Hybridization Transfer Membrane 0.2 μm pore size (Whatman).

Densitometric analysis was performed using ImageJ imaging software.

Antibodies and reagents

The following antibodies were used: anti-Pecam (hamster; MAB1398Z, Millipore); anti-β-galactosidase (chicken; ab9361, Abcam); anti-VE-cadherin (rat monoclonal; 550548, BD Biosciences); anti-VE-cadherin (goat; sc-6458, Santa Cruz); anti-active-β-catenin (dephosphorylated on Ser37 or Thr41, mouse monoclonal; clone 8E7 05665, Millipore); anti-total-β-catenin (mouse monoclonal; 610154, BD Bioscience); anti-S100a4 (rabbit; 07-2274, Millipore); anti-Klf4 (goat; AF3158, R&D); anti-CD44 (rat; 553131, BD Biosciences); anti-Id1 (rabbit; sc-488, Santa Cruz); anti-Ly6a (rat; ab51317, Abcam); anti-GFP (rabbit; A-6455, Invitrogen); anti-Podocalyxin (goat; AF1556, R&D); anti-KI67 (rabbit; Ab1667, Abcam); anti-CCM3 (rabbit; 10294-1-AP, Proteintech); anti-α-tubulin (mouse monoclonal; T9026, Sigma); anti-p-Smad1 (Ser463/465) (rabbit; BA3848, Millipore), anti-p-Smad1 (rabbit; 9516, Cell Signaling); anti-Smad1 (rabbit; 6944, Cell Signaling); anti-p-Smad3 (rabbit; 18801, Epitomics); anti-Smad3 (rabbit; 9523, Cell Signaling); anti-p-Lrp6 (Ser1490) (rabbit; 2568, Cell Signaling); anti-Total Lrp6 (rabbit; 3395, Cell Signaling); anti-Vinculin (mouse; V9131, Sigma); anti-Rap1 (rabbit; Sc-65, Santa Cruz); anti-histone H3 (rabbit; ab1791, Abcam); anti-VE-cadherin (rat, Produced in our laboratories, clone BV13), Biotin-conjugated isolectin B4 (Vector Lab), revealed with Alexa555-conjugated streptavidin (Molecular Probes), was also used to identify ECs in retina and brain sections.

The secondary antibodies for immunofluorescence were anti-Alexa448 and anti-Alexa555, and Cy3-conjugated antibodies raised in the donkey against immunoglobulin of the appropriate animal species (Molecular Probes or Jackson Laboratories).

The secondary antibodies for Western blotting were HRP-linked anti-mouse, anti-rat and anti-rabbit antibodies (Cell Signaling), and HRP-linked anti-goat antibodies (Promega).

Recombinant Wnt3a (Peprotech, 315-20) was used to stimulate cells in culture.

Statistical analysis

Non-parametric Wilcoxon signed-rank tests were used to determine the statistical significance of the lesion burdens after the pharmacological treatments *in vivo*. Student's two-tailed non-paired t-tests were used to determine the statistical significance in the other *in vitro* and *in vivo* analyses. The significance level was set at $p < 0.05$. Pearson test was also used for Affymetrix analysis.

RESULTS

Establishment of a mouse model for CCM3 cavernomas

In order to study the role of *CCM3* gene in cerebral cavernous malformations we developed a mouse model that recapitulates the hereditary form of the human pathology. To this aim *CCM3*-flox/flox mice were crossed with *Cdh5(PAC)-CreERT2* mice[77], for Tamoxifen-inducible endothelial-cell-specific expression of Cre-recombinase and *CCM3* gene recombination. *CCM3*-flox/flox–*Cdh5(PAC)-CreERT2* mice were then bred with *Rosa 26-Enhanced Green Fluorescent Protein* (*EYFP*) mice[177] to monitor the expression of Cre-recombinase through the expression of EYFP.

CCM3-ECKO mice (with endothelial-specific-inactivation of *CCM3* gene induced at early postnatal stage) presented evident malformations and hemorrhages (see **Fig.9a** and Materials and methods) in the cerebellum and retina vasculature comparable to CCM vascular lesions in patients. These lesions began to appear three to four days after treatment with Tamoxifen, and they progressively increased in size. Starting from 10 days after Tamoxifen treatment, *CCM3*-ECKO mice die with evident hemorrhagic cerebellum. In the brain, some superficial vascular malformations can also be observed, but most of the lesions can only be detected after sectioning and immunostaining (**Fig.9b, 9c and 9d**). No vascular malformations have been detected in other organs of *CCM3*-ECKO mice. While constitutive endothelial-selective inactivation of *CCM3* is embryonically lethal with general angiogenic defects[150], this is the first report of endothelial-cell-selective inactivation of *CCM3* after birth.

These malformations exclusively develop on the venous side of the vascular network, which can be distinguished morphologically in the retina (**Fig.9b**) and by Endomucin-positive staining (**Fig.9c**), even though Cre recombinase is also active in the arteries as attested by

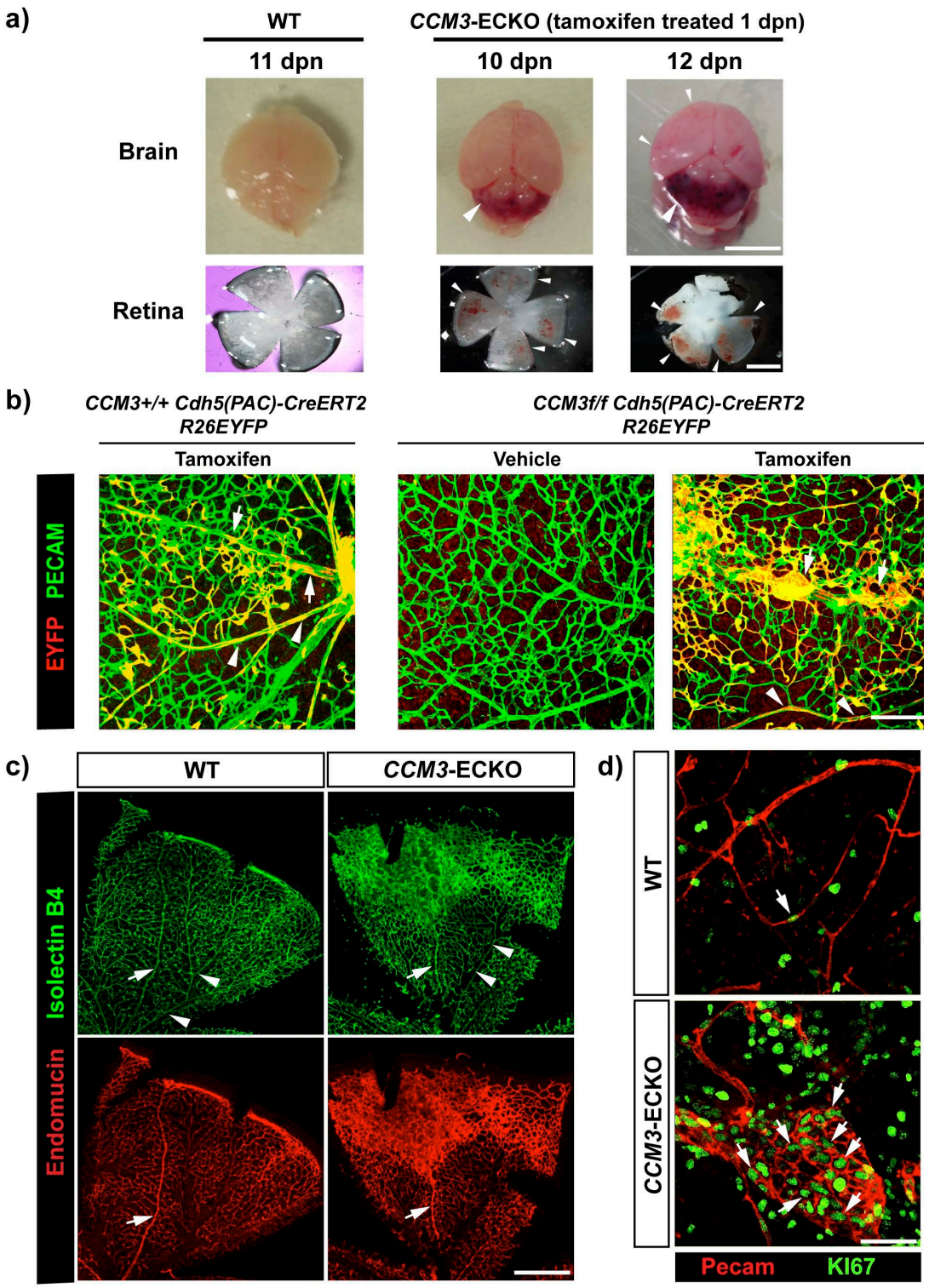

Figure 9. **Establishment of *in vivo* model for endothelial-specific and inducible deletion of *CCM3* gene.** (**a**) The *CCM3*-flox/flox–*Cdh5(PAC)-CreERT2* mice were treated with Tamoxifen (10 mg/kg body weight, as described in Materials and Methods) at 1 dpn to induce endothelial-cell-selective expression of Cre recombinase and recombination of the flox/flox *CCM3* gene (*CCM3*-ECKO mice). The macroscopic appearance following dissection showed evident lesions in the cerebellum and retina (arrowheads). In the brain, some superficial vascular malformations can also be observed (small arrowheads), but most lesions can only be detected after

sectioning and immunostaining, as shown in the main text. Tamoxifen did not induce any phenotype both in *CCM3*-flox/flox–*Cdh5(PAC)* mice negative for *CreERT2*, that did not express Cre recombinase, and in the heterozygous *CCM3*-flox/$^{+}$–*Cdh5(PAC)-CreERT2* mice. The WT mice were *CCM3*$^{+}$/$^{+}$–*Cdh5(PAC)-CreERT2* mice treated with Tamoxifen. *CCM3-flox/flox–Cdh5(PAC)-CreERT2* mice treated with the vehicle used to dissolve Tamoxifen also showed a WT phenotype. Scale bar, 1cm. (**b**) *CCM3*-flox/flox–*Cdh5(PAC)-CreERT2* mice were bred with *Rosa 26-Enhanced Green Fluorescent Protein* (*EYFP*) mice (see Materials and Methods), to monitor the expression of Cre-recombinase through the expression of EYFP. In vessels of the retina from *CCM3*$^{+/+}$–*Cdh5(PAC)-CreERT2–R26-EYFP* mice and *CCM3*-flox/flox–*Cdh5(PAC)-CreERT2–R26-EYFP* (*CCM3*-ECKO) mice, Cre-induced recombination (with Tamoxifen treatment, as above) is indicated by the expression of the reporter gene EYFP. This was frequent in arteries (arrowheads), veins (arrows) and microvessels of both of these mouse models, and was seen as extensive co-localization (yellow) of EYFP (red) and Pecam (green, marker of endothelial cells) labeling. The *CCM3* transcript was reduced by more than 80%, as assessed by rt-PCR in freshly isolated brain microvessels of *CCM3*-ECKO pups, in comparison to the vehicle-treated WT mice. Scale bar, 200 μm. **c.** In the retina of the *CCM3*-flox/flox–*Cdh5(PAC)-CreERT2* (*CCM3*-ECKO) mice, malformations only developed on the venous side of the vascular network, which can be distinguished morphologically in the retina (as in **b**) and by Endomucin-positive staining (red, arrows). Arrowheads indicate arterial vessels, which are Endomucin negative and Isolectin B4 positive (endothelial marker, green). Scale bar, 700 μm. **d**) Higher magnification of brain vessels (red) in WT and *CCM3*-ECKO mice. ECs in the lesions present high number of KI67 positive nuclei (green) indicating an active proliferative state of these cells compared to WT. Scale bar 30 μM. In (**b, c** and **d**) retinas from 9 dpn littermate mouse pups are shown.

EYFP expression (**Fig.9b**). The efficiency of Cre recombinase activation was also assessed by rt-PCR in freshly isolated brain microvessels of *CCM3*-ECKO pups where *CCM3* transcript was reduced by more than 80%, in comparison to the vehicle-treated WT mice. A similar venous-specific defect has been observed after endothelial-specific ablation of *CCM1*[128].

The malformations in *CCM3*-ECKO mice appear both as abnormally enlarged vessels growing on multiple layers and clusters of vascular sacs characterized by a huge lumen. ECs lining the malformations are highly proliferative (**Fig.9d**). Tamoxifen did not induce any phenotype both in *CCM3*-flox/flox–*Cdh5(PAC)* mice negative for *CreERT2*, that did not express Cre recombinase, and in the heterozygous *CCM3*-flox/$^{+}$–*Cdh5(PAC)-CreERT2* mice. The WT mice were *CCM3*$^{+}$/$^{+}$–*Cdh5(PAC)-CreERT2* mice treated with Tamoxifen. *CCM3*-

flox/flox–Cdh5(PAC)-CreERT2 mice treated with the vehicle used to dissolve Tamoxifen also showed a WT phenotype.

As *CCM3*-ECKO mice develop vascular malformations in the central nervous system this model provides a tool for testing pharmacological treatments as described below.

Tgfβ/Bmp pathway is hyper-activated in vivo in endothelial cells of endothelial-cell-specific CCM3-knockout mice only in late stage vascular malformations

In a previous work[128] we demonstrated that CCM lesions develop through an endothelial-to-mesenchymal transition (EndMT) mechanism and that Tgfβ/Bmp pathway significantly contributes to this process. In order to confirm this data also in *CCM3*-ECKO mice we analyzed the phosphorylation state of the Tgfβ/Bmp downstream effector Smad1. Therefore, we performed immunostaining for phospho-Smad1 on *CCM3*-ECKO brains at day post natal nine (9 dpn) when vascular malformations are fully established. In addition, we also investigated CCM lesions at a very early stage that is 3 dpn, in order to assess if the phosphorylation of Smad1 is an early event in CCM progression. Interestingly, we found that, at variance with the late stage (9 dpn) where p-Smad1 staining is significantly increased in the nuclei of ECs lining the vascular malformations, very few endothelial nuclei are positive for p-Smad1 at 3 dpn in comparison to WT vessels (**Fig.10a upper panel, 10b and 10c**). Moreover, we observed that in 9 dpn *CCM3*-ECKO mice only lesions larger than 50 μm (main diameter), which likely developed earlier, express p-Smad1 and that this expression is even more pronounced in the largest lesions (**Fig.11a upper panel and 11b**). Very similar data were obtained using antibody against p-Smad3 (data not shown).

Noteworthy, we also confirmed that EndMT markers expression is up regulated in ECs lining CCM3 lesions starting from 3 dpn in comparison with WT vessels (**Fig.22**) as better described later.

These findings led us to hypothesize that other signaling pathways could be involved in the initiation of vascular lesions. In particular, due to the crucial contribute of the Wnt/β-catenin pathway in the physiology of the BBB, in angiogenesis and in EndMT[74, 76, 139], we investigated the role of this signaling cascade in CCM.

β-catenin-mediated transcription is enhanced in vivo in endothelial cells of endothelial cell-specific CCM3-knockout mice in very early stage vascular malformations

We crossed *CCM3*-flox/flox–*Cdh5(PAC)-CreERT2-R26(EYFP)* mice with *BAT-gal* mice[176], which show β-catenin-activated expression of the nuclear β-galactosidase *(*β-*gal*) reporter gene (see Materials and Methods). In this case β-galactosidase is expressed only in cells in which Wnt/β-catenin pathway is active and could be detected through immunofluorescence using specific antibodies. When we analyzed mice at 3 and 9 dpn we found that β-catenin-dependent transcription of the nuclear *β-gal* reporter gene is highly increased in ECs of brain vessels of the newborn *CCM3*-ECKO, in comparison to matched control animals at both ages **(Fig.10a lower panel, 10b and 10c)**. The percentage of β-gal-positive nuclei is even higher at 3 dpn in comparison to control and this indicates that it is likely to be a very precocious event in the development of the lesions. In contrast with p-Smad1 staining, β-gal staining is present in lesions of any size in 9 dpn *CCM3*-ECKO pups as illustrated in **Fig.11a (lower panel) and 11b**. The quantification by random-field counting using Podocalyxin labeling of ECs showed that small lesions in *CCM3*-ECKO brains have almost 50% β-gal-positive nuclei and that this proportion tends to decrease in larger lesions even if it remains significantly higher in comparison to WT control vessels.

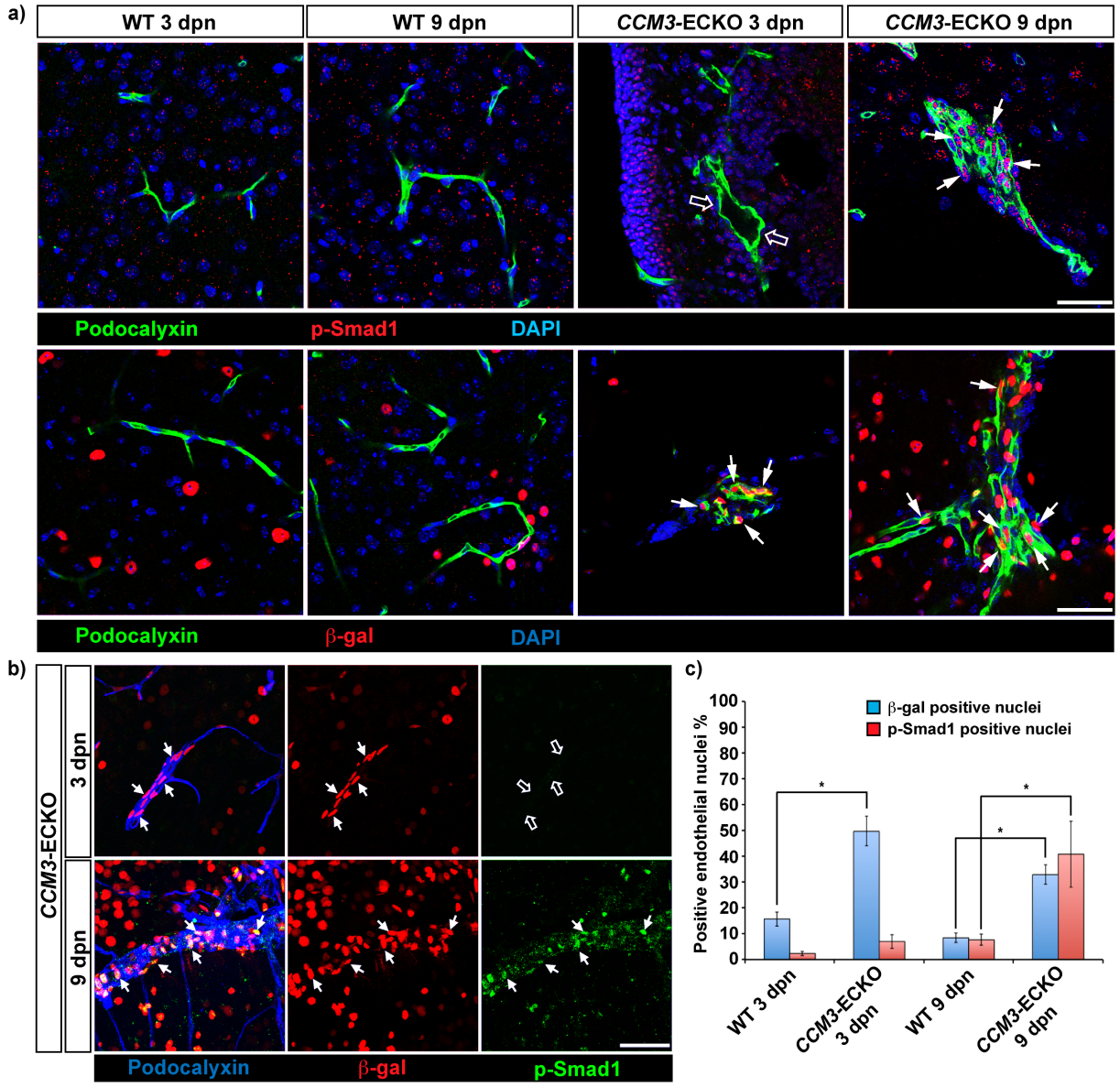

***Figure 10*. Endothelial cells in brain vessels of *CCM3*-ECKO mice show hyper-activation of Tgfβ/Bmp signaling and enhanced β-catenin transcription activity respectively at distinct stages of vascular malformation development.** Representative immunostaining of brain sections (**a, b**) from WT and *CCM3*-ECKO mice at 3 dpn and 9 dpn. (**a**) Upper panel shows p-Smad1 (Ser463/465) expression (red) as a marker of Tgfβ/Bmp active signaling in Podocalyxin-positive (endothelial) cells (green), while lower panel shows β-gal expression (red), as a gene reporter of β-catenin transcription activity in Podocalyxin-positive cells (green). In (**a**) nuclei were stained with DAPI (blue). Arrows, p-Smad1 or β-gal-positive nuclei; empty arrows, p-Smad1 negative nuclei. (**b**) Co-staining of β-gal (red) and p-Smad1 (green) in 3 dpn and 9 dpn brain sections of *CCM3*-ECKO mice. (**c**) Endothelial cell nuclei were counted in 50 random fields at 63× magnification in brain sections from 5 *CCM3*-ECKO mice and 5 WT mice at both time points respectively (see Materials and Methods). β-gal-positive nuclei in brain endothelial cells were more abundant both at 3 dpn and 9 dpn in *CCM3*-ECKO mice than WT mice. p-Smad1 expression is significantly enhanced in endothelial cells in *CCM3*-ECKO mice at 9 dpn in comparison to WT mice but not at 3 dpn. (**a**) and (**b**) Scale bars, 50 μm. (**c**) *, $p<0.05$, t-test.

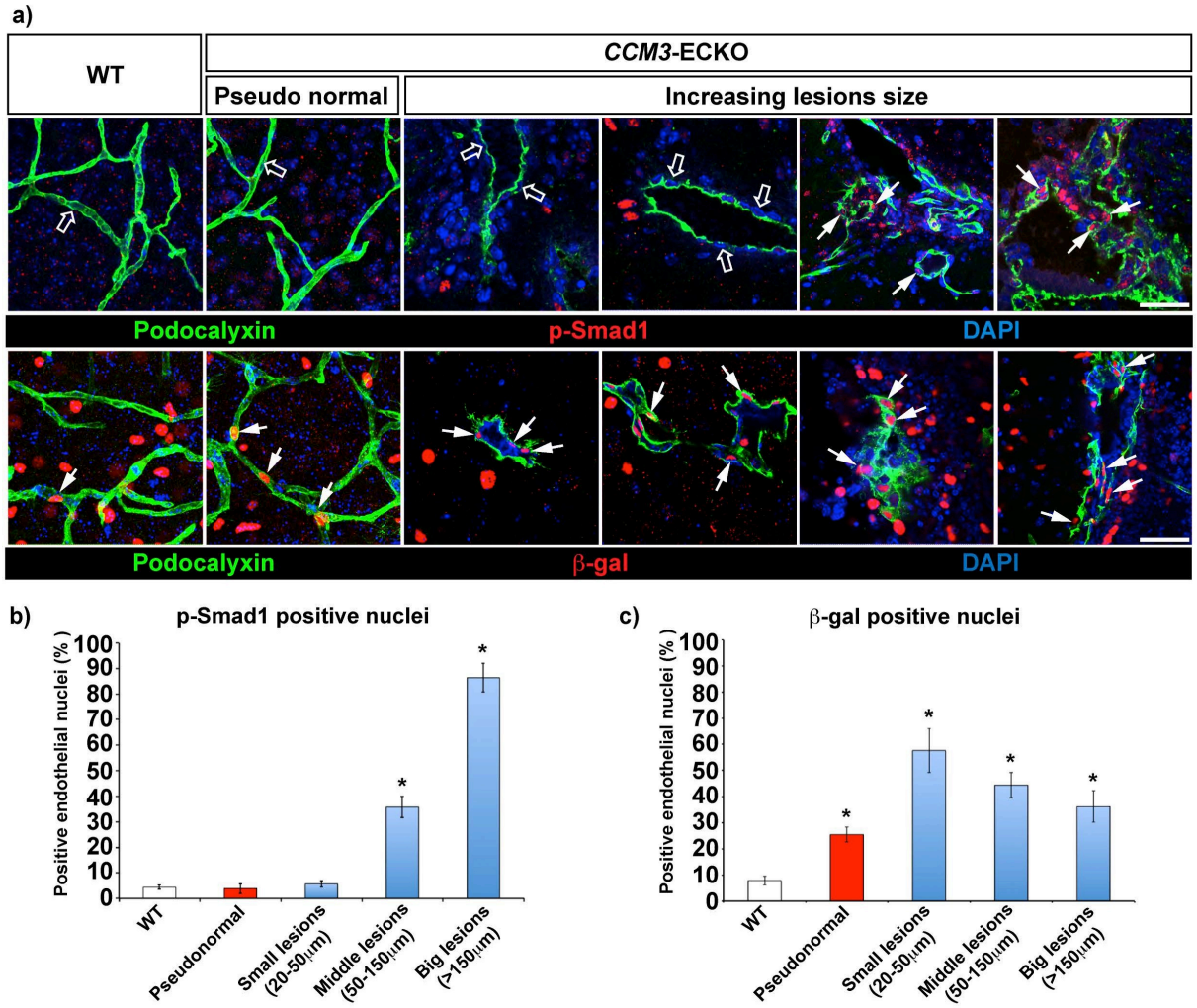

Figure 11. **Tgfβ/Bmp signaling is hyper-activated only in endothelial cells of large lesions while β-catenin-mediated transcription is enhanced in endothelial cells of any size of lesions and in pseudonormal vessels in the brain of *CCM3*-ECKO mice.** Representative immune-staining of brain sections (**a**) from WT and *CCM3*-ECKO mice at 9 dpn. Upper panel shows p-Smad1 (Ser463/465) (red) expression in Podocalyxin-positive (endothelial) cells (green) while lower panel shows β-gal expression (red) in Podocalyxin-positive cells (green). Nuclei were stained with DAPI (blue). Pseudo-normal vessels of *CCM3*-ECKO mice are shown as well as vascular lesions of increasing size (from left to right). Arrows, p-Smad1 or β-gal-positive nuclei; empty arrows, p-Smad1 negative nuclei. Scale bars, 50 μm. (**b)** and (**c**) p-Smad1 and β-gal-positive endothelial cell nuclei were counted in 50 random fields at 63× magnification from 5 *CCM3*-ECKO mice and 5 WT mice (see Materials and Methods). *, $p<0.05$, t-test.

Interestingly, also pseudo-normal vessels in *CCM3*-ECKO mice showed a higher percentage of β-gal-positive nuclei in comparison to WT.

Altogether these data led us to hypothesize that Tgfβ/Bmp pathway could be important for the progression of the lesions and the development of the pathology, but likely Wnt/β-catenin pathway could play an important role in the very initial steps of the lesion establishment.

CCM3 gene ablation induces β-catenin nuclear localization in endothelial cells in culture

In order to better study the role of Wnt/β-catenin signaling in CCM we used different *in vitro* models. In particular we isolated ECs from the brain of the *CCM3*-flox/flox mice (**Fig.12a**, WT, primary culture) and we induced *CCM3* gene recombination *in vitro* (*CCM3*-knockout brain endothelial cells) (**Fig. 12a**, KO, primary culture) using an adenoviral vector expressing Cre recombinase (see Materials and Methods). After recombination *CCM3*-knockout cells showed high level of active β-catenin in the nucleus (i.e., dephosphorylated on Ser37 and Thr41[184]) (**Fig.12a**). This effect paralleled strong alterations to the AJ organization that was seen as delocalization from the junctions of active β-catenin and VE-cadherin (**Fig.12a**).

Due to limitations in both the supply of freshly isolated ECs from the brain and their extremely limited mitotic index after the first *in vitro* passage, detailed analyses of their β-catenin nuclear distribution and signaling were not possible. We therefore established cultured endothelial cell lines where *CCM3* was recombined *in vitro* as above (*CCM3*-knockout endothelial cell line) (see Materials and Methods). In these *CCM3*-knockout endothelial cell line, we confirmed enhanced nuclear localization of β-catenin both by immunofluorescence (**Fig.12b,** KO endothelial cell line) and cell fractionation (**Fig.13**).

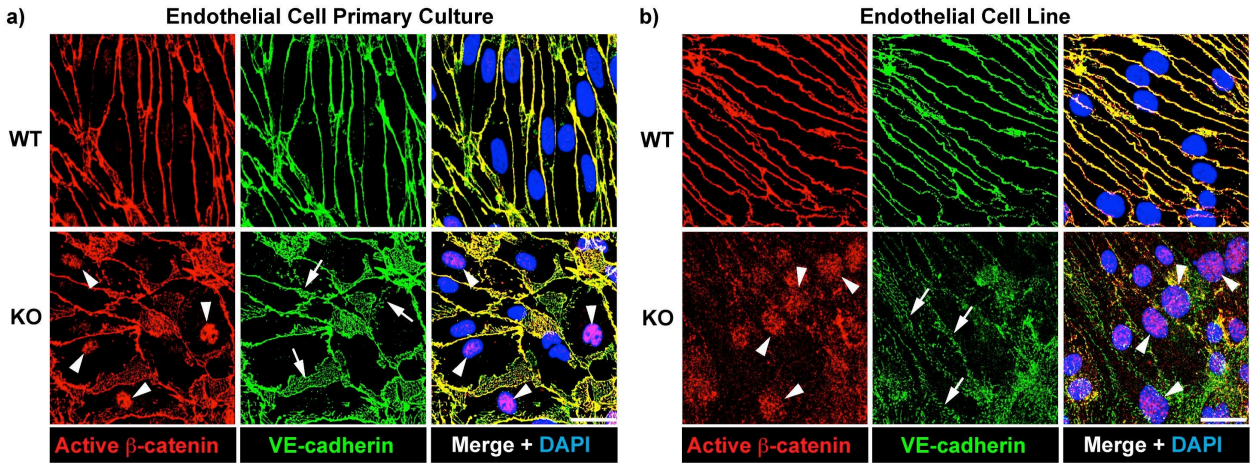

***Figure 12. CCM3* KO endothelial cells in culture show delocalization of active β-catenin from cell-cell junctions and its concentration into the nucleus.** Representative immunostaining of WT and *CCM3*-knockout (KO) endothelial cells for active β-catenin (dephosphorylated on Ser37 and Thr41) (red) and VE-cadherin (green) in primary culture (**a**) and cell line (**b**). Nuclei were stained with DAPI (blue). Arrowheads, β-catenin-positive nuclei. Arrows indicates dismantled cell-to-cell junctions. In these *CCM3*-knockout endothelial cells, the *CCM3* transcript was reduced by 70% to 90% (primary culture) and not detectable (line) by rtPCR. Scale bar, 20 μm.

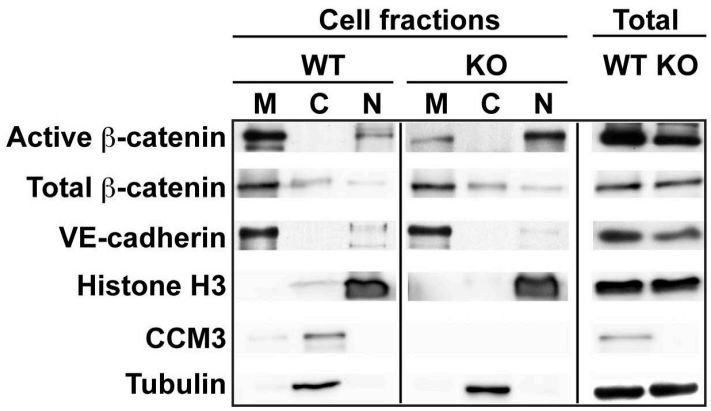

***Figure 13.* β-catenin is concentrated in the nuclear fraction of *CCM3* null endothelial cells.** Representative cell fractionation and Western blotting of membrane (M), cytoplasm (C) and nucleus (N) compartments of WT and *CCM3*-knockout (KO) endothelial cell line. Total, membrane and nucleus active β-catenin were decreased by 34% to 42%, decreased by 58% to 75%, and increased by 51% to 66%, respectively (ImageJ bands quantification); active β-catenin was almost undetectable in the cytoplasm of *CCM3*-knockout *versus* WT endothelial cells. In WT, CCM3 was enriched in the cytoplasm; in the *CCM3*-knockout, no CCM3 was detected by Western blotting. Tubulin and Histone H3 accumulation respectively in the cytoplasm and nuclei confirm a good level of separation of cell fractions. 8 μg proteins per lane were loaded.

CCM3 gene ablation activates β-catenin-driven transcription in endothelial cells in culture

Since nuclear β-catenin is able to interact with Tcf/Lef transcription factors and to drive target gene transcription we investigated whether *CCM3*-knockout cells presented an increased β-catenin-mediated transcription activity. To do this Tcf/Lef-dependent transcription of the exogenous *luciferase* gene was measured in Top/Fop Flash reporter assays. We found that in *CCM3*-knockout endothelial cell line, the transcription activity of β-catenin was significantly increased by 2.7-fold, compared to control WT cells (±0.6 SD; $p < 0.01$) **(Fig.14)**.

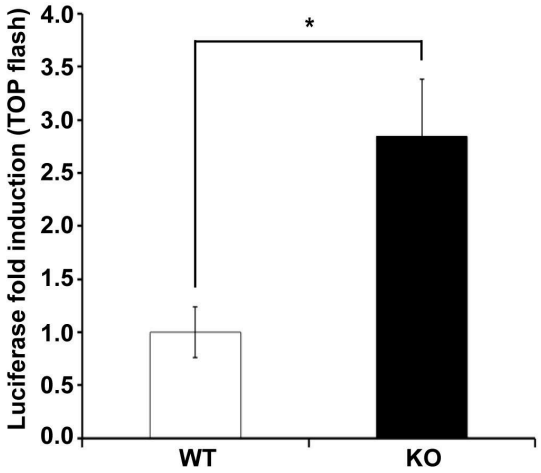

Figure 14. **β-catenin-Tcf/Lef signaling is up regulated in *CCM3*-knockout endothelial cells in culture.** Activation of β-catenin-Tcf4/Lef-dependent transcription in *CCM3*-knockout (KO) and WT cells was assessed using a luciferase reporter gene in the Top/Fop Flash assay (see Materials and Methods for details). The ratio between Top-flash and Fop-flash values normalized over transfection efficiency (β-galactosidase activity) is shown as fold change in comparison to the ratio in WT (Luciferase fold induction). *, $p<0.05$, t-test. Data are means of three independent experiments.

Furthermore, the expression of some typical endogenous targets of β-catenin transcription activity was increased in *CCM3*-knockout endothelial cell line (i.e., *Axin2*, *Nkd1*, *Lef1*, *Ccnd1*[57]) and, importantly, it was inhibited by *in vitro* infection with the adeno viral vector coding for a dominant-negative Tcf4 (dnTCF4) [123] (**Fig.15a**). In parallel we validated this data also in primary ECs where we found that transcription of β-catenin target genes is also enhanced (**Fig.15b**). In these experiments we used as markers for β-catenin transcription

activity *Naked1* gene *(Nkd1)* instead of *Axin2* since it was more sensible to β-catenin activation in this system. These data demonstrated that *CCM3* ablation *in vitro* in ECs lead to β-catenin accumulation into the nucleus where it can directly mediate, in association to Tcf4 transcription factor, the transcriptions of canonical target genes.

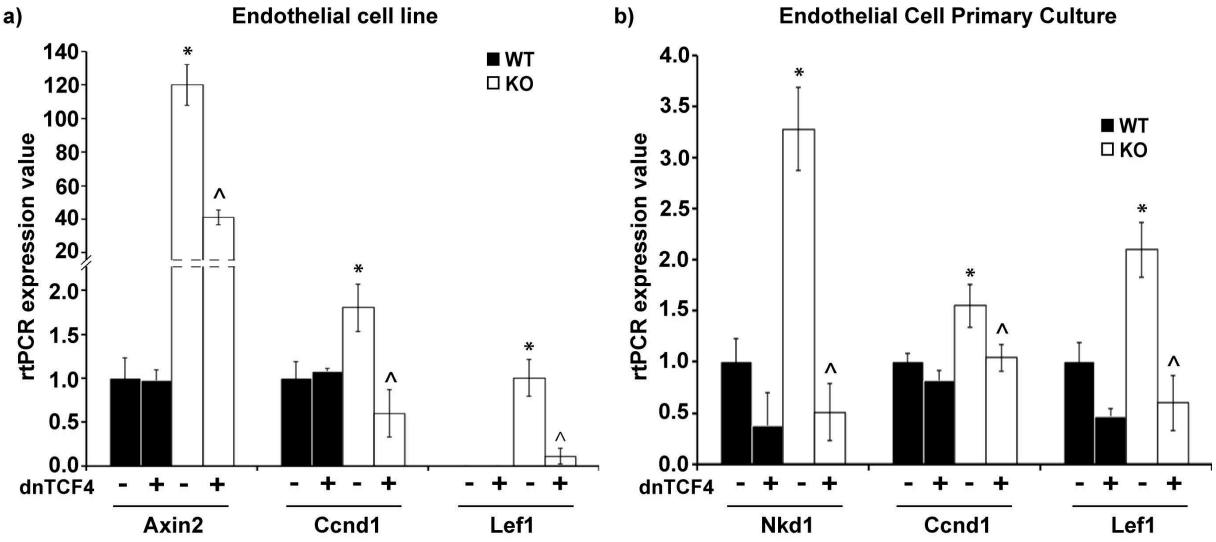

Figure 15. **β-catenin canonical target genes are up regulated in *CCM3* null endothelial cells in culture.** Quantification of typical β-catenin transcription targets without (-) and with (+) expression of dominant-negative Tcf4 (dnTCF4), in WT and *CCM3*-knockout (KO) primary endothelial culture (**a**) and endothelial cell line (**b**). Data are means (±SD) of triplicate rt-PCR assays from three independent experiments. Tubulin transcripts (α, β), which are not targets of β-catenin, were not modified by dominant-negative Tcf4 (data not shown). *, $p<0.05$ for *CCM3*-knockout *versus* control (WT). ^, $p<0.05$ for *CCM3*-knockout plus dominant-negative Tcf4 *versus* *CCM3*-knockout plus GFP (t-test).

β-catenin regulates EndMT in endothelial cells culture

Since we previously demonstrated that endothelial-to-mesenchymal transition (EndMT) is a crucial process for CCM pathophysiology that occurs upon the loss of *CCM1* gene[128], we analyzed the expression of genes related both to acquisition/maintenance of endothelial progenitor phenotype[185] and EndMT[135] in our models taking in consideration that β-catenin transcription signaling has been shown to regulate the processes of differentiation and epithelial-to-mesenchymal transition (EMT) in other cell types[186, 187]as well as EndMT in heart cushion formation[139]. Transcription of *Klf4*[188], *Ly6a*[189], *S100a4*[190] and *Id1*[191] (referred as EndMT markers) were found to be significantly enhanced in *CCM3*-knockout ECs as compared to control cells (**Fig.16a and 16b**). In addition, these increases were dependent on β-catenin transcription activity, as they were inhibited by dominant-negative Tcf4 (**Fig.16a and 16b**). The enhanced transcription of these genes also corresponded to their increased protein expression (**Fig.32**).

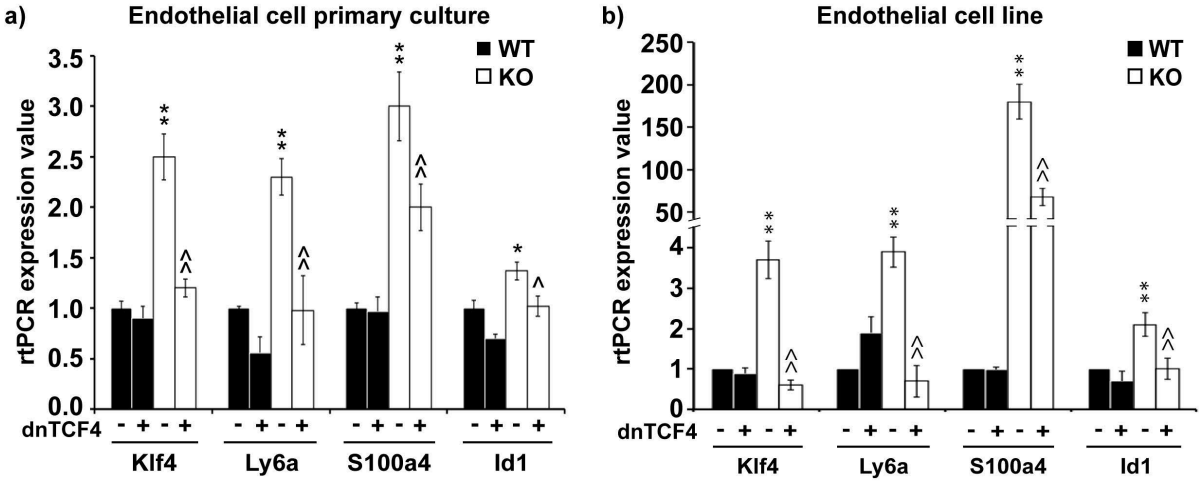

Figure 16. **Nuclear β-catenin activates the transcription of EndMT target genes in *CCM3* null endothelial cells in culture.** Quantification of dominant-negative Tcf4 (dnTCF4) inhibition of transcription of β-catenin target genes *Klf4, Ly6a, S100a4* and *Id1* in WT and *CCM3*-knockout (KO) brain endothelial cells in primary culture (**a)** and endothelial cell line (**b**) by rt-PCR 48h after adenovirus infection. *, $p<0.05$; **, $p<0.01$(t-test) for the comparison *CCM3*-knockout *versus* WT under basal conditions. ^, $p<0.05$; ^^, $p<0.01$ (t-test) for the comparison *CCM3*-knockout plus dominant-negative Tcf4 *versus CCM3*-knockout plus GFP (-). Data are means of three independent experiments.

In addition, WT ECs expressing a constitutive active form of β-catenin, Lef-ΔβCTA[180], after lentiviral infection show higher levels of β-catenin target genes such as *Axin2* and *Nkd1* and of EndMT markers *Id1*, *S100a4* and *Ly6a* in comparison to control cells infected with the vehicle bearing GFP (Ctr) (**Fig.17**). Although far from being conclusive, these data suggest that β-catenin could be directly implicated in the regulation of EndMT genes in ECs. Thus, abrogation of *CCM3* expression in ECs leads to an increase in β-catenin transcription activity and target gene expression and to an increas in EndMT markers gene expression *in vitro*.

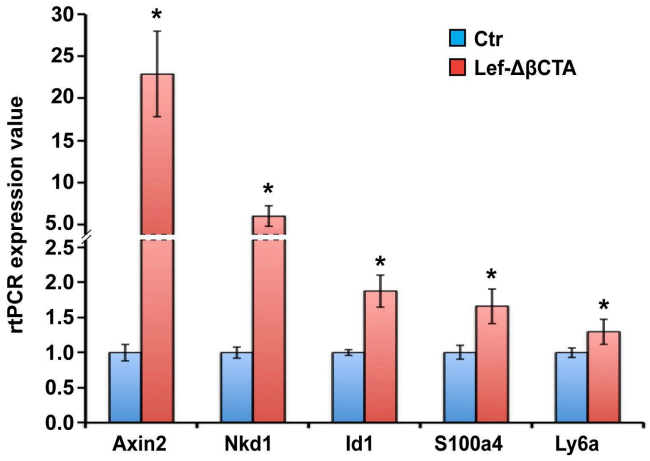

Figure 17. **Constitutive active nuclear β-catenin transcriptionally activates EndMT target genes in endothelial cells in culture.** Quantification of *Klf4, Ly6a, S100a4* and *Id1* transcripts by rt-PCR, in WT endothelial cell line 2 weeks after infection with a lentivirus vector expressing a constitutive active nuclear β-catenin (Lef-ΔβCTA). *, $p < 0.05$ (t-test). Data are means of three independent experiments.

Down regulation of CCM3 transcript after siRNA enhances β-catenin-mediated transcription and the expression of EndMT genes

We also transiently down regulated *CCM3* expression using siRNA and analyzed the time course of activation of β-catenin signaling. We found that at early time point (24h after siRNA transfection with *CCM3* transcript already decreased by more than 80%), (**Fig.18**) β-catenin signaling is up regulated, as indicated by increased *Axin2* transcript (**Fig.18**) and by

nuclear β-catenin accumulation (**Fig.19**) in comparison to control (not-targeting siRNA transfected cells). In addition, *CCM3* down regulation is accompanied by a significant increase of EndMT marker expression (which is delayed at 48h in comparison to *Axin2*) (**Fig.18**) and by a progressive disorganization of cell-to-cell junctions (already detectable after 24h) (**Fig.19**).

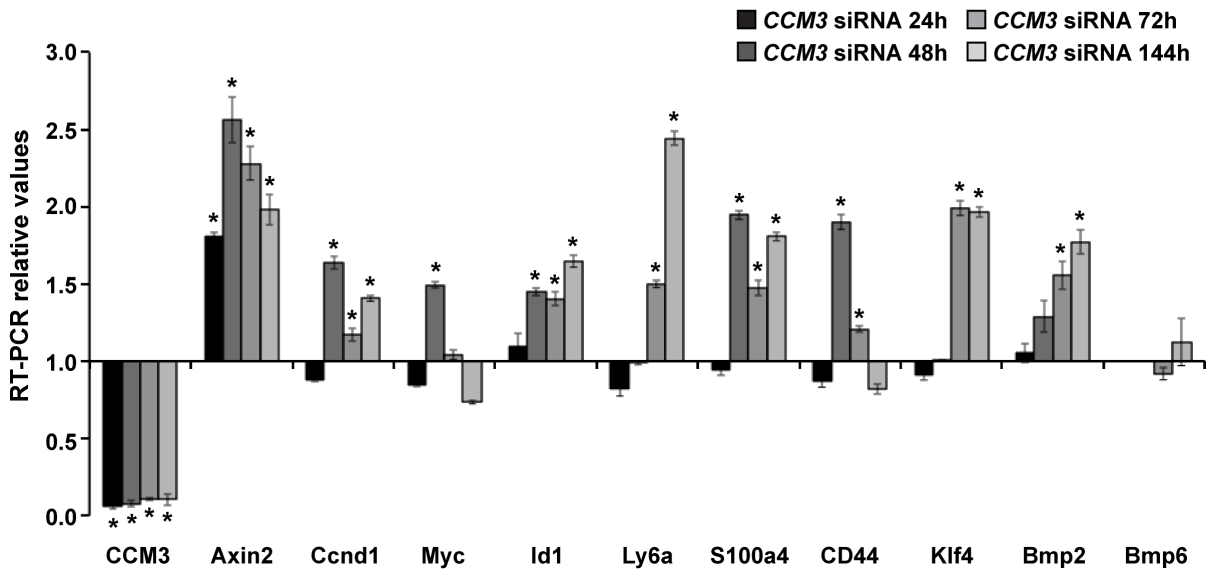

Figure 18. **Acute down regulation of *CCM3* transcript induces transcription activation of β-catenin target genes and Bmp2 with distinct kinetics in endothelial cells in culture.** Acute down regulation of *CCM3* transcript through siRNA (>80%) in WT endothelial cells correlates with transcription activation of β-catenin target genes (*Axin2, Myc, Ccnd1*), EndMT markers (*Id1, Ly6a, S100a4, Klf4, CD44*) and Bmp2 although with different kinetics as discussed in the text. Transcripts were analyzed by rt-PCR 24h, 48h, 72h after siRNA transfection while cells at 144h time point had a second round of siRNA transfection 72h after the first one. Every time point has been compared with time-matched control. Controls were treated with negative (not-targeting) siRNA. *, $p<0.05$, t-test. Data are means of three independent experiments.

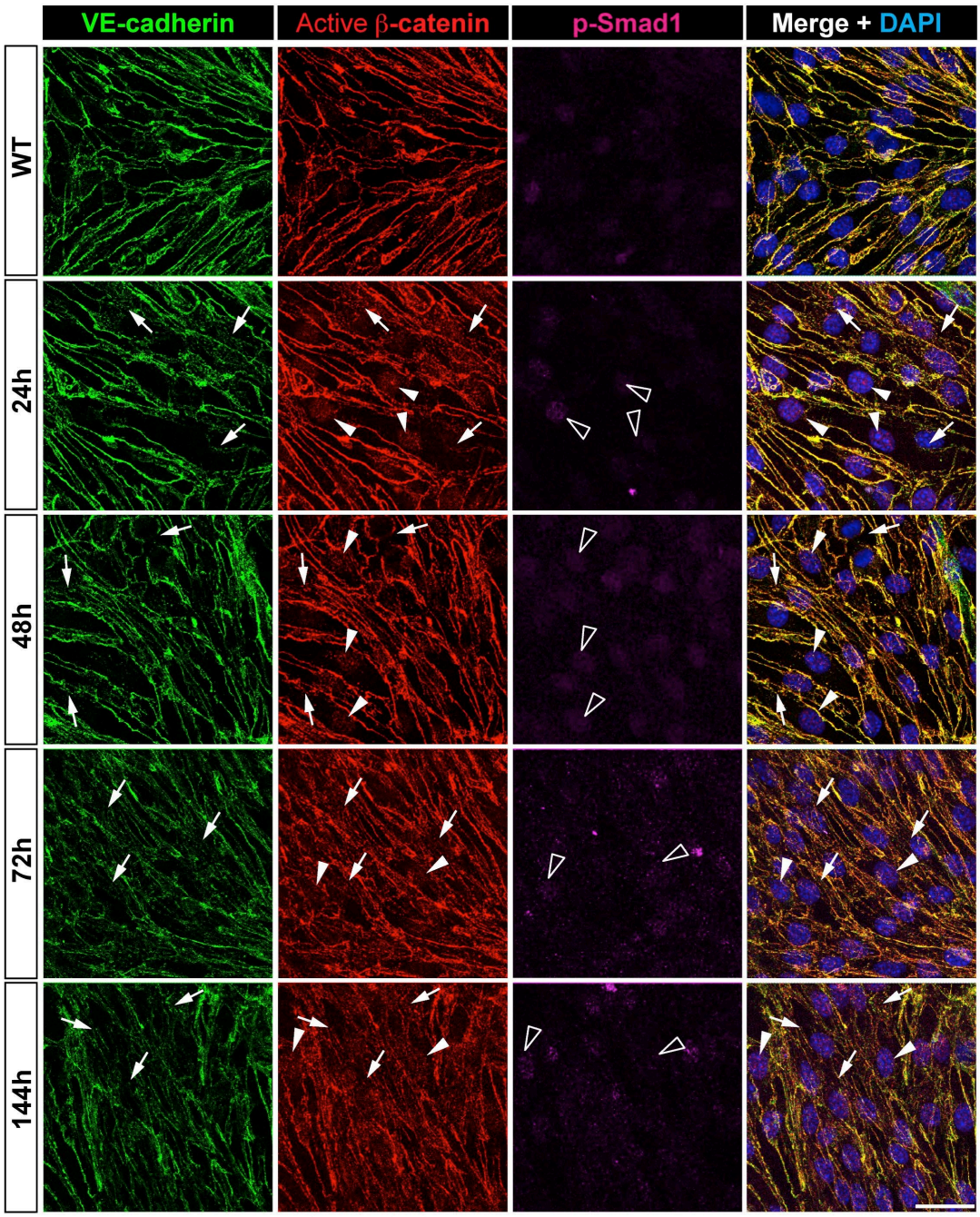

Figure 19. **Acute down regulation of *CCM3* transcript induces junction dismantling together with β-catenin nuclear accumulation in endothelial cells in culture.** Representative immunostaining of active-β-catenin (red), VE-cadherin (green) and p-Smad1 (ser463/465) (purple) at different time points after *CCM3* acute down regulation through siRNA. Junction dismantling is a very precocious event after *CCM3* down regulation (already visible after 24h) (arrows) and correlates with nuclear accumulation of active-β-catenin (DAPI indicating nuclei is in blue). Conversely p-Smad1 accumulation in the nuclei is not significantly increased (empty arrowheads). Controls were treated with negative (not-targeting) siRNA. Scale bar, 30 μm.

We also measured at different time points after *CCM3* silencing the expression of *Bmp2* and *Bmp6*, two important activators of the Tgfβ/Bmp pathways[27]. While *Bmp6* transcript is not modulated, *Bmp2* is significantly increased in *CCM3* silenced cells in comparison to controls (not-targeting siRNA transfected cells). Interestingly, while *Bmp2* expression progressively increased at late time points after *CCM3* silencing, β-catenin signaling tended to decrease in parallel. Although Bmp2 is reported to be able to trigger Smad1 phosphorylation, we couldn't detect any increase of p-Smad1 both in immune-staining and western blot analysis (**Fig.19 and Fig.20**).

Taken together these results confirm, as previously observed *in vivo,* that β-catenin signaling is a very early event upon CCM3 deletion and is able to trigger EndMT in ECs before the activation of Tgfβ/Bmp signaling.

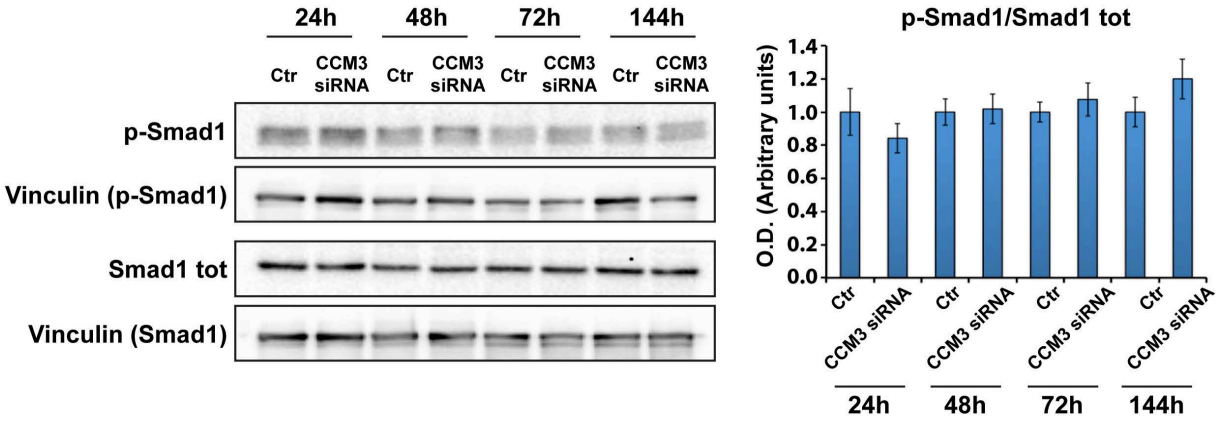

Figure 20. **Acute down regulation of CCM3 transcript is not associated with increased phosphorylation of Smad1.** (**a**) Representative western blot of phosphorylated Smad1 (Ser463/465) protein at different time points after *CCM3* siRNA. (**b**) Western blot bands have been quantified using ImageJ and normalized on respective Vinculin (housekeeper). 20 μg of proteins per lane were loaded. Ratio between p-Smad1 and total Smad1 in (**b**) shows that activation of Tgfβ/Bmp signaling is not an early response to *CCM3* silencing (t-test). Controls were treated with negative (not-targeting) siRNA. Data are means of three independent experiments.

Bmp2 expression is directly regulated by β-catenin in CCM3-knockout endothelial cells

In a previous work we identified Bmp6 as an important mediator of EndMT in *CCM1* null ECs. However, another important member of Bmp family, *Bmp2* is up regulated upon *CCM3* ablation in our model as discussed above. *Bmp2* expression is increased at early time point *in vitro* although delayed in respect to β-catenin transcription signaling. For this reason, we investigated if *Bmp2* could be a target of β-catenin. Experiments using both dominant-negative Tcf4 and Lef-ΔβCTA indicate that *Bmp2* is, indeed, a direct target of β-catenin-mediated transcription (**Fig.21**). However, *Bmp2* transcription activation induced by *CCM3* siRNA fails to trigger Smad1 phosphorylation at tested time points (as discussed before and reported in **Fig.20**). It could be that either longer exposure to Bmp2 or higher level ligand are needed to induce such response (cell autonomous). Interestingly, chronic expression of a constitutive active form of β-catenin (Lef-ΔβCTA) induces both *Bmp2* transcript and phosphorylation of Smad1 (**Fig.2c**).

Although suggestive, the role of Bmp2 in CCM pathology remains to be analyzed.

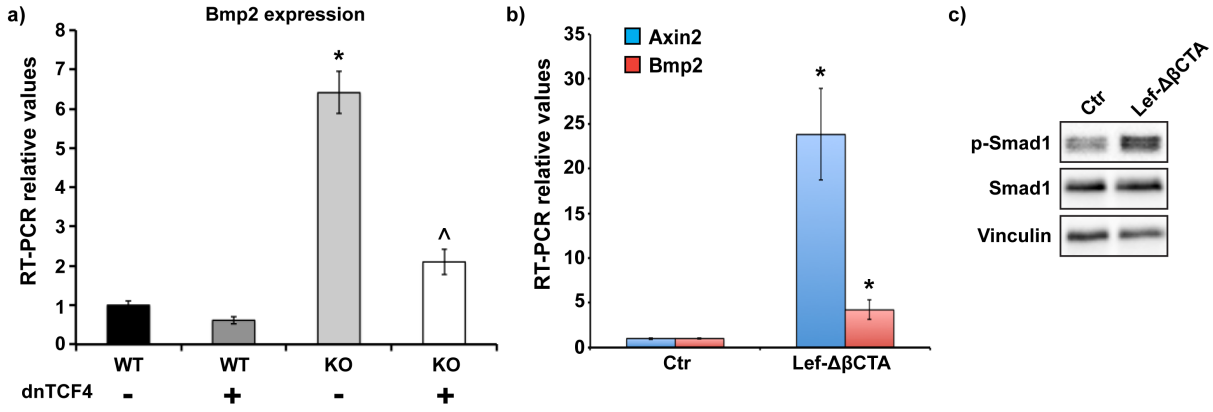

Figure 21. **Bmp2 transcription is directly regulated by β-catenin in *CCM3*-knockout endothelial cells.** (**a**) Bmp2 transcript is strongly up regulated in *CCM3*-knockout endothelial cells line (KO) (*, p< 0.05 WT ctr vs. KO ctr, t-test), and is significantly reduced by dominant-negative TCF4 (dnTCF4) (^, p <0.05 KO dnTCF4 vs. KO ctr, t-test) indicating a direct regulation of *Bmp2* expression by β–catenin/Tcf signaling. (**b**) The expression of β–catenin canonical target *Axin2* and *Bmp2* are up regulated by a constitutive nuclear active form of β–catenin

(Lef-ΔβCTA) 2 weeks after infection. *, p<0.05, t-test. Data are means of three independent experiments. (**c**) The same construct Lef-ΔβCTA is able to induce p-Smad1 phosphorylation. 20 μg proteins per lane were loaded.

Activation of β-catenin-mediated transcription correlates with the expression of EndMT markers in endothelial cells of CCM3 vascular lesions

In order to assess if the expression of EndMT markers *in vivo* was associated to β-catenin-dependent transcription we performed co-staining analysis of β-catenin reporter gene (β-gal) together with EndMT markers in *CCM3*-flox/flox–*Cdh5(PAC)-CreERT2-R26(EYFP)-BAT-gal*. We found that Ly6a (**Fig.22a)**, Id1 (**Fig.22a)**, S100A4 (**Fig.22a)** and Klf4 (**Fig.22a)** expression is significantly increased in ECs lining CCM lesions in comparison to WT vessels both at 3 and 9 dpn. The percentage of nuclei positive either for β-gal and EndMT markers in ECs was also calculated (**Fig.22e**). Here we show that the percentage of endothelial nuclei expressing both β-gal and EndMT markers over the total number of endothelial nuclei analyzed (merge) is significantly higher than in WT vessels and that it tends to decrease at 9 dpn. This is probably due to the fact that the number of β-gal expressing ECs decreases while the number of cells expressing EndMT markers increases. These data are referred to all endothelial nuclei inside CCM lesions. However, considering only EndMT markers-positive nuclei (EndMT markers/β-gal) we found that most (about 80%) of this ECs co-express also β-gal. This is suggestive of a direct association between β-catenin signaling and EndMT marker expression that is particularly high at 3 dpn and decreases (at least for Id1 and Klf4) at the late stage. This finding supports the idea that after an initial phase in which β-catenin is essential to trigger the EndMT, other factors, such as Tgfβ/Bmp, can contribute to the progression of the pathology *in vivo*.

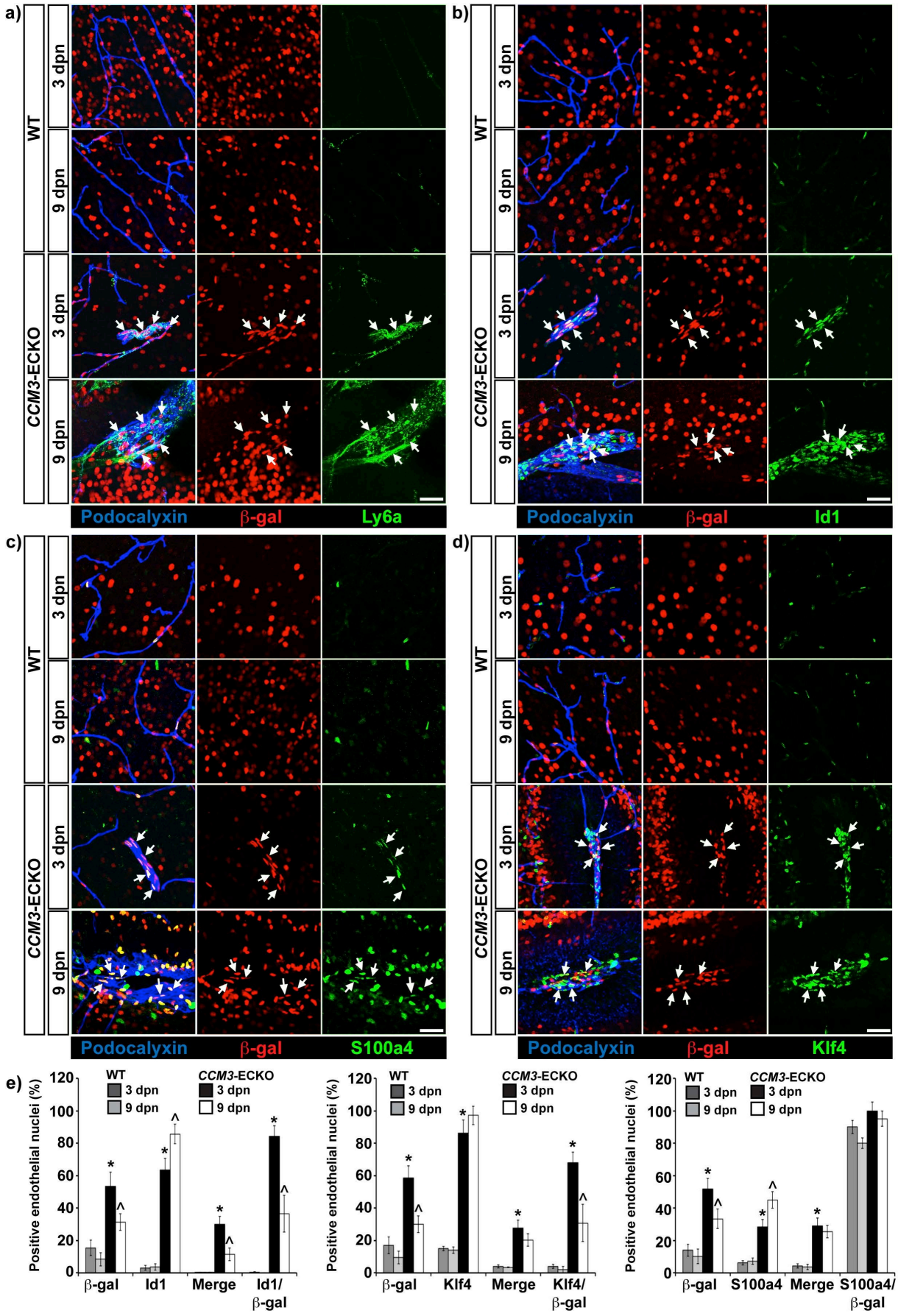
a)
b)
c)
d)
e)
WT
CCM3-ECKO
3 dpn
9 dpn
Podocalyxin
β-gal
Ly6a
Id1
S100a4
Klf4
Positive endothelial nuclei (%)
β-gal
Id1
Merge
Id1/ β-gal
Klf4
Klf4/ β-gal
S100a4
S100a4/ β-gal

Figure 22. **Increased β-catenin-dependent transcription correlates with overexpression of EndMT markers in endothelial cells of *CCM3*-ECKO vessels.** Representative co-immunostaining of β-gal (red), as a gene reporter of β-catenin transcription activity, in Podocalyxin-positive (endothelial) cells (blue) and EndMT markers (green) in *CCM3*-ECKO and WT brains of 3 and 9 dpn mice. Ly6a **(a)**, Id1 **(b)**, S100a4 **(c)** and Klf4 **(d)** concentrated in the nuclei of these *CCM3*-ECKO blood-vessel endothelial cells both at 3 and 9 dpn together with β-gal. Scale bar, 40 μm. **(e)** Quantification of β-gal, Id1, Klf4 and S100a4 positive endothelial nuclei and their co-localization in *CCM3*-ECKO lesions in comparison to WT vessels at 3 and 9 dpn. Endothelial cell nuclei were counted in 50 random fields at 63× magnification in brain sections from 5 *CCM3*-ECKO mice and 5 WT mice at both time points respectively (see Materials and Methods). The percentage of positive nuclei over total nuclei inside lesions is reported. Merge indicates the percentage of endothelial nuclei expressing both β-gal and EndMT markers over the total number of counted endothelial nuclei. EndMT marker/β-gal indicates the percentage of EndMT marker expressing endothelial nuclei, which express also β-gal. *, $p<0.05$ *CCM3*-ECKO 3 dpn *versus* WT 3 dpn; ^, $p<0.05$ *CCM3*-ECKO 9 dpn *versus CCM3*-ECKO 3 dpn, t-test.

The induction of β-catenin transcription activity in CCM3 null endothelial cells is independent from Wnt stimulation

Since β-catenin signaling is usually regulated by Wnt stimuli we investigated whether increased β-catenin-mediated transcription in *CCM3* null ECs could be caused by the activation of Wnt receptors through Wnt ligands.

Wnt ligands are responsible for the activation of a receptor cluster composed by Frizzled receptors and Lrp5/6 co-receptors. In particular phosphorylation of Lrp5/6 is a crucial event in the activation of the canonical Wnt signaling cascade. For this reason we checked for phospho-Lrp6 protein levels in *CCM3*-knockout endothelial cell line in comparison to WT cells and for their response to recombinant Wnt3a stimulation in a time course experiment.

We found that Lrp6 in *CCM3* null cells was less phosphorylated in comparison to WT cells in normal culture conditions and that recombinant Wnt3a stimulates in a similar way the phosphorylation of Lrp6 both in WT and *CCM3*-knockout cells (**Fig.23a and 23b**).

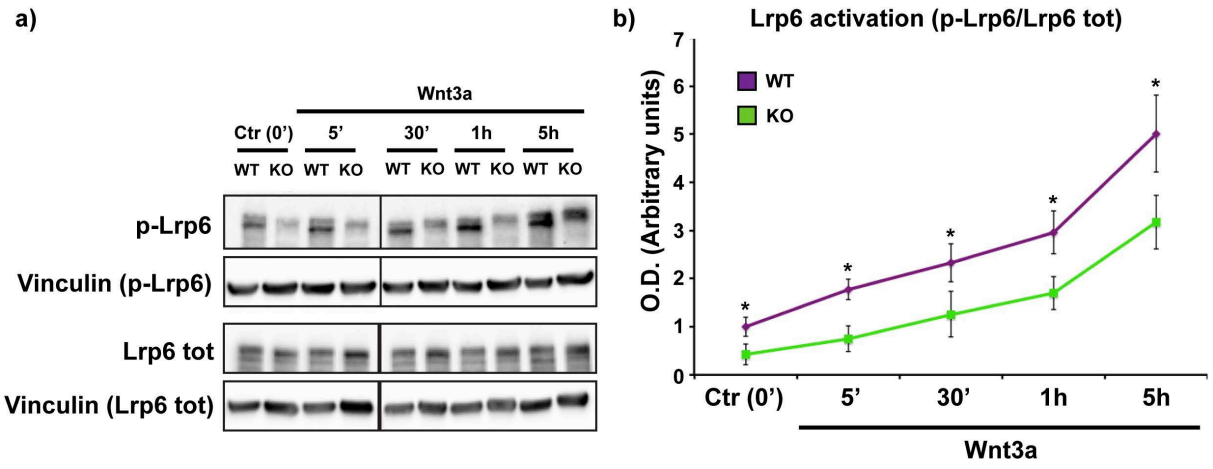

Figure 23. **The Wnt co-receptor Lrp6 is neither constitutively hyper-activated in *CCM3* null endothelial cells in culture, nor more sensible to Wnt stimulation in comparison to WT cells.** *CCM3*-knockout (KO) and WT endothelial cells were treated with recombinant Wnt3a (100 ng/ml) for different time (5 min, 30 min, 1h, 5h). Wnt receptor activation was evaluated as phosphorylation of Wnt co-receptor Lrp6. (**a**) Representative western blots of p-Lrp6 (Ser 1490), total Lrp6 and their respective Vinculin as housekeeper are shown. 20 μg of proteins per lane were loaded. **(b**) Western blot bands were quantified (O.D. assessment by Image J) and the ratio between phosphorylated and total Lrp6, each normalized on respective Vinculin, is reported in the graph (mean of three independent experiments) as index of Lrp6 activation. No differences between WT and *CCM3*-knockout cells are observed at any time points. *, $p<0.05$, t-test. *CCM3*-knockout cells showed lower level of Lrp6 activation both in resting condition (Ctr 0') and at all time points after Wnt3a stimulation.

In addition, *CCM3*-knockout cells were treated with recombinant Dkk1 protein, a physiological inhibitor of Lrp5/6[192] and we checked for the level of *Axin2* and *S100a4* transcripts as readout respectively of β-catenin signaling and EndMT (**Fig.24a**). Despite the ability of Dkk1 to inhibit a Wnt3a-induced stimulation (**Fig.24b**), it failed to reduce the expression of *Axin2* and *S100a4* in *CCM3*-knockout ECs (**Fig.24a**).

Other two inhibitors of Wnt pathway, IWP2 and IWP12[193], targeting Porcupine, an essential enzyme for Wnt processing and secretion, have been used. Also in this case the treatments at 3 different doses showed no effect on *Axin2* and *S100a4* transcripts (**Fig.24c and 24d**) in *CCM3*-knockout ECs.

In order to further confirm that Wnt exogenous stimulus is not responsible for the abnormal β-catenin signaling in *CCM3*-knockout ECs, we treated these cells with Wnt3a. We

found that the stimulation by the ligand is sufficient to trigger the expression of canonical targets of Wnt pathway such as *Axin2* but it is not able to induce the expression of EndMT markers (**Fig.25**).

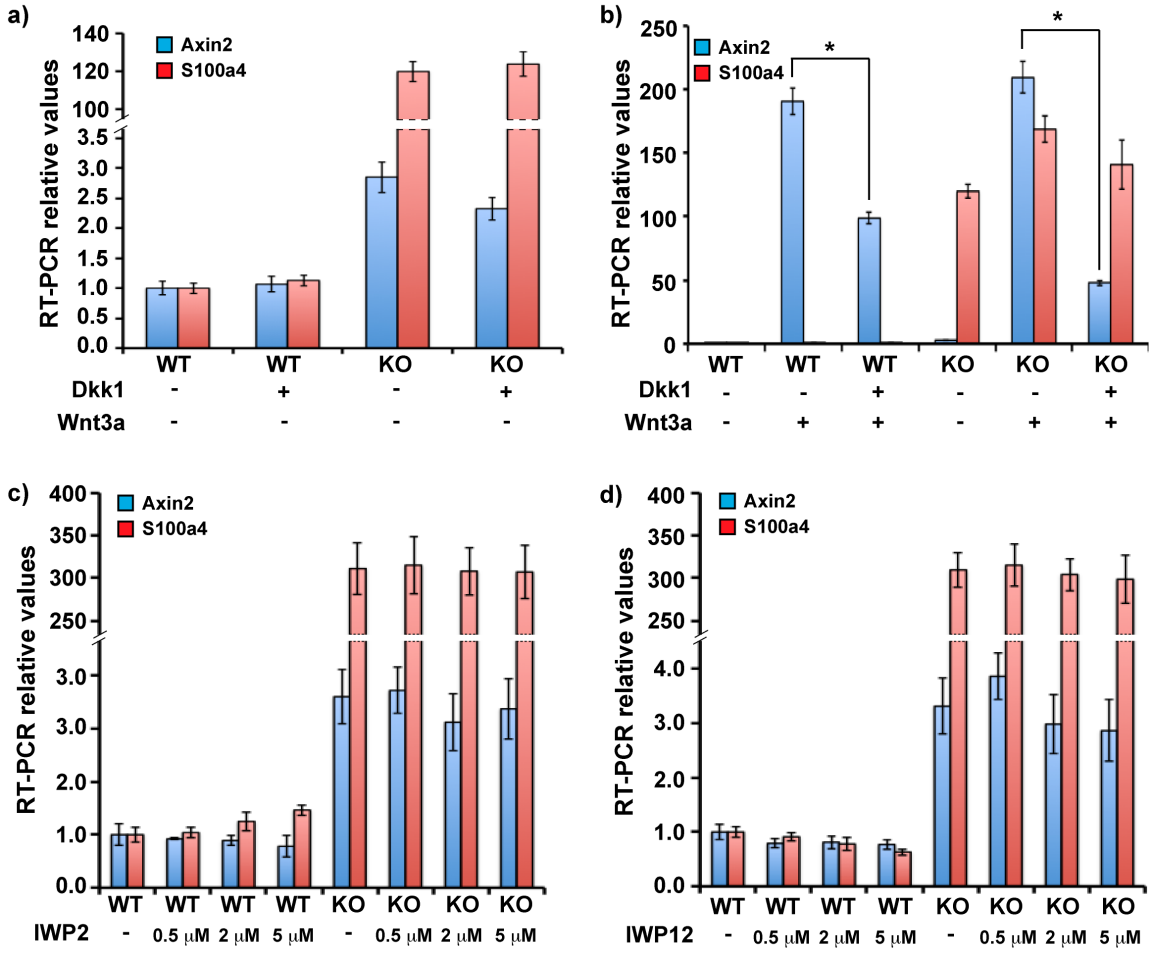

Figure 24. **Inhibitors of Wnt receptor and of Wnt ligand secretion fail to down regulate enhanced β-catenin-mediated transcription in *CCM3* null endothelial cells in culture.** Quantification of the effects of drugs inhibiting the initial steps of Wnt/β-catenin pathway on the overexpression of a β-catenin target gene (*Axin2*) and an EndMT marker (*S100a4*) through rt-PCR. (**a**) Recombinant Dkk1, able to inhibit Wnt receptor activation, (0.5 μg/ml) failed to inhibit the constitutive over expression of *Axin2* and *S100a4* in *CCM3* null endothelial cells while (**b**) it inhibited exogenous Wnt3a activation. *, $p<0.05$. Two different porcupine inhibitors, IWP2 (**c**) and IWP12 (**d**) were used in a range of concentrations reported active in the literature and analyzed at different time point. 48h treatment has been shown as representative of results obtained. No effect on the expression of *Axin2* and *S100a4* was observed. Data are means of three independent experiments.

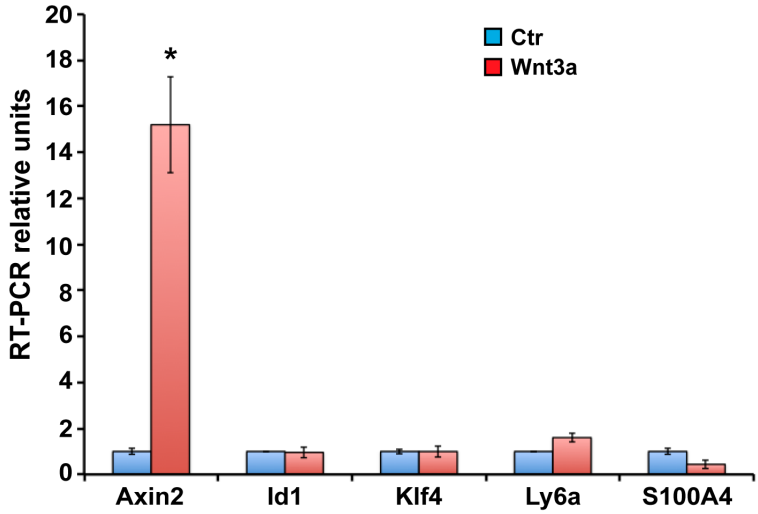

Figure 25. **Exogenous Wnt3a fails to up regulate EndMT markers in endothelial cells in culture.** Quantification of the effects of Wnt3a (100 ng/ml) in WT endothelial cell on the expression of EndMT markers. Despite its ability to trigger a transcriptional response (see *Axin2* up regulation), Wnt3a failed to induce transcription of EndMT markers. Cells were treated with Wnt3a for different time. 72h treatment is shown in figure. *, $p<0.05$, t-test. Data are means of three independent experiments.

High throughput analysis of the transcriptome of CCM3 null endothelial cells

To further analyze the role of Wnt/β-catenin pathway in CCM, we performed high throughput Affymetrix analysis of the transcriptome of *CCM3*-knockout brain ECs in primary culture treated or not with Wnt3a. WT control ECs were analyzed in parallel.

We performed both a qualitative and quantitative analysis of Affymetrix data. In a quantitative analysis, in which we measured the fold change of Wnt target genes expression independently from their starting level, we observed that the gene expression profile is very similar between WT and *CCM3*-knockout cells when treated with Wnt3a ($p>0.05$, paired t-test. $R^2=0.89$, Pearson test), suggesting a similar sensitivity of the two cell type to stimulation by Wnt3a ligand (**Fig.26a**). In addition, in a quantitative analysis, we compared the expression levels of Wnt target genes in WT cells treated with Wnt3a versus *CCM3*-knockout cells (**Fig.26b**). In agreement with previous ratius we found that Wnt stimulation doesn't mimic the

a)

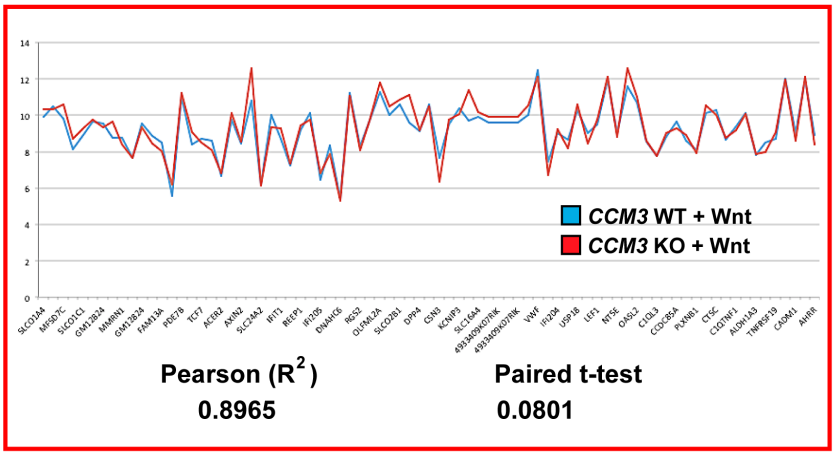
14
12
10
8
6
4
2
0
CCM3 WT + Wnt
CCM3 KO + Wnt
Pearson (R^2)
0.8965
Paired t-test
0.0801

b)

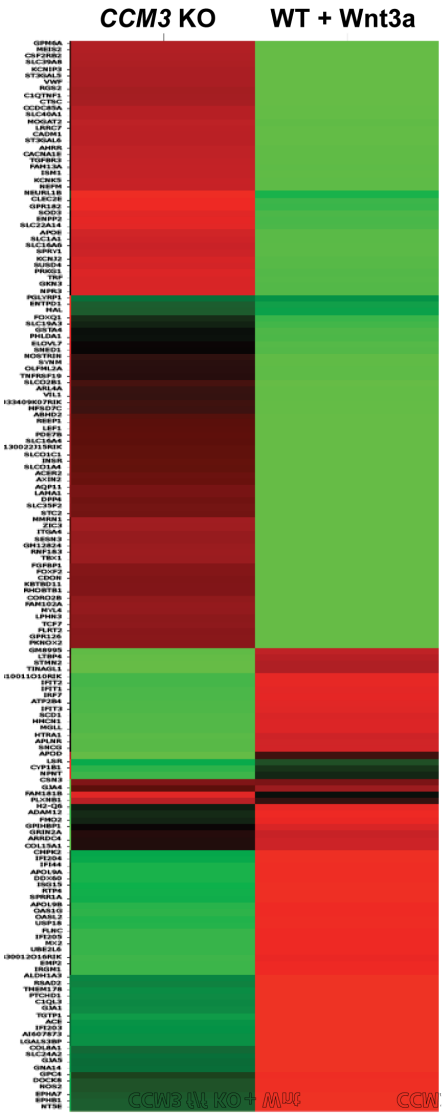
CCM3 KO
WT + Wnt3a

Figure 26. **High throughput analysis reveals no difference in the transcription responses to Wnt3a between *CCM3* null and WT endothelial cells. In addition, the transcriptional profile of un-stimulated *CCM3* null endothelial cells is different from that induced by Wnt3a in WT endothelial cells.** The transcriptome of *CCM3*-knockout (KO) and WT primary cells treated or not with Wnt3a (100 ng/ml, 72h treatment) has been analyzed using Affymetrix technique. (**a**) Qualitative analysis of the transcriptional response to Wnt3a in *CCM3*-knockout and WT cells on Wnt3a target genes (40 genes have been found selectively regulated by Wnt3a *in vitro* in endothelial cells) shows no significant differences between *CCM3*-knockout and WT endothelial cells (paired t-test=0.0801, Pearson test: R^2=0.8965). In this case fold change induced by Wnt3a in comparison to control vehicle is plotted for each condition. (**b**) Quantitative analysis. Genes transcriptionally modulated by the deletion of *CCM3* in comparison to WT cells were selected and analyzed using a color code in a heat map. The same genes in WT cells treated with Wnt3a show a different profile indicating a different regulation. A p-value<0.01 have been calculated using t-test. Data are means of three independent experiments.

ablation of *CCM3* in terms of gene expression levels (**Fig.26b**), confirming that β-catenin transcriptional signaling activation in these cells is independent from regular Wnt/β-catenin signaling pathway. For the list of genes see appendix table 1.

Endothelial cell-to-cell junctions regulate β-catenin transcription activity

Since β-catenin, besides its transcription role into the nucleus, is also a key constituent of AJs we investigated whether junctions dismantling that we observe in *CCM3*-knockout cells could be related to β-catenin nuclear localization and signaling. To do this we induced junctions dismantling through different techniques in WT ECs. In particular we found that upon down regulation of VE-cadherin through siRNA or after treatment with an anti-VE-cadherin antibody (BV13) or with EGTA (a calcium sequestering agent) β-catenin accumulates in the cytoplasm and into the nucleus of treated cells where it can mediate transcription of target genes (**Fig.27 and Fig.28**). Very interestingly down regulation of VE-cadherin through siRNA correlates also with a significant up regulation of some EndMT marker expression (e.g. Id1 and S100a4 but not Ly6a) (**Fig.27**). These findings suggest that

also in *CCM3*-knockout cells, where cell-to-cell junctions are impaired, a similar mechanism could occur.

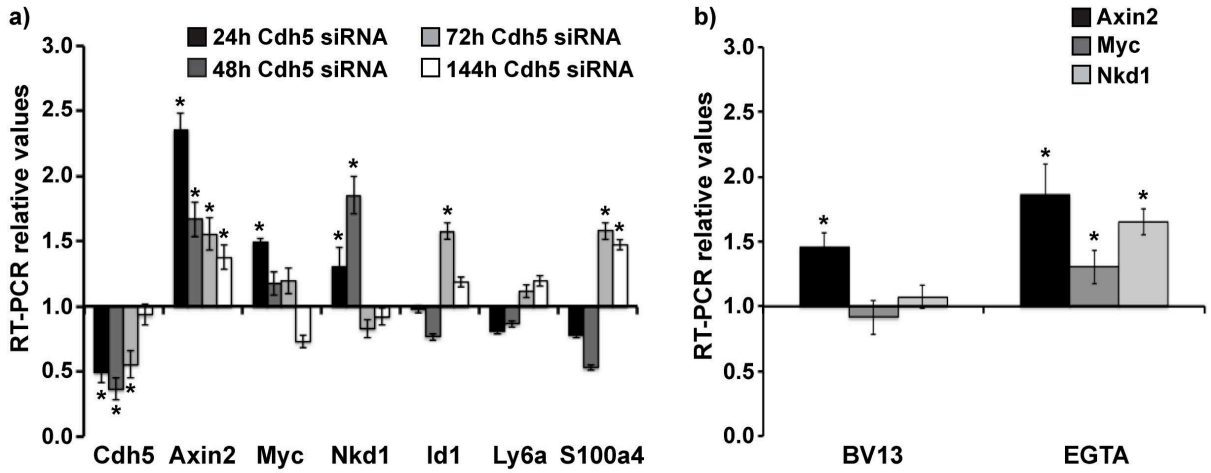

Figure 27. **Junctions dismantling induces up regulation of β-catenin signaling in endothelial cells in culture.** Quantification of the effect of (**a**) VE-cadherin (*Cdh5)* down regulation using siRNA at different time points and (**b**) monoclonal antibody directed against VE-cadherin (BV13 for 72h) as well as calcium-sequestering agent (EGTA for 30 min.) in WT endothelial cells at different time points by rt-PCR. Acute down regulation of VE-cadherin transcript (~60%) (**a**) and protein (see **Fig.19**) correlates with transcription up regulation of β-catenin target genes (*Axin2, Nkd1, Myc)* at 24h. The response of *Nkd1* and *Myc* is lost in long term treatment, while that of *Axin2* declines, but is maintained. EndMT markers like *Id1* and *S100a4* are also increased in these cells even if delayed in comparison to canonical β-catenin target genes. Junction dismantling using BV13 induces only *Axin2* transcript, while EGTA stimulates the three transcripts. Controls were treated with negative (not-targeting) siRNA. * $p<0.05$, t-test. Data are means of three independent experiments.

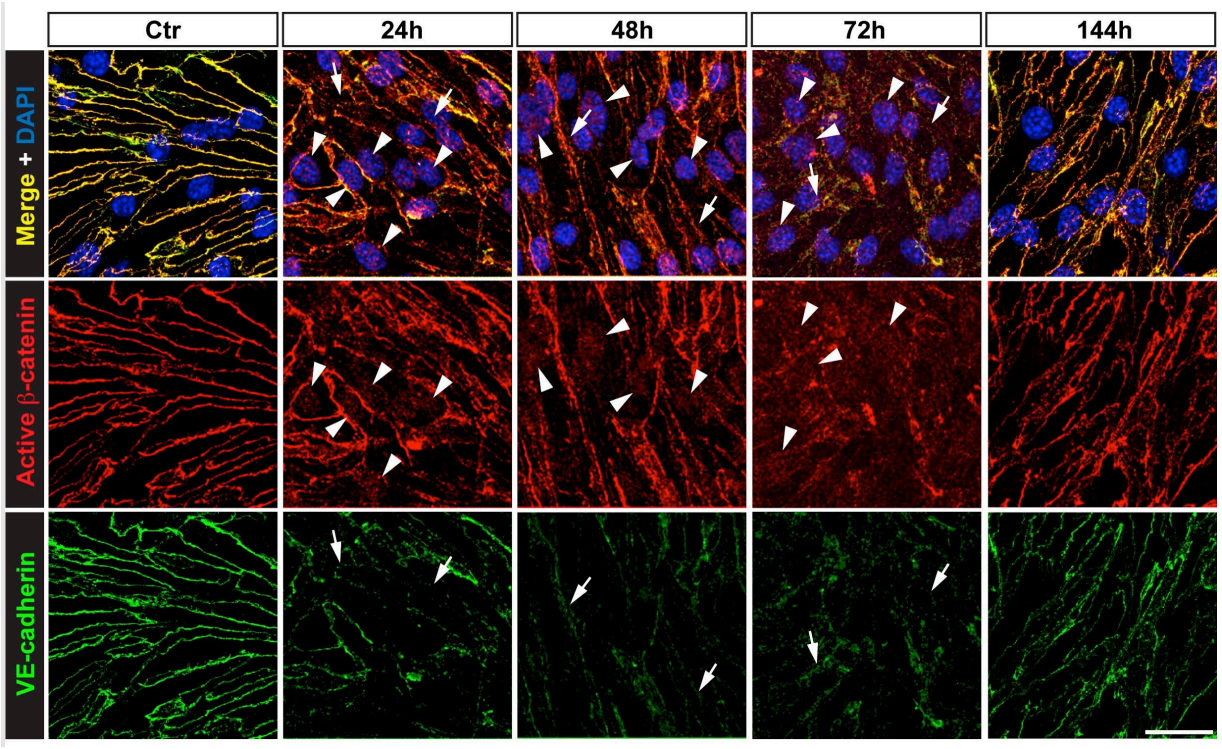

Figure 28. **Junctions dismantling induces β-catenin nuclear accumulation in endothelial cells in culture.** Representative immunostaining of active-β-catenin (red) and VE-cadherin (green) at different time points after VE-cadherin acute down regulation through siRNA. Junction dismantling and VE-cadherin down regulation (arrows) is accompanied by nuclear accumulation of active-β-catenin (DAPI indicating nuclei is in blue) (arrowheads). Controls were treated with negative (not-targeting) siRNA. Scale bar 30 μm.

Sulindac sulfide reduces β-catenin transcription activity and expression of endothelial progenitor and EndMT markers in endothelial cells in culture

Due to the crucial role of β-catenin in mesenchymal transition in *CCM3*-knockout ECs, we investigated whether pharmacological inhibitors of β-catenin signaling could be a real therapeutic opportunity for CCM treatment.

We then initially tested a range of agents in our experimental model *in vitro* that have been described as affecting β-catenin signaling[194] and, most importantly, are already in clinical use: sulindac sulfide, sulindac sulfone[194, 195], silibinin, curcumin and resveratrol[90] (**Fig.29**).

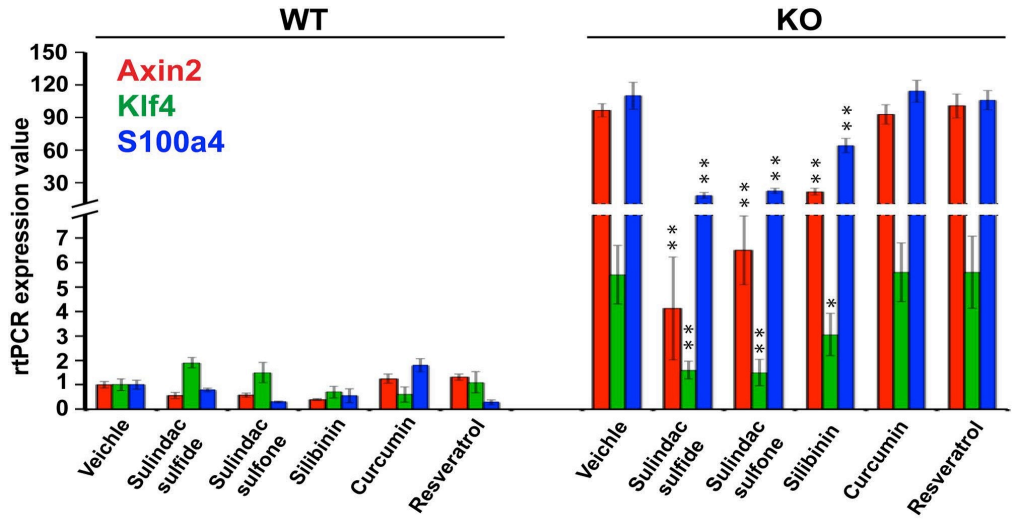

***Figure 29. In vitro* screening of pharmacological antagonists of β-catenin signaling in *CCM3* null endothelial cells in culture.** Quantification of the effect of drugs that have been reported to target different steps of the β-catenin signaling pathway (135 μM sulindac sulfide, 125 μM sulindac sulfone, 200 μM silibinin, 40 μM curcumin, 40 μM resveratrol), on the overexpression of a β-catenin target gene (*Axin2*) and EndMT markers (*Klf4, S100a4*) in WT and *CCM3*-knockout (KO) endothelial cells line 48h after treatment. Sulindac sulfide and sulindac sulfone show the greatest inhibition of the strong induction of transcription of *Axin2, Klf4* and *S100a4* seen in these *CCM3*-knockout endothelial cells. Among the other drugs tested here, silibinin was effective against these three transcripts. Data are mean rt-PCR values from at least three independent experiments, each carried out in triplicate. *, $p<0.05$, **, $p<0.01$ *versus* the respective transcripts in the vehicle-treated *CCM3*-knockout endothelial cells (t-test). See Materials and Methods for further details. Comparable results were obtained with cells from between five and 25 passages after knockout of *CCM3*.

Sulindac sulfide and sulindac sulfone were the most effective of these for inhibition of expression of Axin2, Klf4 and S100a4 as representative endogenous targets of β-catenin transcription activity in the *CCM3*-knockout endothelial cell line (**Fig.29**). In addition, sulindac sulfide reduced β-catenin transcription activity as measured by the Top/Fop Flash reporter assays (**Fig.30**).

We therefore further analyzed the effects of sulindac sulfide on the *CCM3* null phenotype. In primary cultures of *CCM3*-knockout brain ECs, we found that sulindac sulfide effectively inhibited the expression of endogenous β-catenin target genes with efficiency similar to the dominant-negative Tcf4 (**Fig.31**). In parallel, sulindac sulfide

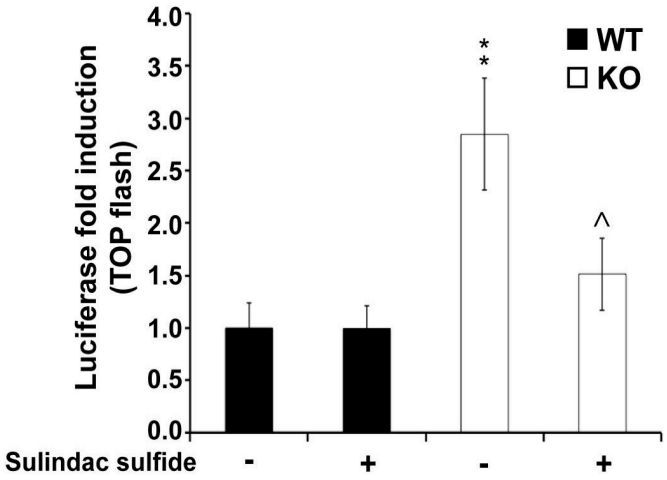

Figure 30. **Sulindac sulfide inhibits β-catenin-mediated transcription in *CCM3* null endothelial cells in culture.** Sulindac sulfide inhibited (^, $p<0.05$, sulindac sulfide KO *versus* vehicle KO, t-test) the significant increase (*, $p<0.05$, vehicle-KO *versus* vehicle-WT, t-test) of β-catenin/Tcf4-dependent transcription of the luciferase reporter gene in the Top/Fop Flash assay (see Materials and Methods for details) in *CCM3*-knockout (KO) endothelial cells. The ratio between Top-flash and Fop-flash values normalized over transfection efficiency (β-galactosidase activity) is shown as fold change in comparison to the ratio in vehicle WT (Luciferase fold induction). Data are means of three independent experiments.

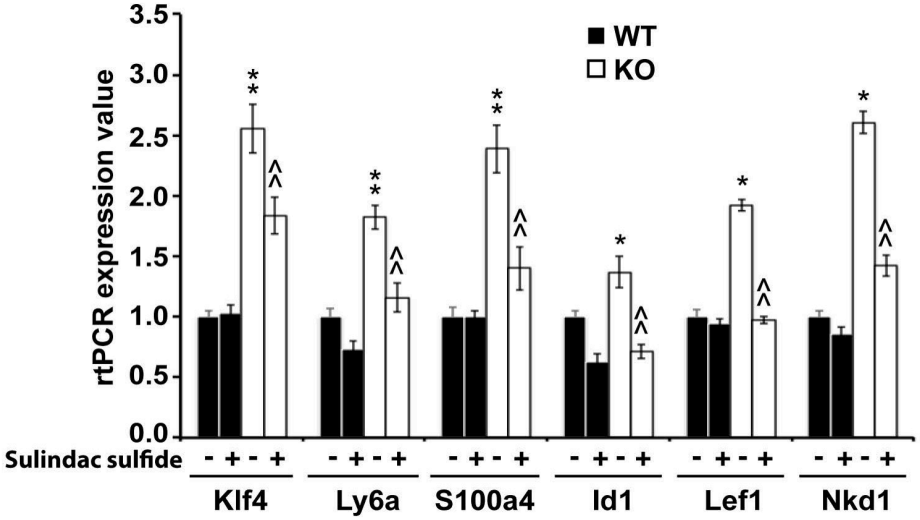

Figure 31. **Sulindac sulfide inhibits the transcription of β-catenin target genes in *CCM3* null endothelial cells in culture.** Quantification of sulindac sulfide inhibition of transcription of β-catenin target genes *Klf4, Ly6a, S100a4* and *Id1* by rt-PCR, in WT and *CCM3*-knockout (KO) brain endothelial cells in primary culture. *, $p<0.05$; **, $p<0.01$ (t-test) for the comparison *CCM3*-knockout *versus* WT under basal conditions. ^^, $p<0.01$ (t-test) for the comparison *CCM3*-knockout plus sulindac sulfide *versus* vehicle treated *CCM3*-knockout. Data are means of three independent experiments.

inhibited the nuclear localization of active β-catenin while increasing its concentration at cell-cell junctions (**Fig.32**). We got the same findings using *CCM3*-knockout endothelial cell line where we observed that VE-cadherin was more localized at cell-to-cell contacts in sulindac sulfide treated cells (**Fig.33**). Sulindac sulfide also restored regular apical polarization of Podocalyxin, which was impaired in *CCM3* null ECs (**Fig.33**).

Consistently, by co-immunoprecipitation and Western blotting analysis sulindac sulfide restored the reduced association between β-catenin and VE-cadherin (minus 35% ±0.32 SD, $p < 0.05$) in *CCM3*-knockout endothelial line (**Fig.34a and 34b**).

The better organization of cell-to-cell junctions after sulindac sulfide treatment is confirmed also by increased activity of Rap1, which is conversely down regulated in *CCM3*-knockout cells in comparison to WT cells (**Fig.35**).

In parallel with inhibition of transcription of β-catenin target genes, sulindac sulfide also inhibited the overexpression of respective proteins in *CCM3*-knockout ECs (**Fig.32 and Fig.36**).

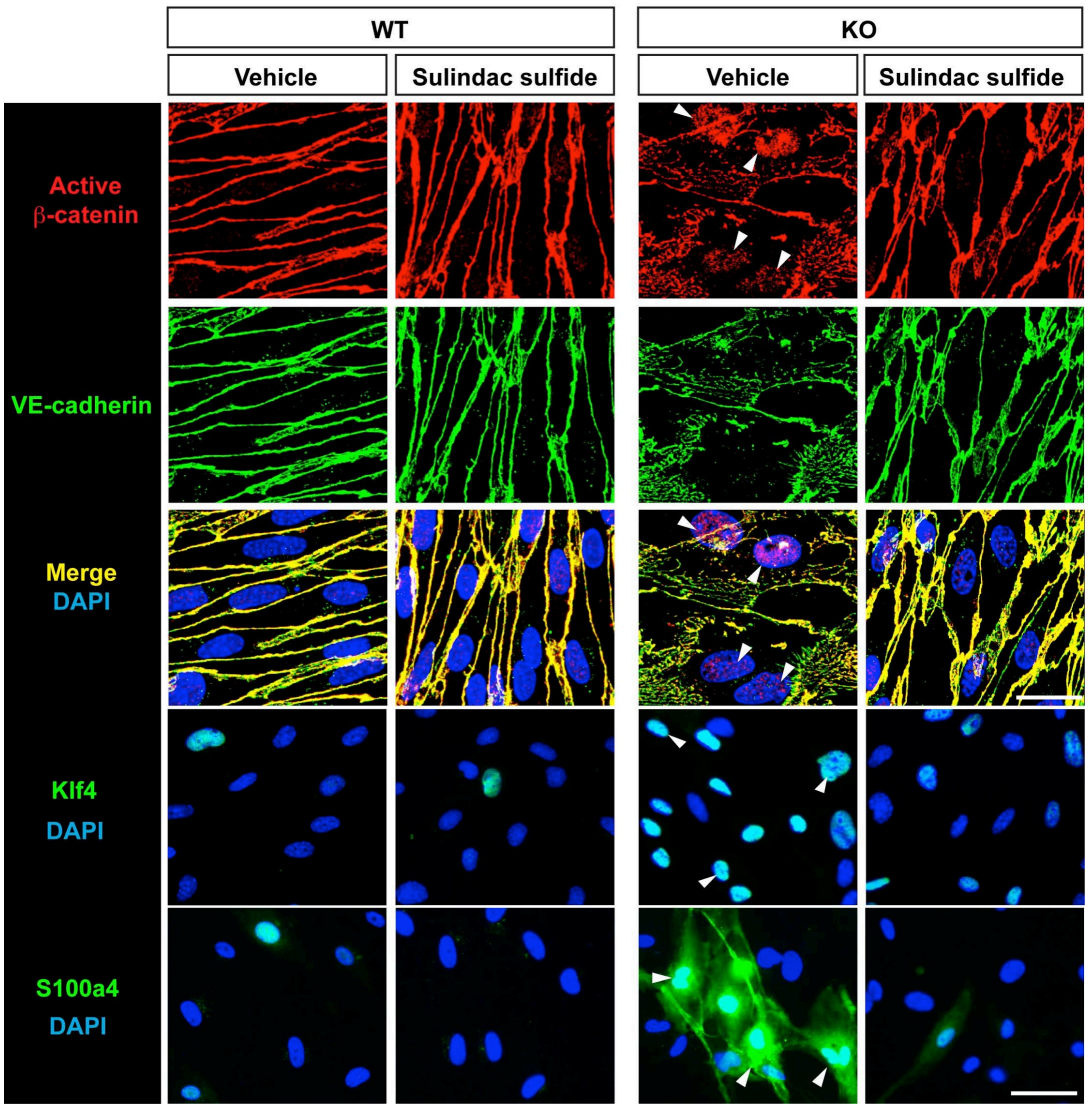

Figure 32. **Sulindac sulfide induces re-localization of active β-catenin from the nucleus to adherens junctions in *CCM3* null endothelial cells in primary culture.** Representative immunostaining of brain endothelial cells in primary culture under sulindac sulfide treatment. Nuclei were stained with DAPI (blue). Top three rows: sulindac sulfide-mediated redistribution of active β-catenin (red) and VE-cadherin (green) from the nucleus (arrowheads) to cell-cell junctions in these *CCM3*-knockout (KO) endothelial cells. Co-localization of active β-catenin and VE-cadherin is shown in the merge (yellow). Scale bar, 15 μm. Bottom two rows: Sulindac sulfide inhibition of overexpression of Klf4 (green) and S100a4 (green) in these *CCM3*-knockout endothelial cells (turquoise shows co-localization with DAPI; arrowheads). Klf4 is exclusively nuclear and S100a4 is both nuclear and cytoplasmic in these *CCM3*-knockout endothelial cells. Scale bar, 30 μm.

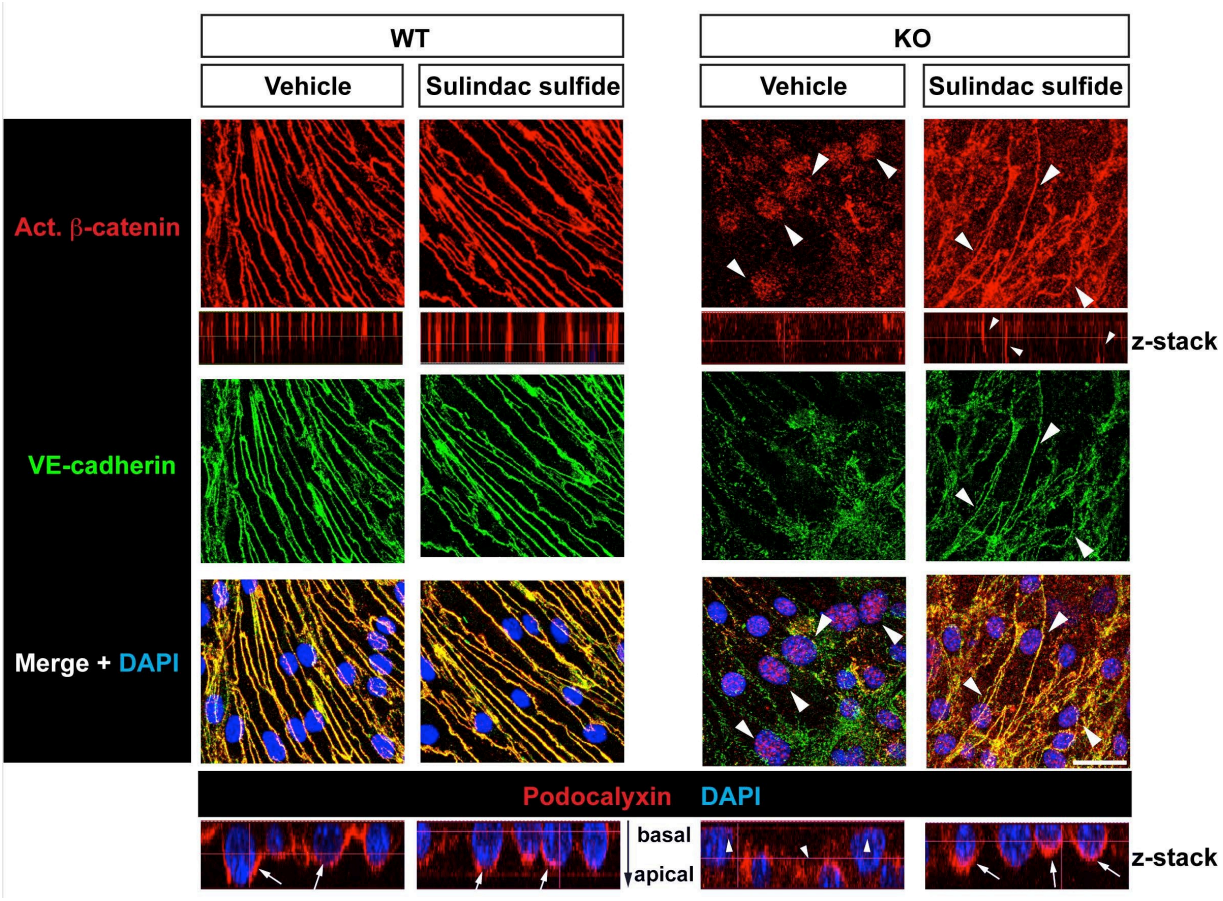

Figure 33. **Sulindac sulfide induces re-localization of active β-catenin from the nucleus to adherens junctions in *CCM3* null endothelial cell line in culture.** Representative immunostaining for effects of sulindac sulfide on re-localization of active β-catenin from the adherens junctions into the nucleus in WT and *CCM3*-knockout (KO) endothelial cell line. Active β-catenin (red) and VE-cadherin (green) were lost from cell-to-cell contacts (adherens junctions) in these *CCM3*-knockout endothelial cells (top main panels, XY axis; small lower panels, Z projection along X axis). The active β-catenin is concentrated into the nucleus, as also seen in the merge with nuclei stained with DAPI (blue) (right panels, vehicle, arrowheads). Co-localization of active β-catenin and VE-cadherin is shown in the merge (yellow). Treatment with sulindac sulfide restored the distribution of active β-catenin (red) and VE-cadherin (green) to the adherens junctions (right panels, sulindac sulfide, arrowheads, and small lower right panels, sulindac sulfide, small arrowheads, for distribution along Z axis). Bottom panels of Z projection along X axis: a marker of apical polarity in endothelial cells, podocalyxin (red), shows loss of apical polarity in *CCM3*-knockout endothelial cells. Podocalyxin is re-localized from the apical surface (left panels, WT, arrows) to be ectopically distributed on the basal side with *CCM3*-knockout (right panel, vehicle, arrowheads), as it has been reported for *CCM1*-knockout[121]. Sulindac sulfide re-establishes the correct apical distribution of Podocalyxin (right panel, sulindac sulfide, arrows). Scale bar, 30 μm.

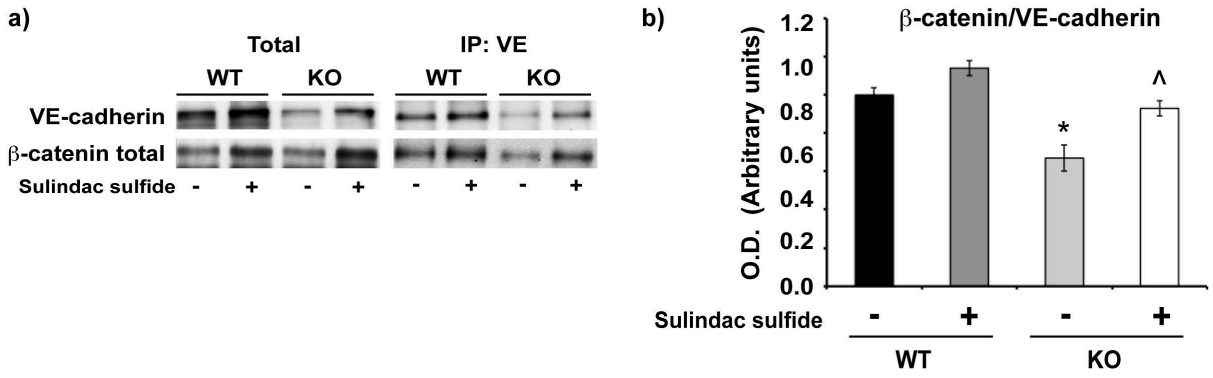

Figure 34. **Sulindac sulfide counteracts β-catenin dissociation from VE-cadherin in *CCM3* null endothelial cells in culture.** Representative Western blotting (**a**) and quantification (**b**) of the effects of sulindac sulfide on the co-immunoprecipitation complex of β-catenin and VE-cadherin. (**a**) Western blotting with the WT and *CCM3*-knockout (KO) endothelial cells of total extracts and immunoprecipitates with VE-cadherin antibodies (IP: VE) are shown. With sulindac sulfide treatment, the reduction in the level of VE-cadherin in the *CCM3*-knockout was restored (compare in total sulindac sulfide KO and vehicle WT). (**b**) With the co-immunoprecipitation complex measured as the β-catenin/VE-cadherin ratio, with sulindac sulfide treatment, the significantly reduced association between β-catenin and VE-cadherin in the *CCM3*-knockout (35% ±0.32 SD, *, $p<0.05$, vehicle-KO *versus* vehicle-WT) was restored to the level observed in the WT cells (^, $p<0.05$, sulindac sulfide KO *versus* vehicle KO, t-test). The quantification of the bands from the Western blotting was assessed as the means of three independent experiments, using ImageJ.

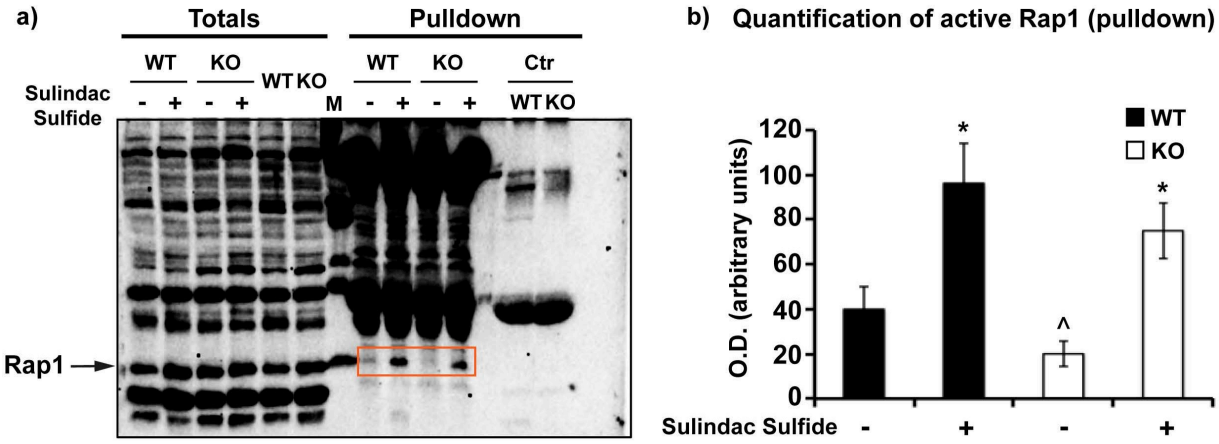

Figure 35. **Rap1 activity is reduced in *CCM3* null endothelial cells in culture and sulindac sulfide induces activation of Rap1 in these cells.** **(a)** Although the total amount of Rap1 protein is slightly increased in *CCM3* null endothelial cells (KO), the amount of active form of Rap1 (GTP-bound) is down regulated in these cells (**b**) as assessed also by quantification of WB bands using ImageJ (data are means of three independent experiments). For controls (Ctr) WT and KO extract were incubated with purified GST. Activity of Rap1 in *CCM3*-knockout and WT cell line treated or not with sulindac sulfide was analyzed using Rap1 activation assay (see Materials and Methods). M=markers. *, $p<0.05$, sulindac sulfide *versus* vehicle, t-test and ^, $p<0.05$, WT *versus* *CCM3*-knockout, t-test.

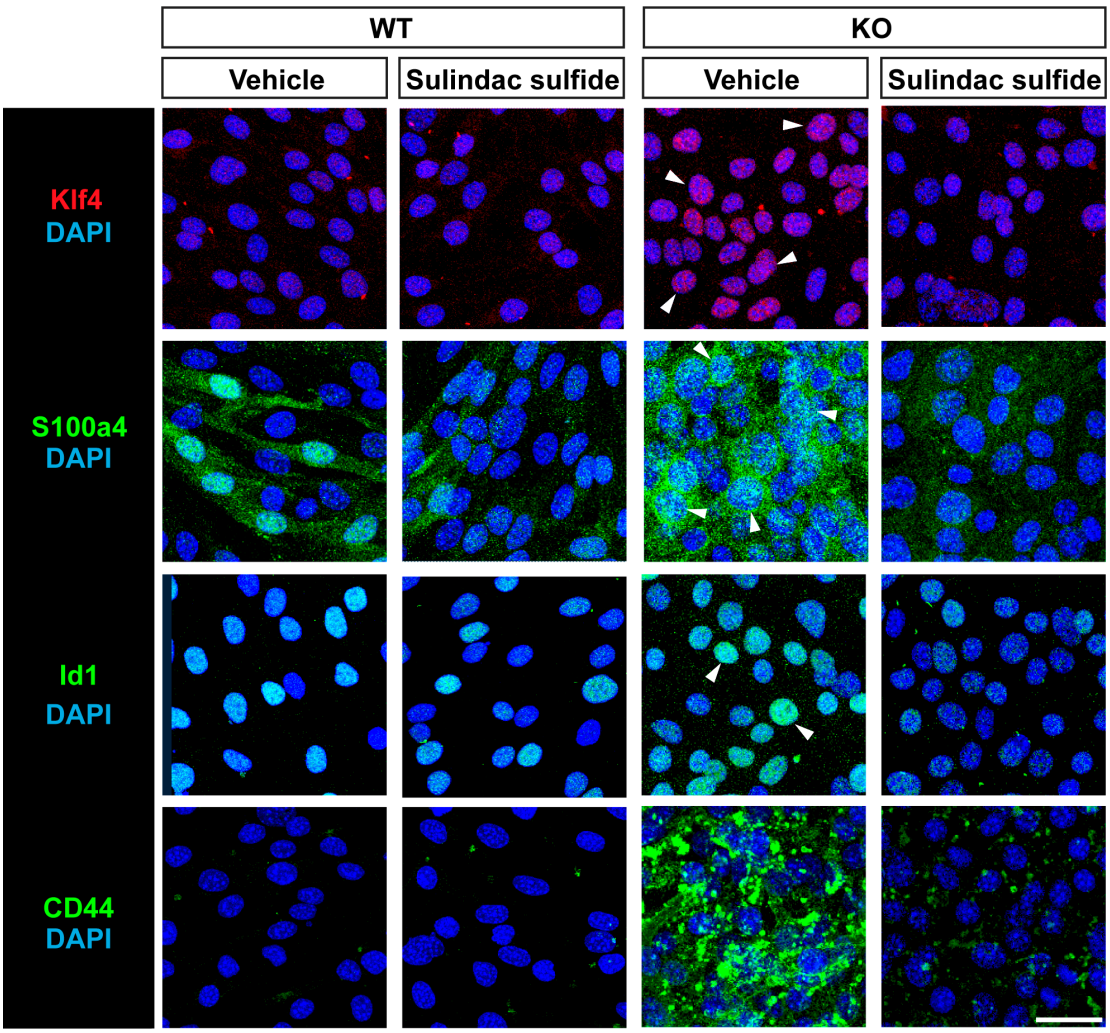

Figure 36. **Sulindac sulfide inhibits the overexpression of progenitor and EndMT markers in *CCM3* null endothelial cells in culture.** *CCM3*-knockout (KO) endothelial cell line shows sulindac sulfide inhibition of overexpression of EndMT markers. Representative immunostaining showing that compared to the WT, there was increased expression of Klf4, S100a4, Id1 and CD44 in *CCM3*-knockout endothelial cells. Nuclei were stained with DAPI (blue). The overexpression of Klf4 (top row, red) and Id1 (third row, green) in *CCM3*-knockout was confined to the nucleus, as shown by double staining with DAPI (blue) (KO, vehicle, arrowheads). Similarly, S100a4 (second row, green) was both nuclear (KO, vehicle, arrowheads) and cytoplasmic (KO, vehicle), while CD44 (bottom row, green) was mostly cytoplasmic (KO, vehicle), Treatment with sulindac sulfide (right-hand panels) strongly reduced the overexpression of these proteins in *CCM3*-knockout endothelial cells. Scale bar, 30 μm.

Sulindac sulfide reduces β-catenin transcription activity and expression of EndMT markers in endothelial cells from the CCM3-ECKO mice

Sulindac sulfide was then investigated *in vivo* in newborn mice after induction of *CCM3*-ECKO in a time course experiment (brain analyzed at 3, 5, 7 and 9 dpn). Macroscopic analysis following dissection showed that lesions present in the brain and cerebellum of *CCM3*-ECKO mice are clearly reduced at different stages in animals treated with sulindac sulfide in comparison to matched control animal (**Fig.37a**) as discussed in the following paragraph. In parallel, sulindac sulfide is also able to strongly inhibit the expression of nuclear β-catenin transcription activity reporter gene β-gal in these brain's vessels (**Fig.37b and Fig.37c**). Noteworthy, some β-gal positive endothelial nuclei are still present in lesions of treated animals. VE-cadherin also appeared to be better localized at endothelial cell-to-cell junctions *in vivo* in the brain vessels of newborn *CCM3*-ECKO mice treated with sulindac sulfide (**Fig.37d**).

In addition, sulindac sulfide is able to inhibit the expression of EndMT markers (**Fig.38, Fig.39, Fig.40 and Fig.41**) in the endothelial cell of the brain vasculature. Interestingly, the lesions still present in the brains of treated animals, even if reduced in number and size (see following paragraph), express EndMT markers at higher levels in comparison to pseudonormal vessels.

Finally, sulindac sulfide is able to reduce cell proliferation as assessed by KI67 immunostaining *in vivo* (**Fig.42**).

Even if there is a tendency of animals treated with sulindac sulfide to live longer in comparison to vehicle treated animals, this increase failed to be significant in a statistical analysis due to the high standard deviation (**Fig.43**).

Taking together this data showed that sulindac sulfide is able to inhibit, in part, β-catenin signaling and that this correlates with a reduction of EndMT markers.

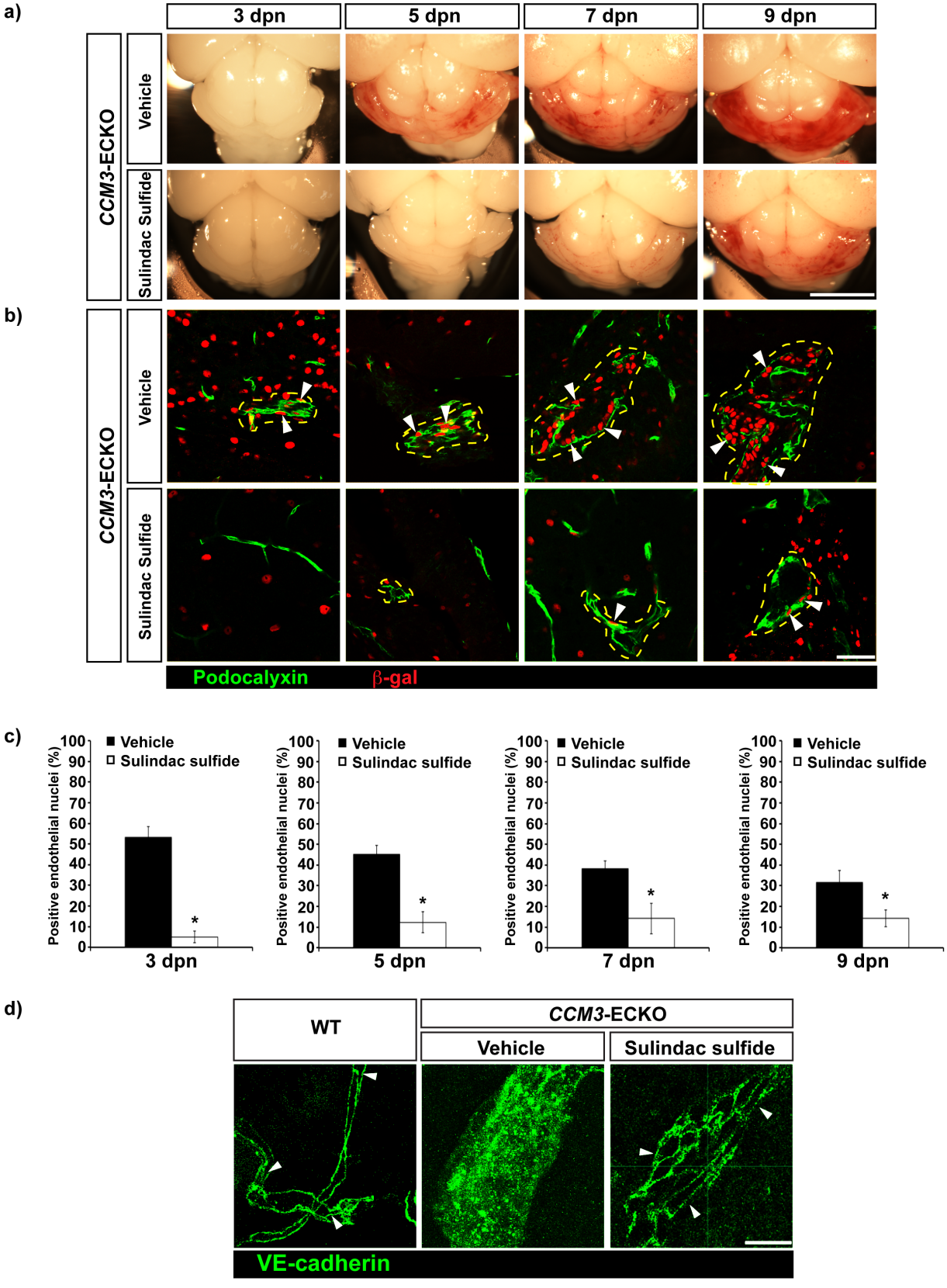
a)
3 dpn
5 dpn
7 dpn
9 dpn
CCM3-ECKO
Vehicle
Sulindac Sulfide
b)
CCM3-ECKO
Vehicle
Sulindac Sulfide
Podocalyxin
β-gal
c)
Positive endothelial nuclei (%)
Vehicle
Sulindac sulfide
3 dpn
5 dpn
7 dpn
9 dpn
d)
WT
CCM3-ECKO
Vehicle
Sulindac sulfide
VE-cadherin

Figure 37. **Sulindac sulfide inhibits β-catenin transcription activity and induces re-localization of VE-cadherin to adherens junctions from diffused distribution in endothelial cells in brain vessels of *CCM3*-ECKO mice. (a)** Representative macroscopic appearance of *CCM3*-ECKO mice brains following dissection without (vehicle) and with sulindac sulfide treatment in pups at different time points. Scale bar, 0.3 cm. **(b)** Representative immunostaining for β-gal (red) as reporter of β-catenin transcription activity in Podocalyxin-positive (endothelial) cells (green) in brain sections without (vehicle) and with sulindac sulfide treatment of the *CCM3*-ECKO mice at different time point. Arrowheads, β-gal positive nuclei. Scale bar, 50 μm. **(c)** Sulindac sulfide mediated inhibition of nuclear β-gal reactivity at different pup ages was quantified, * p, <0.05. (**d)** Sulindac sulfide-mediated re-localization of VE-cadherin (green) from diffused distribution to cell-to-cell junctions (arrowheads) in these blood-vessel *CCM3*-ECKO endothelial cells, for a distribution similar to matched WT mice (right panel, arrowheads). Sections in (**d**) are from 9 dpn littermate pups. Scale bar, 25 μm.

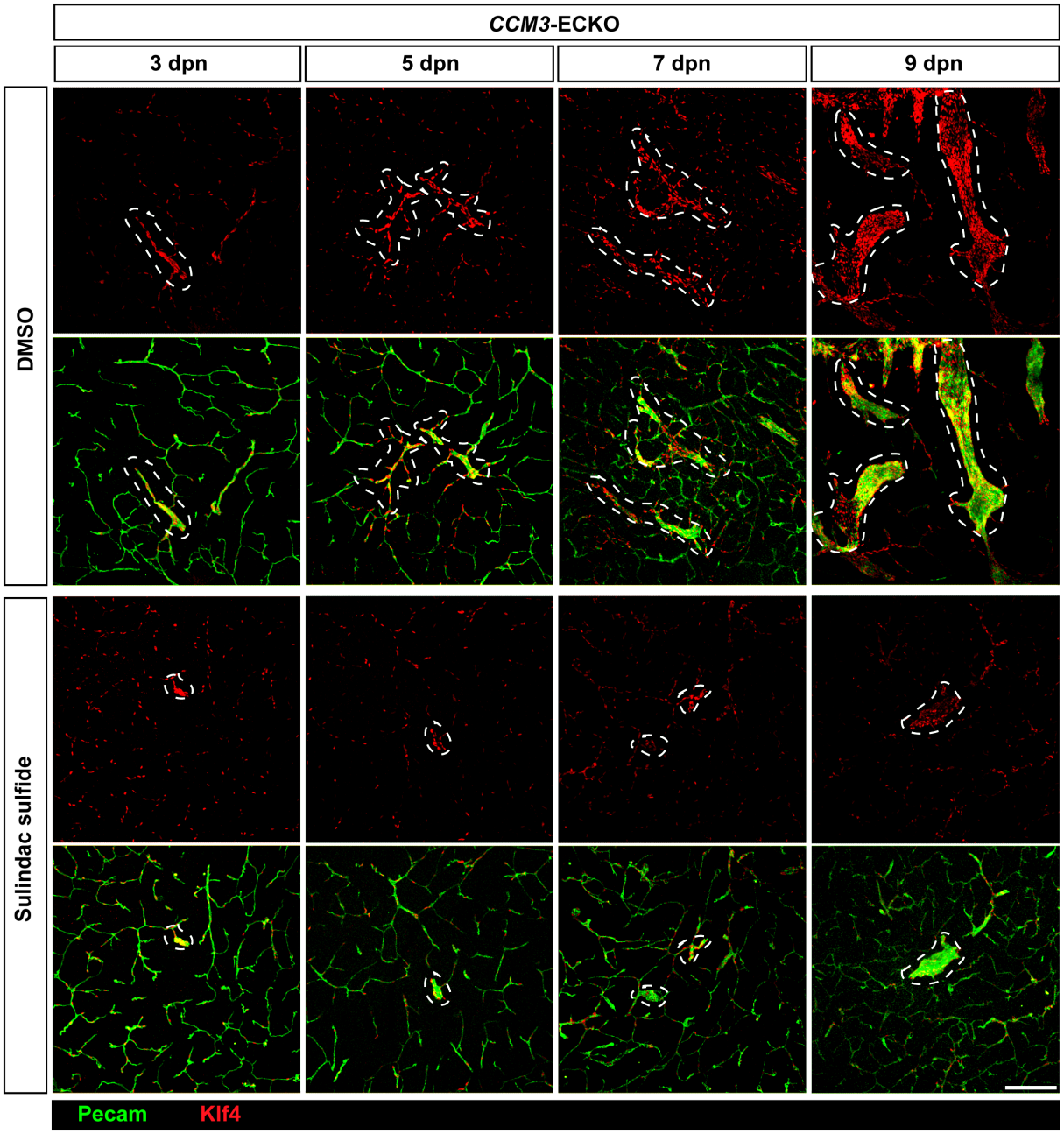

Figure 38. **Sulindac sulfide inhibits overexpression of Klf4 in endothelial cells of brain vessels of *CCM3*-ECKO mice.** Representative immunostaining for effects of sulindac sulfide on Klf4 (red) expression in endothelial cells (Pecam positive) of *CCM3*-ECKO mice brain vessels (green) at different ages after CCM3 ablation. Dashed lines delineate CCM lesions. Scale bar, 700 μm.

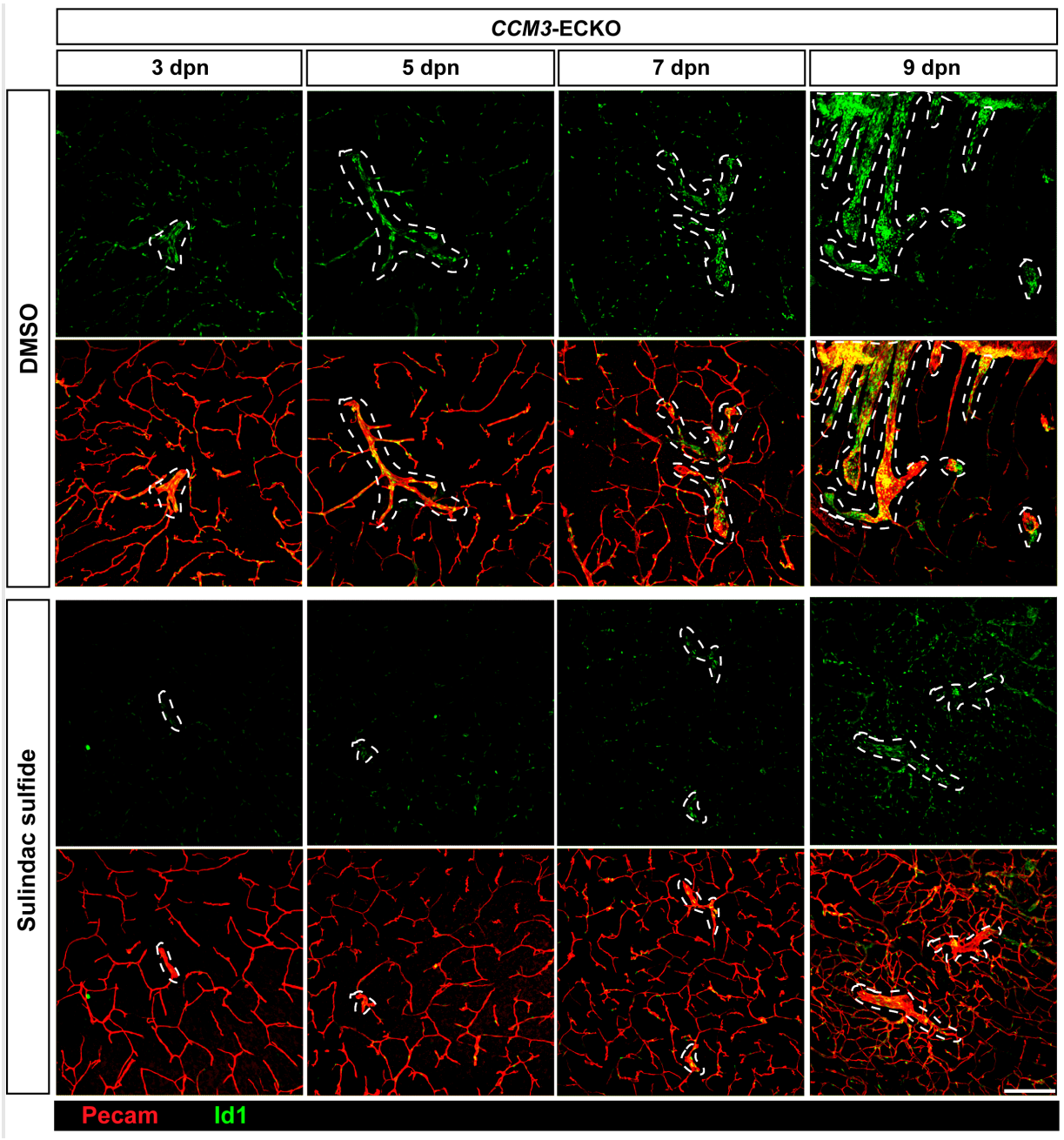

Figure 39. **Sulindac sulfide inhibits overexpression of Id1 in endothelial cells of brain vessels of *CCM3*-ECKO mice.** Representative immunostaining for effects of sulindac sulfide on Id1 (green) expression in endothelial cells (Pecam positive) of *CCM3*-ECKO mice brain vessels (red) at different ages after CCM3 ablation. Dashed lines delineate CCM lesions. Scale bar, 700 μm.

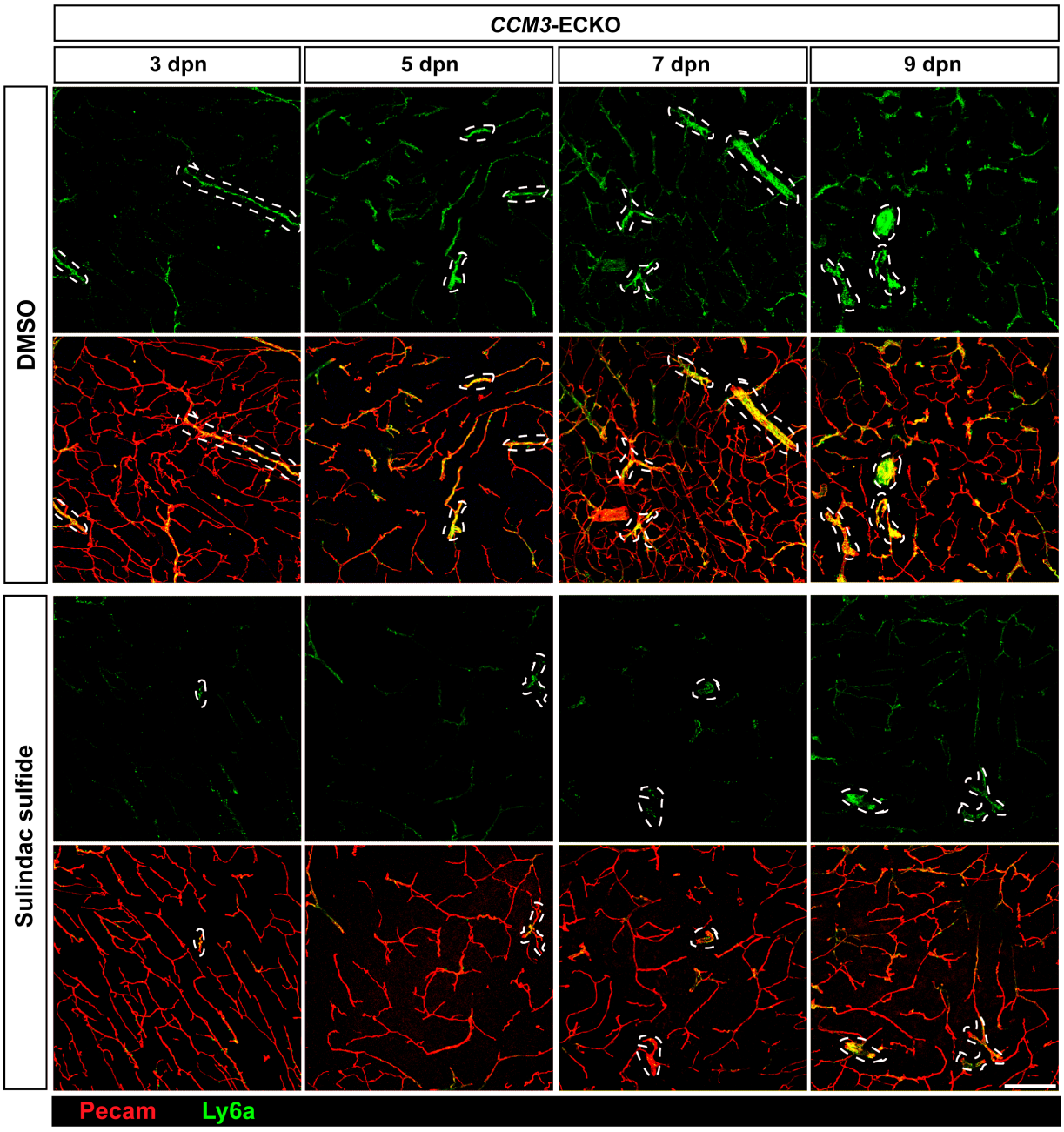

Figure 40. **Sulindac sulfide inhibits overexpression of Ly6a in endothelial cells of brain vessels of *CCM3*-ECKO mice.** Representative immunostaining for effects of sulindac sulfide on Ly6a (green) expression in endothelial cells (Pecam positive) of *CCM3*-ECKO mice brain vessels (red) at different ages after CCM3 ablation. Dashed lines delineate CCM lesions. Scale bar, 700 μm.

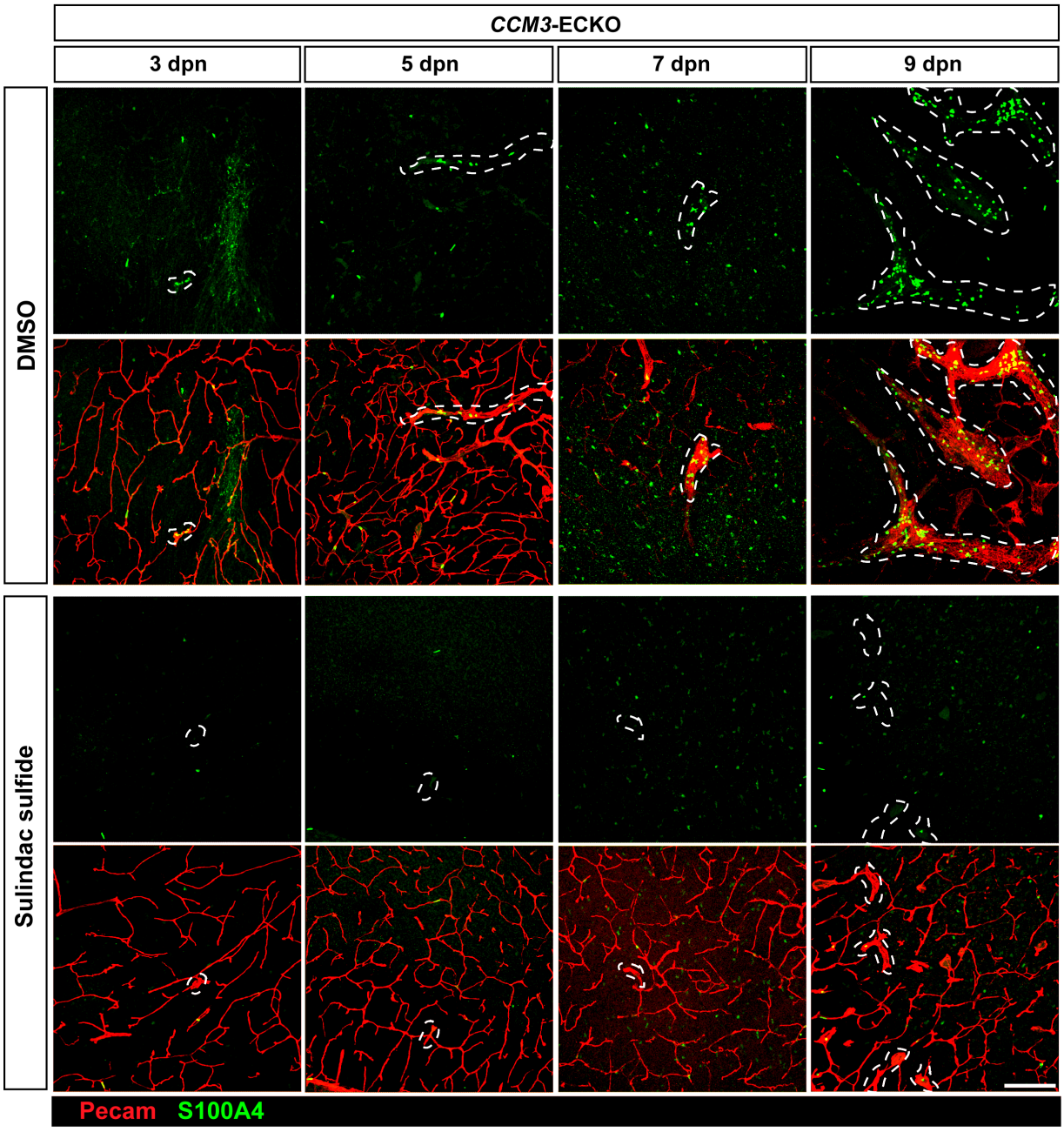

Figure 41. **Sulindac sulfide inhibits overexpression of S100a4 in endothelial cells of brain vessels of *CCM3*-ECKO mice.** Representative immunostaining for effects of sulindac sulfide on S100a4 (green) expression in endothelial cells (Pecam positive) of *CCM3*-ECKO mice brain vessels (red) at different ages after CCM3 ablation. Dashed lines delineate CCM lesions. Scale bar, 700 μm.

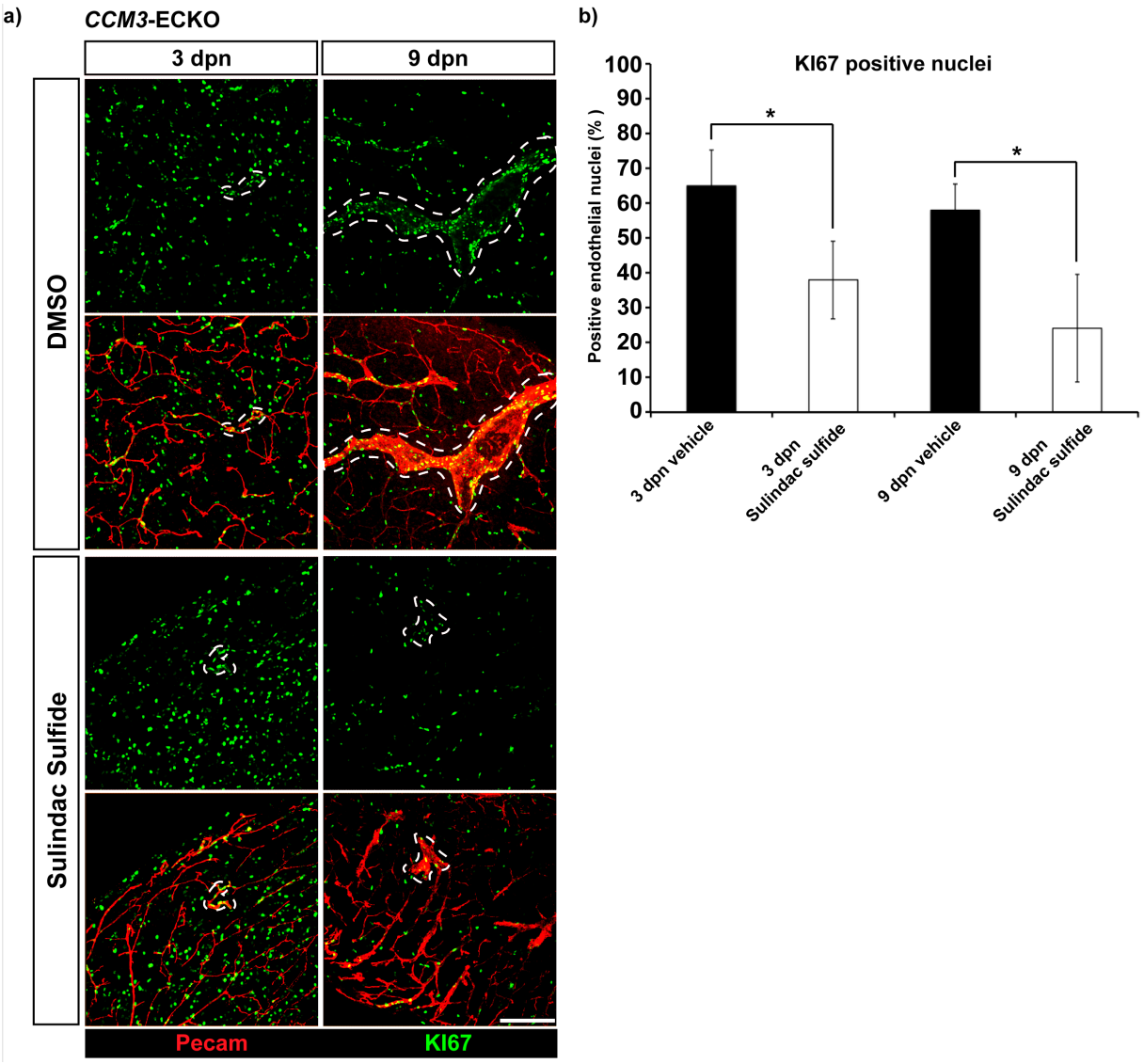

Figure 42. **Sulindac sulfide inhibits proliferation in endothelial cells of brain vessels of *CCM3*-ECKO mice.** Representative immunostaining of the effects of sulindac sulfide on proliferation (**a**) quantified (**b**) as percentage of KI67 endothelial positive nuclei (green) inside lesions in *CCM3*-ECKO mice brain at 3 and 9 dpn. Endothelial cell nuclei were counted in 50 random fields at 63× magnification in brain sections from 5 *CCM3*-ECKO mice and 5 WT mice at both time points respectively (see Materials and Methods). Vessels are in red. Scale bar, 700 μm. *, $p<0.05$ sulindac sulfide treatment *versus* vehicle treated mice.

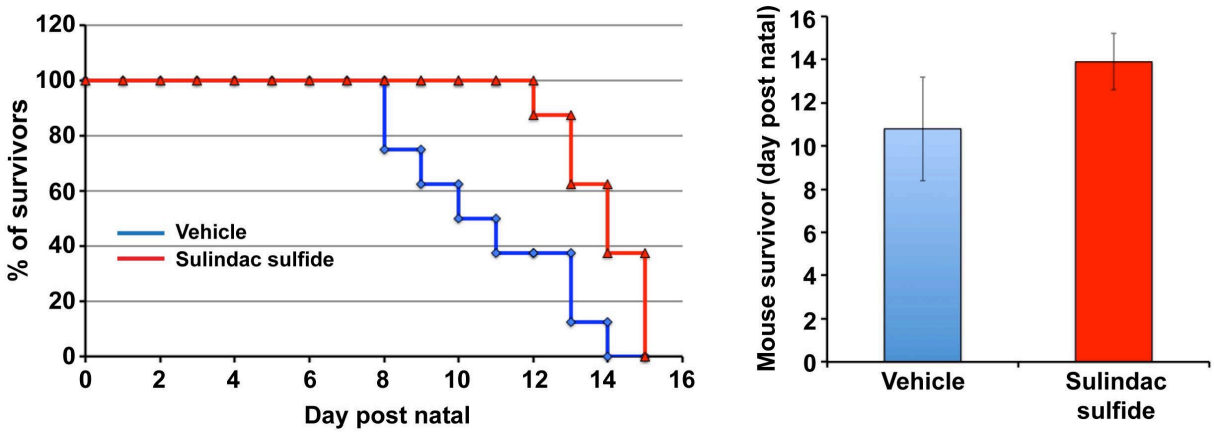

Figure 43. **Sulindac sulfide fails to prolong the survival *CCM3*-ECKO mice.** Survival of *CCM3*-ECKO mice treated or not with sulindac sulfide is reported (as days of survivor after *CCM3* deletion). **a**) Kaplan-Meier curves for mice survival after Sulindac sulfide treatment. **b**) Mean and SD is shown. Although there was a trend for sulindac sulfide treated mice to live longer, no statistical significance was achieved (t-test).

Sulindac sulfide reduces development of vascular lesions in the brain and retina of the CCM3-ECKO mice

A crucial aspect of our study is whether inhibition of β-catenin signaling by sulindac sulfide may also reduce the vascular lesions in *CCM3*-ECKO pups. We found that, indeed, the mean number and size of vascular lesions were reduced by sulindac sulfide treatment. As illustrated in the immunostaining in **Fig.44a** and quantified in **Fig.44b**, the mean number (±SD) of vascular lesions per brain in the vehicle-treated *CCM3*-ECKO pups was 166.8 ±22, with 72.6 ±9 vascular lesions with sulindac sulfide treatment ($p<0.005$; non-parametric Wilcoxon signed-rank test) and the mean maximal diameter of mulberry lesions (±SD) in the vehicle-treated *CCM3*-ECKO pups was 386 ±56 μm and 244 ±38 μm with sulindac sulfide treatment ($p<0.05$, t-test). Sulindac sulfide treatment did not significantly reduce the maximal diameter of single cavernae.

Sulindac sulfide treatment also inhibited the vascular malformations in the retina of *CCM3*-ECKO mice. In these mice the retinas show multiple-lumen vascular lesions that are

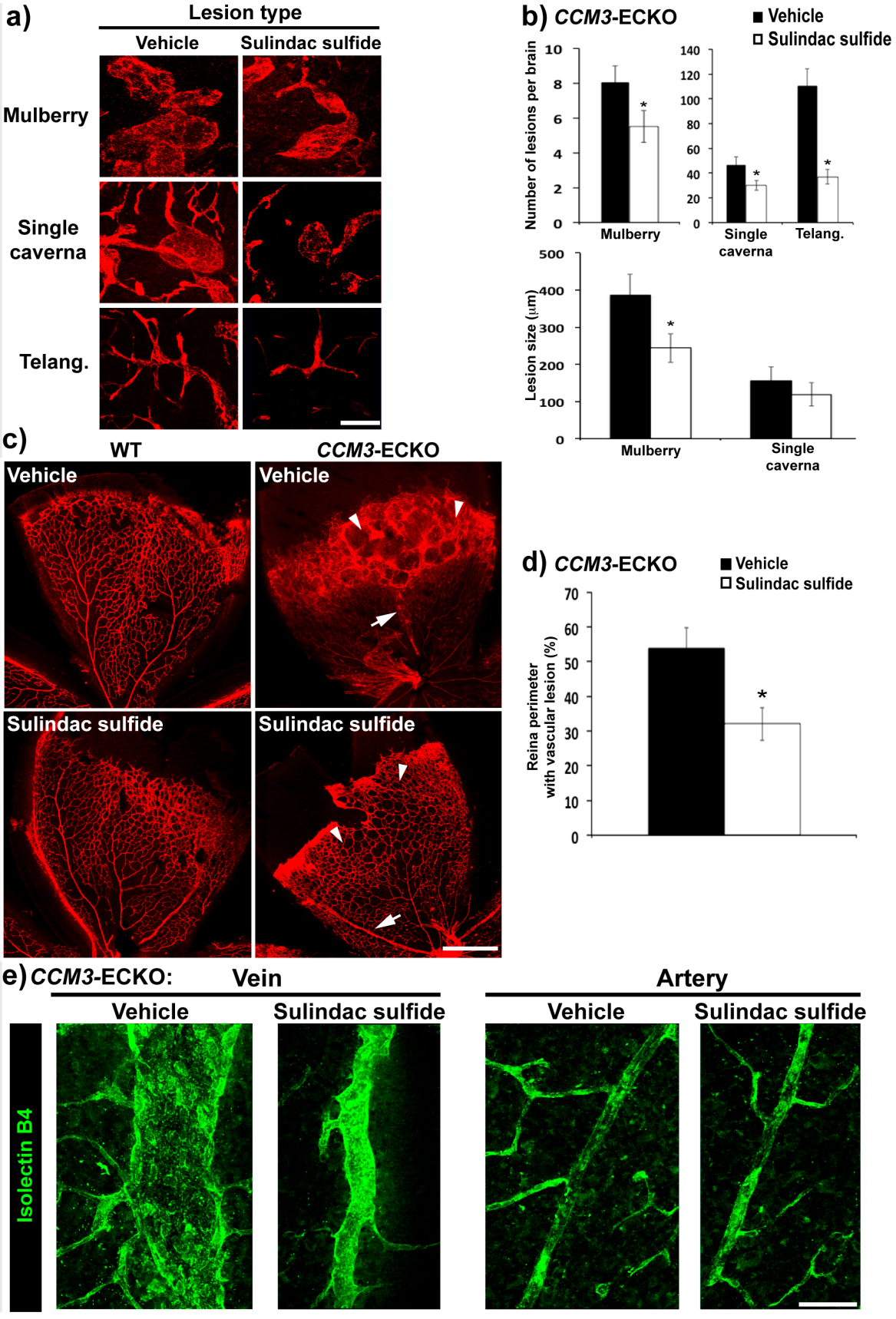
a)
Lesion type
Vehicle
Sulindac sulfide
Mulberry
Single caverna
Telang.
b) CCM3-ECKO
Vehicle
Sulindac sulfide
Number of lesions per brain
Mulberry
Single caverna
Telang.
Lesion size (μm)
Mulberry
Single caverna
c)
WT
CCM3-ECKO
Vehicle
Vehicle
Sulindac sulfide
Sulindac sulfide
d) CCM3-ECKO
Vehicle
Sulindac sulfide
Reina perimeter with vascular lesion (%)
e) CCM3-ECKO:
Vein
Artery
Vehicle
Sulindac sulfide
Vehicle
Sulindac sulfide
Isolectin B4

Figure 44. **Sulindac sulfide reduces the vascular malformations of *CCM3*-ECKO mice.** (**a**) Representative immunostaining of vascular lesions of brain sections without (vehicle) and with sulindac sulfide treatment of *CCM3*-ECKO mice, as mulberry (multiple cavernae), single caverna and telangiectases (Telang.). Lesions classified as in[179]. (**b**) Top panels: quantification of brain lesions as illustrated in (**a**) (see Materials and methods for details). Littermates (9 dpn pups) from five independent litters: vehicle treated (n=8) or sulindac sulfide treated (n=7). *, $p<0.005$, Wilcoxon signed-rank test. Bottom panel: quantification of brain lesion sizes (mm, see Materials and Methods). *, $p<0.05$, t-test. (**c**) Representative immunostaining for Pecam (red; endothelial cells) of vessels in the retina of WT and *CCM3*-ECKO mice (9 dpn littermate pups) treated without (vehicle) and with sulindac sulfide. Multiple-lumen vascular lesions (arrowheads) develop from veins (arrow). Sulindac sulfide (bottom right) reduces the malformations (arrowheads) and vein diameter (arrow), (see also **e**). (**d**) Quantification of the retina vascular lesions illustrated in (**c**) as percentages of retinal perimeter affected by vascular lesions (n=14 for both vehicle and sulindac sulfide, see Materials and methods). *, $p<0.05$, t-test. (**e**) Representative immunostaining of the retina vascular lesions illustrated in (**c**). As well as the peripheral vascular malformations, sulindac sulfide induced reductions in vein diameters (see text for details). Arteries of these *CCM3*-ECKO mice do not show this aberrant phenotype (endothelial cells isolectin B4-labelling: green) Scale bars, 100 μm (**a**); 700 μm (**c**); 60 μm (**e**).

particularly concentrated at the periphery of the vascular network. Such lesions develop from veins, which are enlarged, although straight. Sulindac sulfide partially normalized this aberrant vascular network in *CCM3*-ECKO mice (**Fig.44c** and **44d**). In addition, the enlargement of the most internal tract of the veins that characterizes the retinas of these *CCM3*-ECKO mice was inhibited after sulindac sulfide (89.5 ±7.1 μm in vehicle-ECKO *versus* 35 ±7.8 μm in sulindac sulfide-ECKO, mean ±SD of 30 measurements in 14 retinas each for WT and KO) (**Fig.44e** and **Fig.45**). At variance, arteries do not show this aberrant phenotype (**Fig.44c** and **44e**).

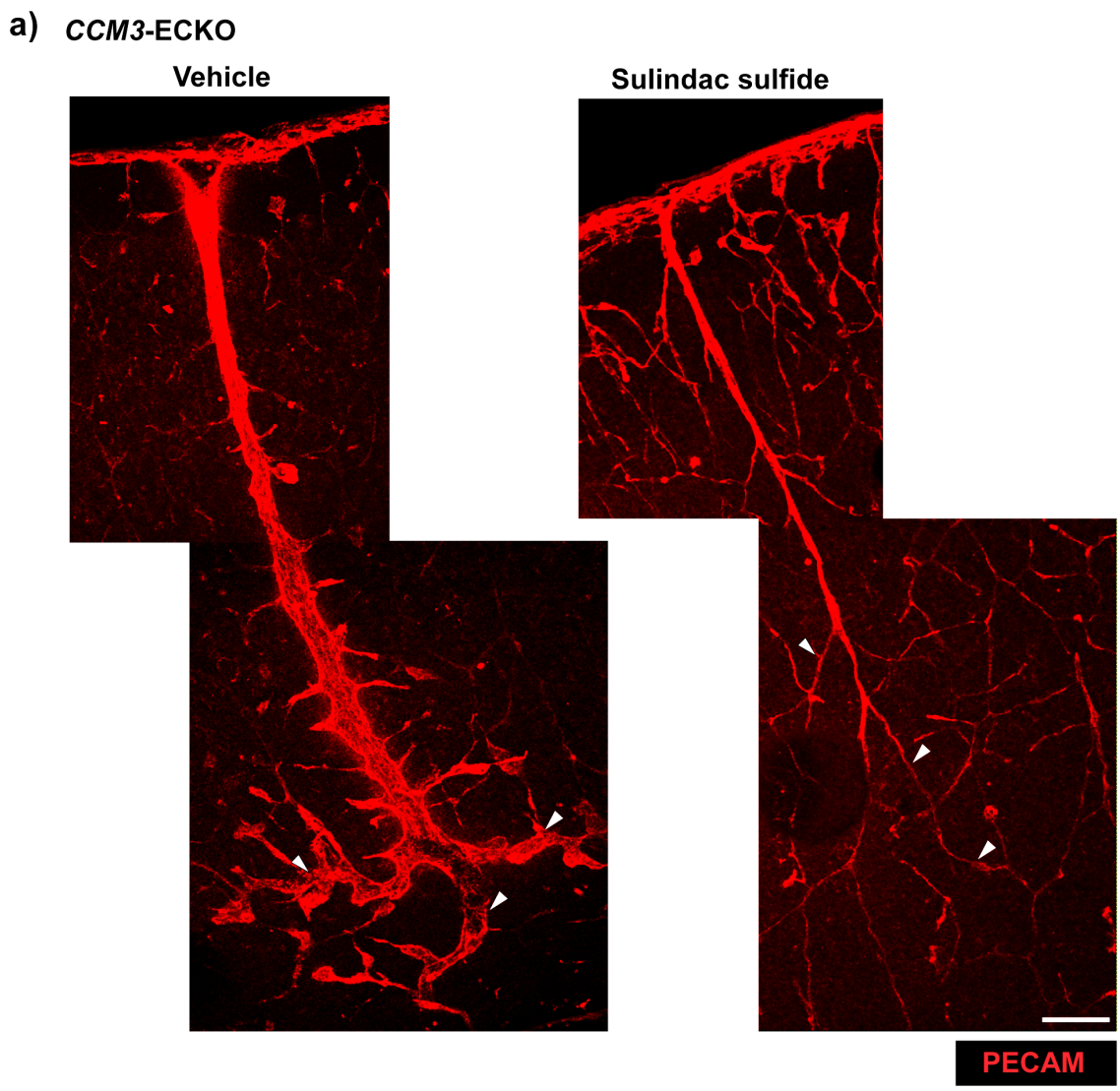

Figure 45. **Sulindac sulfide reduces the diameter of abnormally enlarged vessels in *CCM3*-ECKO mice show.** *CCM3*-ECKO pups (at 9 dpn) treated (from 2 dpn) with vehicle or sulindac sulfide, as described in the Materials and Methods, show sulindac sulfide reduction of the malformations in cerebral vessels. Representative immunostaining of brain sections with Pecam (red, endothelial cells). Vessels of the superior sagittal sinus that enters the brain from the dorsal surface. With the *CCM3*-ECKO (Vehicle), the straight vessels with large diameters are seen to terminate in budding branches that form cavernae. In a comparable vessel, sulindac sulfide treatment in this *CCM3*-ECKO mice greatly reduces the diameters of these vessels and promotes apparently normal terminal branching. The panels show maximal projections of confocal optical sections of samples acquired at 20× magnification. Scale bar, 100 μm.

Sulindac sulfone reduces both β-catenin transcription activity and the expression of EndMT markers in endothelial cells of CCM3-ECKO mice

The data reported above strongly suggest that sulindac sulfide may have a therapeutic activity in CCM patients. However, it has been reported that this drug inhibits cycloxygenease in platelets possibly increasing the risk of hemorrhage. We therefore tested sulindac sulfone, which is devoid of anti-cyclooxygenase activity[196] and does not have an impact on coagulation response. As observed after sulindac sulfide treatment, sulindac sulfone also reduced the nuclear accumulation of active β-catenin and restored cell-to-cell junctions in cultured *CCM3*-knockout endothelial cell line (**Fig.46**). In addition, sulindac sulfone inhibited the expression of β-catenin target genes, (see for instance Klf4 and S100a4 in **Fig.46**), as did sulindac sulfide (see above). When tested *in vivo*, sulindac sulfone reduced the number of lesions in the brain of the *CCM3*-ECKO mice to a level comparable to sulindac sulfide (the mean number of lesions per mouse brain (±SD) in the untreated control was 153.5 ±28 and was reduced to 68.6 ±10 with sulindac sulfone treatment, $p<0.01$; non-parametric Wilcoxon signed-rank test) (**Fig.47a and 47b**). In addition, *in vivo*, in the endothelium of brain vessels of the *CCM3*-ECKO mice, sulindac sulfone inhibited the expression of Klf4 and S100a4 (**Fig.47c**).

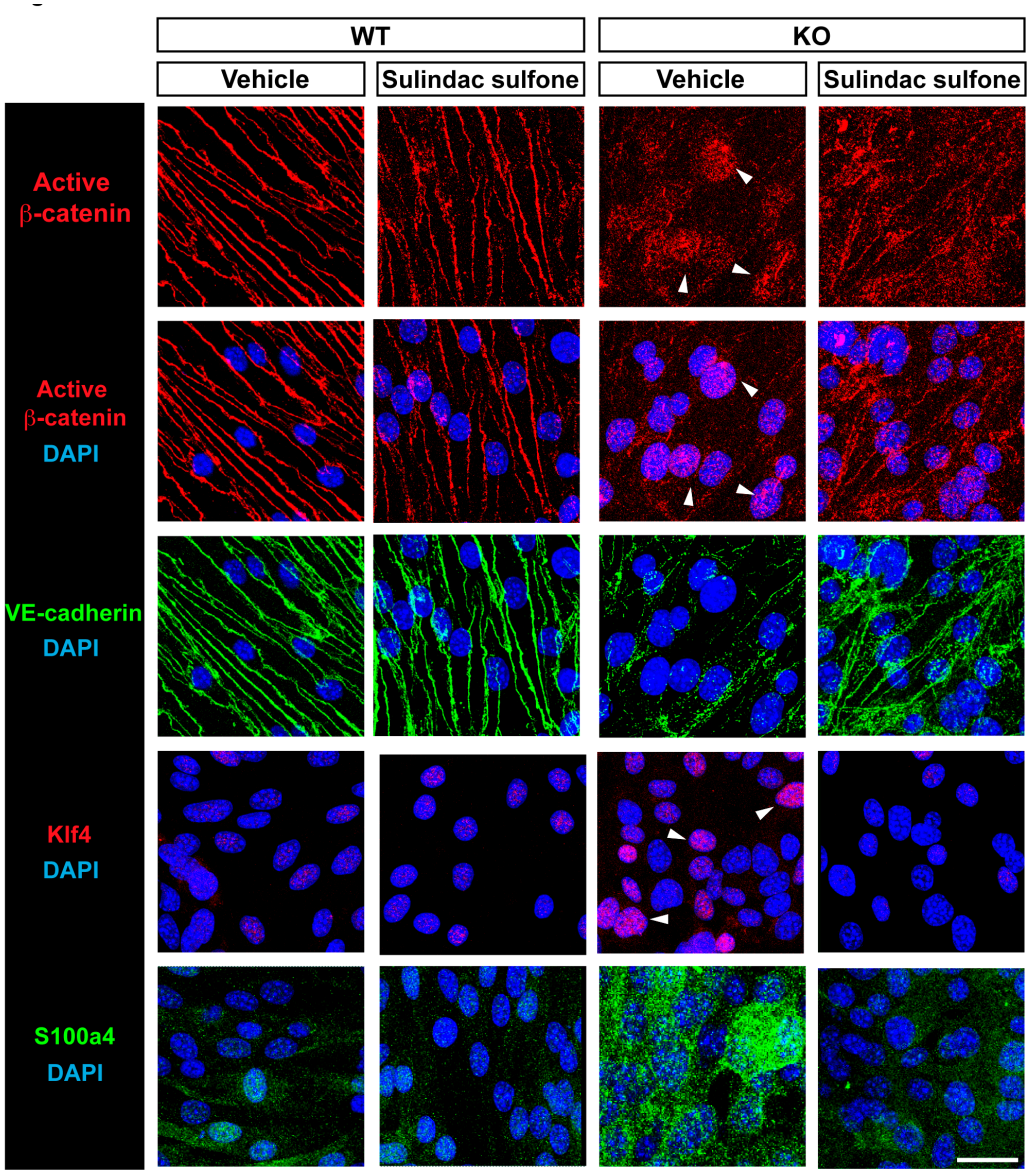

Figure 46. **Sulindac sulfone inhibits the transcription of β-catenin target genes and induces the re-localization of active β-catenin from the nucleus to adherens junctions in *CCM3* null endothelial cells in culture.** Similar to the effects of sulindac sulfide, *CCM3*-knockout (KO) endothelial cell line show sulindac sulfone inhibition of loss of active β-catenin and VE-cadherin from cell-to-cell contacts (adherens junctions), of accumulation of active β-catenin in the nucleus, and of overexpression of EndMT markers. Representative immunostaining showing that the loss of active β-catenin (red) from cell-to-cell contacts (top row) and its relocalization to the nucleus (second row) in these *CCM3*-knockout endothelial cells (Vehicle, arrowheads) was inhibited by sulindac sulfone treatment. Nuclei were stained with DAPI (blue). Similarly, VE-cadherin (green) loss from cell-cell contacts was inhibited by sulindac sulfone treatment (third row). Overexpression of Klf4 (red; nuclear, Vehicle, arrowheads) and S100a4 (green; cytoplasmic and nuclear) in *CCM3*-knockout endothelial cells was also strongly reduced by sulindac sulfone treatment (bottom rows). Scale bar, 30 μm.

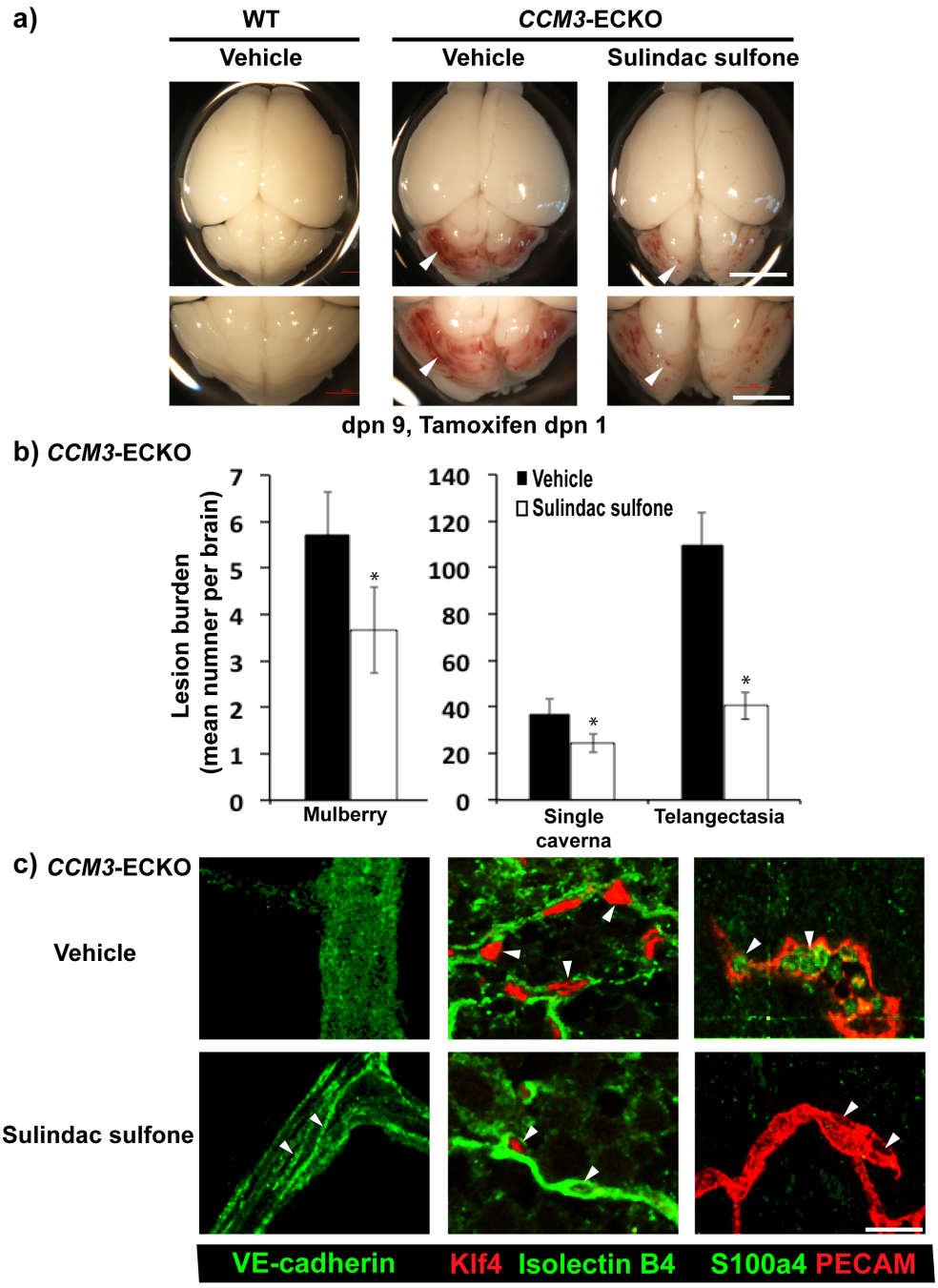

Figure 47. **Sulindac sulfone reduces the vascular lesions in the brain and retina vessels of *CCM3*-ECKO mice.** Similar to the effects of sulindac sulfide *CCM3*-flox/flox–Cdh5(PAC)-CreERT2–BAT-gal (*CCM3*-ECKO) mice show sulindac sulfone reduction of the malformations in cerebral vessels. These mice were treated with Tamoxifen (10 mg/kg body weight, as described in Materials and Methods) at 1 dpn to induce endothelial-cell-selective expression of Cre recombinase and recombination of the flox/flox *CCM3* gene (*CCM3*-ECKO mice). They were also treated with vehicle or with sulindac sulfone (30 mg/kg) daily, starting from 2 dpn. (**a**) The macroscopic appearance of the 9 dpn mouse pup brains following dissection showed evident lesions in the cerebellum of the *CCM3*-ECKO mice (arrowheads). Scale bar, 0.65 cm. Lower panels: Further magnification of the cerebellum. Scale bar, 0.3 cm. (**b**) Quantification of mean brain lesions as the mulberry (multiple lumens), single caverna, or telangiectases lesions in the entire brains (as described in[179], see Materials and Methods) from

five vehicle-treated and five sulindac sulfone-treated *CCM3*-ECKO mice. The brains were sectioned along the sagittal axis (150 mm sections, vibratome), immunostained for Pecam (endothelial cells) and examined by wide-field fluorescence microscopy (10× and 20× magnification). *, p = 0.0053, 0.006, 0.004 for mulberry, single caverna and telangiectase lesions, respectively (Wilcoxon test). (**c**) Representative immunostaining of localization of VE-cadherin, Klf4 and S100a4. Left: from the diffuse state of VE-cadherin (green) in vehicle-treated *CCM3*-ECKO mice, sulindac sulfone restored its localization to cell-to-cell junctions (arrowheads). Middle, right: from the nuclear staining for the expression of Klf4 (middle, red) S100a4 (right, green) in vehicle-treated *CCM3*-ECKO mice, sulindac sulfone reduced this nuclear reactivity for both Klf4 and S100a4. Scale bar, 15 μm.

DISCUSSION

In the present study we investigated the molecular mechanisms behind the development of the vascular disease known as Cerebral Cavernous Malformation (CCM) and we found that endothelial-cell-selective deletion of the *CCM3* gene activates β-catenin transcription signaling *in vivo* in brain ECs. Activation of such signaling pathway appears to play a crucial role in the establishment of vascular malformations in *CCM3* null mice. Indeed, pharmacological inhibition of β-catenin transcriptional activity with the NSAIDs sulindac sulfide and sulindac sulfone reduces the number and dimension of cerebral and retinal vascular malformations in this murine model suggesting that β-catenin transcription signaling in ECs contributes to the pathogenesis of CCM3-mediated vascular lesions.

Definition of murine model of CCM3 pathology

Here, we report that endothelial cell-selective deletion of the *CCM3* gene in mice is able to recapitulate the human pathology as it produces hemorrhagic vascular malformations in the brain, cerebellum and retina. Previous work demonstrated that constitutive endothelial-selective inactivation of *CCM3* gene is embryonically lethal with general angiogenic defects[150]. For this reason we established a model in which *CCM3* gene is deleted postnatally taking advantage of a Cre-lox Tamoxifen inducible system (*CCM3*-ECKO mice). This is also the first report of endothelial cell-selective inactivation of *CCM3* after birth. With this model we have been able to confirm the pathological phenotype observed for *CCM1* and *CCM2* endothelial-specific inducible KO obtained with a very similar protocol linking also in mice the absence of any of the three CCM genes with the same pathological phenotype. Using this tool we have been able to confirm the implication of EndMT in CCM pathogenesis previously observed in *CCM1* KO mice demonstrating the relevance of such process in the familial CCM.

To a microscopic analysis CCM lesions in *CCM3*-ECKO mice are characterized by clusters of enlarged sinusoids (caverns) lined by a thin layer of hyper-proliferative ECs. The fragility of the endothelium within the lesions reflects a compromised BBB responsible for vessels leakiness and breaks, which can lead to intracranial hemorrhages. Since CCM genes are widely expressed in different type of tissues, these findings highlight the importance of CCM genes in endothelial physiology and in particular in brain vasculature.

An important aspect of this work is that since *CCM3*-ECKO mice develop vascular malformations in the central nervous system in short time, this model provides a tool for testing pharmacological treatments.

β-catenin transcription signaling contributes to the pathogenesis of CCM3-mediated vascular lesions

In a recent work we have shown that CCM lesions in a *CCM1*-ECKO mice model develop through the process of endothelial-to-mesenchymal transition (EndMT) and that Tgfβ/Bmp pathway significantly contributes to this process[128]. Here we demonstrated that Tgfβ/Bmp pathway is enhanced also in *CCM3*-ECKO mice but only at late stages of lesion development (9 dpn). In parallel, we found that the activation of β-catenin-mediated transcription is a very early event in lesion formation and it is already high in *CCM3*-ECKO mice brain vessel ECs at 3 dpn when lesions start to appear. However, the expression of EndMT markers, checked as readout of EndMT process, is already increased at very early time point (3 dpn) in ECs of the lesions in comparison to WT vessels.

These findings led us to hypothesize that the activation of β-catenin signaling could represent the first driving event that initiates CCM lesions and activates the mesenchymal transcriptional program. In contrast, Tgfβ/Bmp signaling become hyper-activated only relatively late (increase of nuclear p-Smad1 in ECs of 9 dpn pups) and contributes to the

progression of the pathology. Interestingly, also pseudo-normal vessels of the brain in *CCM3*-ECKO mice show higher levels of β-catenin mediated transcription in comparison to WT vessels even if no regional preference has been observed. Anyway, this is suggestive of the fact that β-catenin signaling is activated in vessels before the onset of phenotype. Moreover, at early stages the over expression of EndMT markers in ECs lining CCM lesions correlates with expression of β-gal. This positive correlation is very high at 3 dpn while it decreases at late stages. To such reduction contributes also the fact that the percentage of β-gal positive nuclei in a lesion decreases at later stages, while EndMT markers positive nuclei increase.

Using *in vitro* model of *CCM3* null ECs we demonstrated that β-catenin signaling is directly implicated in the regulation of EndMT marker genes in these models. Indeed, some β-catenin targets and EndMT markers are activated through β-catenin transcription signaling under basal conditions in the *CCM3*-knockout ECs, as their expression is inhibited by a dominant-negative Tcf4. Consistently, in another model the constitutive activation of nuclear β-catenin shows increased expression of some EndMT markers linking β-catenin transcriptional activity with EndMT regulation.

CCM malformations develop largely, although not exclusively, in the central nervous systems in patients and in mouse models[143, 146]. Wnt/β-catenin canonical pathway exerts a critical role in angiogenesis and in particular in the determination and specification of the phenotype of ECs at the BBB[74, 77, 78]. However, Wnt signaling must be abrogated postnatally to avoid abnormal vascular proliferation and morphogenesis in the CNS[74, 77, 78]. In a model of endothelial specific β-catenin-gain-of-function we observed vascular lesions in the retina comparable to those observed here in *CCM3*-ECKO[28]. In tumor cells, the sustained induction of canonic Wnt signaling is associated to increased growth and invasion[57, 197]. In particular,

upon activation of β-catenin-mediated transcription, carcinoma cells switch from an epithelial-to-mesenchymal phenotype (EMT) [57, 197].

These findings support the hypothesis that β-catenin signaling is important for initiation of the EndMT, while other signaling pathways, such as Tgfβ/Bmp, can sustain further steps of lesion progression.

How is β-catenin signaling up regulated in CCM3 null endothelial cells?

Deregulated β-catenin signaling in CCM could be supported by either endothelial-autonomous activation of the Wnt/β-catenin pathway or by abnormal responses of mutated ECs to environmental Wnt, or by a combination of the two. Our data indicate that at least the first of these mechanisms appears to operate in ECs in culture after ablation of the *CCM3* gene.

Evidences in cultured cells point to cell-autonomus activation of β-catenin signaling. Indeed, we didn't find abnormal activation of upstream mediators of canonical Wnt/β-catenin pathway (ligand and receptors) nor increased sensibility to Wnt stimuli in *CCM3* null cells in culture. In addition, a high throughput analysis using Affymetrix technique revealed that the transcriptome of *CCM3* null ECs is different from the one of WT cells treated with Wnt3a in the sense that the set of genes altered upon *CCM3* ablation (in particular EndMT markers) is different from the one modified in response to Wnt3a stimulus (see appendix table1). Moreover, both WT and *CCM3* null cells respond with the same relative fold change to Wnt3a stimulus. These data reinforce the hypothesis that the abnormal β-catenin signaling that we observed in *CCM3* null ECs is different from the canonical Wnt/β-catenin signaling induced by Wnt in WT ECs.

Nuclear accumulation of active β-catenin appears to be a significant characteristic of the mutated genotype, although we do not have direct indications of the processes that drive the β-catenin concentration into the nucleus of the *CCM3*-knockout ECs. In general, the issue of the molecular mechanisms that regulate nuclear accumulation of β-catenin remain virtually unknown (for review, see[57]).

Concomitant with the accumulation into the nucleus, we observed that β-catenin dissociates from cell-to-cell junctions in both our *in vitro* and *in vivo* models of endothelial-cell-specific deletion of *CCM3*. Junctional β-catenin is mostly associated with VE-cadherin, the transmembrane constituent of the AJs[121], as well as with the β-catenin destruction complex[133]. In the *CCM3*-knockout ECs, the AJs are disorganized, as also observed after ablation of both *CCM1*[117, 120] and *CCM2*[143]. In addition, the β-catenin amount associated with VE-cadherin is reduced here, as it has also been observed after ablation of *CCM1*[117, 201]. We speculate that this decreased association of β-catenin with VE-cadherin is accompanied by accumulation of active β-catenin in the nucleus. This concentration of active β-catenin into the nucleus characterizes conditions of decreased junction stability in ECs, as previously observed in sparse and in VE-cadherin-knockout ECs[123] and as we reproduced using VE-cadherin siRNA. In all of these cases, the total amount of β-catenin is reduced, even to very low levels, although the residual active β-catenin accumulates in the nucleus where it mediates activation of target genes. In particular after VE-cadherin down regulation through siRNA we found that also some EndMT genes start to be up regulated. Inhibition of proteasomal degradation with 'passive' redistribution of active β-catenin into the nucleus appears not to be likely, as the total amount of active β-catenin actually decreases.

Pharmacological approach to inhibit β-catenin signaling and development of CCM3 vascular lesions

The understanding of the molecular mechanisms implicated in CCM pathogenesis is only the first step in the fight against CCM. One of our aims is to lay the foundations for future pharmacological intervention. To this purpose we identified two inhibitors of β-catenin transcription signaling, sulindac sulfide and sulindac sulfone[195, 196], that also inhibit the development of vascular lesions in *CCM3*-ECKO mice.

Sulindac sulfide and sulfone are both able to inhibit β-catenin nuclear translocations upon *CCM3* deletion and subsequent transcription of target genes (canonical targets and non canonical targets such as EndMT markers). Moreover, sulindac sulfide and sulindac sulfone are able, in part, to restore junctions organization, β-catenin association with VE-cadherin and to activate Rap1. Active Rap1 (GTP-bound), which is down regulated in *CCM3*-knockout ECs, has been shown to play a crucial role in junction dismantling after *CCM1* ablation[117] (**Fig.48**).

Sulindac sulfide and sulindac sulfone are both NSAIDs that have significant chemopreventive efficacies against colon cancer in human patients (where β-catenin signaling is hyper-activated), and inhibit tumor progression in experimental models of several types of cancer[198]. The relative efficacy of sulindac sulfide *versus* sulindac sulfone varies depending on the type of cancer[195, 199]. Sulindac sulfone is potentially more interesting than the Sulindac sulfide for therapy of CCM since it lacks anti-platelet activity, which could be detrimental in patients prone to hemorrages. Structural research is very active on sulindac metabolites, to identify chemical modifications (e.g., phosphorylation[200]) that might enhance their activity while reducing their toxicity.

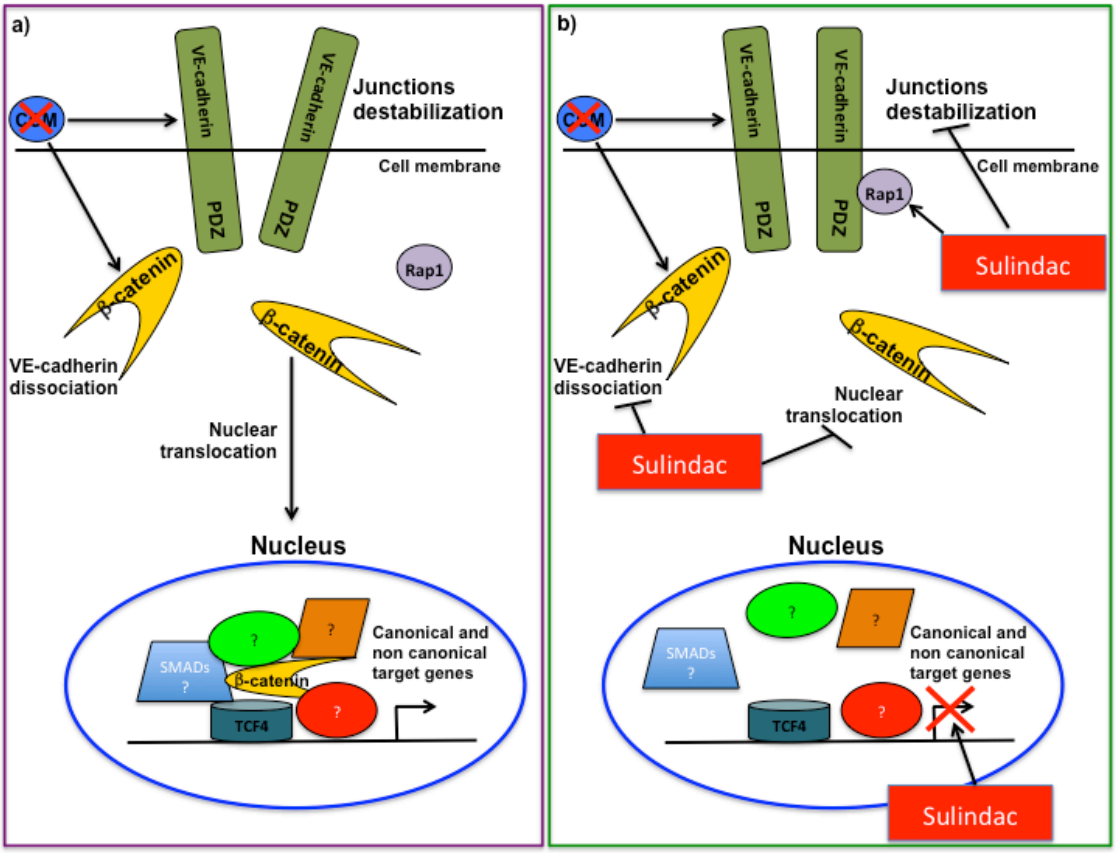

Figure 48. **Schematic representation of key events following CCM deletion and critical points of intervention of sulindac.** (**a**) *CCM3* gene deletion in endothelial cells is associated with adherens junctions dismantling possibly via Rap1 and subsequent β-catenin dissociation from VE-cadherin. Free β-catenin translocates into the nucleus where, in association with Tcf4 and potentially with other transcription factors, regulates canonical and non-canonical (EndMT markers) target genes expression. (**b**) Sulindac treatment (sulfide and sulfone) is able to counteract junction dismantling and to activate Rap1, thus limiting β-catenin nuclear accumulation and subsequently inhibiting β-catenin-mediated transcription.

Which is the relationship between Wnt/β-catenin and Tgfβ/Bmp pathways?

In this work we demonstrated that β-catenin signaling is crucial for the development of *CCM3* vascular malformations since early stages of lesion formation. We previously demonstrated that Tgfβ/Bmp pathway is implicated in CCM progression and EndMT[128] and in the present study we observed that this signaling is likely to intervene in later stages of lesion progression. Various studies report a crosstalk between β-catenin and Tgfβ/Bmp signaling in promoting de-differentiation and EMT. However, it remains still to be investigated whether

cooperation between these two pathways could play a role in the pathogenesis of CCM. β-catenin and Tgfβ/Bmp could cooperate at different levels, in particular at transcriptional level, since Smads and β-catenin can bind to the same promoters[66-68]. In addition, one pathway could activate the other one. For instance we demonstrated that at least Bmp2 is a target gene of β-catenin transcription activity in ECs. Whether Bmp2 can contribute to CCM development and whether this regulation could be important for EndMT still needs to be investigated. However, considering that enhanced β-catenin signaling precedes Tgfβ/Bmp activation during the progression of CCM lesion, we can speculate that β-catenin signaling could, at least in part, activate the Tgfβ/Bmp pathway (see **Fig.49**).

The critical role that both β-catenin and Tgfβ/Bmp pathway play in CCM development is underlined by the fact that inhibitors of both signaling pathways lead to a significant reduction of lesions in murine models of CCM pathology. For this reason it would be interesting to test potential synergistic effect of the two types of treatment on *CCM3*-ECKO mice.

Why CCM arise specifically in CNS? Some speculative hypothesis

Endothelium, such as many others tissues, undergoes a process of maturation and fate specification during development which leads to the acquisition of specific markers and properties fundamental to explain its role in the physiology of the body[4, 5]. However, a great heterogeneity among ECs is necessary in order to fulfill the specific different functions and needs of different organs. The process of differentiation is mediated by different exogenous stimuli coming from the local environment and allowing ECs to enter into a specific specialization program.

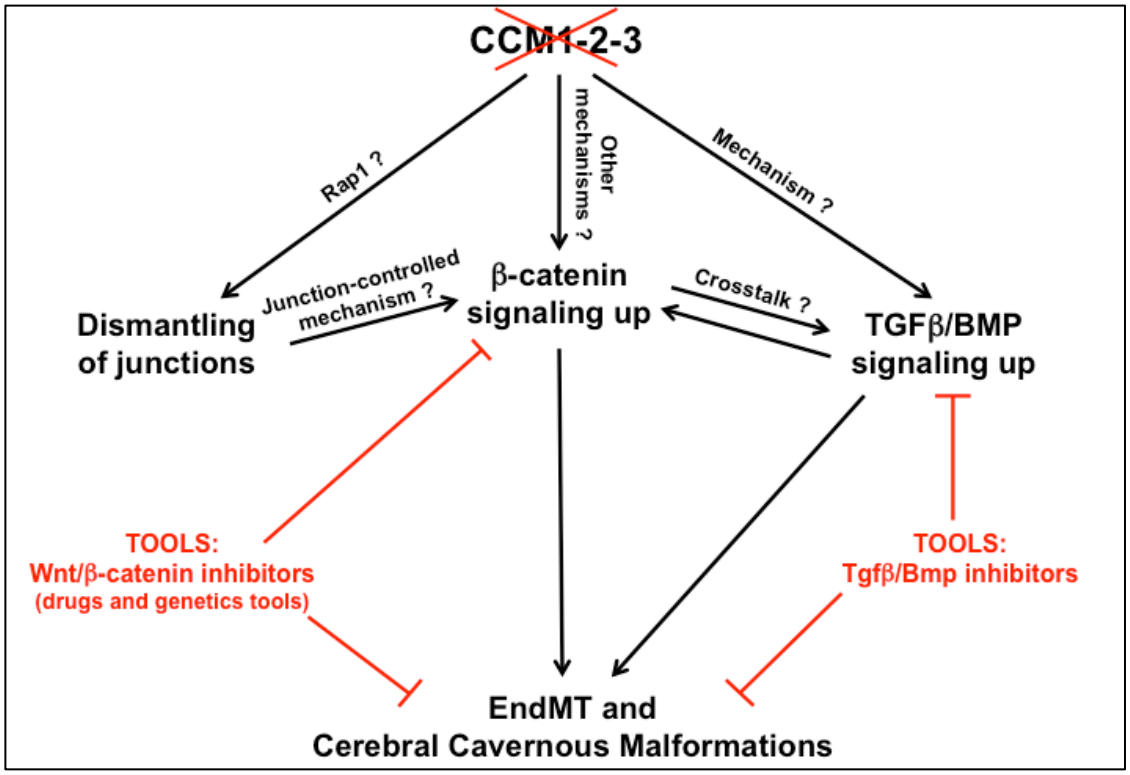

Fig. 49. **Functional model of molecular pathways implicated in CCM3 pathogenesis.** *CCM3* gene deletion in endothelial cells induces enhanced β-catenin signaling through still undefined mechanism, although junctions dismantling via Rap1 is likely involved. In parallel, *CCM3* ablation induces up regulation of Tgfβ/Bmp signaling via unknown mechanism. β-catenin signaling can induce Bmp2 expression, but other points of crosstalk between the two pathways are possible. Both β-catenin and Tgfβ/Bmp signaling contribute to EndMT and CCM development thus pharmacological tools to inhibit these pathways could be employed for CCM treatment also in human patients.

For this reason it is not surprisingly that some pathologies such as CCM arise in certain specific regions, probably reflecting impairment of local molecular and physiological properties[34, 35]. In particular CCM seems to arise specifically in the vasculature of the CNS, the BBB, which is an extremely peculiar vascular entity[49, 143]. Indeed, BBB is unique under different point of view and many factors are responsible for its determination[47]. One of the most relevant is Wnt/β-catenin pathway[77]. It is known that this signaling pathway needs to be finely regulated both in time and levels and any alterations of these parameters can lead to major vascular malformations. In the present work we demonstrated that β-catenin signaling is

up regulated in ECs lacking *CCM3* both *in vitro* and *in vivo*. Thus, a reasonable hypothesis is that CCM lesions originate from de-regulated expression (kinetics and location) of β-catenin signaling in ECs of brain vessels.

Besides its crucial role in BBB angiogenesis, β-catenin signaling is important in other cell types for stem cell maintenance and differentiation[181, 197]. One of the process that we found to be critical for CCM is EndMT, a process of de-differentiation in which ECs lose their mature phenotype to acquire a mesenchymal one[128, 135, 137]. Here we demonstrated that β-catenin is able to mediate this process in ECs upon *CCM3* deletion. We can therefore speculate that up regulation of β-catenin signaling in *CCM3* null ECs in brain induces from one side abnormal angiogenesis and from the other a mesenchymal transition with subsequent loss of peculiar barrier functions. All together this events can contribute to the manifestation of CCM phenotype predominantly in the CNS.

Anyway, not all the vessels in *CCM3*-ECKO brain develop vascular lesions. It has recently been reported in retina and brain ECs that activation of the canonical Wnt pathway by Norrin/Frizzled4 induces development and maintenance programs through both cell-autonomous and cell-non-autonomous signaling[82]. This can explain local vascular phenotypes in different regions of the central nervous system[82]. It is true that different areas in the brain are subjected to different factors and different regulation, but is also true that no preferential association of lesions development with defined anatomical regions has been observed[145, 146].

Glading and Ginsberg[117, 201] reported similar activation of β-catenin transcription activity in bovine aorta ECs and primary human arterial ECs in culture after depletion of CCM1 using RNA interference. They also reported inhibition of β-catenin signaling by CCM1 in epithelial cells, both *in vitro* and *in vivo*. In addition, they reported that the phenotype of β-catenin-driven intestinal adenomas in $Apc^{Min/+}$ mice is exacerbated in a $CCM1^{+/-}$ background. This implies a more general regulatory role for CCM1 and, possibly, CCM3 in β-catenin signaling

in other cells as well as in ECs. As the occurrence of intestinal and other neoplasias in genetic CCM patients does not appear to be increased (E. Tournier-Lasserve, personal communication), the specificity of vascular and organ localization for the CCM pathology suggests that endothelial differentiation and/or local factors in the organ cooperate with β-catenin signaling for the expression of the mutated phenotype. In particular, as far as is known for *CCM3*, mutation of this gene in neuronal cells activates astrocytes and produces vascular lesions that resemble this pathology[162]. This thus reinforces the importance of cellular crosstalk within the neurovascular unit.

In CCM human patients the organ-specific development of vascular lesions can be explained by the two–hits model[149]. Indeed, a good amount of data support the hypothesis that familial CCM patients are heterozygous for LOF mutations in any of the three CCM genes and a second hit, likely a LOF mutation in the other allele, would be the driving force for the development of the pathology[149]. For instance, in our mouse model only homozygous deletion of *CCM3* induce CCM phenotype. This model resembles tumor progression. Indeed, many other characteristics in CCMs are in common with tumors such as hyper-proliferation, acquisition of invasive and migratory properties, formation of abnormal structures, loss of contact inhibition, cadherin-switch, junction disorganization and acquisition of mesenchymal markers[128]. Therefore, we can dare to assume that cavernomas express features of endothelial tumors. One of the characteristics of tumors, even if still controversial, is the presence of cancer stem cell. A hazardous, but suggestive hypothesis could be that CCM arise from endothelial cell progenitors, which lose their control mechanisms and give raise to clonal lesions. Some preliminary data from our lab using reporter mice known as *rosa confetti*[202] support the clonal origin of CCM lesions. In this mice different reporter genes (GFP, RFP, YFP, CFP) are flanked by flox sequences. Expression of Cre-recombinase allows the recombination (by chance) and subsequent expression of only one of these reporter genes per

cell. In this way all the cells generating from a single clone should share the expression of the same reporter protein. Anyway, additional studies are necessary to definitively address this point. CCM3 would act as a tumor suppressor and its loss would trigger β-catenin pathway and tumor/lesion progression. β-catenin pathway is well known to play a crucial signaling role in stem cell maintenance and tumor progression and it is likely that its hyper-activation could lead to ECs de-differentiation and to major defects of vascular structure. The fact that CCM genes deletion in murine models result in CCM phenotype only if genes recombination is performed during the first post natal days and that this ability decreases at increasing ages[143] might fit with the hypothesis of a pool of progenitor ECs which is more numerous in pups and decreases in adults also considering that ECs of BBB acquire their differentiated phenotype early after birth[77].

Another interesting aspect of our observations is that CCM lesions develop exclusively in the venous compartment[128]. Although the reason for this specific location is still unknown, it is interesting to notice that Wnt/β-catenin pathway is important also for arterial-venous differentiation via Sox17/Notch pathway[28, 29]. Failure in arterial-venous differentiation due to the de-regulation of such signaling pathways could be crucial for CCM development in particular in the venous compartment. Moreover, Bmp2, which we demonstrated to be a target of β-catenin-mediated transcription in *CCM3* null ECs, is reported to be crucial for veins development[30]. Taking together this findings suggest that de-regulation of these signaling pathways could be more relevant in venous tract than in arterial one and justify in part the preferential development of CCM lesions within the venous bed. How these pathways can be inter-connected one to the other still need to be investigated.

Future directions

In the present work we have been able to elucidate a new molecular pathway implicated in CCM pathogenesis and in the process of EndMT. Anyway, many important issues remain still obscures, laying the foundations for further studies. In particular for the future it would be interesting to better analyze the molecular mechanisms linking the absence of CCM3 with the activation of β-catenin signaling. Preliminary data produced in the lab suggest that the activation of this pathway is in common at least with *CCM1* KO ECs suggesting that such signaling could play a pivotal role in familial CCM pathology. Further experiments in *CCM2* KO ECs could definitively address this point. Another common feature between *CCM1*, *CCM2* and *CCM3* KO is the dismantling of the junctions that we propose as potential molecular mechanism between CCM proteins and enhanced β-catenin mediated transcription as previously discussed. However, how CCM complex could regulate junction clusters needs still to be addressed. An important player for this process could be Rap1 that is been demonstrated to be a partner at least of CCM1. Whether also other CCM proteins could influence Rap1 activity is not clear even if we observed that in the absence of CCM3 CCM1 protein results down regulated. In this hypothesis CCM protein complex would acquire a great relevance in junction stability by regulating Rap1 thus explaining why deletion of these 3 independent genes could lead to the very same phenotype. Further investigation of the relationship between CCM proteins, Rap1 and junctions stability would help to better understand these issues.

Another open question is linked with the activation of Tgfβ/Bmp pathway in *CCM3* KO ECs. Even if it's clear that enhanced Tgfβ/Bmp pathway plays an important role in CCM pathogenesis, nowadays the reasons behind the up regulation of this pathway are still unraveled. Our data suggest that Tgfβ/Bmp pathway is activated in later stages of CCM development, following β-catenin activation. Whether these two pathways can crosstalk is

now matter of study in our lab. In particular we showed that Bmp2 is a direct target of β-catenin. Now we are trying to understand which is the role of Bmp2 in EndMT and CCM, whether Bmp2 could be responsible of the activation of Tgfβ/Bmp pathway and which is the relationship with Bmp6 that has been demonstrated to be involved in EndMT in CCM. In literature many examples of crosstalk between these pathways have been described even if the subsequent activation of Tgfβ/Bmp pathway by β-catenin signaling seems likely to occur because of time-dependent activation of the two signaling cascades. However, we cannot exclude a synergist effect at transcriptional level between downstream effectors of the two pathways (p-Smad, TCF4 and β-catenin) that has been often observed in literature, in particular for EMT/EndMT genes[66-68].

The molecular mechanisms leading to β-catenin translocation are currently unknown and have not been investigated in the present study. Anyway, an active transport of β-catenin in the nucleus seems to be the most reasonable hypothesis and address this point in *CCM3* KO cells could represent a big step toward the understanding of β-catenin pathway both in pathology an physiological processes.

Since astrocytes-specific *CCM3* deletion leads to CCM in a mouse model, it is clear that the crosstalk between different units in the BBB is a crucial aspect of CCM. In particular we could speculate that CCM3 deletion in astrocytes could activate angiogenic stimuli, which influence EC physiology, junctions state and intracellular pathways thus activating indirectly the same pathways responsible for pathogenesis in endothelial-specific *CCM3* KO. Further study in this direction using different stimuli and co-culture *in vitro* could help to address this point.

We hypothesized that CCM could resemble benign endothelial tumors since they share lot of classical tumor characteristics as we have observed in our work. However, additional experiments could help to better understand this point. For example it would be interesting to

inject WT and *CCM3* KO ECs in nude mice in order to check for their ability to form tumor and their characteristics.

Previously we used Tgfβ/Bmp pathway inhibitors in order to reduce CCM lesion extension. Now we found that also β-catenin inhibitor can strongly counteract CCM development. These finding highlighted the need in the future to try to combine treatments with β-catenin inhibitors (such as sulindac) and Tgfβ/Bmp pathway inhibitors (such as DMH1) in order to define new therapeutic opportunity for CCM patients. Some preliminary studies *in vitro* are already on going in our lab even if the most interesting aspect will be to test these drugs *in vivo*. A synergistic effect between these drugs could lead to an increase of survival of CCM3-ECKO mice.

Concluding remarks

In conclusion, this study highlights the importance of β-catenin signaling for the onset and development of CCM3 pathology and shows that targeting β-catenin signaling in ECs with specific pharmacological tools can effectively reduces vascular malformations in a *CCM3*-ECKO mouse model. These observations suggest a promising strategy for inhibiting the development of vascular lesions and preventing the appearance of new ones in genetic CCM3 patients.

APPENDIX

List of gene generated comparing WT vs. WT + Wnt3a (threshold=1.3)

Affymetrix raw data (log2)

Gene_Symbol	WT WNT3a	CCM3 KO WNT3a	s.d. WT WNT3a	s.d. CCM3 KO WNT3a
ABCB1A	11.9061	12.0066	0.137320137	0.110450079
ABCC6	8.17133	8.432845	0.1738917	0.041118259
ABCC9	7.753295	7.37274	0.081437488	0.10118698
ABHD2	12.6579	12.78735	0.151745115	0.063427478
ACE	10.1855	10.29715	0.518450692	0.518521403
ACP6	10.69235	10.5645	0.206545891	0.188514668
ADAM12	9.997695	9.74413	0.183854834	0.091740034
ADRB2	9.249495	9.3629	0.017486751	0.212867425
AHRR	8.89206	8.411625	0.222413367	0.113398714
AI607873	7.254435	7.369155	0.217074711	0.033608785
AIM1	8.086095	8.283965	0.381533606	0.359599154
AK4	8.672885	8.909055	0.001477853	0.020286894
AKAP12	10.77675	9.780155	0.380777002	1.252208328
ALDH1A3	7.84026	9.55733	0.056766532	2.169219757
AMD1	8.10734	7.87716	0.008315576	0.211085516
ANKRD37	9.065435	8.866555	0.144157859	1.144728097
ANO1	11.1064	10.50695	0.066468037	1.460387635
ANPEP	7.84837	10.212595	0.43043004	1.940732343
APLNR	10.028265	10.20728	1.750280202	1.663709119
APOD	9.12002	10.752705	0.88423703	1.466532393
APOE	12.67315	11.9973	0.181938575	0.788141218
APOL9A	7.362175	9.94893	0.06960052	3.101327916
APOL9B	7.394595	7.58744	0.033820917	0.302585134
AQP11	10.108875	8.9095	0.169740983	2.066590279
ARHGAP20	9.839715	9.8481	0.528046131	0.087638814
ARHGAP28	9.408305	9.45181	0.229491506	0.389530984
ARID3A	8.49664	8.783425	0.193535126	0.541509444
ARL4A	9.06263	9.02347	0.121212244	0.522707475
ARRDC4	9.394075	9.18986	0.09224208	0.111737014
ARXES2	7.63477	7.874225	0.511068497	0.610820051
ATP10A	10.7127	9.48105	0.335027193	2.24711464
ATP13A3	11.96655	11.3257	0.000212132	0.973403195
ATP1B1	7.653015	10.36816	0.170745074	2.517639552
ATP2B4	7.69238	9.05598	0.951214184	0.402654885
AW112010	10.18145	9.163015	0.128198459	1.671296375
AXIN2	8.448225	9.263225	0.221331494	1.24447258
AZIN1	9.93719	9.39811	0.060005081	0.960378288
BEX1	4.89191	7.340645	0.623201491	3.155739783
BHLHE41	6.603545	6.864395	0.19137845	0.219422305
BMP6	11.7271	7.883555	0.229526861	4.789156447
BNIP3	9.86381	11.00995	0.039258568	1.206253458
BOK	10.000385	8.00058	0.024487108	3.23108201
BST2	10.17855	8.4456	0.193110862	2.126468081
C130074G19RIK	10.9595	10.96095	0.026870058	0.193676547
C1QL3	7.762095	8.724295	0.524482313	1.6881538
C1QTNF1	9.376765	10.0032	0.272186613	0.365715627
CACHD1	11.1163	10.54445	0.063073925	0.811970717
CACNA1B	8.55119	9.697085	0.289814785	1.185839285
CACNA1E	7.780715	7.82589	0.107657007	0.200394062
CACNG4	9.143755	8.69819	0.182949737	0.155662487
CADM1	9.00596	9.886765	0.340231499	1.627950729
CAR2	9.91782	8.781265	0.11721002	0.618937637
CASC4	8.48311	7.933045	0.196858528	0.905711863
CCDC134	9.52735	9.18672	0.000608112	0.576065752
CCDC141	8.05143	8.87979	0.192573461	0.57353431
CCDC85A	9.667435	9.10172	0.240098108	0.518549687
CD53	8.195135	7.99313	0.304091271	0.020350533
CDH2	11.6633	10.486645	0.295004949	1.389259764
CDON	9.826565	9.832905	0.139816224	0.035376552
CEACAM2	7.462545	8.70333	0.20905612	0.583688364
CEBPD	8.94837	8.56122	0.117789848	0.783431887
CFH	8.068655	10.25811	1.276334811	1.89701193
CFTR	7.215065	8.27538	1.481565483	2.234839266
CHRM3	9.340905	8.36257	0.793720291	0.78411071
CHST2	9.56272	9.299015	0.479658814	0.600156881
CLCA5	8.17294	7.78949	0.398383961	0.682386328
CLEC14A	11.16215	8.910565	0.121268813	2.932987004
CLIC6	10.417	9.98882	0.18356492	0.38619344
CLVS1	9.25649	9.11216	0.604420734	0.341730565
CMPK2	8.806685	8.80688	0.141159727	0.935290139
COL10A1	8.89344	10.126245	1.166712047	0.661505465
COL15A1	10.74245	10.064325	0.069508597	0.448836029
COL8A1	10.57915	9.64992	0.481186165	1.714988503
COLEC12	10.6326	9.579445	0.103379011	1.401846265
CORO2B	9.91774	8.821815	0.158052508	1.653378289
CPNE7	7.45015	8.658695	0.060797041	2.014554291

Fold change (linear)

Gene_Symbol	KO VS KO WNT	WT vs WT WNT
ABCB1A	1.322942	1.436741
ABCC6	1.452628	1.869335
ABCC9	0.729179	0.808366
ABHD2	1.564932	1.662610
ACE	0.506997	0.483035
ACP6	1.305181	1.400377
ADAM12	0.606359	0.604549
ADRB2	1.517393	1.341266
AHRR	2.002178	1.923455
AI607873	0.396947	0.464835
AIM1	0.646741	0.790512
AK4	0.743624	0.913170
AKAP12	0.709488	0.790343
ALDH1A3	0.487380	0.497566
AMD1	0.804986	0.895075
ANKRD37	0.752845	0.895072
ANO1	0.697251	0.822251
ANPEP	0.592528	0.641998
APLNR	0.440227	0.765397
APOD	0.573464	1.529224
APOE	1.592287	1.380796
APOL9A	0.529306	0.707788
APOL9B	0.507263	0.644854
AQP11	1.761977	1.813561
ARHGAP20	1.443469	1.730405
ARHGAP28	1.381437	1.376715
ARID3A	1.390487	1.381131
ARL4A	1.636122	1.828132
ARRDC4	0.541291	0.445831
ARXES2	3.300673	3.475210
ATP10A	1.491444	1.378023
ATP13A3	0.892330	0.908967
ATP1B1	1.563691	3.575686
ATP2B4	0.560824	0.568724
AW112010	0.698315	0.649657
AXIN2	2.805135	2.997937
AZIN1	0.733892	0.832430
BEX1	1.696469	2.833451
BHLHE41	0.686387	0.848005
BMP6	1.362352	1.025552
BNIP3	0.774359	0.898132
BOK	1.357366	1.368855
BST2	0.701614	0.714928
C130074G19RIK	1.328824	1.168696
C1QL3	0.471262	0.482205
C1QTNF1	2.075746	2.131856
CACHD1	1.380939	1.322392
CACNA1B	1.501365	1.671826
CACNA1E	1.666897	1.361937
CACNG4	0.737835	0.859256
CADM1	2.029255	1.748491
CAR2	1.480731	1.363283
CASC4	1.402072	1.259346
CCDC134	0.768198	0.885010
CCDC141	1.575276	2.892486
CCDC85A	2.094332	1.926778
CD53	1.428291	1.533693
CDH2	1.366324	1.422077
CDON	1.690201	1.721773
CEACAM2	0.677522	1.043869
CEBPD	1.363571	1.233378
CFH	1.411462	1.412749
CFTR	1.445071	1.278365
CHRM3	1.551448	1.759725
CHST2	1.305765	1.387574
CLCA5	0.695065	0.914002
CLEC14A	1.381657	1.189619
CLIC6	0.715860	0.774091
CLVS1	1.639914	1.650331
CMPK2	0.475507	0.585800
COL10A1	1.525947	1.315481
COL15A1	0.584287	0.560641
COL8A1	0.662366	0.703318
COLEC12	1.424198	1.209684
CORO2B	1.872798	1.610440
CPNE7	0.618942	0.659295

CRIP1	10.9661	10.9082	0.251022907	1.10846059	CRIP1	0.745304	0.857673
CSF1	11.446	10.83655	0.035921024	0.873630428	CSF1	1.328364	1.254272
CSF2RB	8.25085	9.143445	0.535067701	0.799575135	CSF2RB	1.646212	1.517083
CSF2RB2	10.26915	8.79048	0.421647774	2.241981045	CSF2RB2	1.801664	1.673218
CSN3	7.67541	9.24738	0.511280629	3.279730957	CSN3	0.428056	0.406450
CST6	8.136885	10.02976	0.206750952	1.720305946	CST6	0.679363	0.688849
CTDSPL	8.80215	8.392865	0.320941626	0.773921301	CTDSPL	1.365965	1.063400
CTLA2A	10.782	9.968965	0.639507373	0.366047967	CTLA2A	1.314396	1.289977
CTSC	10.274225	8.163655	0.628016888	3.363770598	CTSC	2.077617	2.225362
CTTNBP2	9.224445	9.047855	0.011476343	0.101066772	CTTNBP2	1.420565	1.260180
CTXN1	9.99733	9.071865	0.100083894	1.025707884	CTXN1	1.361904	1.556801
CX3CL1	11.0029	11.12765	0.218778838	0.249679404	CX3CL1	0.667898	1.026796
CXCL12	11.2814	10.240595	0.181867864	1.057555973	CXCL12	0.705931	0.682287
CXCL16	8.78597	8.638365	0.058746431	0.079627295	CXCL16	0.651705	0.694798
CYP1B1	8.084105	9.36616	0.086373093	0.110379369	CYP1B1	1.619294	1.977250
CYP39A1	9.584155	10.819855	0.44638944	1.579457346	CYP39A1	1.333234	1.327047
D14ERTD668E	8.495365	10.19145	0.101109199	2.018577728	D14ERTD668E	0.649846	0.716240
D8ERTD82E	10.8034	9.738445	0.18356492	1.525872794	D8ERTD82E	0.756494	0.774668
DAPK2	9.405485	9.39651	0.047312515	0.682612602	DAPK2	0.693842	0.595051
DARC	7.916475	9.069045	0.6216105	0.034655303	DARC	1.426520	1.239304
DDX60	6.70956	7.89802	0.037236243	0.7061734	DDX60	0.546910	0.563327
DHX58	8.090155	9.47435	0.181252681	1.187020154	DHX58	0.611969	0.726616
DISP2	10.86035	9.613525	0.604505587	1.539194686	DISP2	1.325512	1.347747
DNAHC6	5.395045	6.36802	0.128361094	1.560683661	DNAHC6	0.941120	0.929077
DNAJB5	10.1397	8.46858	0.0417193	2.422010431	DNAJB5	1.314715	1.280352
DNM3	8.62547	8.579765	0.304649886	1.089602052	DNM3	1.457236	1.559653
DOCK8	9.28388	10.162495	0.209671303	1.358076355	DOCK8	0.641282	0.630475
DPP4	9.106425	7.232465	0.524496455	2.710248368	DPP4	2.361281	2.532847
DUB2A	7.2474	8.286675	0.401834642	2.46345396	DUB2A	1.407110	0.683987
DUSP2	8.48393	8.745425	0.230559237	0.620974104	DUSP2	1.630727	1.379834
DUSP4	8.85804	8.82139	0.030575297	0.33951025	DUSP4	1.503745	1.387382
EDN1	12.3917	10.377165	0.226557013	1.648315404	EDN1	1.424346	1.381466
EFEMP1	9.683345	8.167145	0.181167828	2.354799932	EFEMP1	1.316584	1.421782
EFNA3	7.43474	8.21441	0.129556104	0.11469272	EFNA3	0.600699	1.141669
EFNB2	11.73645	10.025755	0.01039447	2.271714885	EFNB2	0.742802	0.773059
EGFL8	10.42385	11.3379	0.417687976	0.652518138	EGFL8	0.698460	0.775205
EIF2AK2	9.38805	9.41432	0.12224462	0.383916556	EIF2AK2	0.727198	0.827270
ELOVL7	10.183	10.117035	0.136330187	0.52731074	ELOVL7	1.971167	1.709750
EMP2	10.92785	11.5203	0.518945667	0.027860007	EMP2	0.606740	0.612571
ENPP2	10.38085	10.06362	0.076862507	0.344332718	ENPP2	1.639584	1.492266
ENTPD1	11.5965	10.74188	0.033516861	1.708539689	ENTPD1	1.557303	1.643874
EPDR1	10.14702	10.20078	0.460156809	0.584098486	EPDR1	1.432927	1.369520
EPHA7	8.197895	9.394715	1.143879569	2.432143271	EPHA7	0.585441	0.704197
EPHB1	6.406475	7.72902	0.295238294	2.284958995	EPHB1	0.894765	0.754637
ERN1	11.5621	12.0012	0.035921024	0.658457835	ERN1	1.380939	1.231614
ESR1	7.70649	9.17043	0.206135769	1.933611777	ESR1	1.523532	1.335269
ETL4	9.032965	9.03584	0.017557461	0.49525759	ETL4	0.711534	0.769525
F2RL1	7.943135	7.57795	0.075059385	1.311697221	F2RL1	0.689826	0.795332
FABP7	7.4502	9.27713	0.066100342	2.861618717	FABP7	0.723753	1.025345
FADS3	11.23765	9.35568	0.116884751	2.805403728	FADS3	0.708652	0.803266
FAH	9.225175	9.50837	0.252104781	0.691281731	FAH	0.726679	1.085361
FAM102A	10.8023	9.644185	0.068730779	1.612224674	FAM102A	1.514456	1.605497
FAM102B	10.9563	9.04799	0.267852049	2.909758547	FAM102B	1.425680	1.573323
FAM13A	8.502375	9.779205	0.011702617	1.887260928	FAM13A	3.001035	1.934070
FAM13C	9.23345	9.65643	0.201454722	0.746662335	FAM13C	1.439298	1.324093
FAM181B	6.501635	8.599395	0.08621753	2.892073806	FAM181B	1.045150	0.938361
FAM38B	9.225065	9.70883	0.257167665	1.17262346	FAM38B	1.335259	1.394594
FAM69B	8.66802	8.41363	0.082759778	1.149614205	FAM69B	1.372532	2.288068
FAR2	10.3801	9.790825	0.246638845	1.685424368	FAR2	0.750982	0.699138
FGFBP1	6.947585	6.55314	0.139179828	0.453326157	FGFBP1	1.838463	1.818936
FKBP14	9.543825	9.37765	0.23203709	0.392783675	FKBP14	0.767783	0.928549
FLNC	10.1487	9.79568	0.215950411	0.625817786	FLNC	0.658863	0.744606
FLRT2	8.893245	9.73997	0.060846539	0.869783767	FLRT2	1.675515	1.809047
FMO2	6.899185	6.944285	0.354182716	0.141442569	FMO2	0.543499	0.561001
FOXC1	8.791355	9.40168	0.250223877	0.729027091	FOXC1	1.530916	1.726625
FOXF2	11.9925	11.18345	0.010323759	0.958341821	FOXF2	2.039337	2.166626
FOXQ1	8.15054	8.49029	0.150543034	0.1153574	FOXQ1	1.370127	1.929758
FRRS1	9.719645	7.886205	0.105662966	2.655688009	FRRS1	1.356435	1.399736
FRZB	11.25595	9.8524	0.159594001	1.552523649	FRZB	1.373446	1.305498
FUT11	7.198315	9.4754	0.916601307	3.591961027	FUT11	1.412519	0.906469
FUT4	7.61991	8.318515	0.09442704	1.035211399	FUT4	1.501204	1.439213
FXYD6	11.31815	10.598245	0.419102189	1.405664641	FXYD6	1.335981	1.201553
FZD6	12.21545	11.5472	0.12508719	0.841881334	FZD6	1.344528	1.488026
GADD45G	8.301105	7.771365	0.214755401	1.226285793	GADD45G	0.640995	0.715245
GALNTL2	10.2134	8.63739	0.249467272	1.759479661	GALNTL2	1.449706	1.043764
GJA1	10.79565	10.6874	0.168503546	0.042284986	GJA1	0.618523	0.698291
GJA4	8.675705	10.772875	1.078019643	2.161802207	GJA4	0.445779	0.672215
GJA5	10.6098	9.695385	0.464144891	1.725786023	GJA5	0.423769	0.455430
GKN3	7.16793	8.05886	0.576787001	1.404299925	GKN3	1.838660	1.482827
GLI3	8.931615	9.99881	0.096060456	1.158368187	GLI3	1.603818	1.583915
GM12824	9.54618	8.228365	0.376237376	1.496739995	GM12824	3.200528	2.770603

GM129	8.72687	9.578825	0.354727188	0.726163309	GM129	1.369453	1.653921
GM14005	10.38395	8.43463	0.095105862	2.942087469	GM14005	0.793609	0.850982
GM3893	8.683415	8.963965	0.287559115	0.39778292	GM3893	1.575751	1.807624
GM4884	5.57531	7.25408	0.057996898	3.054729579	GM4884	1.458383	0.978040
GM5972	12.219	10.9956	0.146512525	2.236578749	GM5972	0.698848	0.772657
GM6548	9.997345	9.51682	0.047736779	0.776092119	GM6548	0.767104	0.883070
GM8995	9.8192	10.49785	0.09906566	0.013647161	GM8995	0.652093	0.790014
GNA14	8.121555	8.575875	0.328231897	0.178240406	GNA14	0.601347	0.778066
GNG4	8.014795	6.69	0.178183838	2.06216379	GNG4	0.716081	0.998684
GPC4	10.37855	11.59965	0.074599765	1.883944597	GPC4	0.641557	0.735680
GPIHBP1	8.62062	9.332335	0.07694736	1.227063611	GPIHBP1	0.551677	0.564831
GPM6A	9.510535	9.974675	0.155754411	0.818723587	GPM6A	1.852739	1.737081
GPR126	10.48325	9.285315	0.400717413	2.265407492	GPR126	5.818914	4.486219
GPR143	8.13882	8.238745	0.558373941	0.618414378	GPR143	1.450319	1.413831
GPR182	10.08687	10.142	0.305653977	0.071276364	GPR182	1.609770	1.133398
GPX3	7.950005	8.17243	0.557758758	0.27587064	GPX3	0.670805	0.842746
GRAP	11.7586	10.36068	0.062932504	1.735126904	GRAP	1.394550	1.394212
GRIN2A	8.1589	8.853685	0.13098446	1.372190206	GRIN2A	0.580420	0.710556
GRRP1	9.319025	8.977825	0.541368023	1.169816246	GRRP1	1.323350	1.292666
GSTA4	9.73934	9.87056	0.272731086	0.60081449	GSTA4	1.758877	2.351009
GSTM7	9.05795	8.35576	0.096845345	1.266909078	GSTM7	1.390829	1.783152
GSTO1	10.40685	11.164	0.158604051	0.755048621	GSTO1	0.751998	0.772336
GUK1	10.04486	8.93017	0.332255334	1.535029827	GUK1	0.756132	0.891990
H19	6.91953	7.81973	0.029613632	1.554800533	H19	0.957846	0.884602
H1FX	10.107205	10.5475	0.648268426	0.050487424	H1FX	1.373779	1.373655
H2-Q4	10.75895	10.016185	0.337643488	1.266025194	H2-Q4	0.702149	0.681294
H2-Q6	10.31105	10.66225	0.217293914	0.326754044	H2-Q6	0.501997	0.479699
H2-Q8	9.587475	9.97739	0.210145064	0.253441213	H2-Q8	0.710435	0.670531
H2-T22	10.5004	8.81538	0.102530483	2.499367913	H2-T22	0.740386	0.819832
H2-T23	9.423645	9.826335	0.209819795	0.170391521	H2-T23	0.763913	0.922301
HMCN1	7.099975	8.702945	0.002906209	2.099760658	HMCN1	1.027704	0.968897
HMGA2	10.9496	10.093055	0.131804704	1.04700594	HMGA2	0.722515	0.663009
HS3ST1	8.90974	8.901355	0.202204255	0.021163706	HS3ST1	1.411638	1.087511
HTR2A	9.91791	10.70395	0.167287322	0.051972348	HTR2A	1.447441	1.611356
HTRA1	9.812205	10.21215	0.62153979	0.258871793	HTRA1	0.564073	0.698025
I830012O16RIK	5.542365	6.791585	0.161184991	0.521653886	I830012O16RIK	0.338637	0.522856
ID2	10.046155	10.199375	0.608316893	0.707283558	ID2	1.531839	1.407671
IFI203	8.68193	8.518035	0.046527626	0.990819235	IFI203	0.481434	0.560362
IFI204	9.01195	9.80958	0.341702281	0.66796135	IFI204	0.445522	0.567367
IFI205	6.449275	8.83413	0.055727085	2.670841307	IFI205	0.408331	0.686737
IFI35	9.7472	8.03643	0.038424182	2.93176371	IFI35	0.765699	0.871311
IFI44	9.761535	9.637525	0.151483486	1.532689304	IFI44	0.351718	0.522820
IFIH1	10.03185	9.35723	0.044901281	1.456597543	IFIH1	0.718595	0.805078
IFIT1	8.694595	9.382695	0.038091842	0.412405888	IFIT1	0.393259	0.579381
IFIT2	7.36993	7.395925	0.181500169	0.974060804	IFIT2	0.562933	0.688933
IFIT3	8.77348	9.87436	0.129881374	0.207804541	IFIT3	0.291947	0.478968
IGSF5	9.0834	9.28133	0.136457467	0.396319209	IGSF5	1.352923	1.183915
IIGP1	6.95097	8.64238	0.276903016	1.968047878	IIGP1	0.692344	0.649448
IL17RD	8.19173	8.651735	0.082632498	0.309479425	IL17RD	1.470233	1.365056
IL17RD	8.19173	7.887305	0.082632498	0.771587849	IL17RD	1.470233	1.365056
IL1RAP	8.715505	9.06994	0.083389103	0.293958431	IL1RAP	0.665292	0.823192
INSR	11.97695	10.542835	0.244729657	2.081814288	INSR	2.162575	2.248792
INSR	11.97695	9.139395	0.244729657	4.06657817	INSR	2.162575	2.248792
IRF7	8.405075	8.80988	0.269895587	1.084475528	IRF7	0.347150	0.533188
IRGM1	10.50215	9.42082	0.13767369	1.948475162	IRGM1	0.642692	0.785863
IRGM2	8.84916	9.14389	0.027775154	0.402103342	IRGM2	0.653421	0.884694
ISG15	6.56584	9.587115	0.065463946	3.757968486	ISG15	0.583458	0.692756
ISG20	9.209335	11.002105	0.159162665	1.756870437	ISG20	0.754810	0.964732
ISM1	9.908585	8.95911	0.729755411	0.513034254	ISM1	1.676456	1.738545
ISYNA1	9.11876	10.038385	0.399147636	0.849680721	ISYNA1	1.385830	1.631416
ITGA4	10.28885	9.605605	0.374130198	0.436801072	ITGA4	1.722758	1.991720
JUB	10.3321	8.465175	0.086267027	2.527376413	JUB	1.444565	1.405438
KANK4	7.560505	8.394545	0.195536238	1.189162687	KANK4	1.576893	1.321696
KBTBD11	8.823765	9.444125	0.229816775	0.449005735	KBTBD11	1.684272	2.513696
KBTBD11	8.823765	9.060765	0.229816775	0.093147176	KBTBD11	1.684272	2.513696
KCNE3	8.918345	9.513445	0.056844314	1.149409144	KCNE3	0.640984	0.790929
KCNIP3	10.3748	10.34595	0.226132749	0.113773481	KCNIP3	2.329177	2.257475
KCNJ2	10.8684	9.223975	0.220900158	1.78986404	KCNJ2	1.595380	1.751177
KCNJ8	8.189815	8.063945	0.087207479	0.56359946	KCNJ8	0.623132	0.728378
KCNK5	8.32735	8.12717	0.298837468	0.474185807	KCNK5	2.447129	1.994317
KLHL6	9.095225	8.691955	0.009383307	0.064778052	KLHL6	1.584601	1.217258
LAMA1	8.55841	9.31936	0.364428693	0.537146595	LAMA1	2.130084	2.056541
LBH	10.046655	9.86049	0.169910688	0.108385327	LBH	0.740928	0.810102
LCN2	7.48825	8.48571	0.791252488	0.692031265	LCN2	1.516158	1.708594
LEF1	9.51405	8.96762	0.303263956	1.500452305	LEF1	2.220708	2.733122
LGALS3	8.421985	8.415655	0.020767726	0.275029183	LGALS3	0.705587	0.822718
LGALS3BP	12.0424	10.394795	0.404889343	3.003230992	LGALS3BP	0.600152	0.648173
LIFR	8.500875	9.38695	0.584444968	0.867266467	LIFR	0.737853	0.719589
LIMCH1	10.06985	8.457315	0.09694434	1.961224297	LIMCH1	1.444996	1.431294
LONRF2	7.333885	8.20889	0.729896833	1.871867213	LONRF2	1.605992	1.261968
LPHN2	13.2206	10.854745	0.015132085	3.268749588	LPHN2	0.911554	0.895490

LPHN3	10.138135	10.81765	0.514582818	1.20017234	LPHN3	2.074998	2.106357
LRG1	8.668535	9.701495	1.829391309	2.340389095	LRG1	1.418115	1.653932
LRP8	10.061195	9.911685	0.227836876	0.283853875	LRP8	1.496503	1.441209
LRRC7	6.830385	6.6443	0.439063814	0.253200796	LRRC7	1.608159	1.398921
LSR	9.726295	12.1576	0.091761247	1.419587574	LSR	2.290988	2.453158
LTBP4	10.96635	11.0626	0.583716648	1.311541658	LTBP4	0.612826	0.778841
LYST	9.83102	9.66847	0.060698046	0.506472303	LYST	1.372304	1.340281
MAFB	8.37377	9.06257	0.30077494	1.331524495	MAFB	1.409028	1.177906
MAL	9.58058	8.505595	0.517870864	2.405160077	MAL	2.366754	3.463883
MAOA	11.19675	11.25685	0.184484159	0.426738942	MAOA	1.484729	1.587493
MARVELD2	9.09815	10.31005	0.275785787	2.007122598	MARVELD2	1.624145	1.601191
MDGA2	6.726505	8.52015	0.330070374	2.162403248	MDGA2	0.676525	0.728580
MDGA2	6.726505	7.336165	0.330070374	0.487995603	MDGA2	0.676525	0.728580
MEIS2	8.85288	9.82549	1.639950331	3.084131079	MEIS2	3.154738	2.268612
MEST	10.6621	10.98135	0.189080353	0.449224938	MEST	0.653383	0.748098
MFSD7C	9.799615	9.764545	0.057777695	0.872930392	MFSD7C	4.381394	7.341017
MGLL	7.692625	8.0128	0.145741779	1.04104503	MGLL	0.590183	0.566575
MIR126	8.80776	8.01096	0.438462773	1.038442877	MIR126	1.405701	1.167846
MIR181B-1	9.168395	9.1125	0.273473548	0.226910566	MIR181B-1	1.677846	1.334126
MMP28	9.09793	9.83567	0.161149635	0.435337361	MMP28	1.373384	1.553918
MMRN1	8.75858	9.649695	0.521024561	1.657748209	MMRN1	3.417355	3.457454
MOGAT2	8.6081	8.37165	0.427177349	0.033417866	MOGAT2	2.859336	1.923655
MRPS36	6.344855	7.411745	0.005239661	1.426722281	MRPS36	0.708670	0.869959
MX2	5.578865	7.623005	0.25687068	1.835189585	MX2	0.583533	0.689781
MYH10	12.4171	10.895235	0.233203816	2.004456806	MYH10	1.444179	1.401285
MYL4	11.211	9.684195	0.026162951	1.956571535	MYL4	2.416669	2.670648
NCAM1	8.71035	8.356005	0.250754207	0.883013735	NCAM1	0.654275	0.826399
NEFL	9.90045	7.950335	0.851992961	1.954662346	NEFL	1.402728	1.481347
NEFM	9.147045	6.807655	0.640872089	2.171942118	NEFM	1.823159	1.632514
NEURL1B	10.465	11.385	0.090933932	1.511511455	NEURL1B	1.557401	1.087481
NEURL1B	10.465	10.67595	0.090933932	0.508763329	NEURL1B	1.557401	1.087481
NLRC5	7.206605	7.876995	0.041485955	0.884201675	NLRC5	0.779510	0.707705
NMNAT2	9.451495	10.0416	0.098874741	0.030405592	NMNAT2	0.707239	0.856990
NNMT	10.6838	9.79765	0.605990511	1.051962758	NNMT	0.710152	0.728070
NOMO1	12.19665	11.03122	0.133289628	1.58332522	NOMO1	1.303237	1.327305
NOS2	8.881515	9.3867	0.009142891	0.742377267	NOS2	0.537129	0.556042
NOSTRIN	10.038305	8.752255	0.056702893	2.263088182	NOSTRIN	2.395372	2.376157
NPNT	11.6016	11.4856	0.220758737	1.556907711	NPNT	2.135391	1.475649
NPR3	10.01245	10.054005	1.112066835	1.337697538	NPR3	2.550818	1.557978
NPTX1	8.79984	10.91863	0.347514699	1.891468213	NPTX1	0.646542	0.861958
NQO1	9.7227	9.416355	0.023730504	1.151516322	NQO1	1.316525	1.371134
NR2F1	7.275785	8.727765	0.474899985	2.633456572	NR2F1	1.453121	1.209998
NRBP2	9.30417	11.01287	0.002404163	2.163930598	NRBP2	1.425176	1.376634
NRGN	9.23842	9.70183	0.208059099	0.194539218	NRGN	1.527005	1.754026
NRP2	11.53535	10.226675	0.024960869	1.803581911	NRP2	0.767213	0.681601
NT5E	8.997505	10.078815	0.616660753	0.981867263	NT5E	0.466565	0.459183
OAS1A	7.772885	7.51508	0.443193317	0.660720576	OAS1A	0.629651	0.729207
OAS1G	7.972505	8.984465	0.153887649	0.710734239	OAS1G	0.555938	0.731262
OASL1	8.50484	9.60514	0.151547125	1.337223776	OASL1	0.642547	0.708940
OASL2	10.68945	11.4093	0.06569022	0.093338095	OASL2	0.468412	0.581903
OGDHL	8.625835	8.386865	0.133438121	0.138062599	OGDHL	1.378295	1.302118
OLFML2A	11.26765	9.763635	0.387989491	2.965556343	OLFML2A	2.404472	2.786106
OLFR517	5.60896	6.855315	0.19640598	1.605832429	OLFR517	0.683148	0.889135
P2RY1	9.451755	9.20676	0.190416785	0.953689058	P2RY1	1.314792	1.758445
P2RY2	10.5257	10.8312	0.10323759	0.414505995	P2RY2	0.684062	0.683257
P4HA2	8.753295	8.77494	0.151073364	0.590278599	P4HA2	0.634090	0.745541
PAPSS2	9.7713	10.84499	0.372503852	1.237168166	PAPSS2	0.757491	0.781387
PARP12	11.04655	8.57181	0.066397327	3.880163609	PARP12	0.767958	0.847009
PARP14	9.39497	9.804715	0.152155237	0.024006275	PARP14	0.659281	0.659532
PCDH7	9.771125	10.521585	0.110131881	1.484096926	PCDH7	1.543168	1.301161
PDE7B	11.0368	10.07637	0.041860721	1.48114829	PDE7B	2.949908	3.038965
PGLYRP1	10.8223	10.85702	0.17833233	1.801821216	PGLYRP1	2.802142	3.830811
PHLDA1	8.76589	10.014965	0.154036141	1.405353514	PHLDA1	1.736798	2.658661
PKNOX2	7.95434	8.7622	0.263128575	0.738629601	PKNOX2	1.784018	1.862790
PLAU	12.2266	10.63708	0.051335952	2.15811818	PLAU	0.721915	0.718470
PLEKHF1	7.50424	9.49158	0.162266864	2.634849572	PLEKHF1	0.703831	0.892504
PLSCR2	9.522745	11.26335	0.393851406	2.480884142	PLSCR2	1.340968	1.105340
PLVAP	8.540385	9.36729	0.503650947	0.82543403	PLVAP	0.603362	0.447556
PLXNB1	8.092165	7.80088	0.093684577	0.079026254	PLXNB1	0.976973	0.937600
PPARG	7.70367	9.79695	0.093281527	3.195486255	PPARG	0.708778	0.652123
PPP1R2	12.1662	10.20006	0.124026529	3.326428289	PPP1R2	0.695465	0.788974
PPP1R3C	6.14989	7.189625	0.215116025	1.448373891	PPP1R3C	0.649310	0.913432
PRKG1	8.47991	8.32193	0.135439233	0.078743411	PRKG1	2.051359	1.473391
PROKR2	7.43433	7.814705	0.507504679	0.30461453	PROKR2	0.671449	0.924468
PRRG3	9.40786	8.45342	0.048861079	1.180005654	PRRG3	0.742699	0.883177
PRSS12	8.866695	10.823435	0.100981919	2.90686648	PRSS12	1.511640	1.648467
PTCHD1	10.81355	8.55915	0.171756237	3.119967251	PTCHD1	0.663561	0.674131
PTCHD1	10.81355	9.22592	0.171756237	2.177012074	PTCHD1	0.663561	0.674131
PTER	9.229195	8.246695	0.244680159	1.413966075	PTER	0.740112	0.735061
PTHLH	7.812845	9.125825	0.029012591	0.200952676	PTHLH	0.608228	0.791812
RAMP3	9.404755	9.572155	1.192104251	0.797680089	RAMP3	1.360786	1.733707

RASA4	8.244395	9.58091	0.258355605	1.877495783	RASA4	0.644093	0.543369
RASGRP2	7.45499	9.57312	0.180609214	1.888512507	RASGRP2	0.694427	0.819074
RASSF9	9.732165	9.641925	0.079867711	0.503198399	RASSF9	1.486413	1.657139
RCAN2	10.051265	9.54512	0.464194389	0.046768043	RCAN2	1.336157	1.180465
RDH10	9.662325	10.80577	0.051837998	1.52597886	RDH10	1.318872	1.285941
REEP1	9.18898	8.874005	0.116078649	0.818638734	REEP1	2.490007	2.953345
RERG	7.712935	8.24282	0.517736514	0.156694863	RERG	1.415626	1.739256
RGS2	8.30777	8.81742	0.33951025	1.4537974	RGS2	2.414074	2.822669
RHOBTB1	10.6158	10.1854	0.074387633	0.767210858	RHOBTB1	1.685913	1.808082
RND1	10.52115	9.97616	0.27739799	0.295768624	RND1	0.711063	0.794379
RNF125	10.226785	10.016465	0.390909842	0.857911444	RNF125	0.696833	0.813351
RNF183	9.32662	8.158915	0.029811622	1.403288763	RNF183	1.657409	2.065284
RNF213	10.7687	9.756955	0.219061681	1.95521389	RNF213	0.731510	0.749864
RNF213	10.7687	10.82915	0.219061681	0.438901179	RNF213	0.731510	0.749864
RNU2	10.93595	10.8895	0.091428907	0.478994134	RNU2	0.731662	0.842472
ROBO1	9.916015	9.753345	0.434425193	0.504669181	ROBO1	1.447532	1.819466
RPS6KA2	10.7339	9.825145	0.069437886	0.783976359	RPS6KA2	0.739668	0.737646
RSAD2	9.691005	10.62185	0.300612306	0.467892557	RSAD2	0.414545	0.470472
RTP3	8.93204	10.37187	0.123319423	0.821417663	RTP3	0.751279	0.816271
RTP4	9.50638	10.4491	0.023702219	0.306318658	RTP4	0.428430	0.550447
RUNX1	9.068665	9.458605	0.106115515	0.523449937	RUNX1	0.761125	0.715816
S100A6	11.66845	10.9566	0.259578899	0.818122546	S100A6	0.704099	0.764559
SAMD4	9.25507	9.17947	0.199064701	0.064360859	SAMD4	0.764374	0.766432
SAMD9L	10.2843	10.3354	0.080610173	0.384524668	SAMD9L	0.743188	0.834799
SCD1	8.91039	9.679575	1.01833276	0.565862202	SCD1	0.503576	0.645308
SCGB3A1	8.326195	9.18109	0.662580267	0.473492843	SCGB3A1	1.408662	1.535906
SCN3B	10.73285	11.3486	0.237375746	0.979484313	SCN3B	1.386550	1.437548
SDCBP2	9.50562	9.48696	0.128453018	0.415920209	SDCBP2	0.684198	0.799217
SEMA3G	10.94305	10.716	0.176281721	0.413657467	SEMA3G	0.713062	0.766682
SEMA4B	9.798015	9.38992	0.03449974	0.430670456	SEMA4B	0.755244	0.811805
SERPINA1C	5.108275	6.32095	0.284787256	2.183206329	SERPINA1C	1.530465	1.018806
SESN1	10.3361	10.2789	0.271387583	0.269690526	SESN1	1.365936	1.315891
SESN3	11.458	10.64583	0.138310086	1.004332046	SESN3	1.887204	2.315606
SHISA6	7.196505	8.91183	0.692618163	2.510045225	SHISA6	0.666580	0.802565
SIX1	9.332405	9.25913	0.289850141	0.375784828	SIX1	0.759715	0.894234
SLC16A3	10.65755	7.773	0.085064946	4.605669309	SLC16A3	0.733312	0.972183
SLC16A4	9.91809	9.99845	0.369689567	0.035143207	SLC16A4	2.280595	2.873104
SLC16A6	9.94305	10.358015	0.019813132	1.307560647	SLC16A6	1.703563	1.656336
SLC16A9	4.01685	5.876945	0.05238247	2.363143792	SLC16A9	0.871338	1.018528
SLC19A3	8.70529	9.414285	0.145833703	0.340026438	SLC19A3	1.946328	3.491580
SLC1A1	10.1465	10.6016	0.052325902	0.825617878	SLC1A1	1.323731	1.340206
SLC22A14	7.440135	8.541855	0.495208092	2.569548261	SLC22A14	2.265312	1.550910
SLC22A4	7.996635	8.90467	0.076699873	0.962612746	SLC22A4	0.701371	0.685413
SLC24A2	6.17948	5.095405	0.051505658	1.476813726	SLC24A2	0.381591	0.513576
SLC25A23	8.21742	9.078865	0.225354931	1.265459509	SLC25A23	1.426743	1.342358
SLC25A42	9.50031	9.67834	0.156539299	0.018568624	SLC25A42	1.311402	1.301644
SLC35F2	9.672325	8.195785	0.002227386	2.033872448	SLC35F2	3.640761	3.494849
SLC39A8	10.130845	9.23891	0.298335422	1.218755106	SLC39A8	2.449114	2.331147
SLC40A1	11.7349	8.762835	0.078913117	3.673794495	SLC40A1	1.700313	1.715346
SLC44A1	12.2969	10.14749	0.009475231	2.856159853	SLC44A1	1.350927	1.267688
SLC44A5	7.311155	8.55573	0.071071303	1.410791166	SLC44A5	0.669908	0.667045
SLC9A7	7.939515	8.77883	0.34374582	1.548012308	SLC9A7	1.541602	1.421762
SLCO1A4	9.89261	9.92195	0.100677864	0.747624	SLCO1A4	8.075099	9.987614
SLCO1A5	6.37141	8.91171	0.377962717	3.686557772	SLCO1A5	1.463629	1.822154
SLCO1C1	8.904465	10.875525	0.711738331	1.823451612	SLCO1C1	3.712832	4.901421
SLCO2B1	10.59085	8.995835	0.098641396	2.745787555	SLCO2B1	2.392535	2.352639
SNCG	8.80367	8.816585	0.000410122	1.395383309	SNCG	0.603525	0.706587
SNED1	10.14743	10.35475	0.361996246	0.195515025	SNED1	2.082996	1.758938
SNORA20	6.22496	6.2812	0.180566788	0.536453631	SNORA20	1.451586	1.258583
SOD3	9.015755	8.77494	0.200542554	0.300096118	SOD3	2.234543	1.484097
SP100	10.39765	10.79225	0.017465537	0.004313351	SP100	0.759331	0.844313
SPINT2	9.387575	9.383995	0.203540687	0.020541452	SPINT2	1.324332	1.131860
SPNS2	11.017	10.773	0.040729351	0.218495995	SPNS2	1.338530	1.137329
SPP1	11.84065	9.053465	0.658669967	4.534301021	SPP1	0.760200	0.773032
SPRR1A	8.0627	8.235045	0.439580002	0.171989582	SPRR1A	0.574729	0.610469
SPRY1	9.12422	9.540665	0.085814479	1.164230102	SPRY1	1.893263	1.595579
SPRY4	10.3198	9.74072	0.003676955	0.912139463	SPRY4	0.713557	0.778301
SRPX2	9.41938	9.73956	0.579799276	1.535751076	SRPX2	1.458292	1.388421
SSBP2	9.737765	10.45823	0.285763063	0.875921454	SSBP2	1.445406	1.420585
ST3GAL5	9.425945	8.924555	0.202706301	0.654731382	ST3GAL5	1.736094	1.750491
ST3GAL6	11.4316	9.971945	0.174796796	1.989734843	ST3GAL6	1.624280	1.323905
ST6GALNAC2	10.7901	10.7651	0.178190909	0.518167849	ST6GALNAC2	1.444480	1.418632
ST8SIA6	10.61965	10.060965	0.050416713	1.215566054	ST8SIA6	0.650085	0.781165
STAT1	10.9562	10.32523	0.014849242	1.301599736	STAT1	0.681342	0.743549
STAT2	9.83069	9.68194	0.112599684	0.974053733	STAT2	0.700492	0.826800
STAT4	7.495805	9.571185	0.553021142	2.19360787	STAT4	0.678297	0.943455
STC2	9.596265	10.217295	0.515784899	1.009331291	STC2	1.985490	2.047325
STMN2	9.862255	11.0268	0.238075782	0.033092597	STMN2	0.648467	0.732220
STOM	10.064625	10.64695	0.164720525	0.159028315	STOM	0.673115	0.828573
STXBP5	10.5484	10.27981	0.057134228	0.417461701	STXBP5	1.308261	1.266283
STXBP6	10.13335	8.66914	0.083792154	1.937557433	STXBP6	1.616222	1.612836

SUSD4	8.341465	8.870095	0.315093853	1.158445969	SUSD4	1.866111	1.547645
SWAP70	10.8849	11.143	0.016404877	0.115541248	SWAP70	1.321338	1.347234
SYNM	10.2998	10.4479	0.060669762	0.021496046	SYNM	1.611814	1.586426
SYT5	7.93642	9.953985	1.567585023	1.158686385	SYT5	1.427618	1.477656
TAF1D	7.886175	8.905975	0.26812782	1.105200828	TAF1D	1.097092	1.054066
TBC1D30	8.61631	8.18532	0.171416826	0.604321739	TBC1D30	1.398175	1.687947
TBC1D8	10.001005	10.676835	0.023610295	1.020022745	TBC1D8	1.476207	1.537951
TBX1	12.20035	11.39275	0.207252998	1.122673436	TBX1	1.920524	1.979931
TBX4	9.11201	8.02775	0.010238906	1.651843867	TBX4	1.344976	1.205770
TCF7	8.68668	8.25808	0.07800802	0.665359197	TCF7	2.864692	2.689056
TGFBR3	10.80845	9.87115	0.180807204	1.562776697	TGFBR3	1.537323	1.331355
TGTP1	9.568725	9.944235	0.078043375	0.250690567	TGTP1	0.564844	0.631034
TGTP1	9.568725	11.05395	0.078043375	1.318683436	TGTP1	0.564844	0.631034
THSD1	10.9332	10.03105	0.130531912	1.443275651	THSD1	1.318365	1.393729
TIMP3	12.0599	10.39557	0.162351717	2.962254154	TIMP3	0.743987	1.099616
TINAGL1	10.8676	10.92385	0.347755115	0.952119281	TINAGL1	0.655537	0.778760
TMEM178	9.713295	9.471005	0.078453497	0.245259987	TMEM178	0.647362	0.723144
TNFRSF19	8.71635	9.314725	0.435379787	0.024246692	TNFRSF19	2.047523	2.309771
TPD52L1	9.035165	9.80416	0.1730361	1.604764698	TPD52L1	1.374393	1.433096
TRF	10.69565	11.8491	0.140643539	2.060367739	TRF	1.613010	1.410606
TRIM14	8.575335	10.687715	0.63008164	2.067417594	TRIM14	0.671880	0.749674
TRIM30A	11.1322	10.62889	0.06462956	1.091362748	TRIM30A	0.720840	0.744090
TRIM30D	8.020205	8.585055	0.446926841	0.378874884	TRIM30D	0.691219	0.686340
TRPV4	9.149275	9.79209	0.219549584	1.27818036	TRPV4	0.698262	0.915543
TSHZ2	10.49035	10.28535	0.047164022	0.240345595	TSHZ2	1.437553	1.336477
TSPAN33	8.43354	8.23542	0.307025764	0.201115311	TSPAN33	0.652265	0.687504
TTBK2	10.64115	10.85195	0.213334116	0.376110097	TTBK2	1.454371	1.433011
TTYH2	12.2887	10.004435	0.088388348	2.704351098	TTYH2	1.478670	1.355382
TUBB3	7.541275	9.462725	0.494882823	2.577934548	TUBB3	0.727329	0.670793
UBE2L6	9.950045	10.2671	0.14065061	0.112005714	UBE2L6	0.588880	0.719866
UPP1	12.10385	10.375965	0.017041273	2.8157487	UPP1	0.746182	0.817194
USP18	10.2716	10.77255	0.193322994	0.055366461	USP18	0.447140	0.579207
USP53	10.70555	11.23905	0.32632978	0.938259988	USP53	1.376300	1.285434
VIL1	8.593785	8.327235	0.17256941	0.826105781	VIL1	2.091575	2.218555
VSIG2	11.2033	10.65455	0.075801847	0.692469671	VSIG2	1.365851	1.308805
VWF	12.48365	12.27955	0.083933575	0.065124535	VWF	2.269068	2.436567
WBSCR27	10.02046	10.2089	0.105132636	0.268700577	WBSCR27	1.356195	1.291663
WNK2	8.46679	9.166985	0.108187338	1.11435079	WNK2	1.455298	1.445932
XAF1	9.129845	9.232275	0.052799663	0.473697904	XAF1	0.647726	0.714841
XYLT1	9.23178	10.061225	0.134124014	1.328194022	XYLT1	0.692356	0.767945
ZBP1	7.26186	9.910955	0.076028121	2.854229451	ZBP1	0.676853	0.789702
ZIC2	11.4337	10.668255	0.180029386	1.321080528	ZIC2	1.303734	1.340852
ZIC3	10.41635	9.41748	0.151391562	1.354420613	ZIC3	1.766379	1.794634
ZNRF3	9.44037	9.53958	0.220475894	0.415029254	ZNRF3	1.416671	1.491847

List of gene generated comparing WT vs. CCM3 KO (threshold=1.3)

Affymetrix raw data (log2)

Gene_Symbol	WT+WNT	CCM3 KO	s.d. WT WNT3a	s.d. CCM3 KO WNT3a
A4GALT	9.469495	10.16574	0.329080425	0.284624622
ACER3	8.71395	9.223155	0.076721086	0.320948697
ADAMTS5	10.61755	11.31375	0.23878996	0.165109433
ADAMTSL1	7.166005	8.44057	0.222703281	0.869331219
AFAP1L2	7.516615	8.85352	0.572452437	0.337883904
AHNAK	10.5463	11.0541	0.397394011	0.476165706
AHNAK2	10.9506	11.56765	0.649124025	0.56207918
ALOX5AP	7.19162	8.05255	0.07773932	0.307138901
ANKRD33B	7.40566	7.798225	0.21998092	0.102226427
ANLN	9.94231	10.5551	0.848655417	0.243386154
ANPEP	7.84837	9.574935	0.43043004	0.395944442
APOD	9.12002	11.00205	0.88423703	0.431123004
APOLD1	12.531	12.95265	0.064063874	0.043204224
ARF2	10.45285	10.95755	0.023688077	0.232991684
ARHGAP18	11.2228	10.6572	0.199262691	0.274498852
ARL4D	7.92974	8.65511	0.017140268	0.244871078
ARRDC4	9.394075	9.87393	0.09224208	0.036769553
ASS1	8.823505	9.91264	0.518514332	0.031635957
ASS1	8.823505	9.91264	0.518514332	0.031635957
ATP10D	8.52695	8.86611	0.209727871	0.236216091
ATP2A3	7.30733	8.12221	0.341009316	0.394311025
ATP2B4	7.69238	9.190445	0.951214184	0.275877711
BAIAP2L1	9.117405	9.59039	0.239447569	0.00516188
BCL2L11	10.59175	9.9579	0.287156064	0.545462171
BST1	9.709005	10.5671	0.056179634	0.304763023
C2CD2L	10.5445	10.9087	0.229244018	0.110308658
CACNG4	9.143755	9.01266	0.182949737	0.109898536
CADM3	7.59468	8.47445	0.218439427	0.482020551
CALCRL	11.0602	11.6096	0.245507474	0.074953319
CAPN5	9.74897	10.37175	0.000509117	0.086337738
CAR2	9.91782	8.5299	0.11721002	0.446141953
CAR4	6.731835	7.661025	0.18177594	0.331215887
CAR5B	9.438805	9.89995	0.191746146	0.288570277
CBFA2T3	10.11635	10.6343	0.083085047	0.061094026
CCDC141	8.05143	8.03932	0.192573461	0.28381852
CD24A	8.73289	8.20946	0.493122127	0.518775961
CD276	10.5123	10.35675	0.019657569	0.098782817
CD38	12.9138	12.38555	0.067316566	0.507207694
CD55	7.51668	8.89261	0.251998715	0.823595552
CDC42EP3	10.228	9.759735	0.121339524	0.001237437
CDCA7L	9.87573	9.622215	0.463678201	0.392918025
CEACAM1	11.1053	12.00635	0.062083975	0.058053467
CHST15	10.038335	9.561305	0.148160084	0.883027877
CHST7	9.871655	9.343715	0.137397919	0.091294557
CKB	10.72065	11.6428	0.166382226	0.048931789
CLEC2D	9.825235	9.06648	0.137779756	0.751583798
CLIC5	9.64125	10.88675	0.034407816	0.392514974
CLIC6	10.417	10.37385	0.18356492	0.154785674
CMKLR1	7.242115	8.25133	0.455115138	0.784153136
COL15A1	10.74245	11.0673	0.069508597	0.106773124
CRCT1	8.918805	9.730185	0.026566002	0.328359176
CRIP1	10.9661	11.85075	0.251022907	0.043062803
CRYAB	8.910145	9.07221	1.006191736	0.350838101
CSN3	7.67541	7.655535	0.511280629	0.075794776
CST6	8.136885	9.432595	0.206750952	0.468932004
CTXN1	9.99733	8.982095	0.100083894	0.193754329
CXX1A	12.09905	12.76535	0.235820112	0.02298097
CYP1B1	8.084105	8.600155	0.086373093	0.18634385
CYSLTR1	6.444915	7.376565	0.422050824	0.338598082
DAPK2	9.405485	9.468405	0.047312515	0.095325065
DCN	6.98133	10.67328	0.152126953	1.401513925
DDIT4	10.45	9.87607	0.02602153	0.249368277
DHCR24	10.2094	10.66705	0.099419213	0.044901281
DHH	9.30462	10.010015	0.352591725	0.099963686
DLL1	8.806365	10.4176	0.011575338	0.062225397
DNM3	8.62547	8.62615	0.304649886	0.350229989
DOC2B	8.786095	8.63852	0.399140565	0.310476445
DOK4	9.660245	10.31945	0.005154808	0.03542605
DPY19L3	9.099685	8.30704	0.01489874	0.525408623
DYNC1I1	8.193185	8.93093	0.829895874	0.742122709
E2F8	8.611715	8.82475	0.76444607	0.572289802
EDA2R	10.17765	10.058585	0.099348503	0.13734135
EDN1	12.3917	11.2048	0.226557013	0.115258405
EDNRB	10.444	11.39225	0.136895873	0.019728279
EFHD1	7.628505	8.504835	0.211700699	0.398772869
EFNA3	7.43474	8.828695	0.129556104	0.600171023

Fold change (linear)

Gene_Symbol	WT VS KO	WT vs WT WNT
A4GALT	1.383080	0.853605
ACER3	1.362338	0.957192
ADAMTS5	1.414655	0.873119
ADAMTSL1	2.404488	0.993895
AFAP1L2	2.113714	0.836754
AHNAK	1.321567	0.929451
AHNAK2	1.385590	0.903408
ALOX5AP	1.810314	0.996754
ANKRD33B	1.361687	1.037298
ANLN	1.495746	0.978114
ANPEP	1.960905	0.592528
APOD	2.113758	0.573464
APOLD1	1.397405	1.043261
ARF2	1.528429	1.077248
ARHGAP18	0.752910	1.114310
ARL4D	1.668353	1.009090
ARRDC4	0.754886	0.541291
ASS1	1.745621	0.820517
ASS1	1.745621	0.820517
ATP10D	1.448044	1.144681
ATP2A3	1.620321	0.921081
ATP2B4	1.584124	0.560824
BAIAP2L1	1.357366	0.977945
BCL2L11	0.744942	1.155927
BST1	1.915273	1.056619
C2CD2L	1.444530	1.122255
CACNG4	0.673745	0.737835
CADM3	1.602112	0.870674
CALCRL	1.364952	0.932677
CAPN5	1.487418	0.965956
CAR2	0.565810	1.480731
CAR4	1.625806	0.853797
CAR5B	1.363411	0.990394
CBFA2T3	1.336584	0.933421
CCDC141	1.562109	1.575276
CD24A	0.611581	0.879067
CD276	0.720590	0.802626
CD38	0.753067	1.086057
CD55	2.361903	0.910051
CDC42EP3	0.763571	1.056359
CDCA7L	0.765195	0.912196
CEACAM1	1.478311	0.791631
CHST15	0.731277	1.017846
CHST7	0.762863	1.099948
CKB	1.497961	0.790507
CLEC2D	0.661572	1.119399
CLIC5	1.883068	0.794206
CLIC6	0.694766	0.715860
CMKLR1	1.915658	0.951730
COL15A1	0.731840	0.584287
CRCT1	1.679248	0.956897
CRIP1	1.376066	0.745304
CRYAB	1.470019	1.313822
CSN3	0.422200	0.428056
CST6	1.667822	0.679363
CTXN1	0.673799	1.361904
CXX1A	1.409760	0.888319
CYP1B1	2.315654	1.619294
CYSLTR1	1.670234	0.875634
DAPK2	0.724772	0.693842
DCN	11.239298	0.869664
DDIT4	0.717410	1.067917
DHCR24	1.382855	1.006956
DHH	1.339022	0.821188
DLL1	2.614980	0.855930
DNM3	1.457923	1.457236
DOC2B	0.684558	0.758289
DOK4	1.408100	0.891647
DPY19L3	0.681696	1.180866
DYNC1I1	1.762282	1.056798
E2F8	1.398369	1.206401
EDA2R	0.758586	0.823848
EDN1	0.625638	1.424346
EDNRB	1.499831	0.777304
EFHD1	1.820904	0.991940
EFNA3	1.578627	0.600699

EFR3B	9.113465	9.518005	0.352287669	0.170943064	EFR3B	1.323626	0.999969
ELOVL7	10.183	9.778065	0.136330187	0.185735738	ELOVL7	1.488764	1.971167
EMP3	11.52695	12.0586	0.043487067	0.093055252	EMP3	1.393826	0.964197
ENPP2	10.38085	9.00493	0.076862507	1.071012215	ENPP2	0.631743	1.639584
ENTPD1	11.5965	11.4913	0.033516861	0.091216775	ENTPD1	1.447788	1.557303
ESM1	8.56836	7.31198	0.535110128	0.322214418	ESM1	0.427110	1.020347
F2R	10.76165	10.458	0.070215703	0.084004286	F2R	0.749448	0.925016
F5	6.44601	7.158895	0.316882833	0.037059466	F5	1.761983	1.074984
FABP7	7.4502	7.08596	0.066100342	0.129697526	FABP7	0.562268	0.723753
FAM107A	7.877815	9.470065	0.138628284	0.008647916	FAM107A	2.899070	0.961487
FAM110C	9.2513	8.97724	0.003167838	0.046499342	FAM110C	0.744299	0.900011
FAM189A2	7.76387	9.58435	0.307831866	0.499203245	FAM189A2	3.246308	0.919120
FAM20A	8.785285	9.78255	0.205336738	0.126515545	FAM20A	2.280547	1.142437
FAR2	10.3801	11.18515	0.246638845	0.181938575	FAR2	1.312120	0.750982
FBLN2	8.29856	9.44827	0.246582277	0.063738605	FBLN2	1.692933	0.763032
FNDC1	8.085185	9.717705	0.654476823	0.503311536	FNDC1	2.459525	0.793257
FUCA2	10.4527	11.1911	0.081458701	0.557624408	FUCA2	1.595103	0.956111
GADD45A	9.984515	9.194495	0.150733953	0.21097945	GADD45A	0.737227	1.274737
GALNTL4	9.55237	9.28295	0.185657956	0.39811526	GALNTL4	0.737045	0.888378
GDPD5	11.56315	11.06315	0.087186266	0.353058416	GDPD5	0.728272	1.029933
GEM	6.790545	8.213615	0.198972777	0.84013478	GEM	2.400741	0.895283
GJA4	8.675705	8.780135	1.078019643	1.399625949	GJA4	0.479243	0.445779
GM11428	7.972085	6.769635	0.612121127	0.789590787	GM11428	0.589592	1.356830
GM5972	12.219	13.12655	0.146512525	0.287721749	GM5972	1.310938	0.698848
GM8995	9.8192	10.86095	0.09906566	0.21998092	GM8995	1.342479	0.652093
GPIHBP1	8.62062	9.045125	0.07694736	0.413508975	GPIHBP1	0.740412	0.551677
GPRC5A	10.68475	11.37485	0.073751237	0.116601908	GPRC5A	1.420797	0.880625
GRIN2A	8.1589	8.35705	0.13098446	0.189971308	GRIN2A	0.665873	0.580420
GYS1	10.3389	10.20885	0.025738687	0.097368604	GYS1	0.767533	0.839935
HEY1	11.0533	10.8566	0.00834386	0.264740779	HEY1	0.733592	0.840751
HTR2A	9.91791	9.786275	0.167287322	0.201207235	HTR2A	1.321219	1.447441
HTRA1	9.812205	11.0776	0.62153979	0.28255987	HTRA1	1.355993	0.564073
HYAL1	9.17945	10.034485	0.00456791	0.123906321	HYAL1	1.524816	0.842997
ICOSL	7.07223	8.01002	0.082717351	0.01834235	ICOSL	1.574534	0.821957
ID2	10.046155	8.63319	0.608316893	1.306309068	ID2	0.575266	1.531839
ID3	10.66275	9.53934	0.258447529	0.566109689	ID3	0.514356	1.120583
IGFBP4	10.21144	9.46571	0.626157197	0.941286405	IGFBP4	0.612918	1.027754
IGFBP5	7.93703	9.55137	0.870448448	1.507594084	IGFBP5	3.240486	1.058385
INHBB	9.664415	9.574495	0.418727423	0.270475415	INHBB	0.752107	0.800476
IRX3	8.769385	9.076125	0.326902536	0.25852531	IRX3	1.607318	1.299462
ITGA2	10.05435	9.96941	0.044901281	0.177752503	ITGA2	0.738137	0.782900
ITGA8	10.25755	9.82765	0.165533697	0.081684975	ITGA8	0.761412	1.025729
JAG2	10.9935	11.16365	0.082872915	0.006010408	JAG2	1.303328	1.158333
JAM2	10.88915	11.33395	0.241194123	0.171614816	JAM2	1.351958	0.993265
KCNB1	7.81401	9.04547	0.140728392	0.1640912	KCNB1	2.086797	0.888735
KCNE3	8.918345	9.0118	0.056844314	0.11846867	KCNE3	0.683880	0.640984
KCNJ2	10.8684	9.40504	0.220900158	0.70385409	KCNJ2	0.578561	1.595380
KCNJ8	8.189815	8.288135	0.087207479	0.171381471	KCNJ8	0.667079	0.623132
KCTD12	9.915335	10.0948	0.093359308	0.169281363	KCTD12	1.325062	1.170070
KLF2	9.86349	10.8013	0.092277435	0.154432121	KLF2	1.731545	0.903909
KLF4	9.809585	11.3648	0.178707097	0.337714199	KLF4	2.800239	0.952859
KLK8	7.27614	7.960335	0.074543197	0.337410143	KLK8	1.569342	0.976685
KRAS	10.72345	11.23775	0.064417428	0.052255191	KRAS	1.362258	0.953761
L1CAM	8.59392	9.48771	0.781098435	0.58558341	L1CAM	1.826998	0.983287
LAMB2	10.9262	11.3416	0.058689863	0.017253405	LAMB2	1.312484	0.984116
LBP	9.6743	10.87805	0.472488751	0.290550176	LBP	1.942305	0.843243
LCP2	11.59075	11.16735	0.179675833	0.107268099	LCP2	0.748461	1.003750
LDLR	9.134135	10.086665	0.235516056	0.125631662	LDLR	1.686819	0.871622
LMCD1	9.09464	9.715335	0.040078812	0.132858293	LMCD1	1.529383	0.994646
LPAR4	10.54655	9.952225	0.099631345	0.060577838	LPAR4	0.642147	0.969491
LRG1	8.668535	9.60747	1.829391309	1.64067158	LRG1	2.718687	1.418115
LSR	9.726295	10.061565	0.091761247	0.307358105	LSR	2.890342	2.290988
LTBP4	10.96635	12.22025	0.583716648	0.157048416	LTBP4	1.461500	0.612826
LYNX1	9.548975	10.09322	0.301333555	0.214083649	LYNX1	1.365486	0.936383
MACF1	11.29515	11.64935	0.501267997	0.523895414	MACF1	1.456494	1.139420
MAF1	10.40675	10.01013	0.148421713	0.149298526	MAF1	0.744674	0.980303
MAL	9.58058	9.313905	0.517870864	0.669128076	MAL	1.967325	2.366754
MALAT1	11.0127	11.7876	0.448447121	1.121895619	MALAT1	1.629241	0.952176
MCOLN2	8.58369	8.95246	0.528647172	0.494055508	MCOLN2	1.744266	1.350834
MEST	10.6621	10.8223	0.189080353	0.366988419	MEST	0.730117	0.653383
MGLL	7.692625	9.368135	0.145741779	0.228869252	MGLL	1.885236	0.590183
MIR505	7.98089	8.61456	0.056907954	0.766800736	MIR505	1.823405	1.175248
MKI67	10.278945	10.63525	0.756399195	0.366352023	MKI67	1.392208	1.087541
MN1	9.276835	9.863665	0.103584072	0.179046508	MN1	1.472242	0.980225
MT1	10.1432	10.78135	0.0417193	0.021001071	MT1	1.337603	0.859459
MT2	11.48545	11.1989	0.356169686	0.091499617	MT2	0.690470	0.842180
MTAP6	8.66651	9.263865	0.241278976	0.033835059	MTAP6	1.403438	0.927623
MUSTN1	10.50995	11.25215	0.117591858	0.125228611	MUSTN1	1.785218	1.067251
NBEAL1	10.3731	10.9052	0.280014285	0.350866385	NBEAL1	1.367888	0.945959
NEK7	11.2367	11.94225	0.037759502	0.208667211	NEK7	1.384821	0.849185
NEURL2	8.21281	9.56288	0.237446457	0.415962635	NEURL2	2.942699	1.154341

NKD1	8.76605	8.894885	0.248859161	0.063858813	NKD1	1.388378	1.269768
NKD2	8.443755	8.80376	0.195338248	0.011709688	NKD2	1.563176	1.217967
NMNAT2	9.451495	10.44655	0.098874741	0.113914902	NMNAT2	1.409638	0.707239
NOSTRIN	10.038305	9.222575	0.056702893	0.055345248	NOSTRIN	1.360866	2.395372
NOV	10.6325	10.8576	0.248053059	0.106066017	NOV	1.330944	1.138670
NPNT	11.6016	12.0034	0.220758737	0.307167186	NPNT	2.821183	2.135391
NPPB	6.969335	7.716025	0.060747544	0.153194684	NPPB	1.626640	0.969428
NQO1	9.7227	10.04648	0.023730504	0.10284161	NQO1	1.647770	1.316525
NR4A1	9.951185	10.92605	0.081479914	0.357442478	NR4A1	2.353732	1.197553
NR4A2	8.977235	9.93358	0.004787113	0.076056405	NR4A2	2.025068	1.043641
NRGN	9.23842	9.384375	0.208059099	0.101095057	NRGN	1.689575	1.527005
NUSAP1	9.72959	10.087525	0.925616919	0.576256671	NUSAP1	1.306059	1.019092
OLFR1372-PS1	10.4813	10.71245	0.348179379	0.577494108	OLFR1372-PS1	1.411785	1.202778
OSGIN1	9.888845	9.27374	0.041627376	0.347726831	OSGIN1	0.717883	1.099559
P2RY2	10.5257	11.89715	0.10323759	0.180100097	P2RY2	1.769878	0.684062
PALMD	11.9784	12.24225	0.00311127	0.032597623	PALMD	1.416568	1.179806
PBP2	6.53319	7.65462	0.266013571	0.755218327	PBP2	1.615572	0.742578
PDCD10	8.947135	8.3248	0.130241998	0.507702669	PDCD10	0.590261	0.908627
PDGFA	10.44605	11.4774	0.121410234	0.025455844	PDGFA	1.611663	0.788509
PDZD2	9.148545	9.74156	0.275722147	0.021227346	PDZD2	1.321934	0.876384
PGLYRP1	10.8223	10.6367	0.17833233	0.052608745	PGLYRP1	2.463877	2.802142
PHGDH	9.799555	10.338005	0.547081446	0.620266997	PHGDH	1.325448	0.912584
PHXR4	7.277205	8.135175	0.324625652	0.877710434	PHXR4	1.884818	1.039907
PIK3CG	9.07639	8.32068	0.261403235	0.183536636	PIK3CG	0.691416	1.167429
PIR	10.6491	10.96565	0.002262742	0.052538034	PIR	1.376448	1.105271
PLAGL1	9.746195	10.81015	0.394714076	0.346270191	PLAGL1	1.951631	0.933502
PLOD2	9.51767	9.396485	0.219839498	0.247593439	PLOD2	0.751602	0.817463
PLTP	13.10245	13.68345	0.008555992	0.004454773	PLTP	1.633878	1.092248
PLVAP	8.540385	9.740475	0.503650947	0.112479476	PLVAP	1.386248	0.603362
PMP22	11.58265	12.1775	0.253073517	0.03337544	PMP22	1.346067	0.891249
POLE	8.92238	9.28467	0.612213051	0.35844657	POLE	1.340350	1.042697
PPAP2B	11.4131	11.7467	0.11158145	0.188797511	PPAP2B	1.418238	1.125448
PPP1R2	12.1662	13.0575	0.124026529	0.327673282	PPP1R2	1.289981	0.695465
PRDM1	8.516965	7.78816	0.077505974	0.273537187	PRDM1	0.619594	1.026832
PRKCC	9.14697	9.824475	0.106023591	0.110810704	PRKCC	1.345614	0.841340
PRKCH	7.639705	8.06988	0.067663048	0.343851886	PRKCH	1.600353	1.187737
PRR11	9.729165	10.09482	1.008949453	0.554343432	PRR11	1.308537	1.015577
PTHLH	7.812845	9.58466	0.029012591	0.21667166	PTHLH	2.076998	0.608228
PTPRJ	10.123265	11.0265	0.728086639	0.185261977	PTPRJ	1.604329	0.857813
PTPRJ	10.123265	11.0265	0.728086639	0.185261977	PTPRJ	1.604329	0.857813
RAMP3	9.404755	10.21664	1.192104251	0.98409465	RAMP3	2.388873	1.360786
RASGRP2	7.45499	8.583615	0.180609214	0.017430182	RASGRP2	1.518366	0.694427
RET	8.117725	10.21953	0.540307363	0.611463518	RET	4.636352	1.080111
RGL1	10.2799	9.66841	0.193605837	0.627472415	RGL1	0.729533	1.114607
RGS16	11.03835	10.611	0.043204224	0.031819805	RGS16	0.746700	1.004133
RIPPLY3	8.11768	8.821095	0.082222377	0.069713658	RIPPLY3	1.498802	0.920440
RND3	9.712735	8.96355	0.175807959	0.296009041	RND3	0.581544	0.977484
RNF144A	10.9344	10.6034	0.164614459	0.232213867	RNF144A	0.733643	0.922838
ROBO1	9.916015	8.7491	0.434425193	0.163935636	ROBO1	0.644691	1.447532
RPS6KA1	10.7206	10.3477	0.219485945	0.442648845	RPS6KA1	0.762284	0.987122
RRM2	9.58031	9.988365	0.805804746	0.239475854	RRM2	1.346309	1.014631
RTP3	8.93204	10.22015	0.123319423	0.297904087	RTP3	1.834682	0.751279
S1PR4	8.968775	9.28006	0.107699434	0.349169329	S1PR4	1.340559	1.080388
SAMD5	8.356815	8.68346	0.029960114	0.281527494	SAMD5	1.717714	1.369686
SCARNA13	10.30445	10.67685	0.009687363	0.08237794	SCARNA13	1.337510	1.033222
SCARNA17	10.85005	10.150605	0.231011785	0.890523209	SCARNA17	0.654337	1.062564
SCARNA17	10.85005	10.150605	0.231011785	0.890523209	SCARNA17	0.654337	1.062564
SCN3B	10.73285	9.84849	0.237375746	0.520727576	SCN3B	0.751133	1.386550
SELP	7.99802	9.05292	0.463225652	0.034803796	SELP	1.831690	0.881648
SERPINB1A	6.7888	7.72185	0.062791082	0.014608826	SERPINB1A	1.871487	0.980191
SERPINB8	7.971955	8.431095	0.22826114	0.293739228	SERPINB8	1.678689	1.221112
SERPINB9B	7.36764	9.613135	0.381130555	0.943796634	SERPINB9B	4.820591	1.016574
SESN3	11.458	10.10791	0.138310086	0.164458895	SESN3	0.740289	1.887204
SIX1	9.332405	9.244905	0.289850141	0.380642651	SIX1	0.715007	0.759715
SIX4	9.790655	9.19881	0.17197544	0.146710515	SIX4	0.681483	1.027113
SLC45A4	11.62965	11.4636	0.281216367	0.335310036	SLC45A4	0.720590	0.808489
SLC46A3	10.23715	11.12805	0.000777817	0.091853171	SLC46A3	1.764183	0.951384
SLC6A17	8.737595	8.403395	0.459725474	0.425671211	SLC6A17	0.677470	0.854072
SLC7A6	9.83354	9.19088	0.115173553	0.175404908	SLC7A6	0.708979	1.106862
SLCO2A1	7.79354	8.65313	0.448701679	0.765909781	SLCO2A1	1.810057	0.997539
SLFN2	7.914915	8.990325	0.142984062	0.493313046	SLFN2	1.572168	0.746050
SLFN3	9.99119	10.7422	0.076240253	0.253992756	SLFN3	1.366466	0.811937
SLFN9	9.18195	9.628635	0.677719423	0.422503373	SLFN9	1.328198	0.974534
SNCG	8.80367	10.08743	0.000410122	0.252253273	SNCG	1.469418	0.603525
SNED1	10.14743	9.741045	0.361996246	0.251963359	SNED1	1.571639	2.082996
SNORD57	12.47015	11.98895	0.16680649	0.494479772	SNORD57	0.757674	1.057641
SOX4	10.7837	10.109	0.054588644	0.099277792	SOX4	0.735298	1.173730
STMN2	9.862255	11.5871	0.238075782	0.269690526	STMN2	2.143473	0.648467
SUOX	9.049565	9.287335	0.123496199	0.02225265	SUOX	1.347920	1.143111
SYNE2	8.59955	9.152595	0.209869293	0.413834244	SYNE2	1.434020	0.977399
SYNE2	8.59955	9.152595	0.209869293	0.413834244	SYNE2	1.434020	0.977399

TDG	9.866995	9.43311	0.0235113	0.280990093	TDG	0.716563	0.967981
THBD	11.109	12.1939	0.001838478	0.315793888	THBD	1.889953	0.890971
TINAGL1	10.8676	12.2341	0.347755115	0.164897301	TINAGL1	1.690266	0.655537
TMEM140	9.63001	10.1588	0.095261426	0.044264885	TMEM140	1.359160	0.942082
TMEM173	11.57795	10.9688	0.36394786	0.671327178	TMEM173	0.755917	1.153046
TMEM223	11.919	11.42385	0.008909545	0.357018214	TMEM223	0.763500	1.076128
TMTC1	8.378085	9.731805	0.402661957	0.028715606	TMTC1	2.035510	0.796458
TNFAIP2	10.4653	10.96885	0.246638845	0.231577471	TNFAIP2	1.323630	0.933648
TOMM7	10.186	9.828585	0.088246926	0.112012785	TOMM7	0.755674	0.968115
TOX3	8.935025	7.868995	0.278112168	0.891088895	TOX3	0.513014	1.074079
TRPV4	9.149275	11.11805	0.219549584	0.15747268	TRPV4	2.733255	0.698262
TSC22D3	8.519525	9.31771	0.31686162	0.339991083	TSC22D3	1.723684	0.991243
TUBA4A	8.55442	8.99229	0.206545891	0.079365665	TUBA4A	1.365704	1.008195
UNC5B	12.11965	11.8487	0.073751237	0.188373247	UNC5B	0.757123	0.913546
VWF	12.48365	10.84255	0.083933575	1.089015154	VWF	0.727490	2.269068
XDH	7.914035	9.088095	0.289864283	0.3642802	XDH	1.811456	0.802787
XYLT1	9.23178	9.24315	0.134124014	0.336710107	XYLT1	0.697834	0.692356
ZBTB7C	7.425105	8.173195	0.013159257	0.119706107	ZBTB7C	1.567228	0.933114
ZFP697	9.875725	10.51025	0.586863273	0.5787669	ZFP697	1.601063	1.031329

Table 1. Affymetrix data. Data coming from Affymetrix analysis have been analyzed and listed in this table. The table present raw data about the condition WT+Wnt3a, KO+Wnt3a and KO and the fold changes about the comparison between the following conditions: WT vs. WT+Wnt3a, KO vs. KO+Wnt3a and WT vs. KO. Genes listed here were pre-selected comparing respectively WT vs. WT+Wnt3a and WT vs. KO in order to analyze only genes experimentally regulated by Wnt3a and *CCM3* ablation.

REFERENCES

1. Fishman, A.P. Endothelium: a distributed organ of diverse capabilities. *Ann N Y Acad Sci* **401**, 1-8 (1982).
2. Jaffe, E.A., Nachman, R.L., Becker, C.G. & Minick, C.R. Culture of human endothelial cells derived from umbilical veins. Identification by morphologic and immunologic criteria. *J Clin Invest* **52**, 2745-2756 (1973).
3. Gimbrone, M.A., Jr., Cotran, R.S. & Folkman, J. Human vascular endothelial cells in culture. Growth and DNA synthesis. *J Cell Biol* **60**, 673-684 (1974).
4. Garlanda, C. & Dejana, E. Heterogeneity of endothelial cells. Specific markers. *Arterioscler Thromb Vasc Biol* **17**, 1193-1202 (1997).
5. Le Bras, A., Vijayaraj, P. & Oettgen, P. Molecular mechanisms of endothelial differentiation. *Vasc Med* **15**, 321-331 (2010).
6. Carmeliet, P. Angiogenesis in life, disease and medicine. *Nature* **438**, 932-936 (2005).
7. Schatteman, G.C. & Awad, O. Hemangioblasts, angioblasts, and adult endothelial cell progenitors. *Anat Rec A Discov Mol Cell Evol Biol* **276**, 13-21 (2004).
8. Patan, S. Vasculogenesis and angiogenesis. *Cancer Treat Res* **117**, 3-32 (2004).
9. Carmeliet, P. & Jain, R.K. Molecular mechanisms and clinical applications of angiogenesis. *Nature* **473**, 298-307 (2011).
10. Makanya, A.N., Hlushchuk, R. & Djonov, V.G. Intussusceptive angiogenesis and its role in vascular morphogenesis, patterning, and remodeling. *Angiogenesis* **12**, 113-123 (2009).
11. Folkman, J. Angiogenesis in cancer, vascular, rheumatoid and other disease. *Nat Med* **1**, 27-31 (1995).
12. Marcelo, K.L., Goldie, L.C. & Hirschi, K.K. Regulation of endothelial cell differentiation and specification. *Circ Res* **112**, 1272-1287 (2013).
13. Adams, R.H. & Alitalo, K. Molecular regulation of angiogenesis and lymphangiogenesis. *Nat Rev Mol Cell Biol* **8**, 464-478 (2007).
14. Swift, M.R. & Weinstein, B.M. Arterial-venous specification during development. *Circ Res* **104**, 576-588 (2009).
15. Xin, M., Olson, E.N. & Bassel-Duby, R. Mending broken hearts: cardiac development as a basis for adult heart regeneration and repair. *Nat Rev Mol Cell Biol* **14**, 529-541 (2013).
16. le Noble, F. et al. Flow regulates arterial-venous differentiation in the chick embryo yolk sac. *Development* **131**, 361-375 (2004).
17. Aitsebaomo, J., Portbury, A.L., Schisler, J.C. & Patterson, C. Brothers and sisters: molecular insights into arterial-venous heterogeneity. *Circ Res* **103**, 929-939 (2008).
18. Herzog, Y., Guttmann-Raviv, N. & Neufeld, G. Segregation of arterial and venous markers in subpopulations of blood islands before vessel formation. *Dev Dyn* **232**, 1047-1055 (2005).
19. Wang, H.U., Chen, Z.F. & Anderson, D.J. Molecular distinction and angiogenic interaction between embryonic arteries and veins revealed by ephrin-B2 and its receptor Eph-B4. *Cell* **93**, 741-753 (1998).

20. Adams, R.H. et al. Roles of ephrinB ligands and EphB receptors in cardiovascular development: demarcation of arterial/venous domains, vascular morphogenesis, and sprouting angiogenesis. *Genes Dev* **13**, 295-306 (1999).
21. Gridley, T. Notch signaling in vertebrate development and disease. *Mol Cell Neurosci* **9**, 103-108 (1997).
22. Lawson, N.D. et al. Notch signaling is required for arterial-venous differentiation during embryonic vascular development. *Development* **128**, 3675-3683 (2001).
23. You, L.R. et al. Suppression of Notch signalling by the COUP-TFII transcription factor regulates vein identity. *Nature* **435**, 98-104 (2005).
24. Lawson, N.D., Vogel, A.M. & Weinstein, B.M. sonic hedgehog and vascular endothelial growth factor act upstream of the Notch pathway during arterial endothelial differentiation. *Dev Cell* **3**, 127-136 (2002).
25. Yang, Y. & Oliver, G. Development of the mammalian lymphatic vasculature. *J Clin Invest* **124**, 888-897 (2014).
26. Dejana, E. The role of wnt signaling in physiological and pathological angiogenesis. *Circ Res* **107**, 943-952 (2010).
27. Dyer, L.A., Pi, X. & Patterson, C. The role of BMPs in endothelial cell function and dysfunction. *Trends Endocrinol Metab* **25**, 472-480 (2014).
28. Corada, M. et al. The Wnt/beta-catenin pathway modulates vascular remodeling and specification by upregulating Dll4/Notch signaling. *Dev Cell* **18**, 938-949 (2010).
29. Corada, M. et al. Sox17 is indispensable for acquisition and maintenance of arterial identity. *Nat Commun* **4**, 2609 (2013).
30. Wiley, D.M. & Jin, S.W. Bone Morphogenetic Protein functions as a context-dependent angiogenic cue in vertebrates. *Semin Cell Dev Biol* **22**, 1012-1018 (2011).
31. Henderson, V.J., Cohen, R.G., Mitchell, R.S., Kosek, J.C. & Miller, D.C. Biochemical (functional) adaptation of "arterialized" vein grafts. *Ann Surg* **203**, 339-345 (1986).
32. Othman-Hassan, K. et al. Arterial identity of endothelial cells is controlled by local cues. *Dev Biol* **237**, 398-409 (2001).
33. Roca, C. & Adams, R.H. Regulation of vascular morphogenesis by Notch signaling. *Genes Dev* **21**, 2511-2524 (2007).
34. Aird, W.C. Phenotypic heterogeneity of the endothelium: I. Structure, function, and mechanisms. *Circ Res* **100**, 158-173 (2007).
35. Aird, W.C. Phenotypic heterogeneity of the endothelium: II. Representative vascular beds. *Circ Res* **100**, 174-190 (2007).
36. Bazzoni, G. & Dejana, E. Endothelial cell-to-cell junctions: molecular organization and role in vascular homeostasis. *Physiol Rev* **84**, 869-901 (2004).
37. Atkins, G.B., Jain, M.K. & Hamik, A. Endothelial differentiation: molecular mechanisms of specification and heterogeneity. *Arterioscler Thromb Vasc Biol* **31**, 1476-1484 (2011).
38. Aird, W.C. et al. Vascular bed-specific expression of an endothelial cell gene is programmed by the tissue microenvironment. *J Cell Biol* **138**, 1117-1124 (1997).
39. Warren, M.S. et al. Comparative gene expression profiles of ABC transporters in brain microvessel endothelial cells and brain in five species including human. *Pharmacol Res* **59**, 404-413 (2009).
40. Grau, G.E. et al. Haemostatic properties of human pulmonary and cerebral microvascular endothelial cells. *Thromb Haemost* **77**, 585-590 (1997).

41. Augustin, H.G., Kozian, D.H. & Johnson, R.C. Differentiation of endothelial cells: analysis of the constitutive and activated endothelial cell phenotypes. *Bioessays* **16**, 901-906 (1994).
42. Visconti, R.P., Richardson, C.D. & Sato, T.N. Orchestration of angiogenesis and arteriovenous contribution by angiopoietins and vascular endothelial growth factor (VEGF). *Proc Natl Acad Sci U S A* **99**, 8219-8224 (2002).
43. Suri, C. et al. Increased vascularization in mice overexpressing angiopoietin-1. *Science* **282**, 468-471 (1998).
44. Goumans, M.J. et al. Balancing the activation state of the endothelium via two distinct TGF-beta type I receptors. *Embo J* **21**, 1743-1753 (2002).
45. Davies, P.F., Civelek, M., Fang, Y., Guerraty, M.A. & Passerini, A.G. Endothelial heterogeneity associated with regional athero-susceptibility and adaptation to disturbed blood flow in vivo. *Semin Thromb Hemost* **36**, 265-275 (2010).
46. Cavalcanti, D.D. et al. Cerebral cavernous malformations: from genes to proteins to disease. *J Neurosurg* **116**, 122-132 (2012).
47. Paolinelli, R., Corada, M., Orsenigo, F. & Dejana, E. The molecular basis of the blood brain barrier differentiation and maintenance. Is it still a mystery? *Pharmacol Res* **63**, 165-171 (2011).
48. Abbott, N.J., Patabendige, A.A., Dolman, D.E., Yusof, S.R. & Begley, D.J. Structure and function of the blood-brain barrier. *Neurobiol Dis* **37**, 13-25 (2010).
49. Engelhardt, B. & Sorokin, L. The blood-brain and the blood-cerebrospinal fluid barriers: function and dysfunction. *Semin Immunopathol* **31**, 497-511 (2009).
50. Daneman, R. et al. The mouse blood-brain barrier transcriptome: a new resource for understanding the development and function of brain endothelial cells. *PLoS One* **5**, e13741 (2010).
51. Macdonald, J.A., Murugesan, N. & Pachter, J.S. Endothelial cell heterogeneity of blood-brain barrier gene expression along the cerebral microvasculature. *J Neurosci Res* **88**, 1457-1474 (2010).
52. Obermeier, B., Daneman, R. & Ransohoff, R.M. Development, maintenance and disruption of the blood-brain barrier. *Nat Med* **19**, 1584-1596 (2013).
53. Abbott, N.J. Blood-brain barrier structure and function and the challenges for CNS drug delivery. *J Inherit Metab Dis* **36**, 437-449 (2013).
54. Tanaka, K., Kitagawa, Y. & Kadowaki, T. Drosophila segment polarity gene product porcupine stimulates the posttranslational N-glycosylation of wingless in the endoplasmic reticulum. *J Biol Chem* **277**, 12816-12823 (2002).
55. Willert, K. et al. Wnt proteins are lipid-modified and can act as stem cell growth factors. *Nature* **423**, 448-452 (2003).
56. Hofmann, K. A superfamily of membrane-bound O-acyltransferases with implications for wnt signaling. *Trends Biochem Sci* **25**, 111-112 (2000).
57. Clevers, H. & Nusse, R. Wnt/beta-catenin signaling and disease. *Cell* **149**, 1192-1205 (2012).
58. van Amerongen, R. Alternative Wnt pathways and receptors. *Cold Spring Harb Perspect Biol* **4** (2012).
59. He, X., Semenov, M., Tamai, K. & Zeng, X. LDL receptor-related proteins 5 and 6 in Wnt/beta-catenin signaling: arrows point the way. *Development* **131**, 1663-1677 (2004).
60. Kimelman, D. & Xu, W. beta-catenin destruction complex: insights and questions from a structural perspective. *Oncogene* **25**, 7482-7491 (2006).

61. Schwarz-Romond, T., Merrifield, C., Nichols, B.J. & Bienz, M. The Wnt signalling effector Dishevelled forms dynamic protein assemblies rather than stable associations with cytoplasmic vesicles. *J Cell Sci* **118**, 5269-5277 (2005).
62. Behrens, J. et al. Functional interaction of beta-catenin with the transcription factor LEF-1. *Nature* **382**, 638-642 (1996).
63. Hikasa, H. et al. Regulation of TCF3 by Wnt-dependent phosphorylation during vertebrate axis specification. *Dev Cell* **19**, 521-532 (2010).
64. Lustig, B. et al. Negative feedback loop of Wnt signaling through upregulation of conductin/axin2 in colorectal and liver tumors. *Mol Cell Biol* **22**, 1184-1193 (2002).
65. Derynck, R. & Zhang, Y.E. Smad-dependent and Smad-independent pathways in TGF-beta family signalling. *Nature* **425**, 577-584 (2003).
66. Letamendia, A., Labbe, E. & Attisano, L. Transcriptional regulation by Smads: crosstalk between the TGF-beta and Wnt pathways. *J Bone Joint Surg Am* **83-A Suppl 1**, S31-39 (2001).
67. Hirota, M. et al. Smad2 functions as a co-activator of canonical Wnt/beta-catenin signaling pathway independent of Smad4 through histone acetyltransferase activity of p300. *Cell Signal* **20**, 1632-1641 (2008).
68. Medici, D., Hay, E.D. & Goodenough, D.A. Cooperation between snail and LEF-1 transcription factors is essential for TGF-beta1-induced epithelial-mesenchymal transition. *Mol Biol Cell* **17**, 1871-1879 (2006).
69. MacDonald, B.T., Tamai, K. & He, X. Wnt/beta-catenin signaling: components, mechanisms, and diseases. *Dev Cell* **17**, 9-26 (2009).
70. Bar, T. The vascular system of the cerebral cortex. *Adv Anat Embryol Cell Biol* **59**, I-VI,1-62 (1980).
71. Dermietzel, R. & Krause, D. Molecular anatomy of the blood-brain barrier as defined by immunocytochemistry. *Int Rev Cytol* **127**, 57-109 (1991).
72. Stewart, P.A. & Wiley, M.J. Developing nervous tissue induces formation of blood-brain barrier characteristics in invading endothelial cells: a study using quail--chick transplantation chimeras. *Dev Biol* **84**, 183-192 (1981).
73. Lippmann, E.S. et al. Derivation of blood-brain barrier endothelial cells from human pluripotent stem cells. *Nat Biotechnol* **30**, 783-791 (2012).
74. Daneman, R. et al. Wnt/beta-catenin signaling is required for CNS, but not non-CNS, angiogenesis. *Proc Natl Acad Sci U S A* **106**, 641-646 (2009).
75. Parr, B.A., Shea, M.J., Vassileva, G. & McMahon, A.P. Mouse Wnt genes exhibit discrete domains of expression in the early embryonic CNS and limb buds. *Development* **119**, 247-261 (1993).
76. Engelhardt, B. & Liebner, S. Novel insights into the development and maintenance of the blood-brain barrier. *Cell Tissue Res* **355**, 687-699 (2014).
77. Liebner, S. et al. Wnt/beta-catenin signaling controls development of the blood-brain barrier. *J Cell Biol* **183**, 409-417 (2008).
78. Stenman, J.M. et al. Canonical Wnt signaling regulates organ-specific assembly and differentiation of CNS vasculature. *Science* **322**, 1247-1250 (2008).
79. Cattelino, A. et al. The conditional inactivation of the beta-catenin gene in endothelial cells causes a defective vascular pattern and increased vascular fragility. *J Cell Biol* **162**, 1111-1122 (2003).
80. Grigoryan, T., Wend, P., Klaus, A. & Birchmeier, W. Deciphering the function of canonical Wnt signals in development and disease: conditional loss- and gain-of-function mutations of beta-catenin in mice. *Genes Dev* **22**, 2308-2341 (2008).

81. Paolinelli, R. et al. Wnt activation of immortalized brain endothelial cells as a tool for generating a standardized model of the blood brain barrier in vitro. *PLoS One* **8**, e70233 (2013).
82. Wang, Y. et al. Norrin/Frizzled4 signaling in retinal vascular development and blood brain barrier plasticity. *Cell* **151**, 1332-1344 (2012).
83. Ma, S., Kwon, H.J., Johng, H., Zang, K. & Huang, Z. Radial glial neural progenitors regulate nascent brain vascular network stabilization via inhibition of Wnt signaling. *PLoS Biol* **11**, e1001469 (2013).
84. Yano, H. et al. Differential expression of beta-catenin in human glioblastoma multiforme and normal brain tissue. *Neurol Res* **22**, 650-656 (2000).
85. Polakis, P. The many ways of Wnt in cancer. *Curr Opin Genet Dev* **17**, 45-51 (2007).
86. Castellone, M.D., Teramoto, H., Williams, B.O., Druey, K.M. & Gutkind, J.S. Prostaglandin E2 promotes colon cancer cell growth through a Gs-axin-beta-catenin signaling axis. *Science* **310**, 1504-1510 (2005).
87. Shao, J., Jung, C., Liu, C. & Sheng, H. Prostaglandin E2 Stimulates the beta-catenin/T cell factor-dependent transcription in colon cancer. *J Biol Chem* **280**, 26565-26572 (2005).
88. Voronkov, A. & Krauss, S. Wnt/beta-catenin signaling and small molecule inhibitors. *Curr Pharm Des* **19**, 634-664 (2013).
89. Rajamanickam, S., Kaur, M., Velmurugan, B., Singh, R.P. & Agarwal, R. Silibinin suppresses spontaneous tumorigenesis in APC min/+ mouse model by modulating beta-catenin pathway. *Pharm Res* **26**, 2558-2567 (2009).
90. Teiten, M.H., Gaascht, F., Dicato, M. & Diederich, M. Targeting the wingless signaling pathway with natural compounds as chemopreventive or chemotherapeutic agents. *Curr Pharm Biotechnol* **13**, 245-254 (2012).
91. Dejana, E. & Orsenigo, F. Endothelial adherens junctions at a glance. *J Cell Sci* **126**, 2545-2549 (2013).
92. Steed, E., Balda, M.S. & Matter, K. Dynamics and functions of tight junctions. *Trends Cell Biol* **20**, 142-149 (2010).
93. Eliceiri, B.P. et al. Selective requirement for Src kinases during VEGF-induced angiogenesis and vascular permeability. *Mol Cell* **4**, 915-924 (1999).
94. Giannotta, M., Trani, M. & Dejana, E. VE-cadherin and endothelial adherens junctions: active guardians of vascular integrity. *Dev Cell* **26**, 441-454 (2013).
95. Lampugnani, M.G. et al. A novel endothelial-specific membrane protein is a marker of cell-cell contacts. *J Cell Biol* **118**, 1511-1522 (1992).
96. Nitta, T. et al. Size-selective loosening of the blood-brain barrier in claudin-5-deficient mice. *J Cell Biol* **161**, 653-660 (2003).
97. Nyqvist, D., Giampietro, C. & Dejana, E. Deciphering the functional role of endothelial junctions by using in vivo models. *EMBO Rep* **9**, 742-747 (2008).
98. Hartsock, A. & Nelson, W.J. Adherens and tight junctions: structure, function and connections to the actin cytoskeleton. *Biochim Biophys Acta* **1778**, 660-669 (2008).
99. Simon, D.B. et al. Paracellin-1, a renal tight junction protein required for paracellular Mg2+ resorption. *Science* **285**, 103-106 (1999).
100. Martin-Padura, I. et al. Junctional adhesion molecule, a novel member of the immunoglobulin superfamily that distributes at intercellular junctions and modulates monocyte transmigration. *J Cell Biol* **142**, 117-127 (1998).

101. Wegmann, F., Ebnet, K., Du Pasquier, L., Vestweber, D. & Butz, S. Endothelial adhesion molecule ESAM binds directly to the multidomain adaptor MAGI-1 and recruits it to cell contacts. *Exp Cell Res* **300**, 121-133 (2004).
102. Van Itallie, C.M. & Anderson, J.M. Architecture of tight junctions and principles of molecular composition. *Semin Cell Dev Biol* (2014).
103. Wang, Q. & Margolis, B. Apical junctional complexes and cell polarity. *Kidney Int* **72**, 1448-1458 (2007).
104. Balda, M.S., Garrett, M.D. & Matter, K. The ZO-1-associated Y-box factor ZONAB regulates epithelial cell proliferation and cell density. *J Cell Biol* **160**, 423-432 (2003).
105. Harhaj, N.S. et al. VEGF activation of protein kinase C stimulates occludin phosphorylation and contributes to endothelial permeability. *Invest Ophthalmol Vis Sci* **47**, 5106-5115 (2006).
106. Terry, S., Nie, M., Matter, K. & Balda, M.S. Rho signaling and tight junction functions. *Physiology (Bethesda)* **25**, 16-26 (2010).
107. Kim, J.B. et al. N-Cadherin extracellular repeat 4 mediates epithelial to mesenchymal transition and increased motility. *J Cell Biol* **151**, 1193-1206 (2000).
108. Nelson, W.J. Regulation of cell-cell adhesion by the cadherin-catenin complex. *Biochem Soc Trans* **36**, 149-155 (2008).
109. Ben-Ze'ev, A. & Geiger, B. Differential molecular interactions of beta-catenin and plakoglobin in adhesion, signaling and cancer. *Curr Opin Cell Biol* **10**, 629-639 (1998).
110. Lampugnani, M.G. et al. VE-cadherin regulates endothelial actin activating Rac and increasing membrane association of Tiam. *Mol Biol Cell* **13**, 1175-1189 (2002).
111. Gloerich, M. & Bos, J.L. Regulating Rap small G-proteins in time and space. *Trends Cell Biol* **21**, 615-623 (2011).
112. Birukova, A.A., Tian, X., Tian, Y., Higginbotham, K. & Birukov, K.G. Rap-afadin axis in control of Rho signaling and endothelial barrier recovery. *Mol Biol Cell* **24**, 2678-2688 (2013).
113. Wimmer, R., Cseh, B., Maier, B., Scherrer, K. & Baccarini, M. Angiogenic sprouting requires the fine tuning of endothelial cell cohesion by the Raf-1/Rok-alpha complex. *Dev Cell* **22**, 158-171 (2012).
114. Navarro, P. et al. Catenin-dependent and -independent functions of vascular endothelial cadherin. *J Biol Chem* **270**, 30965-30972 (1995).
115. Monaghan-Benson, E. & Burridge, K. The regulation of vascular endothelial growth factor-induced microvascular permeability requires Rac and reactive oxygen species. *J Biol Chem* **284**, 25602-25611 (2009).
116. Chen, X.L. et al. VEGF-induced vascular permeability is mediated by FAK. *Dev Cell* **22**, 146-157 (2012).
117. Glading, A., Han, J., Stockton, R.A. & Ginsberg, M.H. KRIT-1/CCM1 is a Rap1 effector that regulates endothelial cell cell junctions. *J Cell Biol* **179**, 247-254 (2007).
118. Iden, S. et al. A distinct PAR complex associates physically with VE-cadherin in vertebrate endothelial cells. *EMBO Rep* **7**, 1239-1246 (2006).
119. Nottebaum, A.F. et al. VE-PTP maintains the endothelial barrier via plakoglobin and becomes dissociated from VE-cadherin by leukocytes and by VEGF. *J Exp Med* **205**, 2929-2945 (2008).

120. Lampugnani, M.G. et al. CCM1 regulates vascular-lumen organization by inducing endothelial polarity. *J Cell Sci* **123**, 1073-1080 (2010).
121. Bravi, L., Dejana, E. & Lampugnani, M.G. VE-cadherin at a glance. *Cell Tissue Res* **355**, 515-522 (2014).
122. Dejana, E., Tournier-Lasserve, E. & Weinstein, B.M. The control of vascular integrity by endothelial cell junctions: molecular basis and pathological implications. *Dev Cell* **16**, 209-221 (2009).
123. Taddei, A. et al. Endothelial adherens junctions control tight junctions by VE-cadherin-mediated upregulation of claudin-5. *Nat Cell Biol* **10**, 923-934 (2008).
124. Carmeliet, P. et al. Targeted deficiency or cytosolic truncation of the VE-cadherin gene in mice impairs VEGF-mediated endothelial survival and angiogenesis. *Cell* **98**, 147-157 (1999).
125. Rudini, N. et al. VE-cadherin is a critical endothelial regulator of TGF-beta signalling. *Embo J* **27**, 993-1004 (2008).
126. Claesson-Welsh, L. & Welsh, M. VEGFA and tumour angiogenesis. *J Intern Med* **273**, 114-127 (2013).
127. Lampugnani, M.G., Orsenigo, F., Gagliani, M.C., Tacchetti, C. & Dejana, E. Vascular endothelial cadherin controls VEGFR-2 internalization and signaling from intracellular compartments. *J Cell Biol* **174**, 593-604 (2006).
128. Maddaluno, L. et al. EndMT contributes to the onset and progression of cerebral cavernous malformations. *Nature* **498**, 492-496 (2013).
129. Giampietro, C. et al. Overlapping and divergent signaling pathways of N-cadherin and VE-cadherin in endothelial cells. *Blood* **119**, 2159-2170 (2012).
130. Sanson, B., White, P. & Vincent, J.P. Uncoupling cadherin-based adhesion from wingless signalling in Drosophila. *Nature* **383**, 627-630 (1996).
131. Korswagen, H.C., Herman, M.A. & Clevers, H.C. Distinct beta-catenins mediate adhesion and signalling functions in C. elegans. *Nature* **406**, 527-532 (2000).
132. Kam, Y. & Quaranta, V. Cadherin-bound beta-catenin feeds into the Wnt pathway upon adherens junctions dissociation: evidence for an intersection between beta-catenin pools. *PLoS One* **4**, e4580 (2009).
133. Maher, M.T., Flozak, A.S., Stocker, A.M., Chenn, A. & Gottardi, C.J. Activity of the beta-catenin phosphodestruction complex at cell-cell contacts is enhanced by cadherin-based adhesion. *J Cell Biol* **186**, 219-228 (2009).
134. Zhang, N. et al. FoxM1 promotes beta-catenin nuclear localization and controls Wnt target-gene expression and glioma tumorigenesis. *Cancer Cell* **20**, 427-442 (2011).
135. Medici, D. & Kalluri, R. Endothelial-mesenchymal transition and its contribution to the emergence of stem cell phenotype. *Semin Cancer Biol* **22**, 379-384 (2012).
136. Potenta, S., Zeisberg, E. & Kalluri, R. The role of endothelial-to-mesenchymal transition in cancer progression. *Br J Cancer* **99**, 1375-1379 (2008).
137. Kovacic, J.C., Mercader, N., Torres, M., Boehm, M. & Fuster, V. Epithelial-to-mesenchymal and endothelial-to-mesenchymal transition: from cardiovascular development to disease. *Circulation* **125**, 1795-1808 (2012).
138. Lopez, D., Niu, G., Huber, P. & Carter, W.B. Tumor-induced upregulation of Twist, Snail, and Slug represses the activity of the human VE-cadherin promoter. *Arch Biochem Biophys* **482**, 77-82 (2009).
139. Liebner, S. et al. Beta-catenin is required for endothelial-mesenchymal transformation during heart cushion development in the mouse. *J Cell Biol* **166**, 359-367 (2004).

140. Whitehead, K.J. et al. The cerebral cavernous malformation signaling pathway promotes vascular integrity via Rho GTPases. *Nat Med* **15**, 177-184 (2009).
141. Wolburg, H. et al. Localization of claudin-3 in tight junctions of the blood-brain barrier is selectively lost during experimental autoimmune encephalomyelitis and human glioblastoma multiforme. *Acta Neuropathol* **105**, 586-592 (2003).
142. Schlessinger, K., Hall, A. & Tolwinski, N. Wnt signaling pathways meet Rho GTPases. *Genes Dev* **23**, 265-277 (2009).
143. Boulday, G. et al. Developmental timing of CCM2 loss influences cerebral cavernous malformations in mice. *J Exp Med* **208**, 1835-1847 (2011).
144. Clatterbuck, R.E., Eberhart, C.G., Crain, B.J. & Rigamonti, D. Ultrastructural and immunocytochemical evidence that an incompetent blood-brain barrier is related to the pathophysiology of cavernous malformations. *J Neurol Neurosurg Psychiatry* **71**, 188-192 (2001).
145. Rigamonti, D. et al. Cerebral cavernous malformations. Incidence and familial occurrence. *N Engl J Med* **319**, 343-347 (1988).
146. Batra, S., Lin, D., Recinos, P.F., Zhang, J. & Rigamonti, D. Cavernous malformations: natural history, diagnosis and treatment. *Nat Rev Neurol* **5**, 659-670 (2009).
147. Labauge, P., Denier, C., Bergametti, F. & Tournier-Lasserve, E. Genetics of cavernous angiomas. *Lancet Neurol* **6**, 237-244 (2007).
148. Rosen, J.N., Sogah, V.M., Ye, L.Y. & Mably, J.D. ccm2-like is required for cardiovascular development as a novel component of the Heg-CCM pathway. *Dev Biol* **376**, 74-85 (2013).
149. Akers, A.L., Johnson, E., Steinberg, G.K., Zabramski, J.M. & Marchuk, D.A. Biallelic somatic and germline mutations in cerebral cavernous malformations (CCMs): evidence for a two-hit mechanism of CCM pathogenesis. *Hum Mol Genet* **18**, 919-930 (2009).
150. He, Y. et al. Stabilization of VEGFR2 signaling by cerebral cavernous malformation 3 is critical for vascular development. *Sci Signal* **3**, ra26 (2010).
151. Whitehead, K.J., Plummer, N.W., Adams, J.A., Marchuk, D.A. & Li, D.Y. Ccm1 is required for arterial morphogenesis: implications for the etiology of human cavernous malformations. *Development* **131**, 1437-1448 (2004).
152. Plummer, N.W. et al. Loss of p53 sensitizes mice with a mutation in Ccm1 (KRIT1) to development of cerebral vascular malformations. *Am J Pathol* **165**, 1509-1518 (2004).
153. McDonald, D.A. et al. A novel mouse model of cerebral cavernous malformations based on the two-hit mutation hypothesis recapitulates the human disease. *Hum Mol Genet* **20**, 211-222 (2011).
154. Verlaan, D.J. et al. CCM3 mutations are uncommon in cerebral cavernous malformations. *Neurology* **65**, 1982-1983 (2005).
155. Gianfrancesco, F. et al. ZPLD1 gene is disrupted in a patient with balanced translocation that exhibits cerebral cavernous malformations. *Neuroscience* **155**, 345-349 (2008).
156. Petit, N., Blecon, A., Denier, C. & Tournier-Lasserve, E. Patterns of expression of the three cerebral cavernous malformation (CCM) genes during embryonic and postnatal brain development. *Gene Expr Patterns* **6**, 495-503 (2006).
157. Gore, A.V., Lampugnani, M.G., Dye, L., Dejana, E. & Weinstein, B.M. Combinatorial interaction between CCM pathway genes precipitates hemorrhagic stroke. *Dis Model Mech* **1**, 275-281 (2008).

158. Mably, J.D. et al. santa and valentine pattern concentric growth of cardiac myocardium in the zebrafish. *Development* **133**, 3139-3146 (2006).
159. Voss, K. et al. Functional analyses of human and zebrafish 18-amino acid in-frame deletion pave the way for domain mapping of the cerebral cavernous malformation 3 protein. *Hum Mutat* **30**, 1003-1011 (2009).
160. Mably, J.D., Mohideen, M.A., Burns, C.G., Chen, J.N. & Fishman, M.C. heart of glass regulates the concentric growth of the heart in zebrafish. *Curr Biol* **13**, 2138-2147 (2003).
161. Zheng, X. et al. Cerebral cavernous malformations arise independent of the heart of glass receptor. *Stroke* **45**, 1505-1509 (2014).
162. Louvi, A. et al. Loss of cerebral cavernous malformation 3 (Ccm3) in neuroglia leads to CCM and vascular pathology. *Proc Natl Acad Sci U S A* **108**, 3737-3742 (2011).
163. Riant, F., Bergametti, F., Ayrignac, X., Boulday, G. & Tournier-Lasserve, E. Recent insights into cerebral cavernous malformations: the molecular genetics of CCM. *Febs J* **277**, 1070-1075 (2010).
164. Hilder, T.L. et al. Proteomic identification of the cerebral cavernous malformation signaling complex. *J Proteome Res* **6**, 4343-4355 (2007).
165. Li, X. et al. Crystal structure of CCM3, a cerebral cavernous malformation protein critical for vascular integrity. *J Biol Chem* **285**, 24099-24107 (2010).
166. Stockton, R.A., Shenkar, R., Awad, I.A. & Ginsberg, M.H. Cerebral cavernous malformations proteins inhibit Rho kinase to stabilize vascular integrity. *J Exp Med* **207**, 881-896 (2010).
167. Zheng, X. et al. Dynamic regulation of the cerebral cavernous malformation pathway controls vascular stability and growth. *Dev Cell* **23**, 342-355 (2012).
168. Fisher, O.S. & Boggon, T.J. Signaling pathways and the cerebral cavernous malformations proteins: lessons from structural biology. *Cell Mol Life Sci* **71**, 1881-1892 (2014).
169. Crose, L.E., Hilder, T.L., Sciaky, N. & Johnson, G.L. Cerebral cavernous malformation 2 protein promotes smad ubiquitin regulatory factor 1-mediated RhoA degradation in endothelial cells. *J Biol Chem* **284**, 13301-13305 (2009).
170. Fidalgo, M. et al. CCM3/PDCD10 stabilizes GCKIII proteins to promote Golgi assembly and cell orientation. *J Cell Sci* **123**, 1274-1284 (2010).
171. Fidalgo, M. et al. Adaptor protein cerebral cavernous malformation 3 (CCM3) mediates phosphorylation of the cytoskeletal proteins ezrin/radixin/moesin by mammalian Ste20-4 to protect cells from oxidative stress. *J Biol Chem* **287**, 11556-11565 (2012).
172. Wustehube, J. et al. Cerebral cavernous malformation protein CCM1 inhibits sprouting angiogenesis by activating DELTA-NOTCH signaling. *Proc Natl Acad Sci U S A* **107**, 12640-12645 (2010).
173. Potts, J.D., Dagle, J.M., Walder, J.A., Weeks, D.L. & Runyan, R.B. Epithelial-mesenchymal transformation of embryonic cardiac endothelial cells is inhibited by a modified antisense oligodeoxynucleotide to transforming growth factor beta 3. *Proc Natl Acad Sci U S A* **88**, 1516-1520 (1991).
174. Yoruk, B., Gillers, B.S., Chi, N.C. & Scott, I.C. Ccm3 functions in a manner distinct from Ccm1 and Ccm2 in a zebrafish model of CCM vascular disease. *Dev Biol* **362**, 121-131 (2012).
175. Wang, Y. et al. Ephrin-B2 controls VEGF-induced angiogenesis and lymphangiogenesis. *Nature* **465**, 483-486 (2010).

176. Maretto, S. et al. Mapping Wnt/beta-catenin signaling during mouse development and in colorectal tumors. *Proc Natl Acad Sci U S A* **100**, 3299-3304 (2003).
177. Srinivas, S. et al. Cre reporter strains produced by targeted insertion of EYFP and ECFP into the ROSA26 locus. *BMC Dev Biol* **1**, 4 (2001).
178. McDonald, D.A. et al. Fasudil decreases lesion burden in a murine model of cerebral cavernous malformation disease. *Stroke* **43**, 571-574 (2012).
179. Balconi, G., Spagnuolo, R. & Dejana, E. Development of endothelial cell lines from embryonic stem cells: A tool for studying genetically manipulated endothelial cells in vitro. *Arterioscler Thromb Vasc Biol* **20**, 1443-1451 (2000).
180. Vleminckx, K., Kemler, R. & Hecht, A. The C-terminal transactivation domain of beta-catenin is necessary and sufficient for signaling by the LEF-1/beta-catenin complex in Xenopus laevis. *Mech Dev* **81**, 65-74 (1999).
181. Lluis, F., Pedone, E., Pepe, S. & Cosma, M.P. Periodic activation of Wnt/beta-catenin signaling enhances somatic cell reprogramming mediated by cell fusion. *Cell Stem Cell* **3**, 493-507 (2008).
182. Meani, N. et al. Molecular signature of retinoic acid treatment in acute promyelocytic leukemia. *Oncogene* **24**, 3358-3368 (2005).
183. Self, A.J., Caron, E., Paterson, H.F. & Hall, A. Analysis of R-Ras signalling pathways. *J Cell Sci* **114**, 1357-1366 (2001).
184. van Noort, M., Meeldijk, J., van der Zee, R., Destree, O. & Clevers, H. Wnt signaling controls the phosphorylation status of beta-catenin. *J Biol Chem* **277**, 17901-17905 (2002).
185. Fadini, G.P., Losordo, D. & Dimmeler, S. Critical reevaluation of endothelial progenitor cell phenotypes for therapeutic and diagnostic use. *Circ Res* **110**, 624-637 (2012).
186. Sanchez-Tillo, E. et al. beta-catenin/TCF4 complex induces the epithelial-to-mesenchymal transition (EMT)-activator ZEB1 to regulate tumor invasiveness. *Proc Natl Acad Sci U S A* **108**, 19204-19209 (2011).
187. Li, J. & Zhou, B.P. Activation of beta-catenin and Akt pathways by Twist are critical for the maintenance of EMT associated cancer stem cell-like characters. *BMC Cancer* **11**, 49 (2011).
188. Li, X. et al. LIF maintains progenitor phenotype of endothelial progenitor cells via Kruppel-like factor 4. *Microvasc Res* **84**, 270-277 (2012).
189. Liang, S.X. et al. In vitro and in vivo proliferation, differentiation and migration of cardiac endothelial progenitor cells (SCA1+/CD31+ side-population cells). *J Thromb Haemost* **9**, 1628-1637 (2011).
190. Stein, U. et al. The metastasis-associated gene S100A4 is a novel target of beta-catenin/T-cell factor signaling in colon cancer. *Gastroenterology* **131**, 1486-1500 (2006).
191. Tobin, N.P., Sims, A.H., Lundgren, K.L., Lehn, S. & Landberg, G. Cyclin D1, Id1 and EMT in breast cancer. *BMC Cancer* **11**, 417 (2011).
192. Glinka, A. et al. Dickkopf-1 is a member of a new family of secreted proteins and functions in head induction. *Nature* **391**, 357-362 (1998).
193. Wang, X. et al. The development of highly potent inhibitors for porcupine. *J Med Chem* **56**, 2700-2704 (2013).
194. Kundu, J.K., Choi, K.Y. & Surh, Y.J. beta-Catenin-mediated signaling: a novel molecular target for chemoprevention with anti-inflammatory substances. *Biochim Biophys Acta* **1765**, 14-24 (2006).

195. Boon, E.M. et al. Sulindac targets nuclear beta-catenin accumulation and Wnt signalling in adenomas of patients with familial adenomatous polyposis and in human colorectal cancer cell lines. *Br J Cancer* **90**, 224-229 (2004).
196. Thompson, H.J. et al. Sulfone metabolite of sulindac inhibits mammary carcinogenesis. *Cancer Res* **57**, 267-271 (1997).
197. Holland, J.D., Klaus, A., Garratt, A.N. & Birchmeier, W. Wnt signaling in stem and cancer stem cells. *Curr Opin Cell Biol* **25**, 254-264 (2013).
198. Giardiello, F.M. et al. Treatment of colonic and rectal adenomas with sulindac in familial adenomatous polyposis. *N Engl J Med* **328**, 1313-1316 (1993).
199. Chang, W.C. et al. Sulindac sulfone is most effective in modulating beta-catenin-mediated transcription in cells with mutant APC. *Ann N Y Acad Sci* **1059**, 41-55 (2005).
200. Mackenzie, G.G. et al. Phospho-sulindac (OXT-328) combined with difluoromethylornithine prevents colon cancer in mice. *Cancer Prev Res (Phila)* **4**, 1052-1060 (2011).
201. Glading, A.J. & Ginsberg, M.H. Rap1 and its effector KRIT1/CCM1 regulate beta-catenin signaling. *Dis Model Mech* **3**, 73-83 (2010).
202. Snippert, H.J. et al. Intestinal crypt homeostasis results from neutral competition between symmetrically dividing Lgr5 stem cells. *Cell* **143**, 134-144 (2010).

ACKNOWLEDGEMENTS

If it is true that a “person” is the result of the people he meets and the experiences he does in the life, I’m completely sure that after the last four years I became a better person.

Someone said “life is what happens to you while you’re busy making other plans”. Indeed, during this long journey that was the Ph.D. in the meanwhile of scientific discussion, experiments design and epic fails thinking about the future I found something of exquisitely unexpected but incredibly precious from different people who left me something special that enriched me both as a scientist and as a man.

First of all I want to thank my boss, Elisabetta Dejana, who gave me the possibility to work in her group and grow as a researcher and as a person. She believed in my faculties and guided me always into the complex world of research.

I am particularly grateful to my supervisor Maria Grazia, who was my primary resource for getting my science questions answered and the compass during my entire Ph.D.. She taught me how to work and to move in this complex field and that every unsuccessful experiment was not a failure rather than just the discovery of new ways that won’t work.

I acknowledge my SEMM supervisors during the Ph.D., Giorgio Scita and Stefan Liebner for their very useful suggestions and constructive feedback about my work.

It would not have been possible to write my doctoral thesis without the help and support of the kind people around me, to only some of whom it is possible to give particular mention here. I’d like to give special thanks to Noemi and Roberto who share with me part of the scientific project and not only, helping me in several aspect of every day lab life. I thank all my lab mates, the past members Gigi, Marco, Daniel, Masato, Annamaria and Eleanna and present members Costanza, Monica G, Monica C, Matteo, Marianna, Ferruccio, Fabrizio,

Laura, Cecilia, Ganesh, Surya. All of you are much more than colleagues. I will always keep in mind all of your suggestions.

A special acknowledgement to Azzurra e Benedetta who shared with me the long road to the Ph.D. starting from the first day of selections. Without you every seminar, lesson and report would have been much harder.

A very unique and special thank to Elisabetta who shared with me all my fears, my hopes, every little successes and failures during these years, who gave me a great support and always pushed me to go on. You are the North Star in my little sky, thank you for keeping on shining on me.

I will forever be thankful to my family in particular my parents who always believed in me and gave me the possibility to follow my dreams supporting my choices. They were there every time I needed. I would not have gone so far without them.

Finally, I want to thank also to my friends, in particular Emiliano and Fabio for providing support and friendship that I needed.